Cumulation of Man-Made Radio Noise

A quest for causes of the increase of radio noise in residential areas

Koos Fockens

CUMULATION OF MAN-MADE RADIO NOISE

A QUEST FOR CAUSES
OF THE INCREASE OF RADIO NOISE
IN RESIDENTIAL AREAS

T. W. H. (Koos) Fockens

CUMULATION OF MAN-MADE RADIO NOISE

A QUEST FOR CAUSES OF THE INCREASE OF RADIO NOISE IN RESIDENTIAL AREAS

PROEFSCHRIFT

ter verkrijging van
de graad van doctor aan de Universiteit Twente,
op gezag van de rector magnificus,
prof.dr.ir. A. Veldkamp,
volgens besluit van College voor Promoties
in het openbaar te verdedigen
op vrijdag 20 oktober 2023 om 14.45 uur

door

Tallienco Wieand Harm Fockens
geboren op 8 september 1946
in Groningen, Nederland

Dit proefschrift is goedgekeurd door:

Promotor:
prof. dr. ir. F.B.J. Leferink

The research described in this dissertation was carried out in the Power Electronics and Electromagnetic Compatibility Group, which is part of the Faculty of Electrical Engineering, Mathematics and Computer Science at the University of Twente, The Netherlands.

The noise measurements campaign, as refered to in this dissertation, was partly funded by the Association for Experimental Radio Research in The Netherlands, VERON.

Cover design by: Koos Fockens
Printed by: Gildeprint – www.gildeprint.nl
Written & Typeset in: TechWriter *Professional* © Martin Würthner, 2013.
ISBN (print): 978-90-365-5742-9
ISBN (digital): 978-90-365-5743-6
DOI: 10.3990/1.9789036557436
URL: https://doi.org/10.3990/1.9789036557436

PROMOTIE COMMISSIE

Voorzitter / secretaris:	prof. dr. J. N. Kok
Promotor:	prof. dr. ir. F.B.J. Leferink Universiteit Twente, EEMCS, Power Electronics
Leden:	prof. dr. ir A.B.J. Kokkeler Universiteit Twente, EEMCS, Radio Systems
	prof. dr. ir. F.E. van Vliet Universiteit Twente, EEMCS, Integrated Circuit Design
	dr. ir. P.T. de Boer Universiteit Twente, EEMCS, Design and Analysis of Communication Systems
	prof. dr. ir. M.J. Bentum Technical University Eindhoven
	prof. dr. ir. A.B. Smolders Technical University Eindhoven
	dr. ir. A.P.M. Zwamborn NL Organisation for Applied Scientific Research, TNO

Voor mijn kleinzoon Elio

Summary

Man-Made Noise and Electromagnetic Interference attracted greater attention for some decades now, especially in circles of radio spectrum users. Increasing levels of noise and interference in residential areas hamper the reception of radio signals over a very broad range of frequencies, from long wave via short wave band up to VHF and even UHF bands. Analog radio as well as modern digital radio systems are affected. Also the upper frequency limit of the interference is moving upwards gradually.

The study in this dissertation limits itself to the frequency range from 500 kHz to 50 MHz, and consists of four main parts. The first part consists of a measurement campaign wherein noise floor levels at the locations of radio users have been established, commissioned by the VERON (Association for Experimental Radio Research in The Netherlands), wherein noise floor levels are determined at 59 locations. It also contains extensively statistical processing, by which regression lines of man-made noise levels are calculated, that can be compared with same regression lines that have been published in the ITU-R P.372-15 recommendation. A significant increase of noise in residential areas has been established. The data processing also indicated that the "critical area", wherein the noise floor is determined by the density of habitation, is limited to a range of 100 to 300 m from the measurement location, depending on frequency.

The second part of the study is about propagation of noise and interference through habituated areas. Another measurement campaign was set up and executed by the author with help from a part of the radio amateurs that participated in the first campaign. Extensive processing of the measurement data resulted in a simple and useful statistical propagation model for residential areas.

In the third part a statistical model for the cumulation of man-made noise is derived, using the propagation model. Using this cumulation model it is possible to calculate expectation values for the noise floor at a certain location, depending on the density of habitation, the density of noise/EMI sources, and the available source power.

In the last part of this study the cumulation model is used for simulations, using several combinations of input variable values. The resulting noise field strength levels are compared with the measured levels. The outcome of these experiments is that the hypothesis, that the injection of disturbances with source powers derived from the generic

CISPR limits for the mains port would explain the increase of the man-made noise, is not tenable. Therefore a reasonable conclusion is that the increase of noise levels is caused by radiation from other networks like DC cabling, telecom lines, and/or other wiring.

Especially the higher limit levels for these ports and serious shortcomings in the test methods, not being in accordance with the practical use of the tested equipment, are suspected to cause higher levels of radiation. Another suspected cause for the increased noise levels is formed by limitations in the enforcement of the EMC regulations, whereby too many pieces of illegal equipment circulate on the European market.

At the end this dissitation contains a number of recommendations for further research and proposes a new direction for improving the enforcement of the EU EMC Directive.

Samenvatting

Door menselijke activiteit gegenereerde Electromagnetische ruis en Interferentie zijn volop in de belangstelling sinds enkele tientallen jaren, in het bijzonder in de kringen van radio spectrum gebruikers. Toenemende niveau's van ruis en interferentie in woonomgevingen hinderen en blokkeren de ontvangst van radio signalen over een breed frequentiegebied, van de Lange Golf via Korte Golf tot de VHF en UHF banden. Zowel analoge radio als moderne digitale radio systemen worden geraakt. Ook schuift de bovenste frequentielimiet van de storing geleidelijk naar boven.

De studie in dit proefschrift beperkt zich tot het frequentie bereik van 500 kHz tot 50 MHz, en bestaat uit vier delen. Het eerste deel bestaat uit een meetcampagne in opdracht van de VERON (Vereniging voor Experimenteel Radio Onderzoek in Nederland), waarin ruis niveau's zijn bepaald op 59 locaties. Het bevat ook uitgebreide statistische bewerkingen, waarbij regressielijnen van man-made ruisniveaus's zijn berekend, die kunnen worden vergeleken met dezelfde regressielijnen als die zijn gepubliceerd in de ITU-R P.372-15 recommendatie. Een significante toename of de ruisvloer in woonomgevingen is aangetoond. De data verwerking gaf ook aan dat de "kritieke zone", waarin de ruisvloer is bepaald door de bewoningsdichtheid, is begrensd tot een bereik van 100 tot 300 m vanaf de meetlokatie, afhankelijk van de frequentie.

Het tweede deel van de studie gaat over de propagatie van ruis en EMI door bewoonde gebieden. Een nieuwe meetcampagne was opgezet en uitgevoerd door de auteur met hulp van een deel van de radio amateurs die ook participeerden in de eerste campagne. Uitgebreide verwerking van de meetdata resulteerde in een eenvoudig en bruikbaar statistisch propagatiemodel voor woongebieden.

In het derde deel wordt onder gebruikmaking van het propagatiemodel een statistisch model voor de cumulatie van man-made ruis afgeleid. Met dat cumulatiemodel is het mogelijk om verwachtingswaarden te berekenen voor een zekere locatie, uitgaande van de bewoningsdichtheid, de dichtheid van ruis- en EMI-bronnen, en het beschikbare vermogen per bron.

In het laatste deel van deze studie is het cumulatiemodel gebruikt in simulaties, waarbij diverse combinaties van waarden voor de input variabelen zijn gebruikt. De resulterende ruisveldsterkten zijn vergeleken met gemeten waarden, gevonden in de ruismeetcampagne.

De uitkomst van deze experimenten is dat de hypothese, dat injectie van storingspanningen met bronvermogens afgeleid van de generieke CISPR-limieten voor de netspanningsaansluiting, de toename van de man-made ruis zou verklaren, niet houdbaar is. Een redelijke conclusie zou zijn dat de toename van de ruisniveau's wordt veroorzaakt door de afstraling vanaf andere netwerken zoals DC kabels, telecom lijnen, en/of andere bedradingen.

De oorzaak van deze hogere stralingsniveau's zijn waarschijnlijk gelegen in de hogere limietwaarden voor deze poorten en de ernstige tekortkomingen in de testmethoden, welke niet in overeenstemming zijn met het praktische gebruik van de geteste apparatuur. Een andere verdenking van het veroorzaken van verhoogde ruisniveau's wordt gevormd door beperkingen in de handhaving van de EMC regelgeving, waardoor teveel illegale apparatuur circuleert op de Europese markt.

Het eind van dit proefschrift bevat een aantal aanbevelingen voor verder onderzoek en stelt een nieuwe richting voor om de handhaving van de EU EMC Richtlijn te verbeteren.

Table of Contents

Abbreviations

AMN:	Artificial Mains Network
APD:	Amplitude Probability Distribution
ASTRON:	Netherlands Institute for Radio Astronomy
AuxEq:	Auxillary equipment
AWG(N):	Additive White Gaussian (Noise)
ATG:	Apparant type of ground (defined in this dissertation)
BW:	Bandwidth
C:	A programming language
CEPT:	Conférence européenne des administrations des postes et télécommunications (European Conference of Postal and Telecommunication Administrations)
CENELEC:	Comité Européen de Normalisation Electrotechnique
CISPR:	Comité International Spécial des Perturbations Radioélectriques
CM:	Common mode
CSV:	Comma Separated Values (electronic file format)
DAB:	Digital Audio Broadcasting
DC:	Direct Current
EAS:	Electronic Article Surveillance
ECS:	Equivalent CISPR Source (defined in this dissertation)
EMC:	Electromagnetic Compatibility
EMF:	Electromagnetic Field
EMI:	Electromagnetic Interference
EM:	Electromagnetic
ERC:	European Radiocommunication Committee
EU:	European Union
EUT:	Equipment under test
ETSI:	European Telecommunication and Standardisation Institute

FCC:	Federal Communication Commission (USA)
FS:	Field Strength
FSK:	Frequency Shift Keying
GPS:	Global Positioning System
GUI:	Graphical Users Interface
GW:	Ground-Wave
HAP:	House Access Point
Hz:	Hertz, the SI unit for frequency: one cycle per second
IARU:	International Amateur Radio Union
ID:	Identification signal
IF:	Intermediate Frequency
IN:	Impulsive Noise
ITU-R:	International Telecommunication Union - Radiocommunication Sector
kHz:	kilo Hertz
LED:	Light Emitting Diode
LVDN:	Low Voltage Distribution Network
MHz:	Mega Hertz
MMN:	Man-Made Noise
MW:	Medium Wave
NSW:	Norton Surface Wave
NVIS:	Near Vertical Incident Skywave
OATS:	Open Air Test Site
OSM:	Open Street Map
PDD:	Pulse Duration Distributions
pdf:	1. probability distribution function 2. portable document format - electronic file format
PE:	Protective Earth
PEC:	Perfect Electric Conducting
PLC:	Power Line Communication
PSD:	Pulse Spacing Distributions
PV:	Photo Voltaïc

RA-NL:	Radio Agency of The Netherlands (Agentschap Telecom)
RDI:	Rijksinspectie Digitale Infrastructuur
RF:	Radio Frequency
RFI:	Radio Frequency Interference
RFID:	Radio Frequency Identification
RiscOS:	Operating System for Computers with ARM (Advanced RISC Machine) processors
RISC:	Reduced Instruction Set Computer
SDR:	Software Defined Radio
SE:	Spectrum Engineering
SI:	International System of Units
VERON:	Association for Experimental Radio Research in The Netherlands (Vereniging voor Experimenteel Radio Onderzoek in Nederland)
ZSW:	Zenneck Surface Wave
xDSL:	High speed Digital Subscriber Line
MF:	Medium Frequency (0.3 - 3 MHz)
HF:	High Frequency (3 - 30 MHz)
VHF:	Very High Frequency (30 - 300 MHz)
UHF:	Ultra High Frequency (300 - 3000 MHz)

Chapter 1

1 Introduction

Radio noise forms a fundamental limitation for the reception of radio signals. Its level sets the minimum value for the field strength of a wanted signal to be received, and consequently limits the transmitter range. In this dissertation we will investigate radio noise that is caused by human activity: anthropogenic or Man Made Noise (MMN). That means electromagnetic energy generated as a by-product of electric or electronic processes, but not meant for the purpose of producing an intended, generally information carrying, radio signal.

The research in this dissertation is directed on the subject of cumulation of MMN. That means noise or Electromagnetic Interference (EMI) from many sources, distributed in an certain area, is added into an apparent increased noise floor. In residential areas this increase of the radio noise is seen as an extra layer above the natural levels, as measured in quiet rural areas. As MMN is generated by discrete sources, discrete Electromagnetic Interference (EMI) components are expected, being narrow band or broadband in the frequency domain. Locally these EMI components are detectable indeed, but more than often a broadband shroud of noise is found, covering the natural background radio noise and the intended radio signals.

The ITU-R Recommendation P.372 gives radio noise data of diverse origin including MMN. Allthough the recommendation is updated every few years, the published noise level data is based on measurements in the sixties and seventies of the last century and is not being refreshed. We treat this recommendation further in Section 1.3. Also we will study earlier research into the subject of radio noise in the forthcoming sections, especially in

Section 1.5.

In Chapter 2 we start with a description of the technical requirements for measuring MMN, and that is also the subject of the conference publication [I]. Chapter 3 describes the MMN measurement campaign, including results, which has been published in [II], to get an insight in the current levels of MMN as measured at the actual locations of radio spectrum users. In Chapter 4 a further statistical processing of these measurement data is performed, which is published in [III]. Next we examine the propagation of MMN in residential areas by another measurement campaign, reported in [IV] and in Chapter 5. The results from these propagation measurements are used to build a propagation model, valid for residential areas. Chapter 6 reports on a longitudinal measurements of propagation, depending on weather and seasonal variations. It gives more detailed information about the measurement method and data processing. Finally in Chapter 7 the propagation model becomes a part of a model for the cumulation of electromagnetic radiation from large numbers of MMN sources resulting in MMN field strength levels at a given location. At last we do some exercises in filling the cumulation model with assumptions about MMN source power levels, source densities, and calculate the resulting field strength levels. These levels are compared with the earlier measured field strength levels, from where some conclusion will be drawn.

This investigation will brought to the reader in a narrative style. Very often the word "we" will be used. The author wants to indicate that with the word "we" he means the reader and the author.

1.1 Motivation

During the past decennia several radio services experienced a serious increase in radio frequency interference levels due to Man-Made radio Noise (MMN) as well as local Electromagnetic Interference (EMI) effects. These phenomena lead to a rise of the background noise floor, as has been shown in [1] - [6]. During the standardisation processes of network EMC standards, starting in 2000 in CEPT, later on continued in ETSI, CENELEC, and CISPR, the question of the existing levels of radio noise floor arose, together with how to measure those levels. In The Netherlands an expert group was formed in 2002 consisting of specialists from Agentschap Telecom[1] (RA-NL), Royal Dutch Army, Royal Dutch Navy, Radio Netherlands World Service, ASTRON, Nedap N.V. (industry), and VERON (the Association for Experimental Radio Research in The Netherlands, member of the International Amateur[2] Radio Union, IARU). The results [7], [8] were

1 From 1-1-2023 called Rijksinspectie Digitale Infrastructuur, RDI.

2 Definition Amateur Radio Service in the ITU-R Radio Regulations: A radiocommunication service for the purpose of self-training, intercommunication and technical investigations carried out by amateurs, that is, by duly authorized persons interested in radio technique solely with a personal aim and without pecuniary interest.

submitted to Study Group SG01 of ITU-R, what resulted in Report ITU-R SM.2055, Radio Noise measurements, [9]. This report was extended into Report ITU-R SM.2155, Man-made Noise measurements in the HF range, [10], and finally concluded in Recommendation ITU-R SM.1753-2, *Methods for measurements of radio noise,* [11]. A further study on noise measurement methods is found in [12].

The increase of MMN reached the EMC-EMF committee of the VERON by an increasing number of interference report, sees from her members, so a noise measurement campaign was initiated by the board of the VERON. By letter dated 18/11/2013 an order was given to measure MMN at the locations of our member radio amateurs in the Netherlands with intent to publish the result in a scientific paper. The measurements were carried out in the years 2015 and 2016. The intention was to measure in real life situations in a wide range of densities of habitation, from quiet rural to city areas. Already the author did daily measurements of atmospheric noise levels in the period from 2005 to 2016, driven from a personal interest, using methods as developed in the named expert group. That project does not form a part of this dissertation, but resulted in know how and experience that became relevant for the realisation of the VERON noise measurement campaign.

1.2 Research Question

According the Central Limit Theorem the summation of EMI from a high number of independent sources will result in a stochastic signal that approaches the character of Additive White Gaussian Noise (AWGN). This theorem would be a good explanation for the observed broadband noise. So the central research question in this dissertation is: "Is there a scientific stochastic model possible that explains and predicts broadband noise field strength levels, starting from a distribution of individual MMN sources with a known expectation value of available power?".

1.3 Noise

The English word "noise" has a broad definition, broader than the generally used word "ruis" in the Dutch language. The equivalent word for "noise" in Dutch is "lawaai". It includes all kind of sounds and is not limited by origin or character. Instead, in this dissertation we will talk about noise that is generated in a way wherein random processes are greatly involved and consequently this noise has a mainly stochastic character. An example of fully stochastic noise is Additive White Gaussian noise (AWGN). Herein means "Gaussian" that the samples in the time domain show a normal distribution and "White" mean a constant power density in the frequency domain. "Additive" indicates a linear process wherein noise components mix with wanted signals and other noise

components.

The International Telecommunication Union, Radiocommunication Sector, ITU-R, defines in Recommendation ITU-R P.372-15, reference [13] (further on referred to as ITU-R P.372) radio noise as "A time-varying electromagnetic phenomenon having components in the radio-frequency range, apparently not conveying information and which may be superimposed on, or combined with, a wanted signal."

Clearly, this definition uses the broader meaning of the word "noise" as, for example, a constant and unmodulated radio frequency carrier does not convey information, but is not generated by a random process. It may be generated as a by-product of electric of electronic processes, and as an unmodulated carrier it may cause radio frequency interference (RFI). We will exclude this kind of EMI in our study as we want to focus on cumulation effects that result in a mainly stochastic form of noise.

Noise can be generated by many processes. In (analog) electronic circuits alone we identify thermal noise, shot noise, partition noise, flicker noise, burst noise, and transient time noise, etc. Outside electronic circuits we find other mechanism and sources like electric phenomena in the atmosphere as lightning and corona discharges, together known as atmospheric noise, and other natural sources. In this dissertation we discuss anthropogenic noise, also known as Man-Made Noise (MMN). ITU-R P.372 describes radio noise from most of the natural sources and MMN. More extensive descriptions of natural noise sources, including from celestial bodies and galactic origin, we find in the Handbook of Atmospheric Electrodynamics [14].

Thermal noise is a fundamental phenomenon. Basically it is generated by randomly moving electric charges, for example electrons. Free electrons in a conducting material move by their kinetic energy, causing spontaneous variations of electric potentials. This amount of kinetic energy is depending on the absolute temperature of the material. We call this kind of noise "thermal noise". So for a resistor, defined as a piece of material with a finite conductivity, the unloaded r.m.s noise voltage, e_{rms}, at this terminals is given by:

$$e_{rms} = \sqrt{4kTRb} \tag{1.1}$$

wherein:

k: Boltzmann's constant = $1.38 \cdot 10^{-23}$ [J/K]

T: temperature [K]

R: resistance [ohm, Ω]

b: bandwidth [Hz]

The available thermal noise power, p_n, is given by:

$$p_n = kTb \tag{1.2}$$

Above that, electronic components like amplifiers, etc., produce extra noise. This extra noise, causing the total noise power exceeding the thermal noise level, can be expressed as a ratio of the actual available noise power to the available thermal noise power at a reference temperature $T_0 = 290\,K$, the so called the noise factor, f, and defined as:

$$f = \frac{p_{n,total}}{kT_0b} \tag{1.3}$$

A full description of the noise factor can be found in *IEEE standard dictionary of electrical and electronics terms*. For example R may be the input resistance of an amplifier and $p_{n,total}$ the equivalent noise power, referring to the input of the amplifier. f is here the noise factor of the amplifier.

We can apply this method to a radio receiving system, containing an antenna with a antenna impedance matching circuit, a transmission line, and a receiver. From [13] we learn the next relationship:

$$f_s = f_a + (f_c - 1) + l_c(f_t - 1) + l_c l_t(f_r - 1) \tag{1.4}$$

wherein:

- f_s: the noise factor of the receiving system
- f_a: the noise factor of the lossless antenna, representing the external noise
- f_c: the noise factor of the antenna circuit, caused by circuit loss in case of a passive antenna, or by the noise of the electronic circuit in case of an active antenna.
- f_t: the noise factor of the transmission line, caused by the transmission loss.
- f_r: the noise factor of the receiver
- l_c: antenna circuit loss
- l_t: transmission line loss

Equation (1.4) is a special form of the Friis equation. The gain loss in this equation relates to the available gain and require optimal impedance matching between the system blocks.

For the external noise power, p_{na}, we write:

$$f_a = \frac{p_{na}}{kT_0b} \tag{1.5}$$

Usually the logarithmic noise figure F is used:

$$F_a = 10\log_{10} f_a \tag{1.6}$$

expressed in dB, see footnote[34]. In this way Equation (1.5) is converted into:

$$P_{na} = F_a + B - 204 \text{ [dBW]} \tag{1.7}$$

Available external antenna noise power: $P_{na} = 10 \log p_{na}$

Bandwidth: $B = 10 \log b$

Constant: $-204 = 10 \log kT_0$

The external antenna noise power may be related to a field strength value, but this relationship is depending on the characteristics of the antenna and the environment of the antenna. ITU-R Rec. P.372 [13] gives this relationship for two cases, namely first the case of a vertical monopole, rising up from a perfect electric conducting (PEC) ground plane, and secondly a dipole antenna in free space. A variant to the latter case is the isotropic antenna in free space. In the first case a half space is assumed in combination with a mirror antenna under ground, wherein downward oriented waves are reflected and added to the direct wave. This adding is not the case in free space. In formula:

$$\text{monopole on PEC ground: } E_n = F_a + 20 \log f\,[MHz] + B - 95.5 \text{ [dB(µV/m)]} \tag{1.8}$$

In free space, where there is no interaction with ground or any other object:

$$\text{Hertzian dipole: } E_n = F_a + 20 \log f\,[MHz] + B - 98.5 \text{ [dB(µV/m)]} \tag{1.9}$$

$$\text{half wave dipole: } E_n = F_a + 20 \log f\,[MHz] + B - 98.9 \text{ [dB(µV/m)]} \tag{1.10}$$

$$\text{isotropic antenna: } E_n = F_a + 20 \log f\,[MHz] + B - 96.8 \text{ [dB(µV/m)]} \tag{1.11}$$

The Appendix in reference [15] gives a derivation of these equations. In Appendix A a different derivation is given for the Formulas (1.8) to (1.11). In the latter derivation a important aspect about noise measurement is cleared. In field strength measurements above PEC ground the measured field strength value is doubled in respect to free space value of the arriving EM waves. This is caused by the boundary condition at the reflection point and the fact that we use a field sensor as measurement tool, like a small loop antenna or a small active e-field probe such as the small monopole. These tools are calibrated for a local field in free space, and show a doubled field strength in relation to the arriving wave in free space. This is reflected in Equation (1.8), so guaranteeing for an unambiguous measurement of the value of the arriving noise power.

3 In general the author follows the SI notations in this dissertation, but in cases where ratios expressed in dB are involved the convention is followed to write them in capitals, while the ratios expressed in linear quantities, or the quantities itself, are written in the lower case.

4 Although the centered dot "·" is used for the inner product in vector calculations, here it is used for indicating scalar multiplying in algebraic formulas. No vector calculations are present in this dissertation.

1.4 Types of Radio Noise

When tuning with a receiver over a frequency range we may encounter several types of noise and EMI. Figure 1.2 visualises this schematically. At the very bottom we find the noise, generated by the receiver itself or from any circuits like active antenna amplifiers, matching circuits, feeding line losses, etc. as already quantified as the noise factor f_s in Equation (1.4). We measure this by replacing the antenna by a load, equal to the antenna impedance, consisting of the sum of the radiation and loss resistance and the antenna reactance.

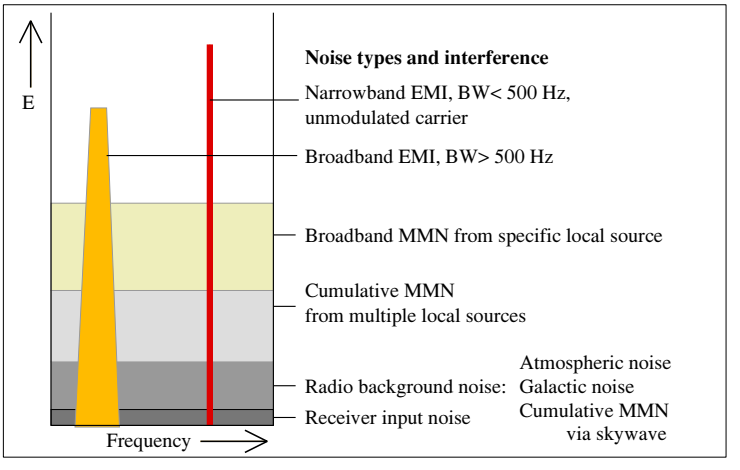

Figure 1.2. Schematic overview of types of noise and EMI.

When the antenna is connected an increase of the noise is measured. In the case that no man-made noise is received, for example at a location in a quiet rural area, only the radio background noise added to the receiver input noise, as shown in Figure 1.2. This background noise may have several sources. The sources for the frequency range of interest (< 30 MHz) are:

a) Atmospheric noise, caused by electric activity in the atmosphere. Result of cumulation of electromagnetic radiation from lightnings in thunderstorms and interaction between electric charges carried inside these clouds. Propagation has a strong influence, so the atmospheric noise is also strongly dependent on the location, especially the latitude, season, local time and activity of the sun (so called space weather).

b) Galactic noise. Noise emitted by celestial bodies like the Milky Way, the sun, planets, stars and other bodies. It is variable because it depends on direction the antenna is looking into the universe, and depends on the status of the earthly

ionosphere. To receive galactic noise on the frequency of interest the ionosphere must be transparent, that means the frequency must be higher than the highest critical frequency of the F-layer, f_xI, see reference [16]. These variables are strongly depending on various factors as season, local time, activity of the sun, and cannot be considered as being constant.

c) Cumulative skywave Man-Made Noise. This category covers a number of noise sources, all depending on ionospheric propagation characteristics as treated above:

   1 intended but weak radio signals received beyond the intended transmitter range;
   2 spurious emissions from radio transmitters;
   3 Man-Made Noise generated by non-radio equipment on the surface of the earth and propagated over large distances by reflection against the ionosphere.
   4 Man-Made Noise radiated by earth orbiting satellites.

Higher in Figure 1.2 we find the next category of noise, being the Cumulative Man-Made Noise, caused by non-radio equipment in the local neighbourhood of the receive location. The level of this Cumulative Man-Made Noise is indicated by the Man-Made Noise curves in [13]. Individual noise sources may cause a higher level of interference. They may produce locally a flat noise spectrum, or a more or less broadband noise or EMI as shown in Figure 1.2. At last the EMI may consist of a narrowband carrier. Those "noise bumps" and carriers may appear repeatedly with a fixed distance in frequency. In such a situation the noise or EMI is formed by harmonics from a much lower fundamental frequency, often the switching frequency of a power convertor.

ITU Rec. P.372-15 [13] gives expectation values of antenna noise figures, F_a. In Figure 1.3 an overview is given in the frequency range from 10 kHz to 100 MHz for the relevant sources in that range. Figure 1.4 is focussed on MMN, broken down by type of environment, and on galactic noise. The regression curves in Figure 1.4 are determined by the Equation (1.12):

$$F_{am} = c - d \log f \tag{1.12}$$

The constants can be found in Table I.

From the point of view of radio engineering, especially in the frequency ranges below 30 MHz, where there is a need to compare field strength values with the (minimum) values of wanted radio signals with noise and interference, it is preferred to calculate noise field

strength values. In Figure 1.5 an overview is given in field strength values for a receiver bandwidth of 2.7 kHz, assuming a monopole antenna over perfect electric conducting ground, using Equation (1.8). The figure is from ERC Report 69 (1999) [17], which report has been written by the author as a member of the working group about short range devices, SE 24 (Spectrum Engineering) of CEPT.

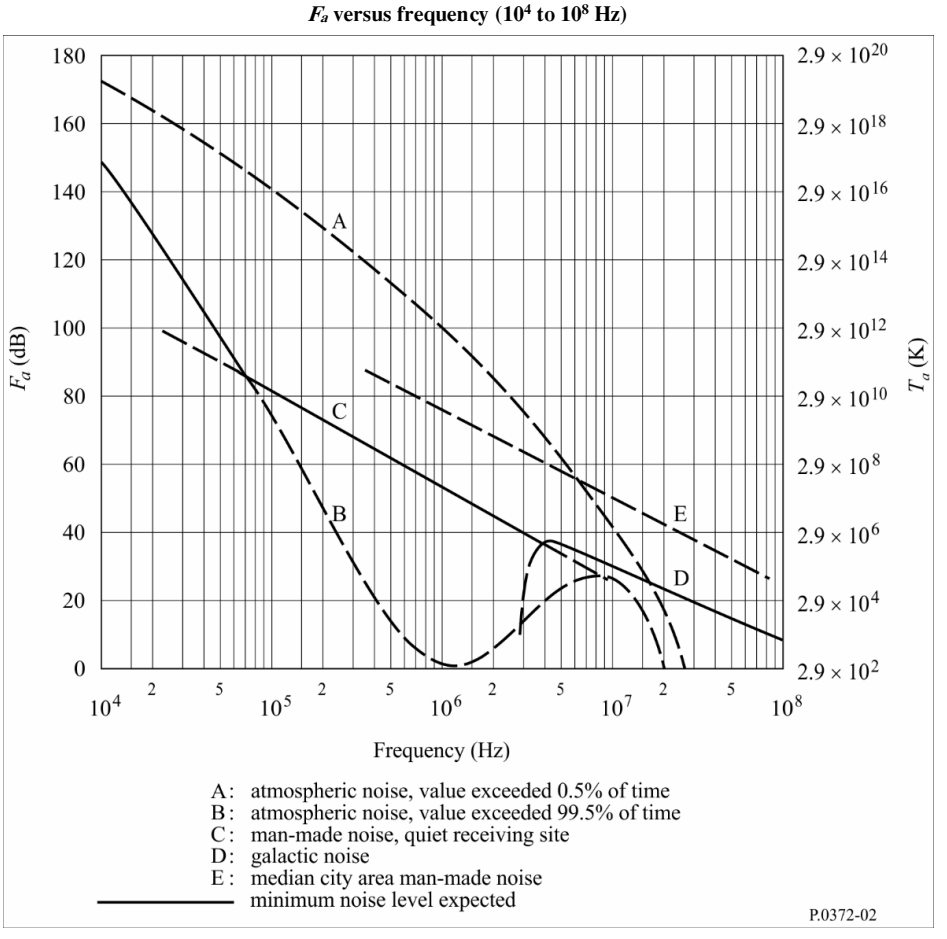

Figure 1.3. Overview of external noise figures. From Rec. ITU-R P.372-15.

Table I. Constants determining the median values for noise factor of MMN and Galactic noise F_{am} according Rec. ITU-R P.372-15.

Environmental category	*c*	*d*
City (curve A)	76.8	27.7
Residential (curve B)	72.5	27.7
Rural (curve C)	67.2	27.7
Quiet rural (curve D)	53.6	28.6
Galactic (curve E)	52.0	23.0

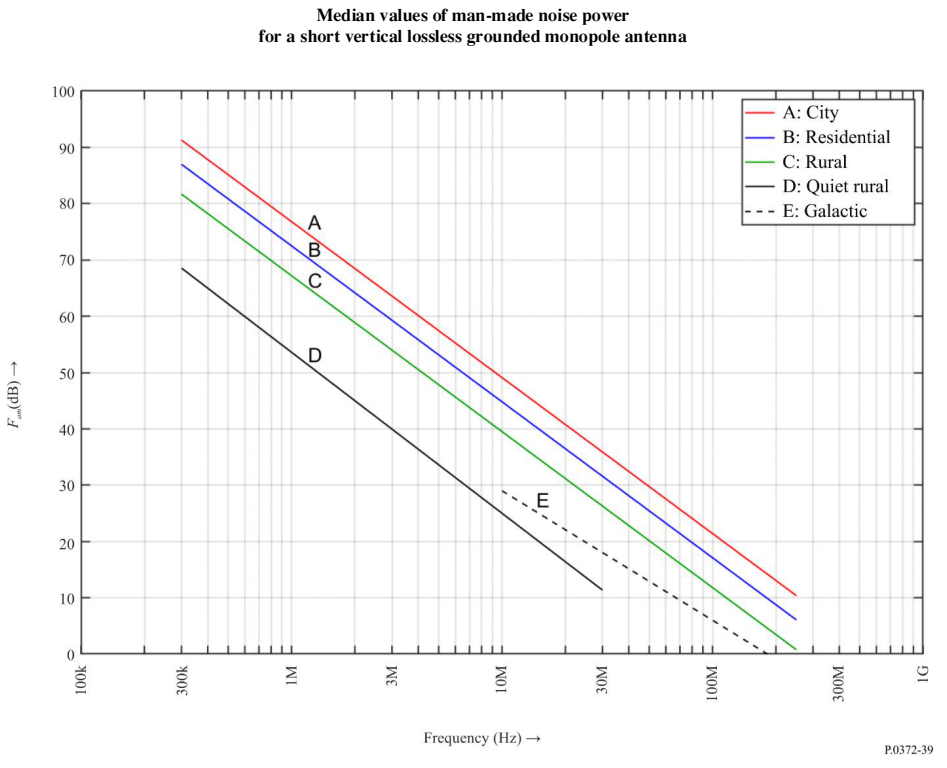

Figure 1.4. Man-Made Noise figures. From Rec. ITU-R P.372-15.

Another advantage of using field strength levels instead of noise figures is that it can be measured directly by field strength measuring equipment, generally consisting of a selective voltmeter, a measuring receiver, or a spectrum analyser, and a calibrated measuring antenna or field probe. The relationship between the measured voltage on the receiver input and the electric field strength is given by:

$$E[\text{dB}\mu\text{V/m}] = V[\text{dB}\mu\text{V}] + K[\text{dB/m}] \tag{1.13}$$

with

E: Electrical field strength [dBµV/m]

V: Input voltage at the measuring receiver antenna input [dBµV]

K: The antenna number [dB/m]

The antenna number is generally given as a calibration number with the antenna. A general derivation of the antenna number for a dipole antenna in free space is given in Appendix B.

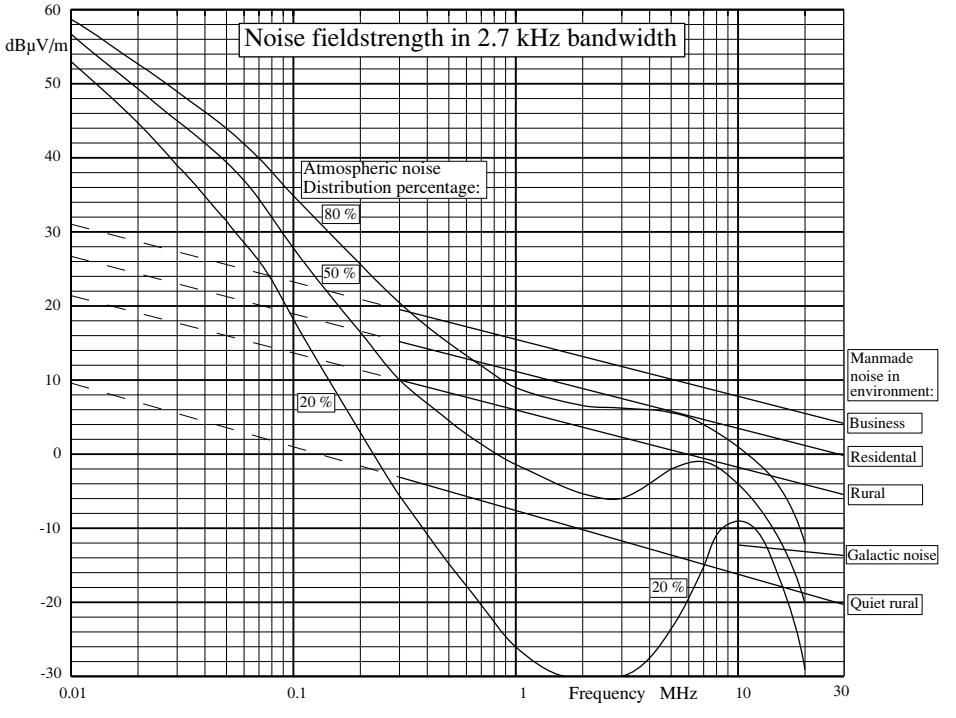

Figure 1.5. Radio noise field strength levels. Atmospheric noise calculated for Western Europe, using a vertical monopole above PEC ground. From ERC Report 69 (1999), based on data in Rec. ITU-R P.372.

1.5 History of the research into Man-Made Noise

Starting in the early fifties of the last century unintended generated man-made radio noise was investigated. The focus was on Very High Frequency (VHF) and Ultra High Frequency (UHF) frequencies mainly. Up to the late 70s the most important sources of man-made radio noise were automotive, power transport and power generating facilities. Other sources were industrial equipment, consumer electric appliances and lighting systems [1], [2], [18]-[27]. From the white Gaussian noise (WGN) and the impulse noise (IN) the latter was dominant by far, especially above 30 MHz, already documented in ITU Rec. P.372. Impulse noise is caused by bursty emissions of short duration and usually with high peak values. Due to the low duty cycle the associated RMS power value is low, while to their short burst time, the spectral occupation is broad. Mathematically, the description of an ideal pulse with zero duration is the Dirac Delta function. For the radio user it is relevant to know that the pulse rate is orders of magnitude lower than the bandwidth of the receiver, while the pulse width is much smaller than the inverse of the receiver bandwidth. In that case the response of the receiver is the impulse response of its filters. This behaviour can technically be used to suppress impulse noise in receiver circuits.

After 1980 more electronic equipment arrived at consumer premises, progressively containing digital circuits. Also computers started to be used by consumers. In power supplies and adapters, the iron transformers were replaced by switching circuits, and appeared in the homes by large numbers. After the millennium-change internet, home networks, and faster computers changed the residential electromagnetic environment even more. New systems arrived like Power Line Communication (PLC) and xDSL networks, both for broadband internet access, extended coaxial cable networks, solar panels with their convertors, battery chargers for electric bicycles etc., and last but not least light emitting diode (LED) lighting. For example reference [28] contains a well-documented case of interference from LED lighting apparatus to Band III DAB (digital audio broadcast) radios. All these new developments, although regulated by the EU EMC Directive [29] and EU Radio Equipment Directive [30], contribute to the current level of MMN.

Also the character of MMN was changed. The increasing source density and the dispersion in the propagation paths, converts IN into WGN as a result of the central limit theorem [31]-[33]. Besides that effect, newer MMN sources produce frequency-dependent EMI like harmonics of switching frequencies, and also broadband WGN. The accumulation of MMN from such sources results in higher levels of broadband WGN. These accumulation effects are also treated in reference [34], and in [35, Chapter 8]. In the composite MMN the share of WGN increased, while that of IN decreased as a result of European automotive EMC standards and/or by burying the powerlines [3], [4], [36]. These changes have a strong influence on the accumulation effect: While the high amplitude, low density, IN propagates over long distances [18], [23], [25], [37] and so determining the accumulated noise floor level in a large area, the lower amplitude, high density, WGN sets the level in a much smaller range of distances.

Current research on MMN is mainly directed towards radio noise inside industrial premises, the interference to short range devices [2], [38], and measurement methods [39]. This reference reports of experiments to perform sensitive noise measurements using commercial available EMC measurement equipment. The conclusion was the available rod antenna was more suitable than a 60 cm broadband loop antenna, still had not enough sensitivity. Further it was concluded in [39] that, despite the increase in electronic equipment, the noise levels were well in line with the noise data in the ITU-R p.372-15. We must add here that the measurements in [39] were conducted on a campus, forming a rural-like area. In the literature the importance of MMN at frequencies below 30 MHz, generated by electronic equipment with a increasing number of switching devices, is addressed [40]. This importance is not only set by the level of unintended radiation per device, but also by the ever increasing number of devices. Other recent papers describe the study of indoor

MMN in relation to digital broadcasting in the Medium Wave Band [41]-[43]. However, the measurement methods, as mentioned in these papers, use E-field antennas without sufficient counterpoise and/or grounding, resulting in large measurement uncertainties. The use of a magnetic loop antenna would be more adequate, also because of the use of ferrite antennas in the MW band receivers. Accumulation of skywave (reflected) MMN is also a threat to the radio users. In [35] a study about F-layer reflected noise from aggregated PLC systems is reported.

The recommendation ITU-R Rec. P.372 [13] contains the MMN levels based on measurements performed in the 1960s, while the electromagnetic environment has been changed drastically, as shown in the overview described before. The data about MMN in [13] has not been updated since 1974, see references [44], [45].

1.6 The VERON noise measurement campaign

In order to quantify the observed increase of the background noise floor by the radio users, and to explore the necessity of modifying noise floor data in [13], VERON carried out a measurement campaign to measure the MMN field strength levels and EMI under representative environment conditions. For this purpose we made use of the hospitality of members of the VERON for reason of the availability of a large number of well-spread locations throughout The Netherlands in very diverse environments. Although we performed the measurements on frequencies in the well spread frequency bands allocated to the Radio Amateur service, it is our intention to assess the harmful effects of increased MMN levels for all radio services.

1.7 The status of Recommendation ITU-R P.372

Recommendation ITU-R P. have been derived from the CCIR Reports 322-3, "Characteristics and Applications of Atmospheric Radio Noise Data" [46], and 258-4, "Man-Made Noise" [47]. CCIR (Comité Consultatif International des Radio-communications, International Radio Consultative Committee) has been merged into ITU-R. The content of these CCIR reports, and also Rec. ITU-R P.372, is fully based on material that has been gained by scientific research. So rightly the CCIR reports have the status of scientific reports, and so this should also apply for Rec. ITU-R P.372. But this last document has the official status of a recommendation, which is not correct in the eyes of the author as it carries only scientific data. Of course, it serves as a reference for radio services to perform calculations concerning transmitter ranges and powers. Although the natural sources of radio noise are not expected to change in time considerably, that is not guaranteed for the MMN levels. The question arises: "Should the MMN data in ITU Rec.

P.372 follow the developments in the MMN levels, or should the original values from [44] be kept as a reference?". In the first case the status of Recommendation ITU-R P.372 should be changed into a Report. In the latter case it will become a real recommendation that sets chosen reference values for radio noise.

1.8 Aspects about the implementation of the research program

The study in this dissertation is based on two measurement campaigns, knowingly the man-made noise level measurements, described in Chapter 3, and the propagation measurements, depicted in the Chapters 5 and 6. Those measurements were setup by the author as a private person. As a consequence the availability of commercial measurement equipment was very limited and consisted only of two measurement receivers from Rohde & Schwarz, type ESH2, and the accompanying loop antenna HFH2 - Z2.

For the field strength measurement antennas there was an additional problem: none of the commercial available antennas had sufficient sensitivity to measure the field strength of low level noise that can be expected in rural and quiet rural areas. Stronger, with the most popular antenna types, used by EMC laboratories, the sensitivity is insufficient, even for measurement in business areas. So dedicated antennas with sufficient sensitivity and low noise floor had to be developed on purpose by the author. Chapter 2 provides some notes on the requirements for such antennas and a short description of this development.

The measurement receiver outputs the measurement results as a DC voltage, which is fed into a datalogger. This datalogger had to be developed on purpose and had as main tasks:

a) digitizing the input voltage;
b) real time processing, including applying calibration figures, averaging, collecting and combining data from consecutive measurement runs, and saving the so obtained data in a CSV file and in a comprehensive plot per frequency range;
c) leading the measurement protocol.

This development included building hardware and writing software. The core of the hardware is a Raspberry Pi microcomputer system card, using the RiscOS operating system[5]. The software is written by the author in the language C in combination with tools from the operating system.

5 An operationg system for Computers with ARM (Advanced RISC Machine) processors. Originally developed for the educational and home market by Acorn Computers Ltd, is an open source project now, and still supported and developed, info: https://www.riscosopen.org/.

For the propagation measurements a beacon transmitter setup had to be build including antenna tuning and circuitry for an identification signal. A calibration of the effective radiated power was included. Also a measurement antenna, to be mounted on a car had to be developed and calibrated.

Another datalogger was developed that incorporated a GPS receiver to record the measurement location in real time. Also the GPS data was used the determine direction of drive of the car and to make an estimation of the direction of arrival of the signal to be measured relative to the car and so make corrections for directivity of the measurement antenna on the car.

For the post-processing of the field strength measurement data existing softwareapplications running under RiscOS was used. The propagation measurements required two dedicated software applications, written by the author. A commercial software application on RiscOS to plot Open Street Map (OSM) data has been extended by its author with the purpose to accept a CSV file with co-ordinates and colour-coded field strength data to plot coloured dots on the map, representing precise measurement positions with their field strength levels. An example of plotting measurement data can be seen in Figure 1.6.

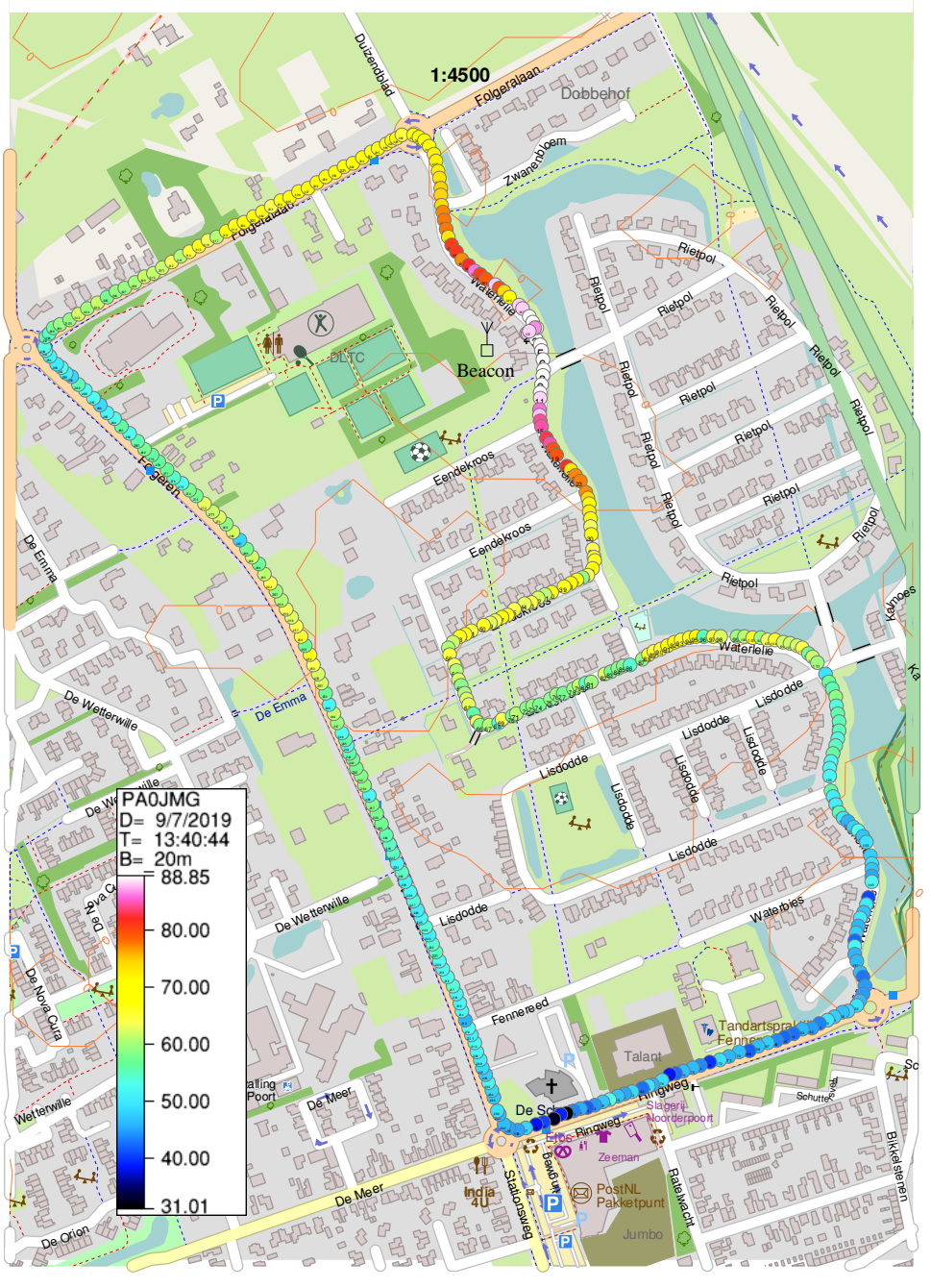

Figure 1.6. Example of plotting propagation measurement data on an OSM sheet.

Chapter 2

2 Noise measurement system

In Chapter 2 investigations have been performed into requirements and technical solutions for noise measurement antennas, especially those for portable operation. This chapter is for a large part based on the conference paper "Issues Concerning Radio Noise Floor Measurements using a Portable Measurement Set-up", EMC-Europe 2018, publication [I]. More information about the technical solutions has been added.

2.1 Introduction

Although Recommendation ITU-R SM.1753-2, [11] gives a comprehensive overview of requirements for noise measurements in general, some more detailed aspects are depending on precise purpose and kind of the measurements. As already mentioned in Chapter 1 some recent papers describe the study of indoor MMN in relation to digital broadcasting in the Medium Wave Band [41]-[43] using Electric(E)-field antennas without sufficient counterpoise and/or grounding. This results in large measurement uncertainties, which subject will be discussed in this chapter in Section 2.3. The results for this research activity has been applied in a MMN measurement campaign from which the results are published in [II] and treated in Chapter 3.

This chapter is organized as follows. First the requirements for man-made noise measurement are described in Section 2.2. Section 2.3 focus in on the choice of measurement antennas and Section 2.4 on the technical solutions, including the datalogger.

2.2 Requirements for noise floor measurements

Chapters 2 and 3 deal with outdoor measurements of the noise floor in habituated areas, where a statistical relation is sought between the level of the noise floor and density of habitations. The main sources of noise in these environments are man-made, although under certain conditions natural sources may contribute too. So, the target is measuring MMN that may hamper or disturb residential radio reception in a wide variation of environments, from quiet rural to city areas. The chosen frequency range is 0.5 to 50 MHz. The sensitivity has to be sufficient high to measure the lowest noise level that can be expected under the relevant measurement circumstances. Measurements had to be done at a large number of locations, divided over all kinds of environment, for a reliable statistical assessment. As a consequence the measurement setup has to be designed for portable use. This differs from reference [9], wherein the measurement locations were assumed to be fixed. The difference has consequences for the selection of antennas.

2.2.1 Determination of sensitivity requirements

To get a good understanding of the relationship between the density of habitation and the level of MMN it is necessary to measure in all kinds of environments, from Quiet Rural, where only natural kinds of noise are received, to the City environment, where high levels of MMN and Electromagnetic Interference (EMI) can be expected. Recommendation ITU-R P.372-15 [13] delivers data about relevant noise sources: atmospheric, galactic, and man-made noise. These data, given as noise power density numbers, measured with a vertical rod antenna, has been transferred to noise field strength levels in a bandwidth of 2700 Hz (Reference bandwidth, see Ch. 3, Subsection 3.3.2.). According [13] the given atmospheric noise levels are depending on location, season, and time slot[1]. Western Europe was chosen as regional location, and for the timing the summer season the time slot 08.00 - 12.00 hours local time for the frequencies 14 - 30 MHz, and 12.00 - 16.00 hours for 0.47 - 10 MHz were selected. For an illustration of the variations in atmospheric noise floor see next subsection. Figure 2.1 shows the expected noise levels of the noise sources separately, and the sum of all sources combined, depicted as Minimal Expected Noise Floor. The noise floor of the measurement system should be lower than this minimum, preferably 10 dB, so that the error caused by the system noise, is less than 0.5 dB. If the difference is smaller than 10 dB a correction should be made by subtracting the system noise power from the measured noise power. This requirement implicates that the system noise floor is a calibration parameter for each band separately, and should be determined in advance, after the antenna factor for each band and corresponding antenna has been measured.

1 It is plausible that also the activity of the sun and the moment in the 11 year cycle has an effect on the atmospheric noise level, but in [13] only averaged values are shown.

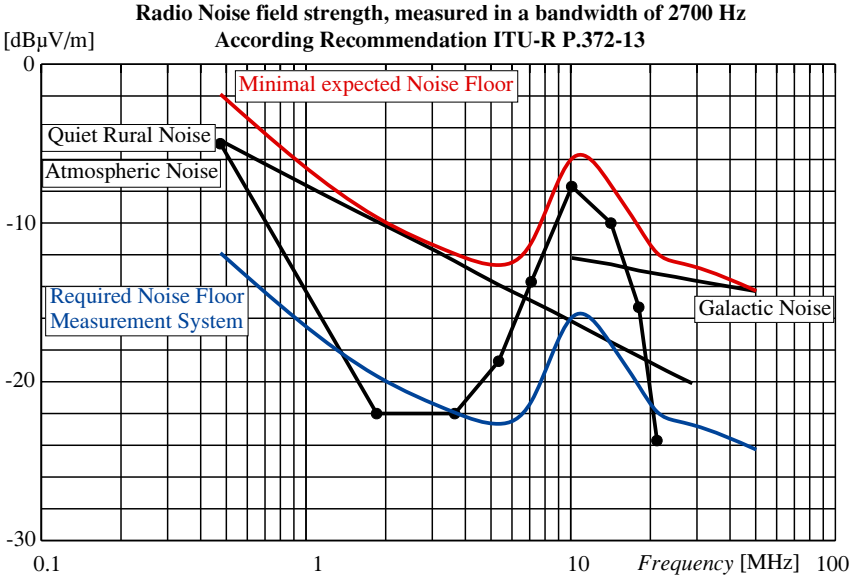

Figure 2.1. Minimum expected noise floor and required noise floor measurement system.

2.2.2 Daily cycle of atmospheric noise floor

For illustration of the daily cycle of the level of atmospheric noise, as mentioned in Subsection 2.2.1, a single measurement from an earlier atmosheric noise measurement campaign has been taken. This campaign by the author, mentioned in Chapter 1, Section 1.1, consists of an eleven years, one sunspot activity cycle, lasting measurements of radio noise. In a period of 24 hours background noise level has been measured continuously, concurrently using two antennas. Figure 2.2 depicts the measurement results. One antenna, named German Quad, is only sensitive for nearly vertical incident skywaves (NVIS). In addition the polarisation is strictly horizontal. The other, the tuned active monopole, is sensitive for waves from low and middle elevations, but has a zero for the vertical direction and receives vertical polarisation.

Both antennas show a daily cycle in the noise floor with a minimum at local noon. This lower level is mainly caused by the damping by the D-layer in the ionosphere, which is only present during the daylight hours and disappears when the sun sets. The limitation in the reduction of noise during the daylight on the monopole antenna is caused by the amount of MMN from the environment, which is vertically polarized and arrives from low elevation angles, in fact ground-wave propagation. Figure 2.2 also shows the levels of man-made noise for the diverse environments and the expectation values for the atmospheric noise. These values are dependent on the local time, the season, and the geographical location. Rec. ITU-R P.372-15 provides the data to calculate this curve.

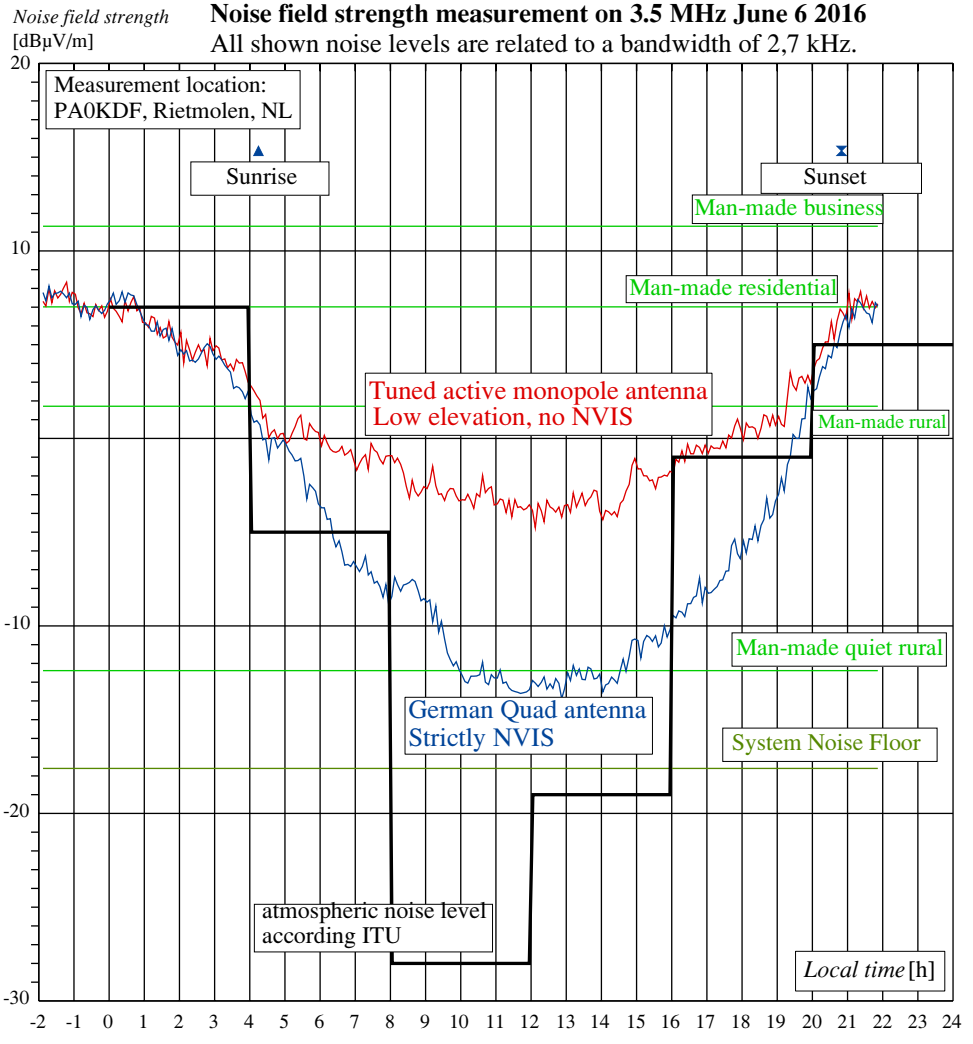

Figure 2.2. Illustration of the daily cycle of the atmospheric noise level.

2.3 Selection of Antennas

2.3.1 Field strength measurement using an E-field rod antenna

The E-field rod antenna is a well-known antenna used for field strength measurements in many applications. Rod antennas were used for radio noise measurements in the frequency range 9 kHz to 30 MHz, for example in studies used in the ITU-R P.372-15 [13] for measuring atmospheric and man-made noise. In [50] we find a description for the antenna used for the measurements reported in [13]. A vertical rod has been used, which is matched to the receiver input impedance using a passive matching circuit. A high number of long

radial rods form a ground plane. The constructing implies the installations to be fixed.

For the purpose of portable measurements setups several manufacturers developed active rod antennas. Figure 2.3 shows an example of such a rod antenna. The rod often has a length of 104 cm, resulting in an effective height of 0.5 m. The ground plane, which has limited dimensions too, may be formed by a set of radial rods, or by a metal plate. An active circuit, often called an impedance convertor, matches the antenna to the characteristic impedance of the cable towards the receiver and to the receiver input impedance. Another example of a rod antenna is shown in [42]. The sensitivity of rod antennas is relative high with respect to broadband magnetic loop antennas, but the use of E-field rod antennas encounters a few problems as we will discuss below. Reference [51] already points out that there are accuracy problems. Reference [52] shows the influence of antenna cable, without a detailed analysis of the cause either.

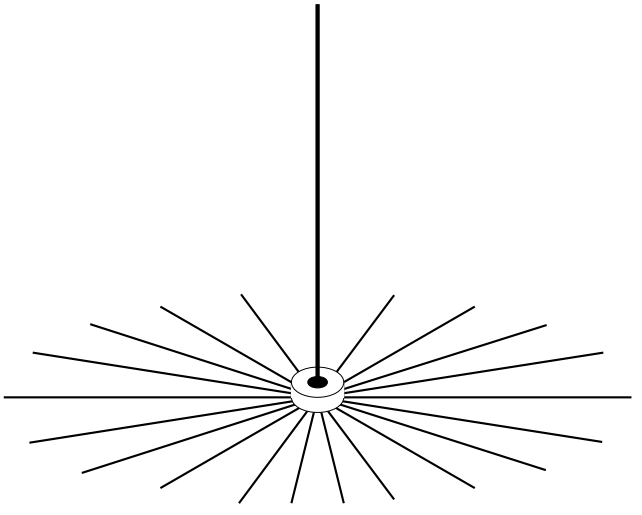

Figure 2.3. Example of an Active Rod Antenna for E-field measurements.

These problems are:

a) calibration uncertainties;
b) Measurement errors by noise pick-up by the cable between antenna and receiver, thus parasitic behaviour as an antenna, resulting in extra calibration uncertainty and a disturbed directivity;
c) Measurement errors by noise originating from mains network and data processing equipment when the receiver is connected to the mains and eventually other equipment.

Reference [53] gives a solution for these problems, using optical fibre communication

between antenna and measurement equipment, and grounding to ground plane of the measurement setup. However, this solution is only useful for the EMI measurements mentioned therein, but not for noise floor measurements in general. Reference [54] shows a design for an active E-field rod antenna, which is tunable and narrow band, but meant to be used on the roof of a car, thus using the metal work of the car as counterpoise and reference plane. In reference [55] the grounding of the counterpoise is subject for investigation, and reveals large calibration uncertainties. Some solutions are shown, but only useful in the special cases of EMI measurements. Another problem with the rod antenna, the groundplane resonance, is shown in [56].

2.3.2 Calibration uncertainties

In Figure 2.4 we see a detailed schematic view of an electric vertical rod antenna, as is commonly used for E-field measurements at a non-fixed location. A vertical antenna rod is loaded by an impedance convertor, which has a high input impedance and a low, 50 ohms, output impedance, with a voltage gain *g*. *g* may be unity or higher.

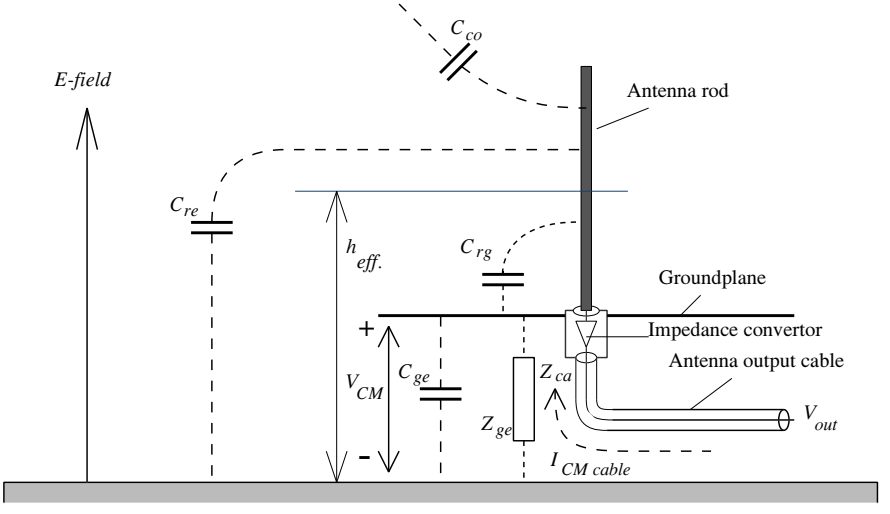

Figure 2.4. electric schematic with parasitic elements of a rod antenna.

The antenna rod is loaded by the following capacitances:

a) The input capacitance of the impedance convertor, C_{in},
b) the capacitance between the rod and the ground plane, C_{rg},
c) the capacitance between the rod and earth, C_{re}, not coupled with the EM field,
d) the capacitance between the rod and space, representing displacement currents, not direct resulting in earth return currents, but coupling with the EM field, C_{co}.

The ground plane, positioned close or at some distance above earth, shows a capacitance, C_{ge}, to earth. In case the ground plane is connected to earth, for example using a network of radials or a grounding rod, an additional grounding impedance, Z_{ge}, is connected parallel tot C_{ge}.

The ground plane is also loaded by the common mode (CM) impedance Z_{ca_CM}, caused by CM currents $I_{CMcable}$ on the coaxial antenna cable. Z_{ca_CM} is strongly dependent on the length of the cable relative to the wavelength, and on the characteristics of the underground, suspending the cable. As the length is in the same order of the wave length the impedance at the end may strongly be influenced by resonance effects. These effects can be mitigated by applying lossy ferrite tubing over the cable.

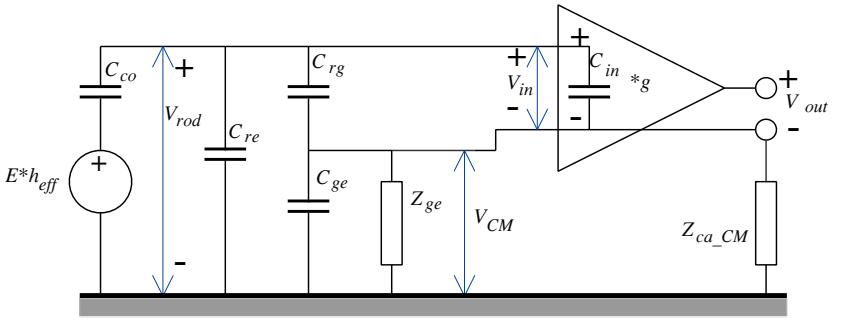

Figure 2.5. Equivalent circuit of an active rod antenna.

Figure 2.5 shows the equivalent-circuit. To simplify the calculations we combine C_{ge}, Z_{ge}, and Z_{ca_CM} to one impedance from the ground plane to earth: Z_{gp}.

$$\begin{aligned} Z_{gp} &= (1/j\omega C_{ge})//(Z_{ge})//(Z_{ca\_VM}) \\ &= \frac{Z_{ge}Z_{ca\_CM}}{j\omega C_{ge}Z_{ge}Z_{ca\_CM} + Z_{ge} + Z_{ca\_CM}} \end{aligned} \tag{2.1}$$

In a further simplification we assume that $C_{re} \ll C_{co}$ and $C_{re} \ll C_{rg}$, so C_{re} may be omitted. Also, we may add C_{in} to C_{rg} in $C_{base} = C_{in} + C_{rg}$. Now the schematic is simplified into Figure 2.6. The antenna rod is loaded by Z_{rod_load} consisting of the series circuit of C_{base} and Z_{gp}:

$$Z_{rod\_load} \approx 1/j\omega C_{base} + Z_{gp} \tag{2.2}$$

The loaded voltage on the antenna rod is now:

$$V_{rod} \approx \frac{C_{co}(1 + j\omega C_{base}Z_{gp})}{(C_{co} + C_{base}) + j\omega C_{co}C_{base}Z_{gp}} \cdot E \cdot h_{eff} \tag{2.3}$$

$$V_{CM} = \frac{j\omega C_{base}Z_{gp}}{1 + j\omega C_{base}Z_{gp}} V_{rod} \tag{2.4}$$

$$\approx \frac{j\omega C_{base} Z_{gp}}{1 + j\omega C_{base} Z_{gp}} \cdot \frac{C_{co}(1 + j\omega C_{base} Z_{gp})}{(C_{co} + C_{base}) + j\omega C_{co} C_{base} Z_{gp}} \cdot E \cdot h_{eff} \tag{2.5}$$

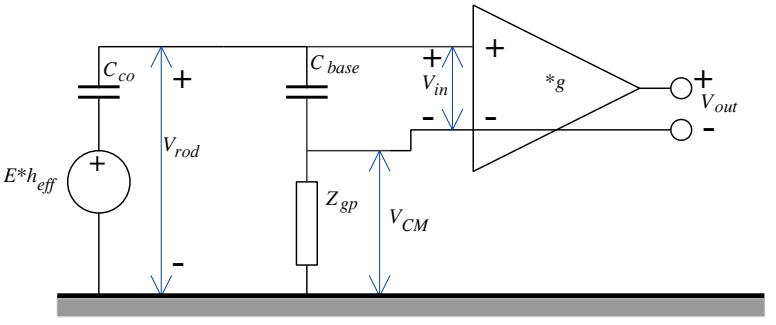

Figure 2.6. Simplified equivalent circuit.

When $Z_{gp} = 0$, then $V_{CM} = 0$.

$$V_{in} = V_{rod} - V_{CM}$$

$$V_{out} = V_{in} \cdot g$$

$$= \frac{C_{co} + j\omega C_{co} C_{base} Z_{gp}}{(C_{co} + C_{base}) + j\omega C_{co} C_{base} Z_{gp}} \left(1 - \frac{j\omega C_{base} Z_{gp}}{1 + j\omega C_{base} Z_{gp}}\right) E \cdot h_{eff} \cdot g \tag{2.6}$$

The antenna factor k, used as a calibration factor, is defined as:

$$k = \frac{E}{V_{out}}$$

$$= \frac{1}{\frac{C_{co} + j\omega C_{co} C_{base} Z_{gp}}{(C_{co} + C_{base}) + j\omega C_{co} C_{base} Z_{gp}} \left(1 - \frac{j\omega C_{base} Z_{gp}}{1 + j\omega C_{base} Z_{gp}}\right) h_{eff} \cdot g} \tag{2.7}$$

We conclude that the calibration of the E-field rod antenna is depending on the impedance from the ground plane to earth, Z_{gp}, which consists of variable components like the capacitance between ground plane and earth, C_{ge}, the common mode impedance of the output cable at the output connector, Z_{ca_CM}, and the impedance of the earth connection of the antenna, Z_{ge}, if present. All three impedance values are more of less undefined, variable and frequency dependent, especially Z_{ca_CM}. They have a considerable influence on the calibration of the antenna. The only way to solve this problem is to make Z_{ge} very small, for example by using a low impedance grounding system like a wire mesh or radial network. This requirement can only be met in fixed installations and makes the E-field rod antenna unsuitable for portable measurement setups.

2.3.3 Measurement errors by noise induced in the cable between antenna and receiver

So far we did not assume that noise or interference is arriving from the antenna cable into the antenna system, effectively the cable acting as a parasitic antenna. However, the antenna cable is a common mode conductor that lays over the ground between the antenna and the measuring receiver. This situation is pictured in Figure 2.7. Cable lengths of 4 to 10 meters are common. In the real world the soil is not a good conductor, but has certain values of permittivity and conductivity. Depending on the type of soil, the permittivity, ε_r, may vary between 3 and 40, and the conductivity, σ, between 0.1 and 30 mS/m. Not only this variance has an effect on Z_{ca_CM}, but more important the skindepth has a considerable depth in the relevant frequency range, 0.5 - 50 MHz.

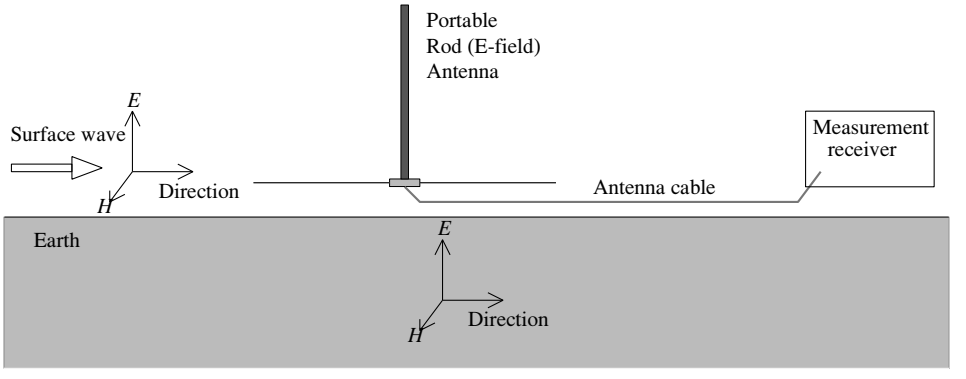

Figure 2.7. Pick up of noise by antenna cable.

Table 2.1 gives an overview of the characteristics of various types of ground as defined by ITU-R PN.368-9 [57], the Handbook on Ground-wave propagation [58] and the resulting skin-depth values. For example, for a medium soil type as "Land", according to ITU-R definitions, with $\varepsilon_r = 22$, and $\sigma = 3$ mS/m, the skindepth varies from 30 m at 0.5 MHz to 8 m at 50 MHz. This means that an EM-wave, arriving from a high elevation, or propagating over the surface, is penetrating in the soil, and is surrounding the antenna cable. This EM field will induce a voltage in the cable in a common mode way. Part of this CM voltage will arrive at the antenna connection and will be added to V_{CM}. As the length of the cable is considerable larger than the length of the antenna rod, this CM voltage, arriving from the cable, may be in the same order, or even stronger than de received voltage V_{rod}. Figure 2.8 shows an equivalent-circuit diagram for this situation. Source e_{CM} represents the common mode voltage induced in the antenna cable over the full length, $Z_{s\_ca\_CM}$ the effective source impedance, frequency dependant, and Z_{Rx_e} the series impedance from the body of the receiver to earth. In case the receiver is connected to the mains, Z_{Rx_e}

determined by the conducting of the RF currents from the body of the Rx to the mains too. A voltage V_{CM_ext} is developed over the common mode impedance of the antenna, the parallel combination of C_{ge} and Z_{ge}, see Figure 2.8.

Table 2.1. Conductivity and skindepth of various types of ground.

Type of ground	σ [S/m]	ε_r	Skindepth [m] @ frequency [MHz]							
			0.1	1	5	10	20	30	50	100
Sea water, av. salinity	5	70	0.7	0.225	0.10	0.07	0.05	0,04	0.032	0.023
Sea water, low salinity	1	80	1.6	0.50	0.22	0.16	0.11	0.10	0.08	0.06
Fresh water	0.003	80	31.3	16.6	15.9	15.8	15.8	15.8	15.8	15.8
Wet land	0.030	40	9.22	3.02	1.52	1.30	1.17	1.15	1.13	1.12
Wet ground	0.010	30	16.0	5.47	3.25	3.03	2.97	2.92	2.91	2.91
Land	0.003	22	29.7	11.2	8.50	8.36	8.31	8.31	8.30	8.30
Medium dry ground	0.001	15	52.5	23.3	20.7	20.6	20.6	20.6	20.6	20.6
Dry ground	0.0003	7	98.0	49.8	46.9	46.9	46.8	46.8	46.8	46.8
Very dry ground	0.0001	3	173	95.7	92.1	92.0	92.0	92.0	92.0	92.0
Fresh water ice, -1 °C	0.00003	3	379	308	307	307	307	307	307	307
Fresh water ice, -10 °C	0.00001	3	957	920	920	920	920	920	920	920

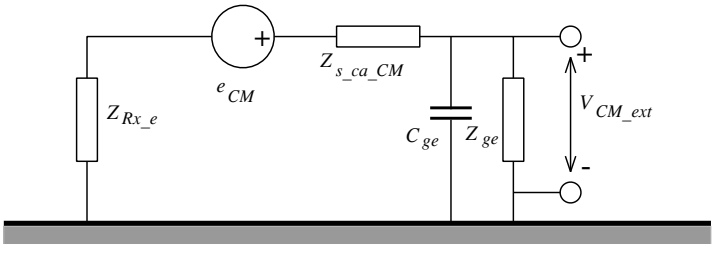

Figure 2.8. Equivalent circuit for external noise pick up by antenna cable.

Z_{ge} is only relevant when an earth connection is present. We can calculate V_{CM_ext} as:

$$V_{CM\_ext} = \frac{Z_{ge}\left(Z_{Rx\_e} + Z_{s\_ca\_CM} + Z_{ge}\right) - j\omega C_{ge}\left(Z_{Rx\_e} + Z_{s\_ca\_CM}\right)Z_{ge}}{\left(Z_{Rx\_e} + Z_{s\_ca\_CM} + Z_{ge}\right)^2 + \omega^2 C_{ge}^2\left(Z_{Rx\_e} + Z_{s\_ca\_CM}\right)^2} e_{CM} \qquad (2.8)$$

Now we see the result of the erroneously measured noise by e_{CM} on the output voltage V_{out}:

$$\begin{aligned} V_{out} &= gV_{in} \\ &= g\left(V_{rod} - \left(V_{CM} + V_{CM\_ext}\right)\right) \end{aligned} \qquad (2.9)$$

This added voltage in V_{out} causes loss of calibration and a serious deforming of the directivity of the antenna, as well as in the azimuth direction as in the elevation. It may be acceptable for EMC measurements, where the antenna cable is lying over a good conducting floor and can be routed optimal, but certainly not for noise floor measurements, without very large ground planes.

2.3.4 Measurement errors by noise originating from mains network

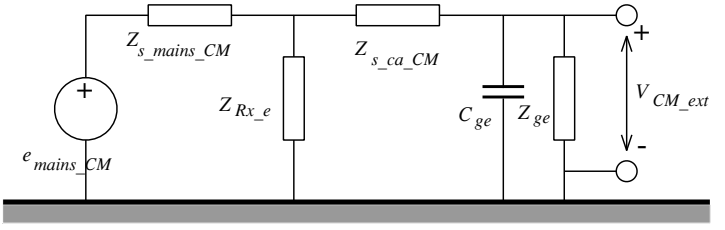

Figure 2.9. Equivalent circuit for leaking noise from mains network.

A second way of erroneous measured noise is caused by noise that is arriving from the mains connection, when present. Figure 2.9 shows an equivalent-circuit diagram for this measurement setup. Without an exact calculation, and referring to the foregoing calculation, we can conclude from Figure 2.9 that also noise from the mains network may arrive at the antenna ground plane and so pollute the output of the antenna. When Z_{Rx_e} is kept to a low value, for example by connecting the receiver case to a separate clean ground network, this mains-originated noise may be reduced. Also applying lossy ferrite chokes on the antenna cable, as on the cabling to the mains or other equipment may reduce external noise to a certain extend. But uncertainties still remain, and especially in noise floor measurement no certainty can by acquired about the origin of the measured noise floor.

For noise floor measurements we can conclude that an E-field rod antenna should only be used in a fixed installed antenna system, including a well-designed extensive ground network. For portable applications an E-field rod antenna should be avoided.

2.3.5 Loop antennas

With loop antennas we mean electric small loop antennas with a circumference smaller than a quarter of a wavelength, that are designed to couple only with the magnetic field component in the EM-wave. Figure 2.10 (left) shows a screened realization of a loop antenna, and Figure 2.10 (right) the working principle. We can calculate the unloaded voltage of the loop for far field as:

$$V_{loop,max} = -j\omega\mu_0 A\frac{E}{120\pi} \tag{2.10}$$

Herein is the constant $120\pi = 377$ ohm, often in dB expressed as 51.5 dB. This is only valid for far field conditions. The sensitivity is depending on the enclosed surface A and is linear with frequency. The loop is directly coupled to an active circuit. Often this is a circuit with a very low input impedance, which effectively short-circuits the loop. The short-circuit current is given by:

$$I_{short} = -\frac{\omega^2 L + j\omega R}{\omega^2 L^2 + \omega^2 R^2}\frac{\mu_0 A}{120\pi}E$$
$$\approx -\frac{\mu_0 A}{120\pi L}E \quad \text{for } |\omega L| \gg R \tag{2.11}$$

wherein L is the self inductance of the antenna loop and R the sum of the loss resistance of the loop, R_{loss}, the (here neglectable small) radiation resistance, R_{rad}, and the input resistance of the active circuit, R_{in}. The current is frequency independent and makes the antenna wideband. Relevant for the sensitivity of the antenna is the power delivered into the active circuit:

$$P_{in} = I_{short}^2 R_{in} \tag{2.12}$$

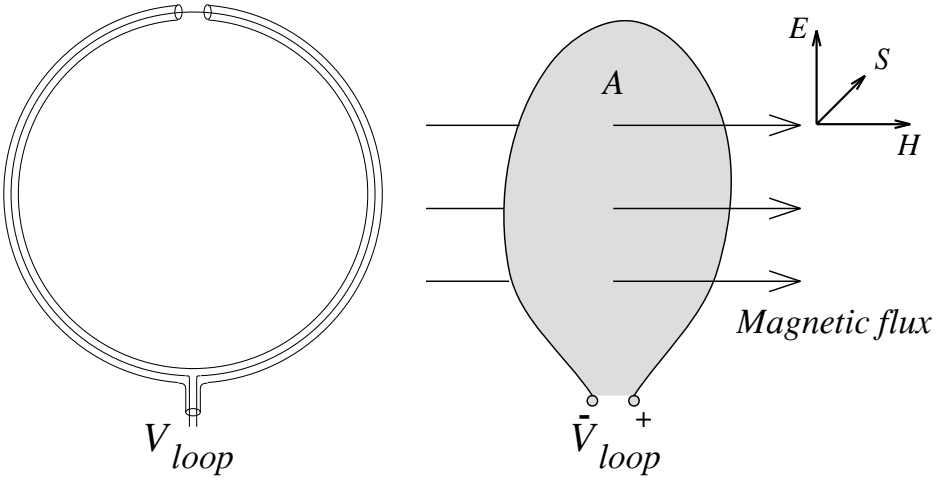

Figure 2.10. Screened realization of a loop antenna.

For a low value of R_{in} the frequency range is large, but the sensitivity low, while for a higher value of R_{in} the sensitivity increases, but the useful broadband frequency range is limited. Still, the sensitivity is relative low compared to a full size electric antenna, and not enough to match the above mentioned requirements. By tuning the loop by a parallel capacitor, and loading that with high input impedance amplifier, the resonance effect of the resulting L/C circuit accumulates energy from the H-field at the cost of a small bandwidth. The voltage over the loop connection and tuning capacitor is now:

$$V_{tuned,max} = V_{loop,max}Q = -j\omega\mu_0\frac{QA}{120\pi}E \tag{2.13}$$

wherein Q is the Quality factor, determined by the combination of the antenna loop, the tuning capacitor, the sum of the loss and radiation resistance, and the loading of the high input impedance of the active circuit. Q may have values from 10 to 100 or higher. So a

sensitive antenna can be constructed with limited dimensions. As common mode voltages on the antenna loop do not couple with the antenna output voltage, the problems with calibration and measurement errors by erroneous noise pick-up, as described for the rod antenna, do not occur. These characteristics make the loop antenna very useful for portable measurement setups.

2.3.6 Directivity of loop antennas

An important difference with the rod antenna is the directivity. As the polarization of the arriving low angle EMI just above ground is mainly vertically directed because of the strong damping effects by the conductivity of the ground for horizontal electric field and vertical magnetic components (boundary conditions for the Maxwell equations), the vertical standing rod antenna is optimal coupled with the EM field. For vertical polarisation the loop antenna need to be positioned so that the plane of the loop is vertical, as the magnetic field is horizontal. The azimuthal directivity of the loop antenna has a shape of a figure 8, and is described by a spherical system with the axis on the axis of the loop as:

$$\begin{aligned} V_{loop} &= V_{loop,max}\sin(\theta) \\ &= V_{loop,max}\cos(\pi/2 - \theta) \end{aligned} \tag{2.14}$$

wherein $V_{loop,max}$ is the maximal value when the plane EM-wave is arriving from any direction in the plane of the loop. θ is the deviation angle from the axis. In a transformed spherical system with its axis vertical directed with elevation angle E and azimuth A, see Figure 2.11, we can apply the relation $\cos(\alpha) = \cos(\beta)\cdot\cos(\gamma)$, valid for a rectangle triangle on a sphere, and arrive at:

$$\begin{aligned} \cos(\pi/2 - \theta) &= \cos(\pi/2 - A)\cos(\pi/2 - E) \\ V_{loop} &= V_{loop,max}\cos(\pi/2 - A)\cos(\pi/2 - E) \end{aligned} \tag{2.15}$$

We want to measure the noise floor omnidirectional, like the rod antenna does. To achieve that with a magnetic loop antenna, we may use two loops orthogonal to each other, or do two measurements with the same loop, but at the second measurement the loop turned by 90 degrees in azimuth. Both measurement results have to be vectorial added to get a final result that is directly comparable with noise measurement results used in [13], that came from measurements with vertical rod antennas. In Appendix C it is shown that the vectorial adding of powers gives the wanted result for horizontal arriving EMI.

The vertical rod antenna has a horn toroidal shape for the directivity with a null in the vertical direction. This means that the rod antenna is not sensitive in high elevation directions, but is equal sensitive in all azimuth directions. However, high angle sky-wave

signals and noise will not be received. In our investigations for man-made radio noise we expect to find the sources of man-made noise on the ground, and that the man-made noise floor, that we measure, is the result of accumulation of ground wave propagated man-made noise signals from a number of sources. So, the man-made noise to measure arrives at low elevation angles, and the difference between the rod antenna and the combination of loop antennas with respect to the high elevation sensitivity, is not relevant. Of course, we have to make sure that the level of atmospheric noise, arriving from high angles, is low. This can be achieved by choosing optimal time slots during the day wherein the D-layer absorption is maximal. It means we have to allocate the measurement periods around noon local time.

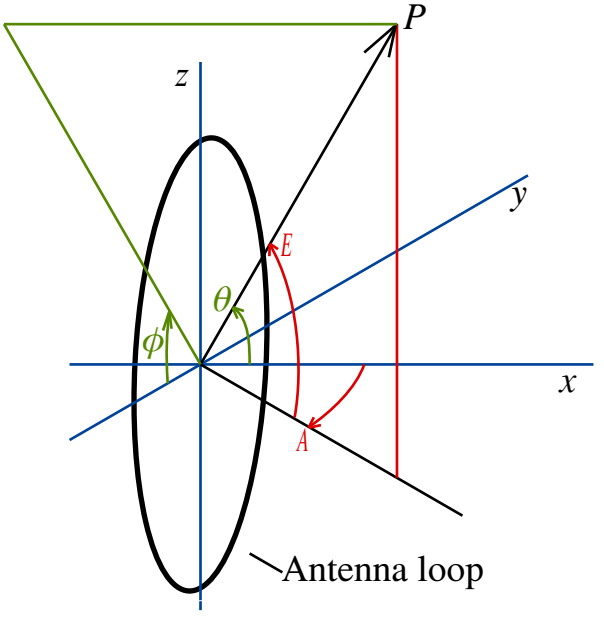

Figure 2.11. Transformation of spherical co-ordinates, θ, ϕ, of upright standing loop antenna (green) into azimuth, A / elevation co-ordinates, E (red).

2.4 Technical solutions

The measurement equipment for the noise and EMI measurements are depicted in Figure 2.12, and consists of a measurement receiver, three antennas, and a datalogger. The measurement receiver is a commercial Rohde & Schwarz ESH 2, self-calibrating. The datalogger digitises the receiver output voltage, does all necessary processing and stores the results. Photo 3.1 in Chapter 3 and photos on the backside of the cover illustrate the measurement setup.

2.4.1 Choice of the type of antenna

In the comparison between the electric rod and the magnetic loop antenna the last type has been chosen. First of all because of the difference in reliability of the calibration factors as discussed. Secondly there is another consideration in relation to the kind of measurement location. Generally this location is in a garden with limited dimensions. In the direct surrounding of the measurement antenna there may be vertical objects, mostly connected to earth, like small trees, bushes, poles, etc. These objects, which mostly have a certain amount of electric conductivity, may attenuate the vertical polarized electric field components. Especially in the range around such an object, being in the near field region from the object (*range* $\leqslant$ *lambda*/2π), the field impedance is higher than the free space impedance. In that case the magnetic field is less attenuated, so a magnetic antenna will give a more reliable measuring result.

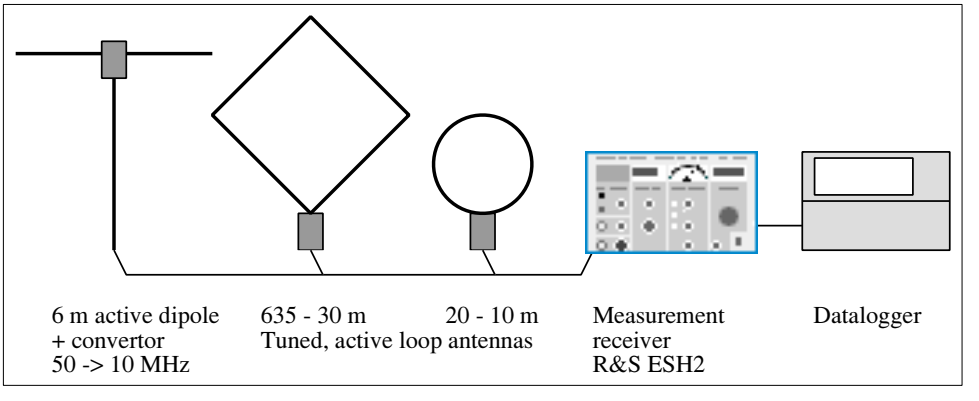

Figure 2.12. The measurement equipment setup for noise FS measurements.

2.4.2 Measurement Antennas

For the measurements a dedicated combination of loop antennas has been developed and built. For maximal sensitivity tuned loops are used, and the frequency range has been split up in two subranges: 0.470 - 10.2 MHz and 10 to 30 MHz. Figure 2.13 shows simplified schematics. For the low band a foldable construction has been designed, wherein the lower half of the loop is electrically shielded. The four sides of the loop have lengths of 1.40 m.

The high band loop antenna is made of an aluminium wheel chair handle, which is cut on one side, and is not shielded. The opposite side is connected to a vertical bar. The electronic circuits are the same for both bands. The tuning circuits, which contain parallel capacitors and additional means for optimal tuning in each subband including relays for switching, are optimised for each band. One of more tuning diodes makes tuning on the measurement frequency possible by applying a tuning voltage from a manually operated potmeter.

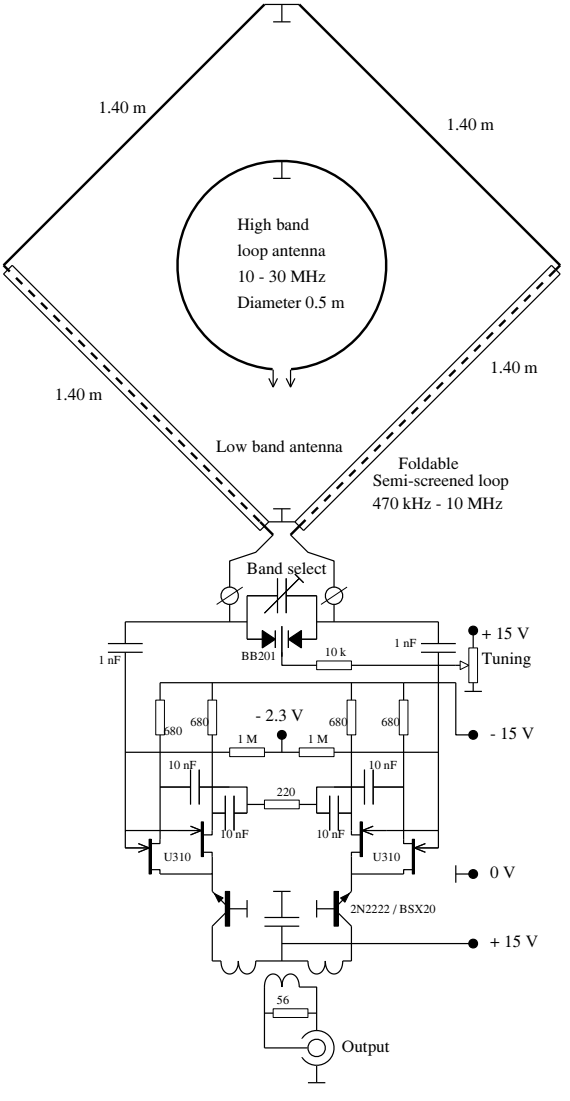

Figure 2.13. Simplified schematic of the loop antenna system.

Photo 2.1. The low-band antenna unfolded. The vertical limb is retractable. The lower parts of the loop exists of square aluminium profiles wherein an aluminium rod is mounted as an inner conductor with screws on both ends. The upper parts are made of 1.5 mm diameter copper wire, isolated. In the lower corner the box with tuning and amplifier is situated.

Photo 2.2 below: The upper part of the pcb contains the loop tuning circuit, including the relays for switching between frequency bands, controlled by the switch above, left. The fine tuning is done by means of multiple varicap diodes, which tuning voltage is set by the multi-turn potentiometer above, right. The lower part of the pcb contains the balanced amplifier with output transformer. Below, left, is the output connector, right hand the power connector with the + 15 and - 15 volt power lines.

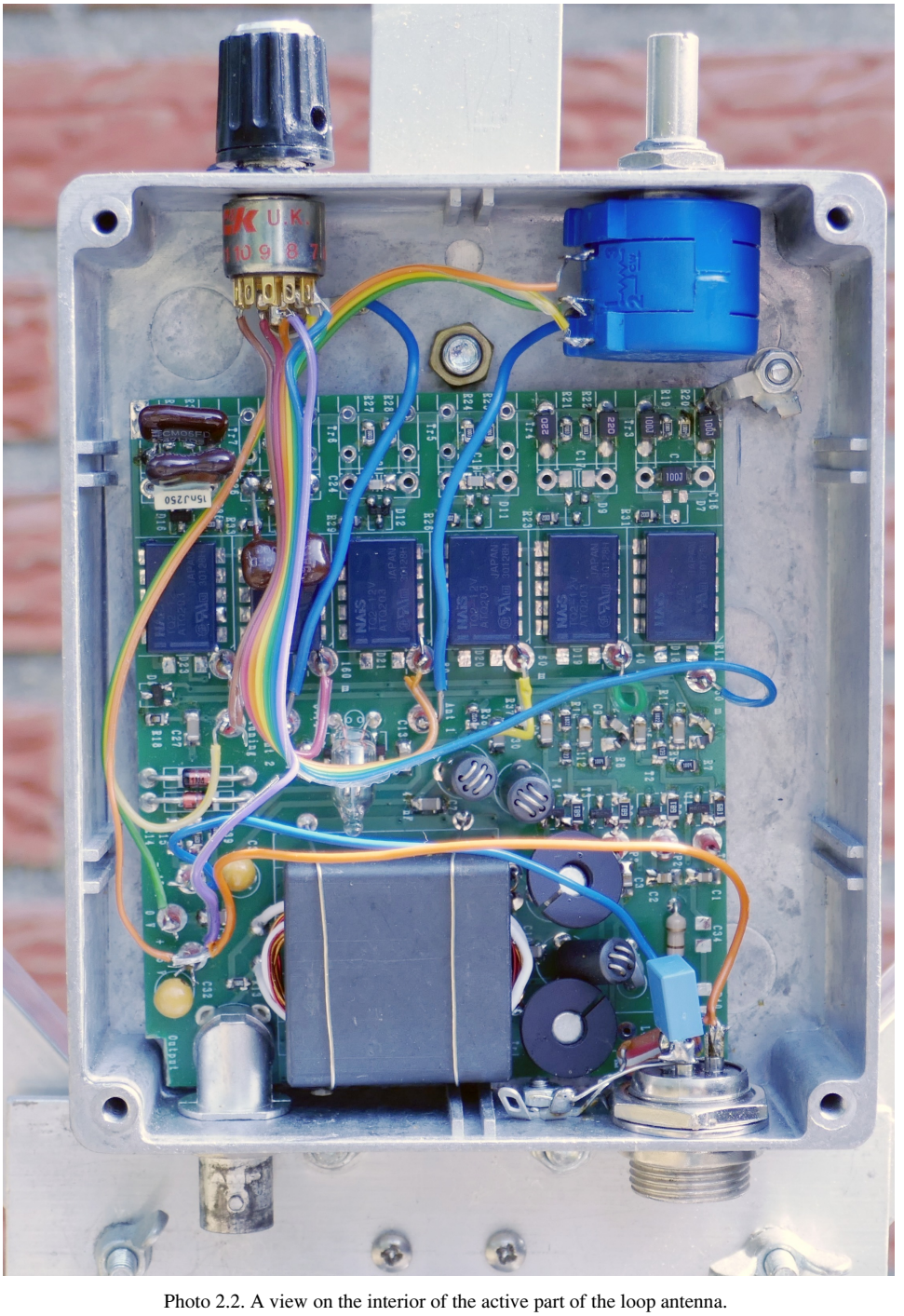

Photo 2.2. A view on the interior of the active part of the loop antenna.

With the band switch the frequency band is selected, and with the fine tuning the antenna is tuned on the measurement frequency by adjusting for maximum receive signal. In case the external noise has a low level, comparable with the noise from the internal antenna circuits, an auxiliary signal (comb) generator is used in combination with small loop antenna. Every 50 kHz a carrier frequency component is produced. The combination is manually kept close to the measuring loop, so that this loop can be tuned by maximizing the auxiliary signal from the comb generator with a small coupling loop.

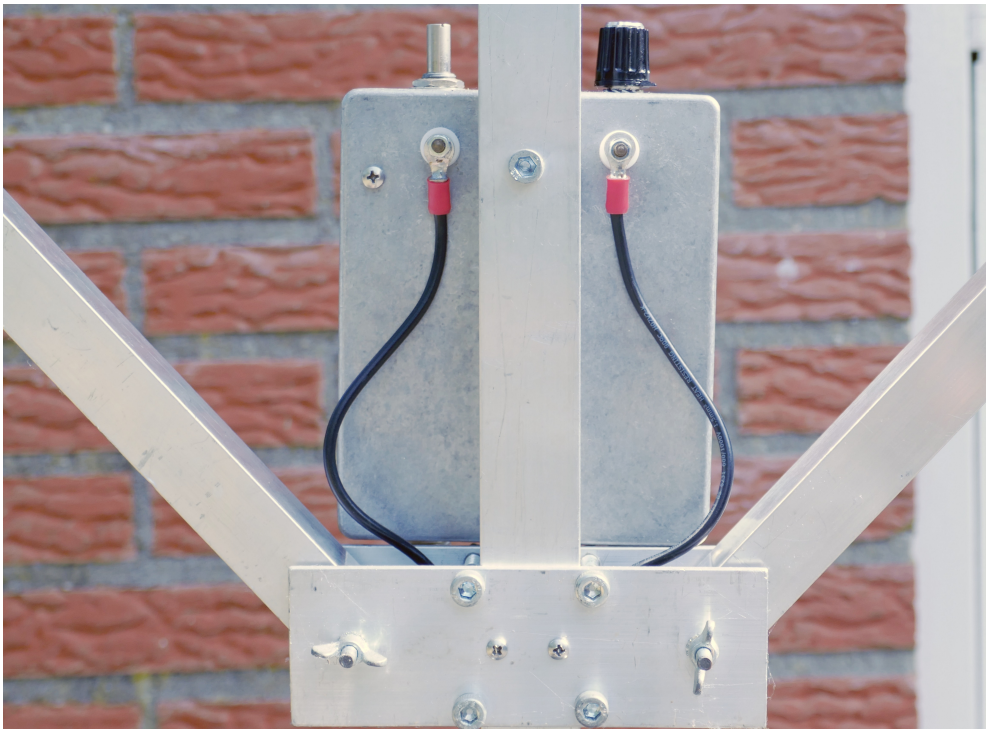

Photo 2.3. The backside of the active part. Here the flexible connections to the rods inside the Alu profiles are visible.

Photo 2.4. The high-band loop antenna. The basis is formed by a wheel-chair handle and is cut on the lowest part, and connected to the active part. Here the fine tuning potmeter and the band switch are mounted on the backside.

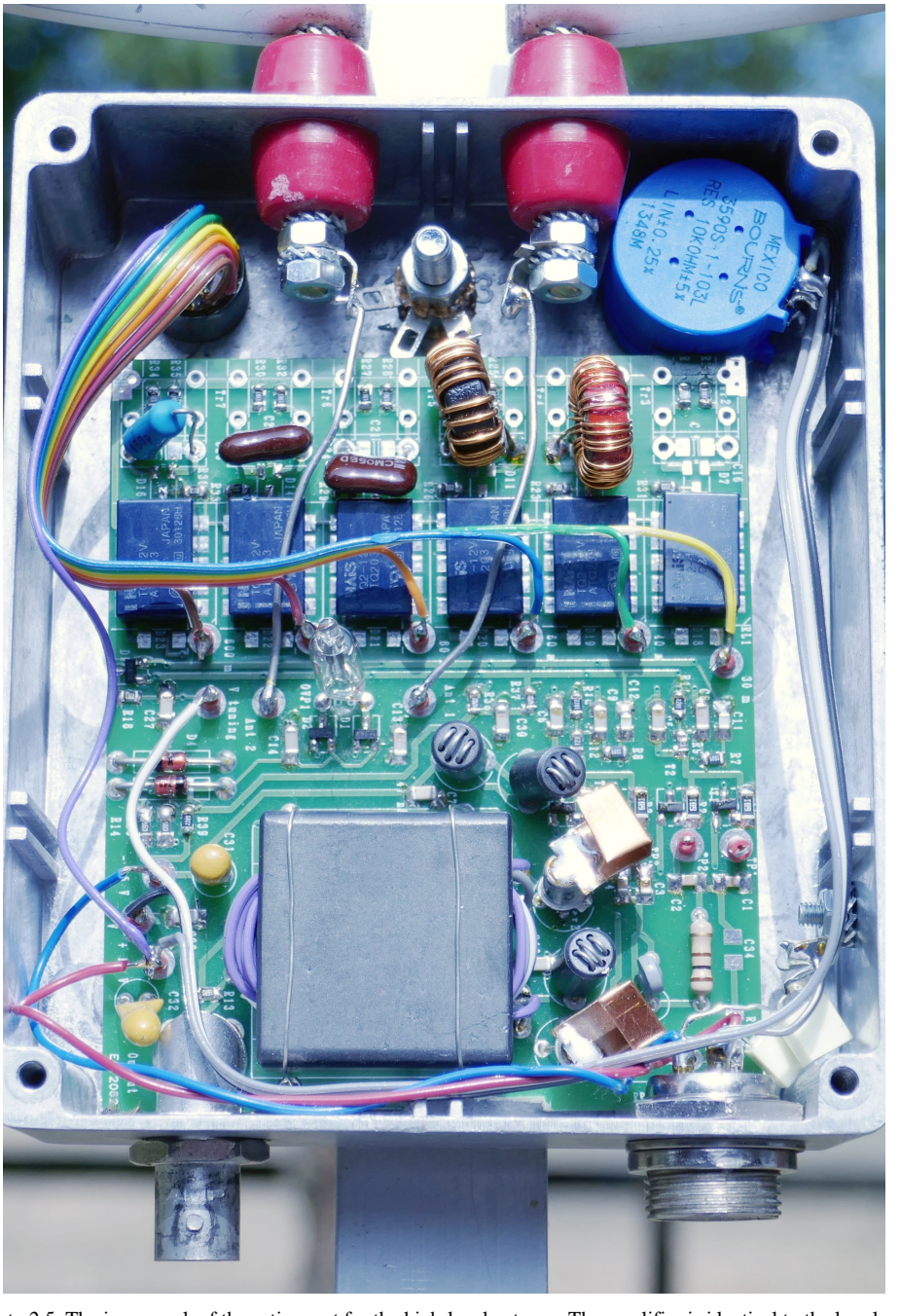

Photo 2.5. The inner work of the active part for the high-band antenna. The amplifier is identical to the low-band antenna, but the tuning components are different.

2.4.3 Datalogger

The function of the datalogger is multiple:

a) It digitises the analog recorder output voltage, 0 to 5 V;

b) it processes the measurement samples in real time, incorporating calibration factors;

c) per frequency band it collects all results from subsequent measurements and stores it in a single CSV file and in an overviewing graphic;

d) it contains the chargeable battery that feeds the datalogger and the connected antenna.

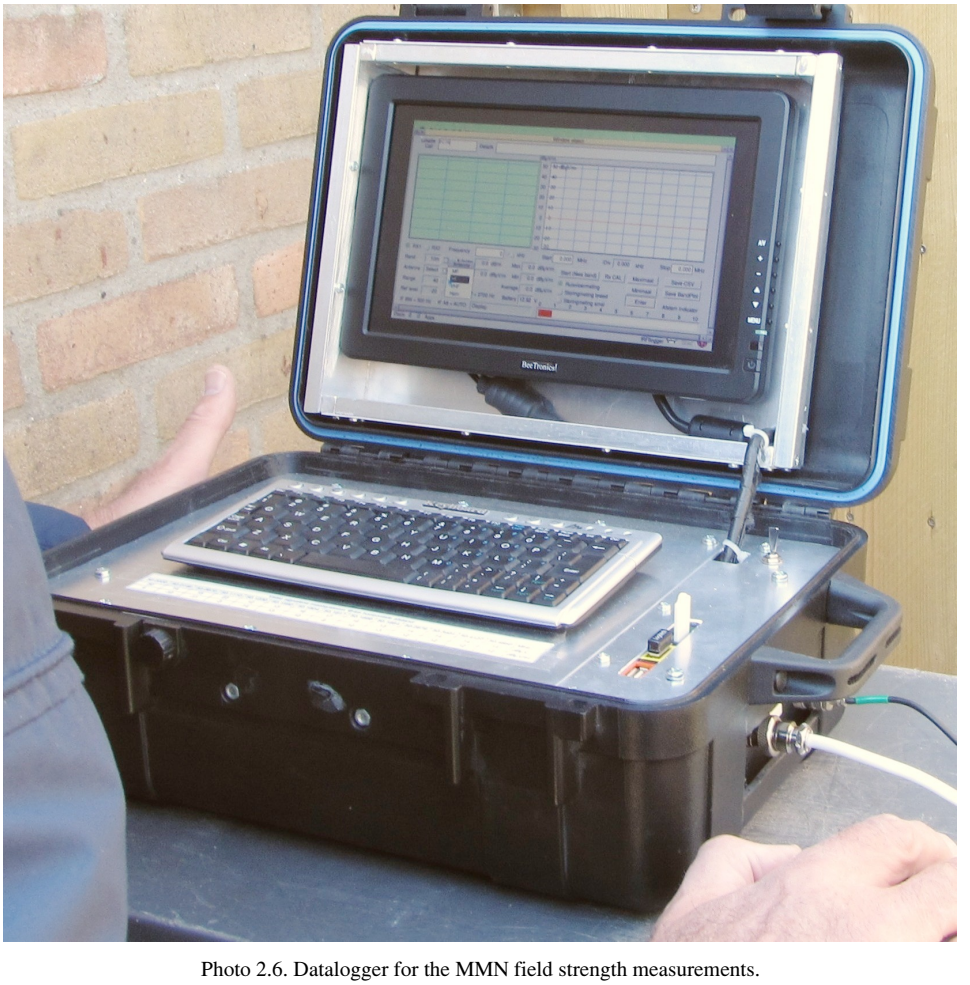

Photo 2.6. Datalogger for the MMN field strength measurements.

A special requirement for the datalogger is that it does not radiate EMI of its own and so pollute the measurement results. Therefore shielding of the whole unit is necessary, including partly screening of the display, see Photo 2.6. Also the DC-DC convertors, needed for the powering of the Raspberry Pi and for the antenna, are placed in a double screened box, including double filtering of the input and output lines, see Figure 2.14. Another measure is to use a cordless mouse and a fixed mounted keyboard. The result is that up to 30 MHz no EMI is noticeable above the external noise. Only in the range 50 - 50.5 MHz some internal EMI is measurable, and is indicated on a scale below the keyboard.

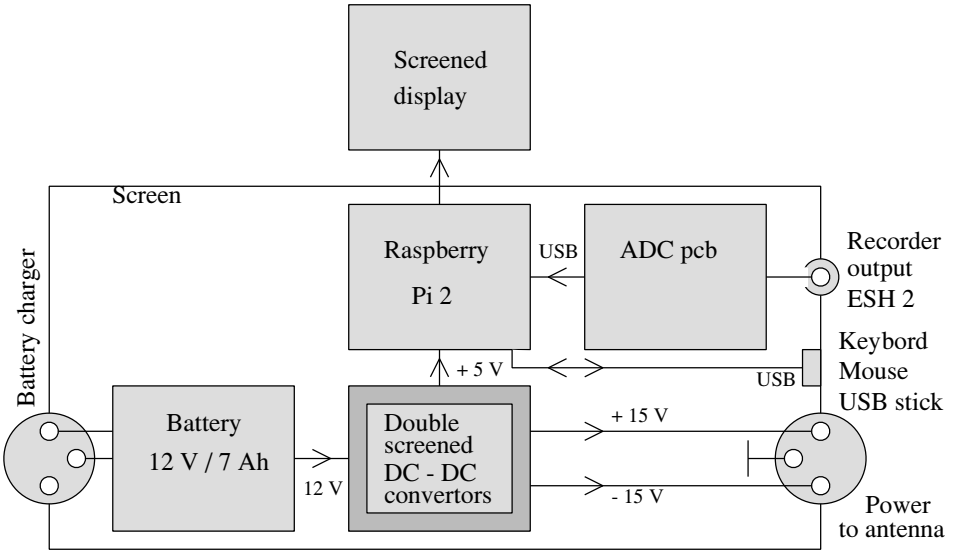

Figure 2.14. Block diagram of data-logger for noise FS measurements.

2.4.4 Measurement receiver

For the measurements two measurement receivers were available. The manufacturer of the receivers is Rohde & Schwarz, the type is ESH2. During the noise measurements the Average detector was used in combination with a 500 Hz bandwidth (measurement bandwidth, see Chapter 3, Subsection 3.3.2.) and the logarithmic 40 dB measurement range. The reference level was adjusted according received noise levels by selecting the input attenuation. The unfiltered analog recorder output voltage, 0 - 5 Volt, proportional with the meter deflection, was used as input to the datalogger.

These measurement receivers use a calibration system, based on an internal calibration generator. For the purpose of the noise measurement campaign both receivers were individual calibrated on

a) absolute amplitude corrections, caused by small differences in the output of the calibration generators;
b) the effective noise bandwidth of the 500 Hz IF bandpass filters;
c) the receiver Noise Figure for 0 dB IF attenuator, as well for 10 dB IF attenuator settings and higher.

The calibration data was applied by means of a calibration file inside the datalogger application software together with the frequency band depending calibration of the antenna sensitivity and the noise floor of the antennas.

2.5 Conclusion

An investigation into requirements for measuring the radio noise floor, using portable equipment, shows issues in the field of sensitivity, calibration accuracy, and directivity, besides the general requirements as described in Recommendation ITU-R SM.1753-2 [11]. A minimum sensitivity requirement for antennas is derived, and causes of uncertainty in the calibration of E-field rod antennas are analysed. E-field rod antennas were found to be unsuitable for noise floor measurements when they are not grounded using a low impedance. For H-field loop antennas it is found that they do not show those accuracy problems, but require to be tuned in frequency for sufficient sensitivity, and that there is a need to measure in two orthogonal directions with vectorial composing of both results to produce a radio noise floor that is direct comparable with the MMN levels as mentioned in Recommendation ITU-R P.372-15 [13]. Technical solutions were described in short and some essential elements therein were highlighted.

3 Man-Made Noise field strength measurement campaign

In this chapter the Man-Made Noise measuring campaign and the results thereof are described. The chapter is mainly based on the publication "Measurement Methodology and Results of Measurements of the Man-made Noise Floor on HF in The Netherlands" [II].

3.1 Introduction

In Chapter 1 already the motivation for an investigation into the current levels of Man-Made Noise (MMN) is given. Also the existing scientific knowledge about this subject has been discussed. In Section 3.2 we a description of the measurements is given, in Section 3.3 the measurement setup and results. Section 3.4 will contain a statistical analysis and an evaluation of the measurement results, and Section 3.5 will finalise this chapter with a conclusion.

3.2 Description of the measurements

In this dissertation we use the Euclidean reference frame. To denote a point in space we use the vector $\boldsymbol{x}=x\boldsymbol{i}_x+y\boldsymbol{i}_y+z\boldsymbol{i}_z$ in which x,y,z are scalars given in the SI-unit [m], $\boldsymbol{i}_x$, $\boldsymbol{i}_y$ and $\boldsymbol{i}_z$ are orthonormal unit vectors in the x, y and z direction respectively and bold face denotes a vector quantity. Time is denoted by the scalar t in [sec]. Time-harmonic signals are easily considered in the frequency domain by the well-known Fourier Transform. For the sake of simplicity the time factor will be omitted when working in the frequency domain. In case of a time-harmonic signal with period T the pertaining frequency is $f=1/T$, in Hertz [Hz].

3.2.1 Scope of the measurements

The methodology of the measurement campaign, described in this chapter, differs from earlier MMN measurements. Instead of using measurement locations at large distances from buildings and homes, locations are sought representing the normal living conditions of radio spectrum users. Therefore 54 premises of VERON members were selected. These premises were well spread over rural areas, urban areas with a large variation in habitation densities, city environments, and also spread over the whole of the Netherlands: eleven of the twelve provinces were included. To complete the data set the measurement environment is extended with three locations representing a quiet rural environment and two locations to represent atypical environments. This extensive measurement campaign cover thus a representative geographic area of the main categories of the ITU-R. The measurements are carried out in the frequency range of 470 kHz up to 50.5 MHz. In this range impulse noise (IN), see Section 1.5, is not an item of interest to the radio user, due to the general availability of noise blanker circuits. In modern Software Defined Radio (SDR) systems the noise blanker technique is also available, even in analog to digital convertors, [61]. So the measurements in this chapter are restricted to measuring WGN field strength levels, and will be compared to field strength levels, derived from noise power levels given in ITU-R P.372 [13].

The strict limitation to the frequency bands of the Amateur Radio Service has one drawback: In these bands Powerline Communication equipment (PLC) should be notched, and often are. Although in many places strong PLC signals were seen outside these bands, they do not fully contribute to the measured MMN levels, and we may expect higher MMN levels outside the notches, especially in the evening hours when PLC systems are mostly in full use.

3.2.2 Types of Noise Signals

In Chapter 1 we already discussed the different kinds of noise we may encounter when listening on the MF and HF frequency bands. For the purpose of the measurement campaign we differentiate between the following types of noise:

1 Interfering signal, EMI: an unwanted signal, usual man-made which is divided into two sub-classes:

  1.1 Narrowband EMI: Bandwidth $\leqslant$ 500 Hz, often an unmodulated carrier.

  1.2 Broadband EMI: Bandwidth > 500 Hz, but smaller than the observed frequency band. Signal over the pertaining bandwidth may be partly

Gaussian.

2 Noise*:* a stochastic signal or an accumulation of uncorrelated signals, not necessary Gaussian; Bandwidth much larger than the width of the observed frequency band. Within Noise three subclasses are identified:

2.1 Man-made noise originating from an individual specific local source.

2.2 Man-made noise originating from multiple local sources, generally cumulative.

2.3 Radio background noise, like atmospheric noise, galactic noise, and cumulative skywave MMN.

In Chapter 1, Section 1.4, a detailed description is given of the types of noise that can be found when measuring, see also Figure 1.2. Man-made noise can be characterized by several parameters like the power spectral density, the amplitude probability distribution (APD), pulse spacing distributions (PSD), pulse duration distributions (PDD) [13], [45]. In this investigation we indicate the power spectral density by using a bandwidth of 2700 Hz, representing the standard channel bandwidth for radio communication systems in the High Frequency (HF) bands.

3.3 The measurement setup and results

3.3.1 General description of the measurement campaign

Radio noise measurements have been performed at the premises of 54 radio amateurs, and at 5 other locations. For purpose of this measurement campaign six categories of environment are defined:

1 *Quiet Rural area*: No residences, no infra structures within 1.5 km radius.

2 *Rural area*: up to 10 residences within a radius of 100 m, but at a distance of at least 100 m outside built-up area.

3 *Residential area-1*: 11 - 50 residences within 100 m.

4 *Residential area-2*: 51 - 100 residences within 100 m.

5 *Residential area-3*: >100 residences within 100 m.

6 *City area*: large apartment buildings, commercial & city centres. In this campaign we used the definition for *City area:*

1 the residence is directly surrounded by shops and other city centre activity, or

2 the number of residences within a radius of 100 m is larger than 150, or

3 the number of residences within a radius of 500 m is larger than 2000.

For every environment category a number of 10 locations measurements was targeted; practically the numbers were: Quiet Rural: 3, Rural: 10, Residential area 1: 14, Residential area 2: 14, Residential area 3: 8, and City: 8. Two locations were atypical and the measurement data were not used in this chapter. Appendix D, Table D.1 gives an overview of the measurement locations divided in their categories, and showing the numbers of homes at given distances from the measurement location. Table D.2 gives an overview of the measurement data. Figure D.1 shows the map of measurement locations.

3.3.2 Measurement details

For the measurements a small receiver bandwidth of 500 Hz is used because of the difficulty to find frequency spaces free of radio signals, while the results are converted to the reference bandwidth of 2700 Hz. For this conversion we assume the noise to be Gaussian. Table 3.1 lists all the frequency bands wherein the measurements are performed.

Table 3.1. Frequency ranges and time slots.

Frequency Ranges and time slots used in the measurements		
Name of the amateur radio frequency band	Frequency range of the measurements	Aproximate timeslots of the measurements
635 meter	470 - 480 kHz	12.00 - 14.00 h local time
160 meter	1.8 - 1.9 MHz	
80 meter	3.5 - 3.8 MHz	
60 meter	5.25 - 5.45 MHz	
40 meter	7.0 - 7.2 MHz	
30 meter	10.10 - 10.15 MHz	
20 meter	14.0 - 14.35 MHz	9.00 - 11.00 h local time
17 meter	18.068 - 18.168 MHz	
15 meter	21.0 - 21.45 MHz	
12 meter	24.89 - 24.99 MHz	
10 meter	28.0 - 29.7 MHz	
6 meter	50.0 - 50.5 MHz	14.00 - 15.00 h

All measurements are carried out in periods with long daylight hours in the months from April until October, and in time slots wherein the level of atmospheric noise is minimal. At the MF (0.3 - 3 MHz) and HF (3-30 MHz) frequencies we assume that the dominant way of propagation of cumulating MMN is caused by the surface waves, inherently resulting in a mainly vertical polarization. The measurement antennas are matched for this polarization. Appendix G studies the error on estimating the field strength by neglecting the wave-tilt of a ground-wave over lossy ground, and concludes that in most cases the error is far below 1 dB. At the lower VHF band (6 m / 50 MHz) an antenna for horizontal polarization is used, assuming free space propagation. All measurement positions were in the open air, about 10

Photo 3.1. Noise measurement setup with magnetic loop antenna, datalogger and measurement receiver.

meters from outside wall of the premises, where applicable. Photo 3.1 shows the measurement set-up.

3.3.3 Reference noise field strength values

Table 3.2. Existing MMN regression line constants from [13].

Constants for calculating Man-made Noise field strength levels			
Environmental category	*c*	*d*	Frequency range [MHz]
City	76.8	27.7	0.3 - 250
Residential	72.5	27.7	0.3 - 250
Rural	67.2	27.7	0.3 - 250
Quiet rural	53.6	28.6	0.3 - 30
Galactic noise	52.0	23.0	10 - 150

In [13] the MMN levels are given as linear regression curves, wherein the median values F_{am} of the antenna noise figure, F_a, depending on frequency f [MHz], is given by:

$$F_{am} = c - d \cdot \log f \tag{3.1}$$

The constants c and d are given by Table 3.2. According to Equation (3.2):

$$E_n = F_a + 20 \log f_{\mathrm{MHz}} + 10 \log b_{\mathrm{Hz}} - 95.5 \text{ [dBµV/m]} \tag{3.2}$$

the noise field strength levels, E_n, can be calculated for a short monopole antenna above a perfect ground plane. These levels are plotted in Figure 3.2.

3.3.4 Measurement results

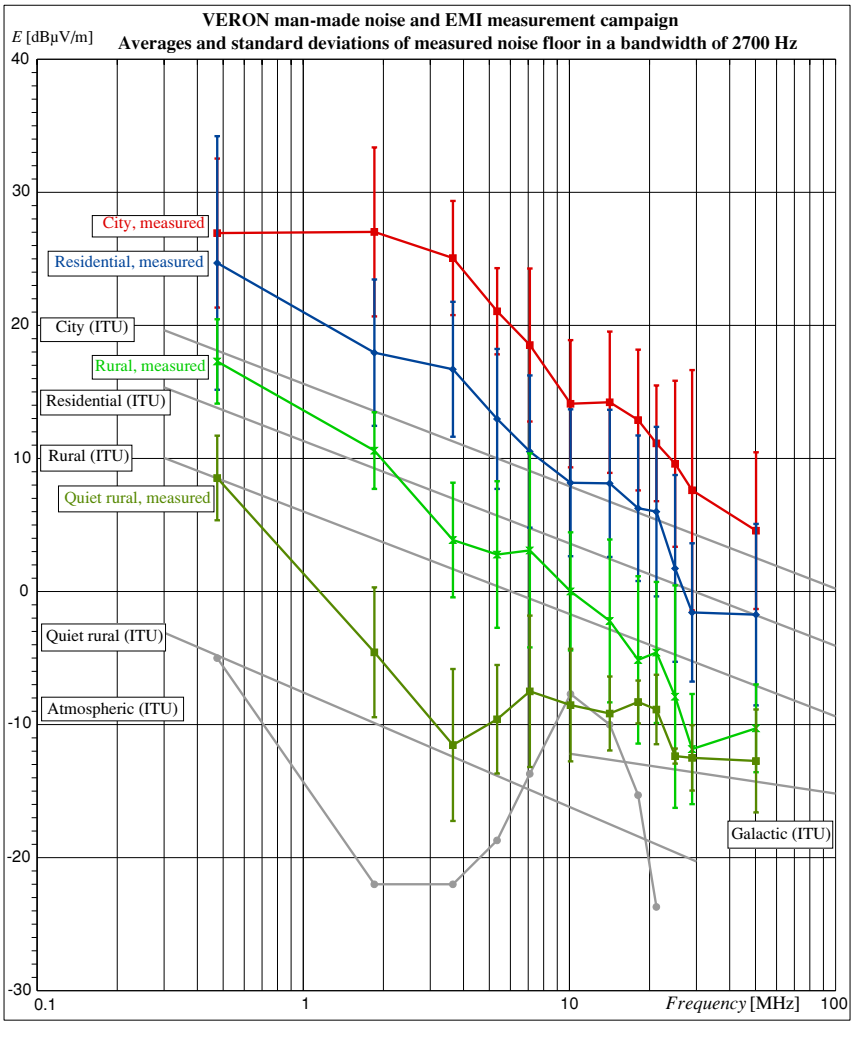

Figure 3.2. Measurement results and reference curves of MMN.

The average values of the measured field strength levels for each frequency band were calculated, including the related standard deviation values. The measurement data for the four categories of environment are plotted in Figure 3.2. The curves and main markers indicate the averaged noise field strength value pertaining to the associated environment. For completeness the standard deviations in the measurement results are plotted as well as the noise floor field strength levels as they are derived from [13]. It should be noted that Figure 3.2 does not show the worse case measurement results. The worst case measured MMN levels exceed the Average levels by more than twice the shown values of the standard deviation. De measurement results are summerized in Appendix D, Table D.2.

3.4 Statistical analysis and evaluation

Statistical tests are performed on the measurement data using the Student t-test as described in [60]. A two-tail test is chosen, using a level of significance, $\alpha = 0.05$, which means a Type I error risk of 5 %, a common used value. The population is the total number of enrolled amateur radio station in The Netherlands per type of environment, including the measurement locations in Quiet Rural environments. The population means, μ, are given by the noise field strength levels as given in Figure 3.2. The sample in the statistical meaning is the set of noise floor field strength measurements within a type of environment. The null hypothesis, H_0, is formed by the assumption that noise levels have not changed since the time and method of measurement of the data in [13]. The alternative hypothesis, H_1, assumes a change of the noise floor. So the rejection of H_0 means a statistical relevant increase of the noise floor, or a statistical relevant decrease of the noise floor. The number of samples, n, differs for the individual environments: $n = 3$ for Quiet Rural, $n = 10$ for Rural, $n = 36$ for Residential, and $n = 8$ for City.

Table 3.3. Results of the statistical analysis of the increase of the radio noise.

VERON man-made noise measurement campaign		**Statistical analysis of increase of noise floor**											
Band	n	635m	160m	80m	60m	40m	30m	20m	17m	15m	12m	10m	6m	
City	8	+ 8.8 ±5.6	+13.4 ±6.4	+13.8 ±4.3	+11.1 ±3.2	+9.4 ±5.8	+6.2 ±4.8	+7.5 ±5.3	+7.0 ±5.3	+5.7 ±4.4	+4.7 ±6.2	+3.2 ±9.0	+2.1 ±5.9	AV SD
Resi-dential	36	+10.9 ±9.5	+8.7 ±5.5	+9.7 ±5.1	+7.3 ±5.3	+5.7 ±5.7	+4.3 ±5.5	+5.7 ±5.5	+4.7 ±5.5	+4.9 ±6.4	+1.1 ±7.0	-1.7 ±5.2	0.1 ±6.8	AV SD
Rural	10	+8.8 ±3.2	+6.6 ±2.9	+2.2 ±4.3	+2.4 ±5.5	+3.6 ±7.3	+1.7 ±4.4	+0.7 ±6.1	-1.4 ±6.3	-0.4 ±8.4	-3.2 ±8.4	-6.6 ±4.1	-3.2 ±3.3	AV SD
Quiet rural	3	+13.3 ±3.2	+5.3 ±4.9	+0.9 ±5.7	+4.3 ±4.1	+6.2 ±5.7	-0.8 ±4.2	+0.8 ±2.8	+4.7 ±1.6	+4.3 ±2.6	+1.0 ±0.6	+1.1 ±2.5	+1.6 ±3.9	AV SD
Statistical relevance:				Increase			Neutral			Decrease		AV: [dBµV/m] SD: [dB]		

Table 3.3 shows the results of the statistical analysis, and is denoted as follows. The red cell colour indicates that for that frequency band a statistically significant increase in the noise floor has been found. The blue cell colour means that a statistically significant

decrease has been observed. For the sake of completeness the average values and standard deviations of our measurements are given per frequency band.

From the results, shown in Figure 3.2 and Table 3.3, several things can be learned:

1 Although the measurement results for the quiet rural environment shows a statistical significant rise in the noise floor at the lowest frequency band, its not clear that this is caused by MMN only. From the expected levels of MMN Quiet Rural and of Atmospheric Noise, as shown in Figure 3.2 where they coincide at 470 kHz and cross between 7 and 19 MHz, one may conclude that Atmospheric noise may contribute to the measurement results too.

2 For the rural environment the rise in MMN is statistically significant on the two lowest frequency bands. On the other side of the spectrum we see a relative decrease of MMN on the 10 and 6 meter bands. Reduced ground wave propagation, caused by low conductivity of the ground (the measurements were performed during the summer half year, see Chapter 5), may explain this reduction.

3 In residential environments the increase of the noise floor level by MMN is very clear, and is statistically significant for all frequencies, except the highest three bands.

4 In city environments the rise of the MMN level, relative to ITU-R P.372-15, is complete, and is statistically significant for all frequencies, except the highest three bands.

3.4.1 Regression lines

In a second step of the statistical analysis the correlation between the mean values of measured field strength levels and the frequency bands is determined per type of environment, and so calculating regression lines. Figure 3.3 shows the change of the slopes and of the mean levels of the regression lines from the basic Report CCIR 322-4 (1988) [46] / Report 258-4 (1982) [44], which is just copied in the later ITU-R P.372 versions, into the measured values. The slope and the Man-Made Noise field strength level at a frequency of 1 MHz are shown in Table 3.4.

Table 3.4. Results of correlations of measured MMN FS levels.

Slope and level of regression curves according the measurements			
Environment type:	*Slope* [dB/log (MHz)]	$E_{N@1\ MHz}$ [dBµV/m]	Correlation coefficient *r*
City	-12.58	28.00	-0.9459
Residential	-13.61	22.06	-0.9752
Rural	-14.64	13.53	-0.9808

Also shown are the Pearson correlation coefficients r, which show a high level of correlation. The slope and field strength levels in Table 3.4 can be calculated back to Noise Figures as used in ITU-R P.372-15. Inverse use of formula (3.2) results in new values for the constants c and d. The frequency range is limited to 50 MHz, because there is no measuring data available for higher frequencies. Based on the measurements results we might anticipate a modification of ITU-R P.372-15. In Table 3.5 our proposition for possible modifications is presented. For the question as whether we want to modify ITU-R P.372-15 the author will refer to Chapter 1, Section 1.7: "The status of Recommendation ITU-R P.372".

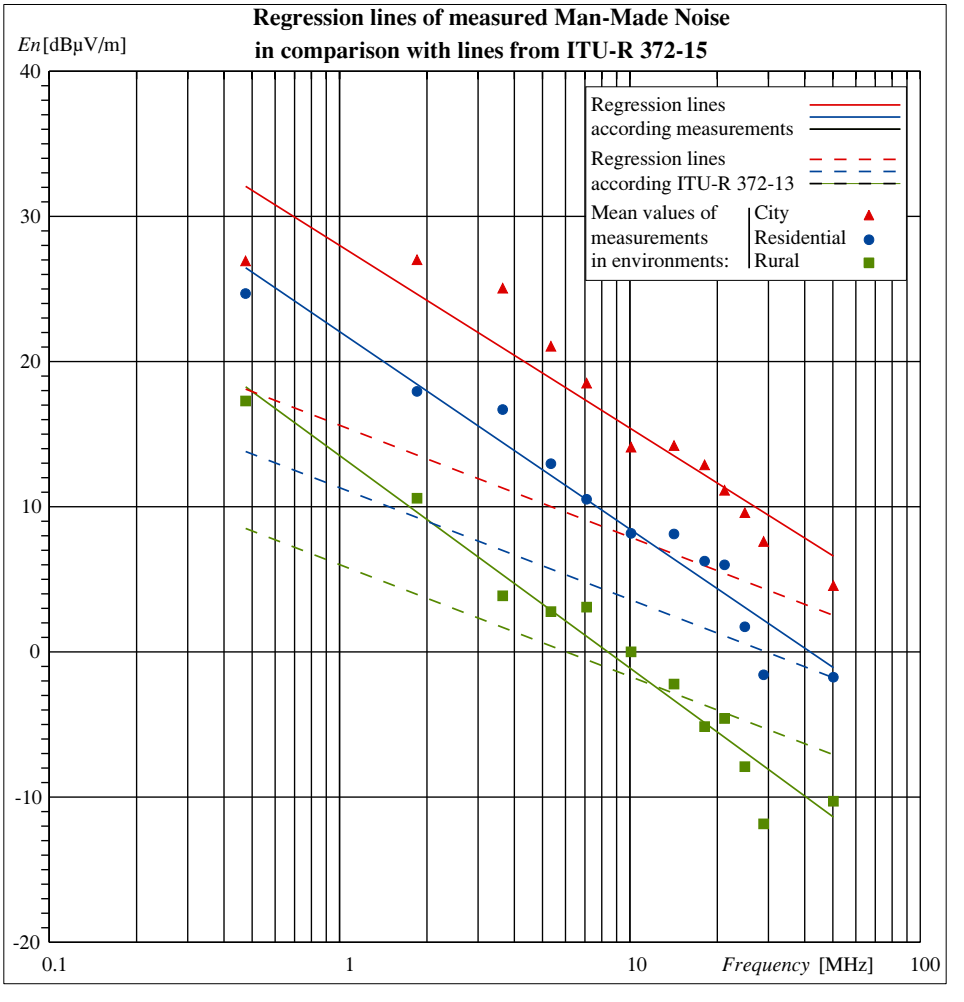

Figure 3.3. Regression lines of measured Man-Made Noise in comparison with the regression lines in ITU-R P.372-15

Table 3.5. MMN regression line constants according the measurements.

Proposed constants for future version of ITU-R 372			
Environmental category	*c*	*d*	*Frequency range* [MHz]
City	89.2	32.6	0.3 - 50
Residential	83.3	33.6	0.3 - 50
Rural	74.7	34.6	0.3 - 50

3.4.2 Discussion

We see that the so found regression lines consistently show a different and steeper slope than those in ITU-R P.372-15. For an explanation we could think of the different type of sources, as we already concluded in Section 1.5, differences in the distances, and in the propagation losses. In Chapter 5 we will see that the propagation losses in residential areas are higher than expected from pure ground-wave propagation and increase with frequency.

3.5 Conclusion

The measurements at 54 different locations in inhabited areas show that man-made activities generate an increase of the Man Made noise floor in the Netherlands. In general there is a statistically significant increase of the MMN floor in comparison with the reference levels as given in Recommendation ITU-R P.372-15 [13]. This increase is highest in dense build-up regions like city centre, where increases up to 14 dB averaged, with peak values over 20 dB, exist. In residential environments the increase is also very significant, although gradual lower with lower habitation densities.

As the measurements were performed in various locations, from lakes and woods at far distances from the built-up area to residential areas in various densities of habitation and in city centres, it is our opinion that we have gained a representative picture of noise floor levels in the Netherlands. After many years of EMC-regulation in the European Union and the assumption that the MMN-environment in the Netherlands does not differ from other developed (EU) countries, we have no reason to believe that performing our measurements in other countries under similar circumstances would lead to different results. In order to verify that other countries have similar MMN-environments, we encourage other groups to conduct measurements too. Consequently, we conclude from our measurements that the data about Man-Made Noise in Recommendation ITU-R P.372-15 is not representing the current state. Depending on the status of the Recommendation, see Section 1.7, we suggest to define reference values for MMN (recommendation) and enforce those reference values, or transform ITU-R P.372-15 into a Report that follows the developements of the MMN levels.

As known from previous work [34], [35] our measurements and analysis have

confirmed the accumulation effect caused by the increasing density of interfering sources in close proximity. From this observation we can conclude that the paradigm of Man-Made Noise has shifted over time: In conventional EMC-standards it is assumed that only one single (sub)system is present in the close vicinity of a radio receiver, but clearly, this is not the case any more. Finally it is noted that due to the constant change in our modern day society similar noise-floor measurements should be conducted frequently to keep track on the evolution of the MMN floor.

4 Correlation Between Measured Man-Made Noise Levels and the Density of Habitation

In this chapter we will further process the measurement data, found in Chapter 3, and correlate that with the density of habitation. The chapter is based on the publication "Correlation Between Measured Man-Made Noise Levels and the Density of Habitation" [III].

4.1 Introduction

In Chapter 3 the author described a measurement campaign in which on 59 locations man-made radio noise (MMN) was measured on 12 frequency bands in the range from 470 kHz to 50.5 MHz. The basic result of that measurement campaign was that a clear increase of MMN levels was found, relative to the data in [13]. A further research question is wether a correlation can be found between the measured noise levels and the density of habitation. And to what range this correlation is measurable? For answering these questions a further statistical study into the measurement data is required.

In the literature little evidence is found in the relation between density of habitation and MMN noise floor. MMN and electromagnetic interference effects (EMI) has been studied for a long time. Measurements of time and frequency domain characteristics of noise and types of sources, affecting high-frequency (HF) communication sites, are presented in [1]. Analysis of sources of MMN as mains circuits with switching pulses, corona radiation and silicon controlled rectifier noise, automobile ignition noise, and ISM. In [20] results are presented of spatial MMN measurements around Seattle (USA) for a frequency of 1 MHz.

MMN levels are measured up to 100 miles. In [22] it is concluded that at frequencies below 25 MHz low voltage transmission lines and radio frequency stabilized arc welders are the major incidental radio noise sources when the observer is within 30 m of the source.

In [23], [24] and [31] the same author concludes for the range 20 to 200 MHz interference ranges of 0 to 5 miles (urban), 5 to 15 miles (suburban I), and 15 to 35 miles (suburban II). Impulsive noise is the dominant form of interference in these early papers, 1966 to 1970. In [6] the results of measurement in the VHF and UHF range (1995) are presented, discussing the observation that the technological advances had significantly changed the man-made noise emissions. In contrary in reference [3] a decrease in MMN levels in business and residential areas in Canada (1993) is concluded. A noise measurement program in the UK [4], [61] conclude an increase of additive white Gaussian (AWG) noise in city centres, factory estates and business centres. This increase is attributed to the high number of emission sources in those environments, so an accumulation of noise powers is assumed here. For the suburban and major road junction areas a low MMN level has been measured, concluding a low number of emitters. The frequency range of these measurements starts from 60 MHz upwards. In reference [62] measurements in Sweden around the year 2000 are evaluated, concluding that the MMN levels between 30 and 300 MHz did not exceed the ITU-R P.372 levels. It was remarked that these measurements were hampered by the large physical dimensions of the measurement system, and the actual measurement locations did not fully represent residential locations. Due to increase of electronic equipment in residential and city environments they expect a increase in MMN noises floor after 2000. In [5] radio noise in the frequency range 2 to 30 MHz has been measured and studied. As there are also several natural sources of noise in this range no conclusions about MMN is given. In [2] an overview of MMN studies is presented, including cases of interference, with special interest for indoor, industrial, environments. Much scientific information about radio background noise and noise floor levels, including MMN, has been gathered in the ITU-R Recommendation P.372-15 [13]. Methods how to measure radio noise has been discussed in [10], [11]. Reference [13] does not give information about the accumulation of the emissions from a collection of MMN sources, spread in a certain environment.

Renewed interest in HF communications, now triggered by interests in broadband NVIS data communication using channel bandwidths up to 24 kHz, [63] concludes that doubling the channel bandwidth results in a 3.5 dB increase of noise power. The measurements were performed in a urban environment, on frequencies from 3 to 9 MHz, and we conclude from the result that the measured noise was mainly consisting of Gaussian MMN. In [64] a reconnaissance into interference by several kinds of MMN is done for modern wireless

telecom systems below 3 GHz. Indoor and outdoor measurements are done in the range 500 to 2500 MHz. Especially spurious emissions of several electronic equipment in house of office were found strongly interfering, resulting in capacitance reduction. Interference risks from accumulation of MMN is theoretically studied in [65]. Herein propagation via ground wave, as well as via sky wave is involved.

In our measurements in Chapter 3, we already concluded that as a result of the huge increase of electronic devices in residential homes in the last decades, especially by all kind of switching power supplies, the AWG noise became more dominant as MMN. In these foregoing papers we did not find any measurement concerning the relation between MMN floor and registered density of habitation. So we do not know the origin of that noise power in the geographical meaning. Also we do not know whether the measured MMN originates from a single source, a small number of sources with high power, or from a very large number of sources each with a very limited power. The latter is indicating a wide accumulation process, where is referred to in [65].

This chapter does make an attempt to fill this gap in our knowledge by using the measurement data from the measurement campaign described in Chapter 3, combine the data with the number of residential livings as registered for each measurement location, and correlate the noise level in relation to the density of livings. The chapter is organized as follows. In Section 4.2 a short description of the measurement method is given. The results are being connected to the geographical density of habitation. In Section 4.3 a statistical analysis of the relation between MMN levels and that density is performed. Section 4.4 shows the results of the analysis, and in Section 4.5 conclusions are drawn.

4.2 Description of the measurements

In the measurement campaign the subject of the measurements was man-made radio noise as experienced by the radio users, for example radio amateurs or worldwide broadcasting listeners, living in residential areas. This means that the measurement locations had to be situated at the livings of those people. Radio users were expected to use outdoor antennas of reasonably quality, so that their reception quality was optimal for their surroundings. Therefore the measurement antennas were placed outdoors, most in gardens, with a projected distance of 10 meters from the nearest building wall. The ITU-R P.372-15 [13] shows expected values of MMN for a series of defined environments: quiet rural, rural, residential and city. We used these specification of environments, and extended the type residential into three subtypes: residential 1, residential 2, and residential 3, see Table 4.1.

Table 4.1. Definitions of types of environment

Definitions of types of environment	
Environment	Number of homes, $n_{range[m]}$
Quiet Rural	n_{1500}= 0, no infra structures
Rural	$n_{100} \leqslant 10$
Residential 1	$10 < n_{100} \leqslant 50$
Residential 2	$50 < n_{100} \leqslant 100$
Residential 3	$100 < n_{100} \leqslant 150$
City	n_{100}>150, n_{500}>2000, city centre

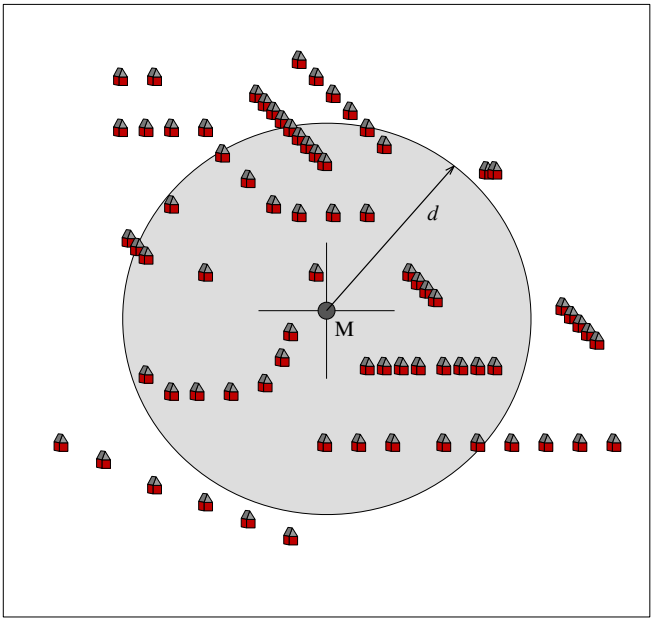

Figure 4.1. Map of a residential environment with a cumulative area marked within a circle.

Measurements were performed at a total number of 59 locations, but five were excluded for this study because they are in Quiet Rural areas (no habitation) or are the atypical, see Appendix D. For each measurement location the number of homes in circular rings around the measurement point has been counted on maps from [66] and registered. The annulus are: 0 to 50 m, 50 to 100 m, 100 to 200 m, 200 to 300 m, 300 to 400 m and 400 to 500 m. We want to investigate the cumulative noise field strength as a function of the density of habitation in (a) in a cumulative areas from zero up to a distance 50, 100, ... 500 m from the measurement location, see Figure 4.1, and (b) in annuluses from zero up to a distance 50, 100, ... 500 m, see Figure 4.2. In these figures the measurement location is indicated by M, the range of the cumulative area by d, and in the annuluses the minimal and maximal distance to the measurement location by respectively d_{min} and d_{max}.

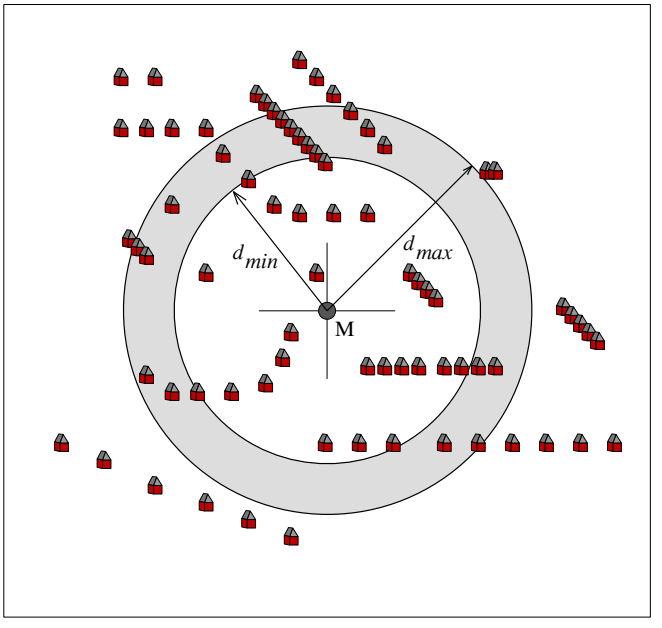

Figure 4.2. Map of residential environment with a cumulative area marked with an annulus.

Table 4.2. Frequency ranges used in the measurements.

Name of the frequency band	Frequency range of the measurements
635 meter	470 - 480 kHz
160 meter	1.8 - 1.9 MHz
80 meter	3.5 - 3.8 MHz
60 meter	5.25 - 5.45 MHz
40 meter	7.0 - 7.2 MHz
30 meter	10.10 - 10.15 MHz
20 meter	14.0 - 14.35 MHz
17 meter	18.068 - 18.168 MHz
15 meter	21.0 - 21.45 MHz
12 meter	24.89 - 24.99 MHz
10 meter	28.0 - 29.7 MHz
6 meter	50.0 - 50.5 MHz

The measurements were performed in twelve frequency bands, according Table 4.2. The results are grouped along these frequency bands and in this chapter these bands are indicated by their associated wavelength handle from here. The processing of the data is done for each band separately. The numbers of homes, in circular rings, are known for each measurement location, for example a location in the city of Meppel, see Table 4.3.

Table 4.3. Examples of number of homes in annuluses.

Distance from measurement location [m]	**0 - 50**	**50 - 100**	**100 - 200**	**200 - 300**	**300 - 400**	**400 - 500**	**Total**
Number of homes	52	106	369	511	533	575	2146

For purpose of the statistical analysis the original measurement data from Chapter 3, reproduced in Appendix D, was organized in two tables as follows:

Table D.1:

1 The first column contains a serial number of the location,
2 The second column contains the location name.
3 The third column gives the category of location.
4 The 4rd to 9th columns, labelled 0 to 50m, 50 to 100m, up to 400 to 500m, contain the number of homes in each annulus for each location.
5 The 10rd to 15th columns, labelled 0 to 50m, 0 to 100m, up to 0 to 500m, contain the number of homes in the cumulative distance ranges for each location.

Table D.2 contain the measured field strength level in each location for all the subsequent frequency bands. By selecting one of the columns with the habitation data, and ordering the table on basis of the increase of homes in that column, a relation between measured field strength levels and habitation density in the area, described in that column, has been extracted per frequency band.

4.3 Statistical analysis

4.3.1 Correlation testing

The purpose of the statistical analysis of the measurement data is to study if there is a statistical relationship between MMN field strength and the density of habitation. In this research the number of homes, n, within a defined area is the quasi-independent variable, while the measured electric field strength, e, of the MMN noise floor is the dependent variable. We want to test if a positive correlation exists between the density of homes, as calculated from the number of addresses, found on the Open Street Map, and the measured noise level. That means that for the hypothesis H_0 the correlation coefficient $\rho = 0$, (no correlation) and for H_1, $\rho \neq 0$ (certain amount of correlation). In this case we expect $\rho > 0$, meaning an increasing of the noise floor with a higher density. This is a directional (one-tailed) test [60].

Remark that $\rho < 0$ is also possible, but only in a situation of one or a very small

constant number of noise sources. In this case the decrease of field strength, caused by the increasing path loss by higher density of buildings, is higher than the increase of the number of sources. In our measurement data we did not find this.

Assuming that the number of noise sources per home is constant and that the generated noise power per source is constant on average, the cumulative noise power-flux density pfd_{cum} is proportional with the number of homes, n_d, within an area limited by a radius d. We can write for the electric field strength at a measurement point:

$$pfd_{cum} = \frac{{e_d}^2}{Z_0} \equiv C \cdot n_d \tag{4.1}$$

$$e_d = \sqrt{C \cdot n_d \cdot Z_0} \tag{4.2}$$

Wherein C is a constant and Z_0 is the impedance of free space. C stands for the mean of the combinations of the radiated power of the source with the propagation loss for each source. It includes also the number of sources per home. Transferring formula (4.2) into dB and the field strength E in dBµV/m results in formula (4.3)

$$E_d\,[\text{dB}\mu\text{V/m}] = 10 \log n_d + 10 \log C - 94.2 \tag{4.3}$$

Now we define

$$a_{hyp} \equiv 10 \log C - 94.2 \tag{4.4}$$

$$slope_{hyp} \equiv 1 \tag{4.5}$$

$$N_d \equiv 10 \log n_d \tag{4.6}$$

so we may write (4.3) as:

$$E_d = slope_{hyp} N_d + a_{hyp} \tag{4.7}$$

Now we arrive at a linear relation between E_d in dBµV/m and N_d. With this relation we assume a case of interval measures, implying we may apply the Pearson correlation test, using the Pearson product-momentum coefficient. The degrees of freedom is given by $df = m - 2$, where m is the total number of measurement samples.

We write for every measurement sample i:

$$N_i = 10 \log n_i \tag{4.8}$$

The averaged values are determined from:

$$av_N = \frac{1}{m} \sum_{i=1}^{m} N_i \tag{4.9}$$

$$av_E = \frac{1}{m} \sum_{i=1}^{m} E_i \tag{4.10}$$

The Pearson product-moment correlation coefficient r is following from:

$$r = \frac{covar\,(E_i, N_i)}{\sigma_N \sigma_E} \text{ with:} \tag{4.11}$$

$$covar\,(E_i, N_i) = \frac{1}{m} \sum_{i=1}^{m} \{(N_i - av_N)(E_i - av_E)\} \tag{4.12}$$

$$\sigma_N = \sqrt{\frac{1}{m} \sum_{i=1}^{m} (N_i - av_N)^2} \tag{4.13}$$

$$\sigma_E = \sqrt{\frac{1}{m} \sum_{i=1}^{m} (E_i - av_E)^2} \tag{4.14}$$

After r has been determined we must check whether the level of r is sufficient high for concluding hypothesis H_1 to be true. Therefore we must select a level of significance for the one-tailed test (α-level), which is giving the probability value for concluding H_1 is true while H_0 is true (false positive). In our study we select the much used value $\alpha = 0.05$.

Knowing m and α we read a minimum value for the Pearson correlation, r_{min}, from statistical tables, for example Table B6 from [60], or Table VI from [67]. In our study $m = 54$ in all cases. For example, a measurement series on all locations for the 80 m band, frequency 3.5 - 3.8 MHz, considering an area limited by a radius $d = 0 - 200$ m, we find a correlation $r = 0.831$, while $r_{min} = 0.227$ [$df = 52$; $\alpha = 0.05$]. So, for this band we may conclude that hypothesis H_1 is true, see reference [60].

4.3.2 Regression analysis

In the subparagraph above we showed that theoretically the accumulated MMN field strength, expressed in dBµV/m, is proportional with ten-fold the logarithm of the number of homes, with a hypothetical $slope_{hyp} = 1$. But what is the measured value of the slope?

To investigate this we calculate the regression line for each measurement ensemble. The regression line is described by:

$$y = slope \cdot x + a \tag{4.15}$$

The slope follows from the measurement results:

$$slope = \frac{\sum_{i=1}^{m} (N_i - av_N)(E_i - av_E)}{\sum_{i=1}^{m} (N_i - av_N)^2} \tag{4.16}$$

and

$$a = av_E - slope \cdot av_N \tag{4.17}$$

Herein is α the MMN field strength under assumption of $N = 0$, $n = 1$: so one home present in the measurement area. The level of confidence of the regression line can be

indicated by the F-ratio. For that the Squared Sum of the deviations from the regression line in the measurement samples, SS_{fs}, split up in a part related to the regression line, *predicted variability*, $SS_{regression}$, and a part that is related to the coincidence, *un-predicted or residual variability*, $SS_{residual}$, see ref. [60].

$$SS_E = \sum_{i=1}^{m} (E_i - av_E)^2 \tag{4.18}$$

$$SS_{regression} = r^2 SS_E \tag{4.19}$$

$$SS_{residual} = (1 - r^2)\, SS_E \tag{4.20}$$

From here the Mean Square values $MS_{regression}$ and $MS_{residual}$ are determined by dividing by the degrees of freedom, df, valid for these parameters:

$$MS_{regression} = \frac{SS_{regression}}{df} \quad \text{with } df = 1 \tag{4.21}$$

$$= SS_{regression}$$

$$MS_{residual} = \frac{SS_{residual}}{df} \quad \text{with } df = m - 2 \tag{4.22}$$

$$= \frac{SS_{residual}}{m - 2}$$

$$F = \frac{MS_{regression}}{MS_{residual}} \tag{4.23}$$

The regression line is considered to be significant when $F \geqslant F_{limit}$. This F_{limit} is depending on the number of sample pairs, and on α. Values for F_{limit} can be found in Table B.4 from [60], and Table A14 from [68]. F indicates whether the amount of variance accounted by the regression equation is significantly greater than would be expected by chance only, [60]. The outcome of this test is consistent with the result of the test using the Pearson correlation. So it is not necessarily to calculate F and do the test when the correlation test is already done.

A measurement series on all locations for the 80 m band, considering an area limited by a radius $d = 0$ to 200 m, is used here as an example. Figure 4.3 show the results of the regression analysis. The most important output parameter here is the slope. The level of confidence, F, is here 116.4, very much above the minimum $F_{limit} = 4.03$ [$df = 52$; $\alpha = 0.05$]. For this band we may conclude that hypothesis H_1 is true, like in the correlation test.

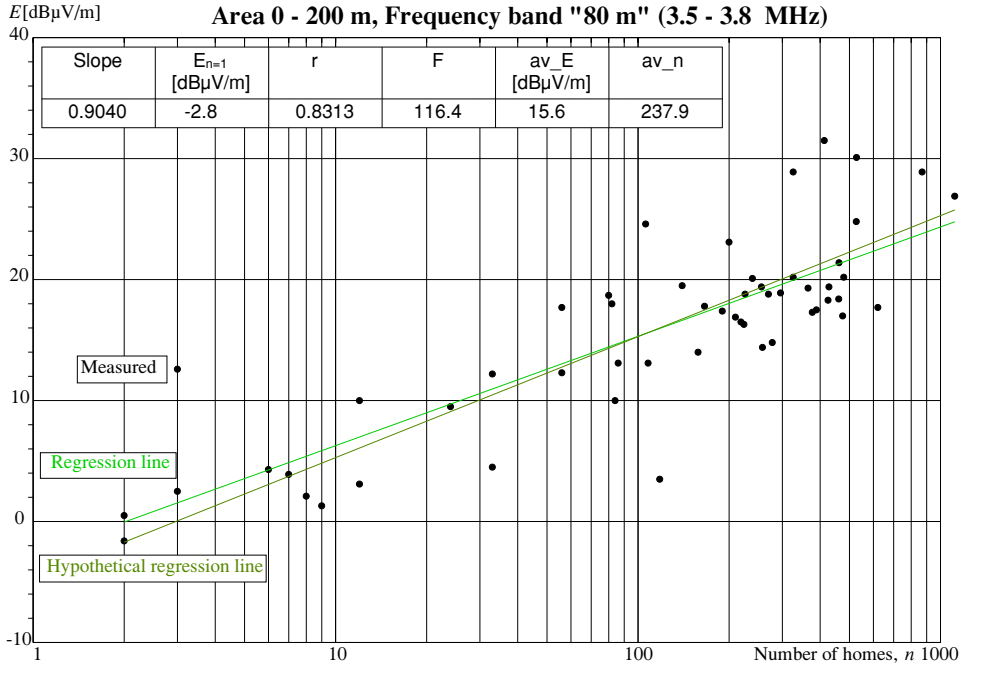

Figure 4.3. Example of a result from a regression analysis.

4.4 Results of the analysis

The results of the analysis concerns two metrics: (a) the correlation coefficient *r* and (b) the slope of the regression line *slope*. The results are ranked in order of the frequency band and in order of the selected part of the area wherein the number of homes has been counted. For all the 54 measurement locations the MMN field strength levels *E* are combined with the number of houses in that selected part. Thereby must be remarked that *E* is determined by all the noise sources in the wide area around the measurement locations, not only by those in the selected part. The goal of this analysis it to find out which parts have a dominant influence on *E*, and which parts have less influence. These parts may differ for each frequency band.

The correlation coefficient has a maximum value $r = 1$, indicating a 100 % correlation between field strength *E* and the logarithm of the number of houses within the selected area *N*. This means that *E* is proportional with *N*. In that case all measured values appear on a linear regression line, see Figure 4.3, and the constant *C* in the formulas (1) to (4) is invariable. *C* stands for the mean of the combinations of the radiated power of the source with the propagation loss. It includes also the number of sources per home. In practical situations there are strong variances in the radiated power and in the propagation loss for each sample, reflected in variances in *E*.

In case of $slope \neq slope_{hyp}$ (= 1) the slope of the measured regression line indicates a systematic deviation in the proportionality of E to N, deviating from the assumption that the field strength e increases with the square root of the number of homes. It shows to what extent sources in homes in the selected area part are participating in the accumulation that lead to the measured level E. Nearby the measurement location this participation is nearly 100 %, resulting in $slope \approx 1.0$. Further away the influence of the sources will decline because of the increased propagation loss, although the number of sources is increasing by the larger radius. Especially the increase of the propagation loss with distance is an unknown factor. Ground-wave propagation is assumed to be the main propagation mode, but the complex conductivity of the ground in residential areas is not well known, and besides that the houses and buildings will scatter the MMN radiation, as well as providing extra loss and shielding. Also buried cables and pipelines may influence the propagation in a positive, as well as in a negative way. Overhead cables cannot have effects in this study, because there are no there are no overhead cables in the Netherlands. Propagation loss is a subject of further study, to be treated and measured in the Chapters 5 and 6.

Assume that in a certain part A of the studied area on all measurement locations, for example the most outward ring 400 - 500 m, no MMN radiation reaches the measurement location M, and so will not attribute to the total noise power, indicated by the measured field strength E. The other parts of the area do contribute noise power. In that case we expect no correlation, thus $r = 0$. However, in practice this is not completely true because in general the habitation density in that ring 400 - 500 m and the density at other distances are correlated to a certain extent. So we see a reduced correlation factor r, but not being zero.

Likewise we expect in this situation that $slope = 0$ because E must be independent of N for the homes in area part A. Again, in practice the slope will be higher because of the correlation in the habitation densities between different parts. The conclusion is that a strongly reduced influence of sources in more distant homes will be visible as a reduced correlation factor r and a reduced slope, without r and $slope$ necessarily approaching zero. Taking this into consideration, we conclude that already small differences in r are meaningful.

Measurement data from 54 measurement locations and 12 frequency bands have been processed according the earlier described methods. Two sub-methods have been used. In the first method areas has been defined using cumulated distances from zero up to a limit 50 m, 100 m, ... 500 m. In the second sub-method annuluses has been defined with a minimum and a maximum radial distance, 0 to 50 m, 50 to 100 m, ... 400 to 500 m. Two sets of graphs are resulting. Figure 4.4 shows the correlation factors for each frequency

band as a function of the maximal distance *d*. The figure is split up into four subgraphs, each containing three of the twelve frequency bands.

Except the 635 m band all bands show a maximal value of the correlation factor *r* for the distance of 100 to 200 meter. The 635 m band shows a maximum at 300 m. Generally spoken, the shorter the wave length the stronger is the roll-off of *r* with distance. This is in line with the expectation that the noise components with shorter wave lengths experience higher propagation losses than those with longer wave lengths. Examining these results one must bear in mind that in all analyses all measurement data from all 54 locations is used.

Figure 4.5 shows the slope of the regression lines as function of the radius of the area of accumulation. The hypothetical value of this slope is also plotted here. One can observe that the deviation from the hypothetical value increases with distance, implying that noise sources at larger distances have a reduced influence on the total noise level at the measurement position.

The roll-off of the correlation factor *r* with distance is visible with cumulated area parts (Figure 4.4) as well as with annulus area parts (Figure 4.6). However with annular area parts there is a small dip at the annulus 50 - 100 m for the most frequency bands. This dip is not visible with the cumulated area parts (Figure 4.4). For both types of area parts can be concluded that there is a maximum in the correlation at distances from 100 to 200 m, except the lowest band (635 m) where the maximum with cumulated area parts occur at 300 m distance. It is remarkable in the Figure 4.5 and Figure 4.7 that *slope* is around 1.0 in the first area part, 0 - 50 m, and decreases sharply at larger distances. The reason for this effect is not clear. As it is visible with long and with small wave length a cause by the near field effect is not plausible. The effect is stronger when area parts are taken as annuluses (Figure 4.7) than as cumulated area parts (Figure 4.5).

Summarizing, the perceived correlation factor *r* between MMN field strength at the measurement positions and the number of houses in all parts of the measurement areas is high and supporting hypothesis H_1. The decline of the correlation factor, as well as the slope of the regression lines, over distances of 300 m indicates that mainly the noise sources at distances below 300 m determine the cumulated noise floor.

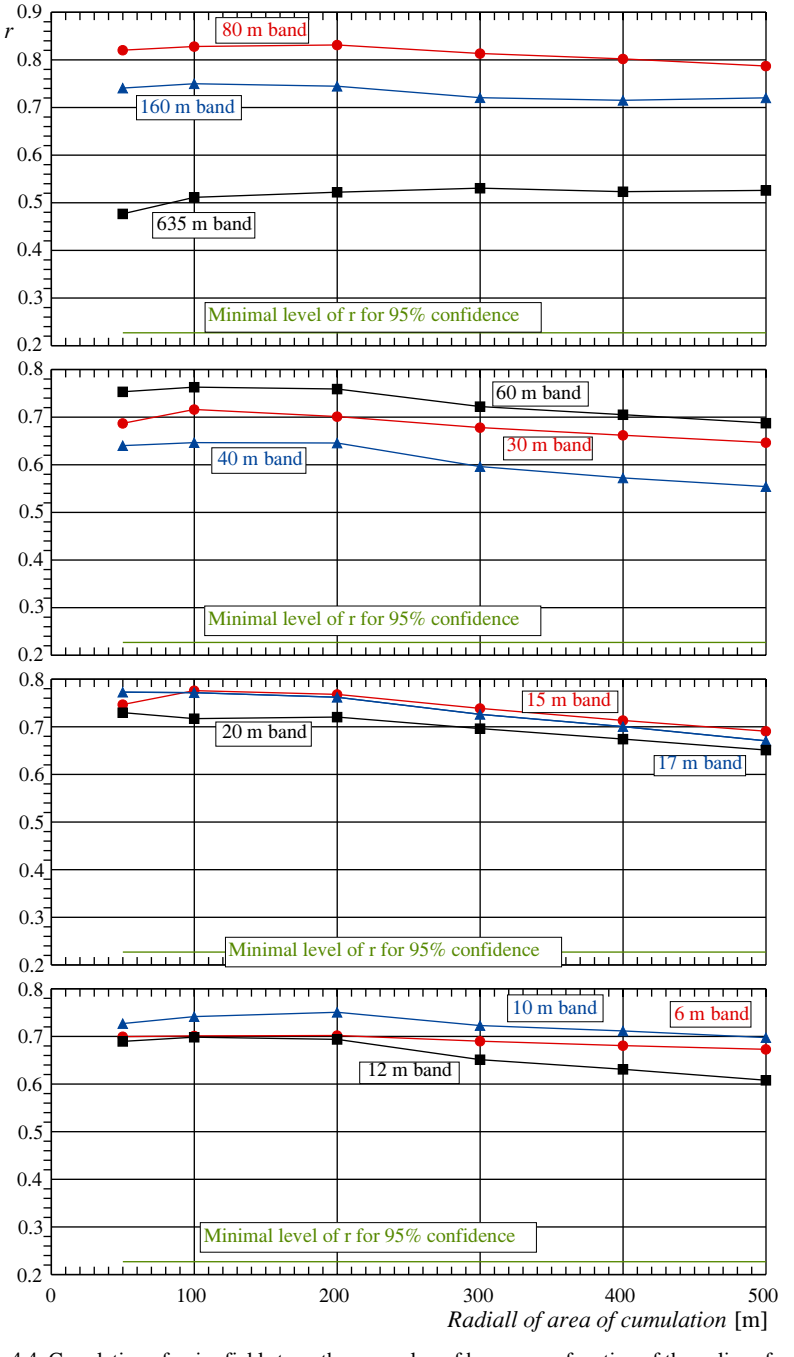

Figure 4.4. Correlation of noise field strength vs. number of homes as a function of the radius of area of accumulation.

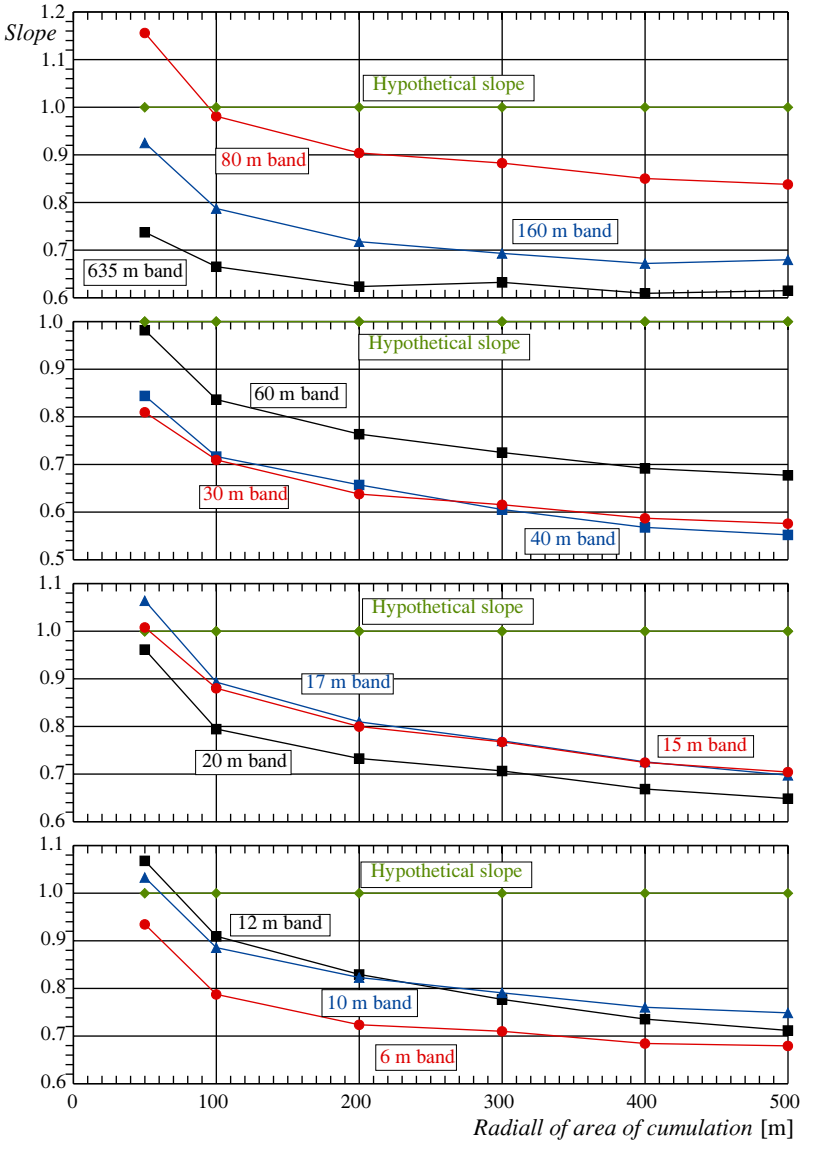

Figure 4.5. Slope of regression line of noise field strength [dBμV/m] vs. number of homes as function of the radius of area of accumulation.

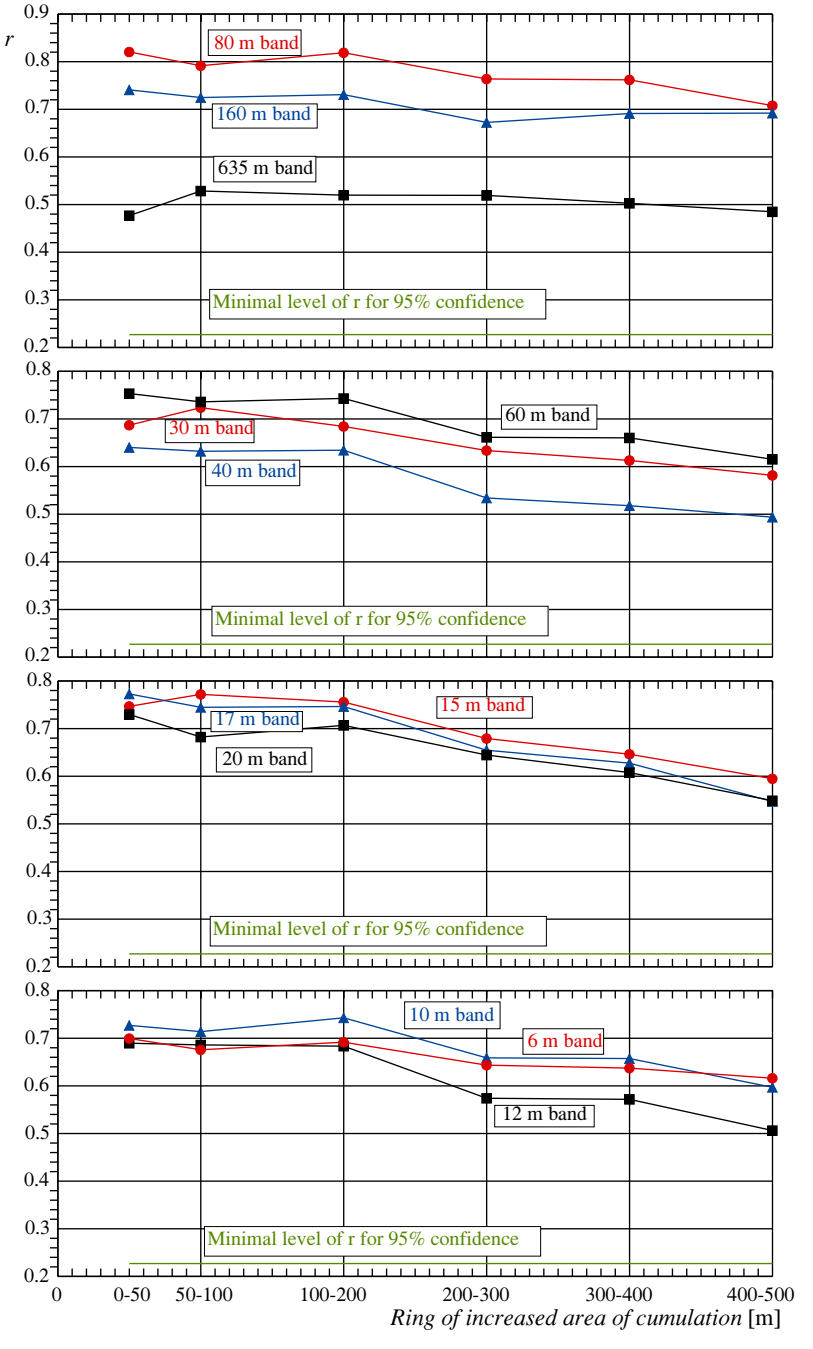

Figure 4.6. Correlation of noise field strength vs. number of homes as a function of the annulus of accumulation.

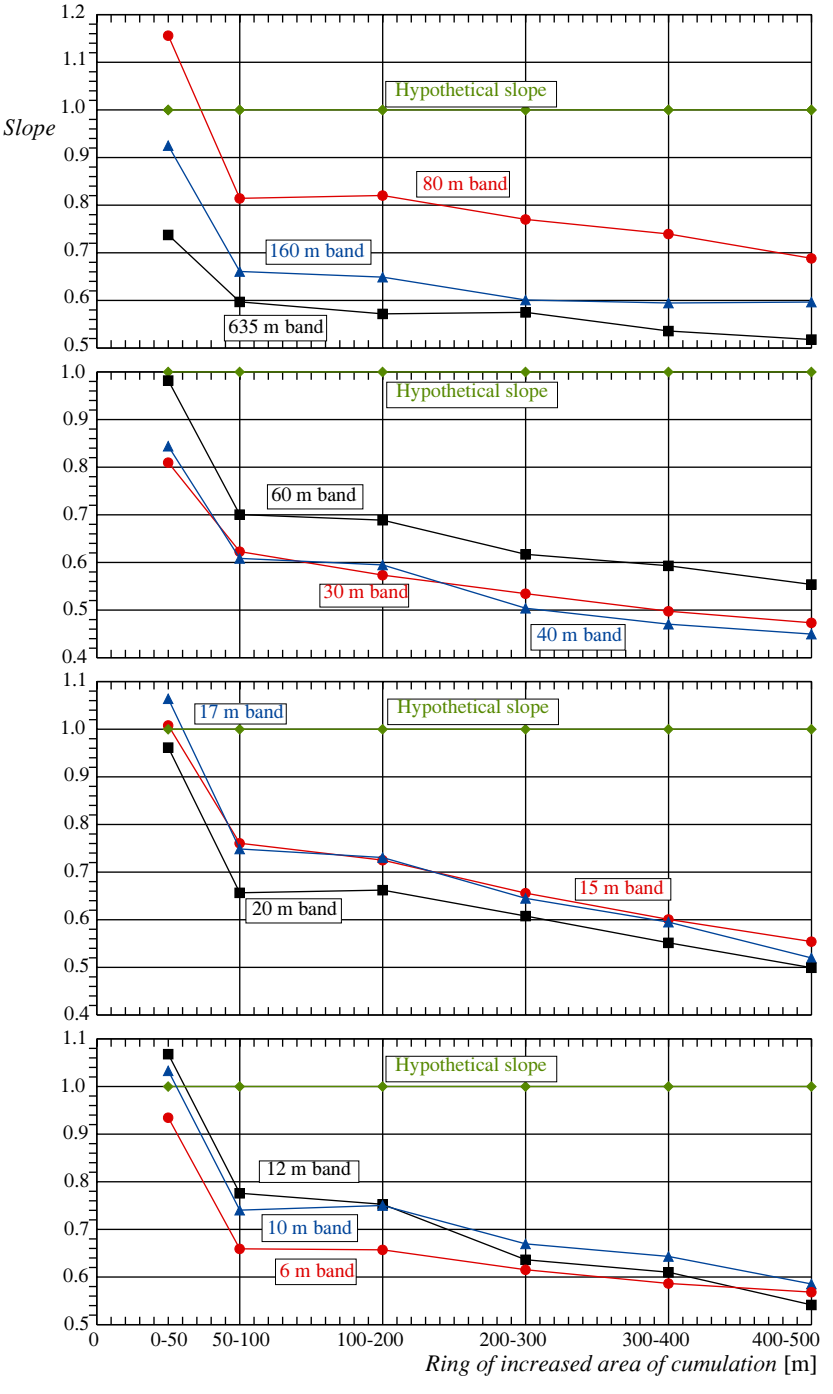

Figure 4.7. Slope of regression line of noise field strength [dBμV/m] vs. number of homes as a function of the radius of the annulus of accumulation.

4.5 Conclusions

In this study a strong correlation is found between the density of homes in any area around the measurement location and the measured MMN field strength, at least up to a distance of 500 meter from the measurement location, confirming the hypothesis of a logarithmic relationship between the density of habitation and field strength. This result proves that the in this campaign measured noise floor levels are mainly the result of accumulation of noise power from a large number of small sources spread in the houses, instead of being caused by a single, or a few, strong sources. This strong correlation is decreasing at distances over 300 m, implicating that the noise floor is mainly determined by the source densities at short distances up to 300 meter. Aforementioned conclusion is further supported by the observation that the slope of the regression lines increasingly deviates from the hypothetical slope at ranges over 300 m from the measurement location.

Chapter 5

5 Propagation measurements and analysis on MF and HF bands in urban areas in The Netherlands

A second measurement campaign is described in this chapter, based on the paper "Propagation measurements and analysis on MF and HF bands in urban areas in The Netherlands", publication [IV].

5.1 Introduction

In a study on the accumulation of man-made radio noise (MMN) by large numbers of noise sources, the propagation of the EM waves from individual noise sources to the point of aggregation is very relevant. MMN in the frequency range of 0.47 to 50 MHz was investigated earlier [II] and treated in Chapter 3. A further statistical study of the measurement results revealed that there is a strong correlation between the measured noise floor and the density of habitation [III], reproduced in Chapter 4. These results raise the question of how does the radio noise propagate in these populated areas, and what is the propagation loss with distance. In the earlier mentioned frequency range, the wavelength vary from 6 to 600 m. As the field strength measurements were done at an antenna height of 2 meters, and the sources are located in homes mostly at the first, second or third floor, or in more dense areas in higher apartment buildings, these heights are also relatively low compared with the wavelength. So, a very reasonable presumption is that the propagation may be described by the theory of the ground-wave (GW) propagation.

For a good understanding of this theory we will look into a part of the history. After

Marconi had proven the ability of long range radio communication by his transatlantic experiments in 1901 the need for a theoretical explanation was first fulfilled by Zenneck [69] and Sommerfeld [70]. Zenneck introduced a surface wave as a solution for the Maxwell equations. Sommerfeld analysed the case of a vertical Herzian dipole over a lossy ground, and came also to the surface wave as described by Zenneck, hereafter called "Zenneck Surface Wave", ZSW. The main property of this ZSW is that the energy is trapped on the surface, and that the roll-off with distance is 10 dB/decade, instead of 20 dB/ decade for a wave in free space. Starting in 1936 Norton showed in [71], [72], [73] that the ZSW could only exist under extreme conditions, and that Sommerfeld had made a mistake in his theory by a faulty interpretation of the square root of a complex variable, this resulting in the so-called "sign controversy". A complete overview of this history can be found in [74] and in [75].

Norton defined in [76] the GW as "A Radio Wave that is propagated through space and is, ordinarily, affected by the presence of the ground", with excluding any other reflections than against ground, as for example the ionosphere. In his solution the field strength E at a distance d from a transmitting antenna, a vertical dipole or a magnetic loop with the winding in a vertical plane, is given by an equation in [76], showing a sum of three terms:

$$E = \frac{E_0}{d}\left[\cos^3\psi_1 e^{i2\pi r_1/\lambda} + R\cos^3\psi_2 e^{i2\pi r_2/\lambda} + (1-R)f(P,B)\cos^2\psi_2 e^{i[2\pi(r_2/\lambda)+\phi]}\right] \quad (5.1)$$

Direct wave, Ground-reflected wave, Surface wave.

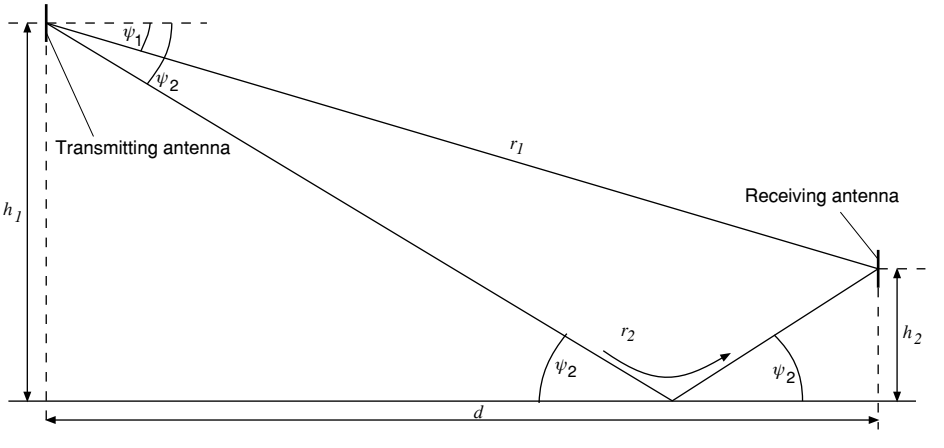

Figure 5.1. Ground-wave model according Norton.

Most parameters are defined in Figure 5.1. R is the reflection coefficient of the ground, P and B are the "numerical distance" and his phase angle for elevated antennas, as defined by Sommerfeld. The three terms are corresponding respectively to the direct wave, the ground reflected wave, and the surface wave. The last one is generally called the "Norton

Surface Wave", NSW. In the derivation by Norton the NSW is mathematically the result of the subtraction of the optically reflected Reflected Wave from the total of wave energy that is interacting with the ground. When the transmitting and the receiving antenna are close to the ground with respect to the wavelength the direct and the reflected wave will cancel, so the NSW is left. It is important to realize that the NSW is not trapped on the surface, in contrast to the ZSW, and that the roll-off with distance is minimal 20 dB/decade of distance. The values of the attenuation can be looked up on graphics in [57], a description is given in [58], and may be calculated by means of a computor program GRWAVE [77].

In this study, propagation in urban areas, all three wave paths in the GW theory are involved. The distance varies from 50 to 1000 m. In the measurements the transmitter antenna is at a level of 3 m and the receiving antenna at 2 m. That means that generally the direct and reflected wave are cancelling each other, but that especially for the short distances and for the upper part of the frequency range, the direct and reflected wave may play a role, next to the NSW. For all three paths the buildings may damp, reflect, or scatter all three waves. Especially tall vertical constructions as street lamps, towers, etc. may cause scattering, which, depending on conductivity and the ratio between height and wavelength, may cause forward, back, and random scattering. Buried conductors in the earth, like all kinds of cables and metal pipes, may enhance the ground conductivity, so decrease the attenuation of the surface wave. This is especially the case at the lower frequencies with the greater skin depth, see Table 2.1 in Chapter 2. Also overhead cables may cause a considerable increase of propagation, but the mechanism is very different from propagation by cables in the ground. We must remark here that overhead cabling is not used in The Netherlands, so does not play a role in our measurements.

In the last decades propagation studies, theoretically and empirical, [78], [79], are mostly concentrated on VHF and UHF frequencies, especially in urban areas. In this frequency range the wavelength is small to very small with relation to the dimensions of the objects in that environment. For the MF and HF range the wavelengths are larger or equal to these dimensions. This also means that in the VHF/UHF range the wave interaction with the ground is less relevant and that free space, reflected, and scattered paths dominates. As a consequence these studies are not relevant in our case.

There is a very limited number of studies about propagation in urban areas on frequencies below 30 MHz, and they are in essence limited to Medium Wave broadcasting signals. In [80] an extensive measurement campaign and theory building has been performed about the propagation from a local MW transmitter site North of London, through the city centre to the South of London, with a total range of 60 km. Three frequencies were involved, and interesting phenomena were recorded and theoretically

explained. Herein the built-up environment with its buildings was modelled as a "bed of nails" like structure. However, in our study the relevant frequency range is higher, and the distance much shorter. In [81] field strength measurements were performed on the propagation of a local MW transmitter in São Paulo, Brazil. One of the results that were reported is: "the prediction model of Rec. ITU-R P.368-9 overestimates the measured field during daytime". Consequently the GW propagation losses were higher than expected. In [82] propagation measurements on HF frequencies were reported in open desert areas, as well as in urban environments. The conclusion in this report was that the losses in open areas matched the expectation within a few dB, but in urban areas a diversity of propagation losses was found when measured the GW propagation path, and varied all over the city. Reference [83] reports a new MF and HF GW propagation model for urban areas. It includes a fundamental addition to the Norton model by building-complex parameters and height-gain factors. The model applies for areas with high and tall buildings in particular. Only validating measurements at the medium wave frequencies were reported.

We conclude that the existing models for propagation below 30 MHz handle urban areas as a local disruption in a wider area, mainly for the purpose of coverage studies of broadcasting transmitters. For our application, being short range intra-urban propagation of man-made noise in the MF and HF range, there is no sufficient scientific information available about measurement data, nor theoretical models, useful for a statistical modelling of accumulation of spatial spread noise sources, so leading to a conclusion that a measurement campaign was necessarily.

The chapter is organized as follows. In Section 5.2 we describe the measurement methods, in Section 5.3 the data processing and some theoretical aspects. Section 5.4 describes the statistical analysis and the results thereof. Our conclusions are summarized in Section 5.5. In Subsection 5.6.1 we describe validation measurements. In Appendix E we calculate the field strength above Perfect Electric Conducting (PEC) ground. In the end Appendix F derives the equations to make field strength measurement corrections in the near and intermediate field.

5.2 Description of the Measurements

The goal of the measurement campaign is to gather statistical data about transmission loss as a function of distance, frequency, and of density of habitation. Thereto we need measurements on several locations in diverse environments. From the list of measurement locations, earlier used in Chapter 3, we selected a number of 16, and enumerates them in Table 5.1.

TABLE 5.1. Overview of measurement locations.

Location			Number of homes in radii of the annuluses [meter]							Environment	
No.	Call sign	City	0-50 [m]	50-100	100-200	200-300	300-400	400-500	Total	Type	Group
1	PA0RLM	Driebergen	6	2	48	108	258	249	671	Rural	I
2	PA3AWN	De Heurne	3	10	11	35	26	23	108	Res. 1	
3	PA0RYL	Huis ter Heide	5	15	98	147	54	49	368	Res. 1	
4	PA0JMG	Drachten	7	7	66	110	107	130	427	Res. 1	
5	PA0WTA	Apeldoorn	6	14	62	225	261	225	793	Res. 1	
6	PA0HTT	Ommen	12	54	153	176	144	112	651	Res. 2	II
7	PC7M	Goor	23	43	158	133	158	193	708	Res. 2	
8	PA0VBR	Nijmegen	27	71	160	184	338	379	1159	Res. 2	
9	PC0WP	Hengelo(Ov)	11	39	108	358	313	423	1252	Res. 2	
10	PA1AT	Assen	24	63	152	382	406	308	1335	Res. 2	
11	PB0AIR	Hengelo(Ov)	31	64	366	363	447	626	1897	Res. 2	
12	PA0WJG	Nieuwegein	22	55	348	540	446	518	1929	Res. 2	
13	PA0RSM	Amersfoort	30	86	210	407	323	452	1508	Res. 3	III
14	PA3BME	Driebergen	21	94	274	446	407	441	1683	Res. 3	
15	PA3GXD	Meppel	52	106	369	511	533	575	2146	City	
16	PH1E	Eindhoven	34	57	274	448	656	715	2184	City	

They all belong to contributing radio amateurs, the locations are coded in the table and further on in accordance with their radio call signs. Also the city is given and numbers of homes around that locations. The type of environment is given as defined in Chapter 3, and listed below:

1 Quiet Rural area: No residences, no infra structures within 1.5 km radius.

2 Rural area: up to 10 residences within a radius of 100 m, but at a distance of at least 100 m outside built-up area.

3 Residential area-1: 11 - 50 residences within 100 m.

4 Residential area-2: 51 - 100 residences within 100 m.

5 Residential area-3: >100 residences within 100 m.

6 City area: large apartment buildings, commercial & city centres:

   a residences directly surrounded by shops and other city centre activity, or

   b the number of residences within a radius of 100 m is larger than 150, or

   c the number of residences within a radius of 500 m is larger than 2000.

The location groups, as defined in Table 5.1, are based on the types residential 1 - 3, but supplemented with one rural (location no. 1, which literally fulfils the definition of type rural, but is enclosed in urban area), and for group 3 the residential type 3 is supplemented with two location from the city type. The decisions here and the cut-offs are based on a study of the topographic maps of the locations, resulting in heuristic decisions. The

measurement locations are in the Netherlands, and so have some restrictions. First, the areas are all flat, and secondly, the focus is primary on the civil HF listeners/users, they mostly live in residential areas. Metropole-like city centres with large numbers of high-rise buildings are not included.

Photo 5.1. View of the beacon transmitter.

The principle of the measurements is based on placing a low power beacon transmitter at a fixed location and drive with a mobile field strength (FS) measurement system in a fixed trajectory from that location away up to a distance of about 1 kilometre and back via a different path, depending on the local topography, and selectively measuring the field strength generated by that beacon transmitter. This drive is repeated for all test frequencies over the same trajectory: 1.85 (160 m wavelength), 3.57 (80 m), 7.07 (40 m), 14.07 (20 m), 21.07 (15 m), and 28.07 MHz (10 m). During the drive repeatedly measurement samples

are taken at random varying distances 8 - 16 meters between themselves, resulting in a high number of samples.

The special designed beacon transmitter consists of a 19 inch cabinet, a 4 m high rod antenna, and two metal plates forming a counterpoise grounding, see Photo 1. Next to the transmitter, a commercial Elad FDM-DUO SDR transceiver, the cabinet contains an antenna matching circuit and a Morse code ID generator, which modulates the transmitter carrier in Frequency Shift Keying (FSK) with a shift of 100 Hz. That shift is well within the bandwidth of the measurement receiver, so that the measurement is not disturbed by the ID transmission. The transceiver output power is set at 1 Watt. The RF carrier is measured at the measurement receiver. In principle this includes noise within the receiver bandwidth, but during the measurements the level of the beacon signal is that strong that external and internal noise does not contribute to the measurement result significantly.

For calibration the field strength has been measured at a distance of 25 m on a flat and undisturbed piece of grass land by using a calibrated magnetic antenna, the Rohde & Schwarz Z2 loop antenna. For the near and intermediate field regions (lower frequencies) corrections were made according correction factors, derived in Appendix F. Also for ground losses (upper frequencies, very small) compensations, calculated with GRWAVE, [77], has been calculated and applied. From these measurements the actual effective isotropic radiated power (eirp) has been calculated for each test frequency. The eirp values are to be used as calibration numbers in the post-processing of the field strength measurements.

The mobile FS measurement system was build in a passenger car. On the roof an active E-field antenna system is mounted, see Photo 5.2. The antenna groundplane as shown is well grounded on the roof and the bodywork of the car by a low impedance capacitive coupling through two self-adhesive copper strips on the roof, behind the luggage carrier strips. The capacitance per strip is 10 nF. Figure 5.2 shows the principle diagram of the measurement system, and Photo 5.3 the equipment inside the car.

The calibration of the mobile FS measurement system has been carried out for the system as a whole, including the car. The reference antenna method has been used, using the same Rohde & Schwarz EZ2 loop antenna as a reference as also used for calibration the transmitter. A beacon transmitter at a distance of 40 meters produced a vertical polarized test signal.

The reference antenna was positioned at the same height as the E-field antenna on the car. For the frequencies, where the E- and H-field diverge because of the effects in the near and intermediate field regions, a compensation has been made, see Appendix F. Also the directivity of the mobile setup has been measured at 5 directions from 0° (front) to 180°

(back of the car). For all test frequencies a small difference in antenna factor was observed, maximal sensitivity for a signal arriving at the front of the car, and a minimum in the sensitivity for signals arriving from the back side of the car.

Photo 5.2. Antenna system for propagation measurements. Mobile receiver side.

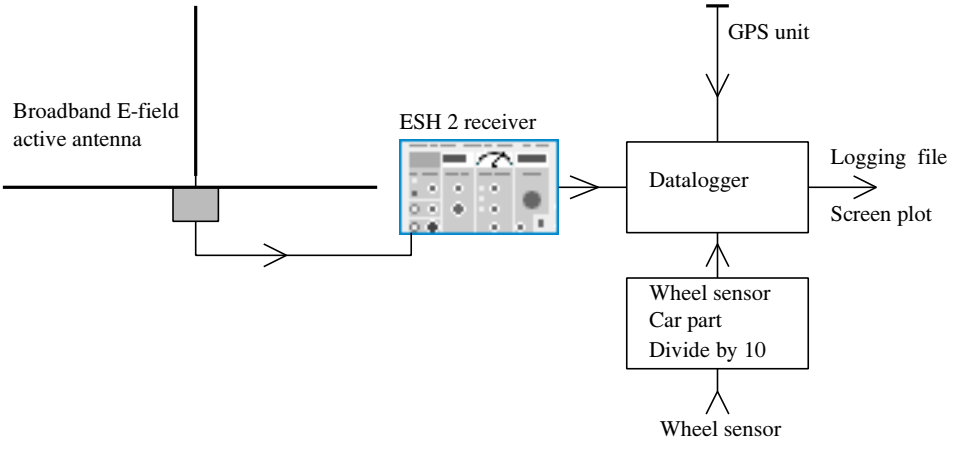

Figure 5.2. Setup of the mobile field strength measurement system.

The amplitude of this directional variation is lowest at 1.8 MHz: 0.3 dB, and highest at 25 MHz: 1.3 dB. For each test frequency a cosine function approximation has been derived. An algorithm has been developed for a real time estimation of the direction of arrival of the beacon signal during the measurement drives from the GPS data, using the stored location of the beacon, and so to compensate for directional variations in the antenna-factor.

For validating the measurement system and method measurement drives has been performed in flat and open areas as described in Subsection 5.2.1. Concerning seasonal effects on the propagation loss, monthly measurements were carried out throughout a full year, from September 2019 to November 2020, on a fixed traject, partly in populated area, and partly over open land. A clear relation with seasonal variation in soil humidity was found, but the maximal deviation from the median on the loss measurement, as caused by a total of 10 % to 90 % spread, was very limited, and varied from 1 (1.8 MHz) up to 3 dB (28 MHz). As a result no corrections were applied in our urban measurements. A more extensive description of this experiment is given in Chapter 6.

Photo 5.3. Measurement equipment installed in a Peugeot 307 passenger car.

5.2.1 Validation Measurements

To validate this method of measurement of the propagation loss a number of validation measurement has been carried out. By definition these measurements should be done outside residential areas in open fields where the ITU GW propagation model according [57], [58], [77] should apply. As the ground in residential areas has been paved for a large part, also for the reference measurements two traject with a concrete surface were sought. The three trajects, all in the Netherlands, were:

1 A 3 km long, nearly straight, farmer's road near Kloosterhaar, brick road, vast open area, grown crops, only two trees halfway the road. Groundwater level: -

1.2 m.

2 A 1000 m long, 25 m wide, runway of the general aviation airstrip near Drachten, asphalt concrete. Small airport building 150 m from the beacon location, business area at 150 m distance next to the runway at the far end.

3 A 2 km long, 50 m wide, decommissioned part of the 3 km runway of the military airbase Deelen, asphalt concrete, forest at 400 m distance at one side next to the runway. Dry sandy soil.

The measurement results are shown as normalized field strength levels next to calculated field strength levels according the ITU GW propagation model for a series of standardized types of ground, and for Perfect Electric Conducting ground (PEC), all for an isotropic effective radiated power of 1 Watt. The measurements are performed at ten frequencies in the range from 1.8 to 28 MHz. Because of limited space we will show the plots of six well spread frequencies here, showing the three locations together.

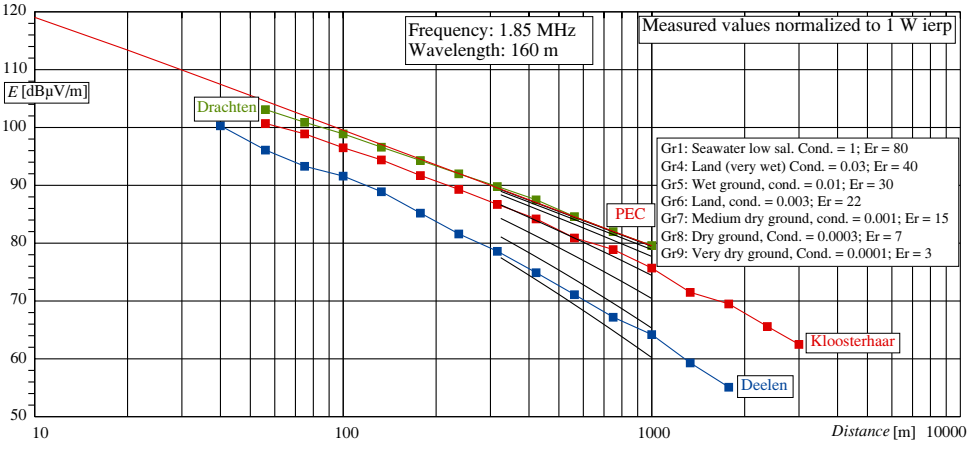

Figure 5.3. Field strength roll-off with distance, measured and compared with ITU GW propagation model at 1.85 MHz. Notice: the curve Gr1 for sea-water is fully covered by the PEC curve, and so invisible.

A few observations we will mention here. In the measurements at Kloosterhaar we see a good propagation for lower frequencies and bad propagation for the higher frequencies. We explain that by the influence of the groundwater causing an enhanced conductivity deeper in the ground, having influence at the longer wavelength. At the higher frequencies the extra losses caused by vegetation is having an effect, especially the effect of the 2 meter high crops in the distance range of 200 to 700 m is visible. At Deelen the underground is sandy and dry, so bad propagation for low frequencies, but for the high frequencies the effect of the runway pavement appear to be relevant. In the measurement on the runway of

Drachten the conducting effect of buried cables from decommissioned runway lighting is showing up on the lower frequencies. We conclude that these measurements show results being well inside the range we might expect, and so validate the measurement system and method.

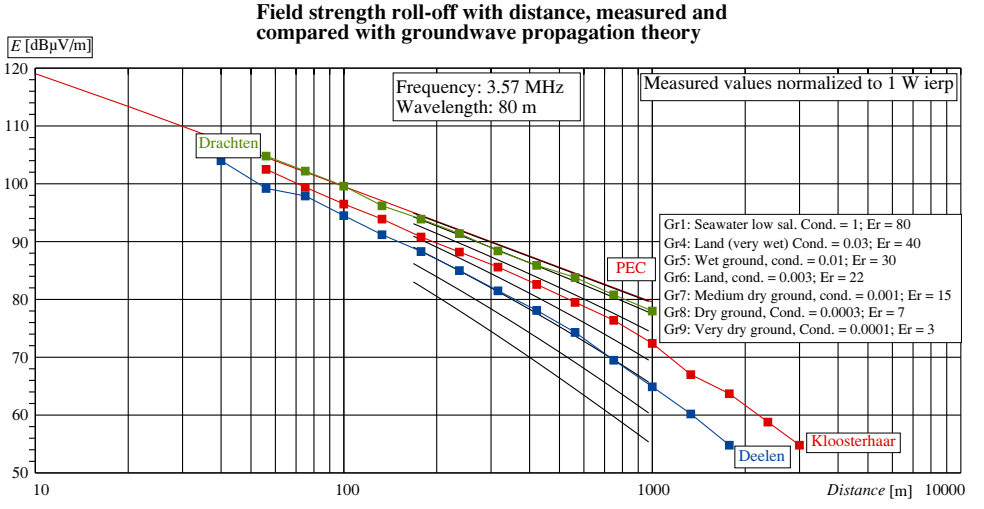

Figure 5.4. Field strength roll-off with distance, measured and compared with ITU GW propagation model at 3.57 MHz.

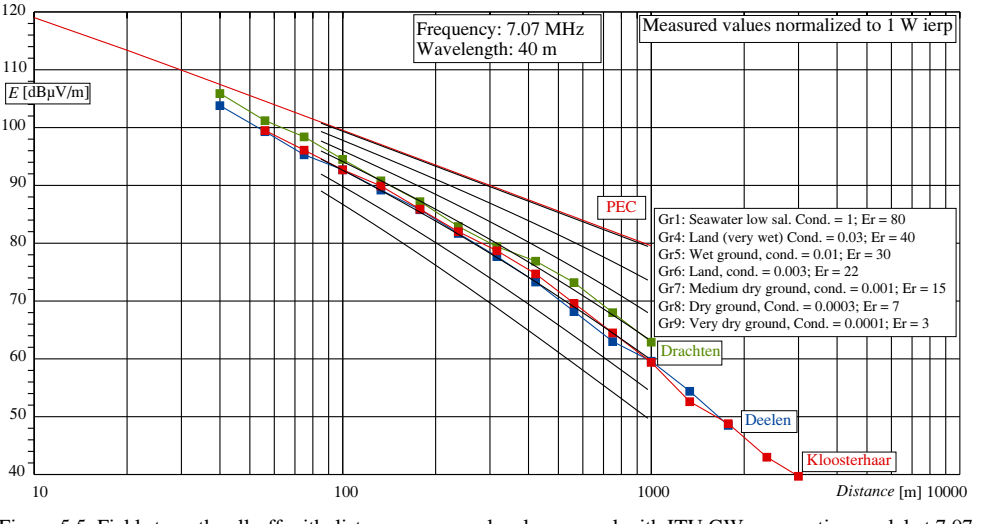

Figure 5.5. Field strength roll-off with distance, measured and compared with ITU GW propagation model at 7.07 MHz.

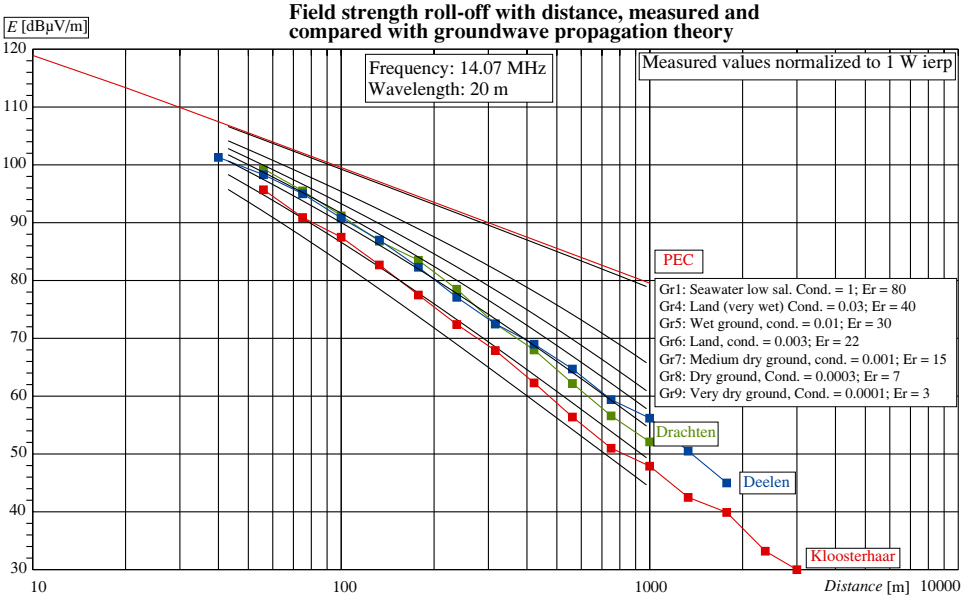

Figure 5.6. Field strength roll-off with distance, measured and compared with ITU GW propagation model at 14.07 MHz.

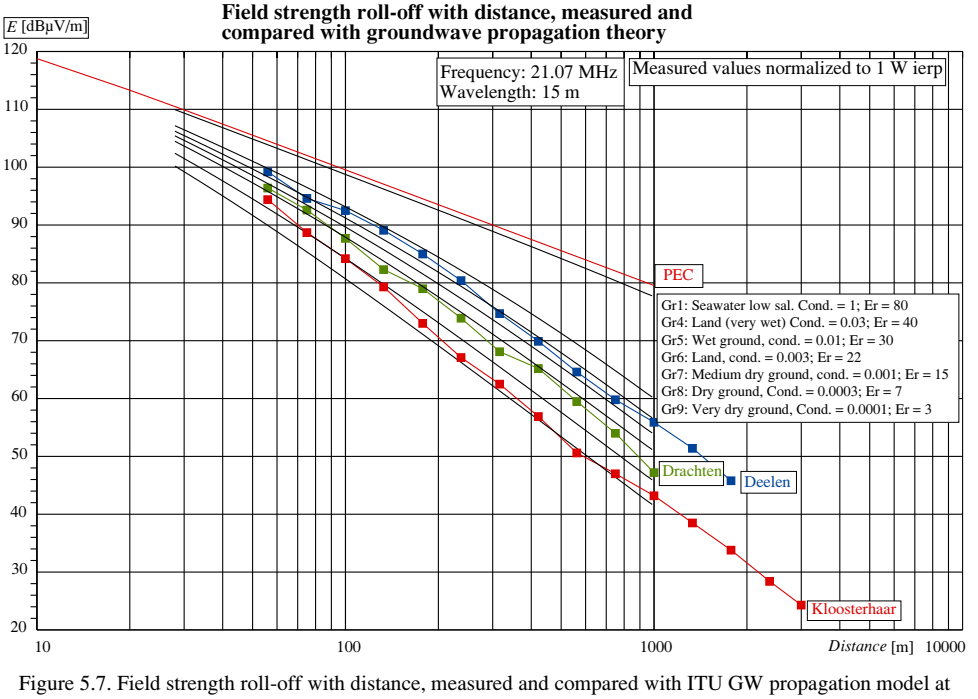

Figure 5.7. Field strength roll-off with distance, measured and compared with ITU GW propagation model at 21.07 MHz.

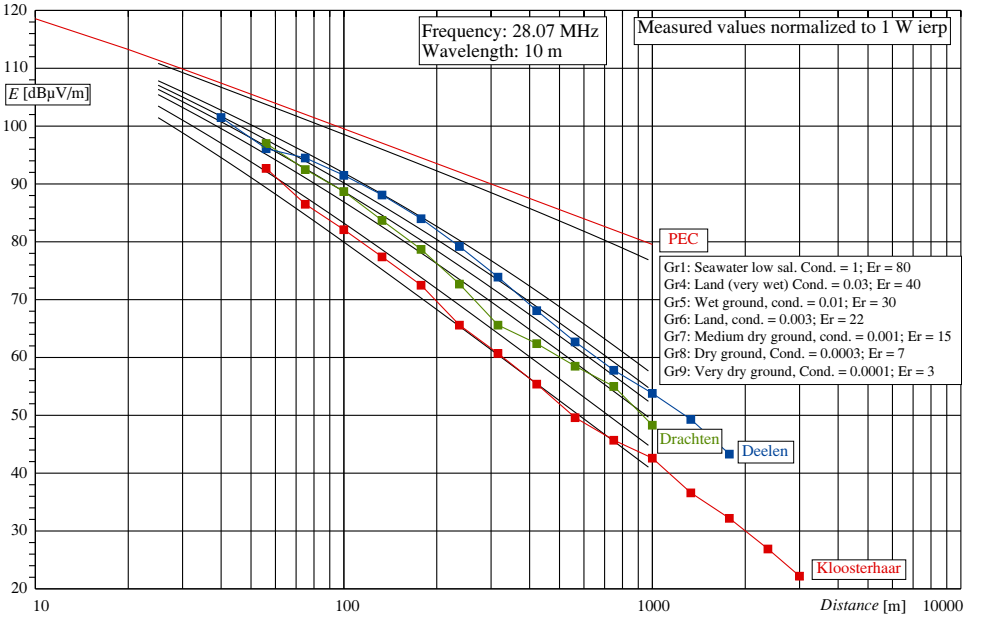

Figure 5.8. Field strength roll-off with distance, measured and compared with ITU GW propagation model at 28.07 MHz.

5.3 Data Processing

5.3.1 Decimation of samples and the statistical approach thereof

For the purpose of the accumulation study an estimator is required in this experiment that is representing the propagation loss. We take here the expected value from the probability distribution function (pdf) of the propagation loss, thus the mean value μ in the pdf. But actually, samples of FS levels are measured and normalized for an effective isotropic radiated power of 1 Watt. These FS levels are used as an intermediate result, they can be used to compare with the FS levels that are resulting from calculations according the ITU GW propagation model.

In the post processing the measurement samples are grouped into bins, representing ranges of distances. The samples, inputted in those bins, can be measured on a single location, on a group of locations, or on all locations. They may be combined during the post processing in those bins. In this way a kind of parallel processing is achieved from: 1st the individual locations, 2nd the three groups of locations with comparable density of habitation, and 3rd from all measurement locations totalized together.

From each bin an average value *Av* and a median value *Me* from *N* samples can be calculated. Generally, *Av* appear to equal μ nearly in the measurement results. For higher numbers of *N Av* and *Me* approach the pdf mean, and so the mean value, μ. In this case we

use the linear values of the field strength e for the statistical calculation, and the results are converted back in logarithmic values E [dBμV/m]. The statistical processing is complicated by the fact that we need to convert FS values into a linear quantity, μV/m, on which we can apply the statistics. Further arithmetic and presentations are usually done in logarithmic quantities, e.g. in dBμV/m (FS) or dB (propagation loss). For the average and median values this is not a problem as they can be converted from linear quantities into dB and *vice versa* unambiguously. But deviations translate from linear into logarithmic values for a negative and for a positive deviation differently. This makes it necessarily to define and describe the complete processing procedure.

Each bin delivers an average value e_{Av}, $E_{Av} = 20 \log e_{Av}$, and an estimated Standard Error e_{SE}. The error will be split up in the logarithmic quantities E_{SE+}, and E_{SE-},:

$$E_{SE+} = 20 \log \left(\frac{e_{Av} + e_{SE}}{e_{Av}} \right) \tag{5.2}$$

$$E_{SE-} = 20 \log \left(\frac{e_{Av} - e_{SE}}{e_{Av}} \right) \tag{5.3}$$

Herein is $E_{SE+} \geqslant 0$, $E_{SE-} \leqslant 0$, and because of the asymmetry in the ratios $|E_{SE-}| \geqslant E_{SE+}$. The median FS value E_{Me} has to be normalized for an effective radiated power from the beacon transmitter of 1 Watt:

$$E_{N,Me} = E_{Me} - P_{tx} \text{ [dBW]} \tag{5.4}$$

P_{tx} is the effective isotropic radiated power as measured by the calibration of the beacon transmitter. To calculate the propagation loss L the FS median is subtracted from the FS that would be measured when the ground is Perfect Electric Conducting, PEC:

$$L_{Me} = E_{PEC} - E_{N,Me} \text{ [dB]} \tag{5.5}$$

$$l_{Me} = 10^{(L_{Me}/20)} \tag{5.6}$$

Because of the sign in (5.4) the standard errors in L will be reversed:

$$L_{SE+} = E_{SE-} \quad (\leqslant 0) \tag{5.7}$$

$$L_{SE-} = E_{SE+} \quad (\geqslant 0) \tag{5.8}$$

Inversely, the linear standard error in the propagation loss l is:

$$l_{SE} = l_{Me}(1 - 10^{(L_{SE+}/20)}) \tag{5.9}$$

$$= l_{Me}(10^{(L_{SE-}/20)} - 1) \tag{5.10}$$

In this way we arrive at the same value for both polarities of l_{SE}, so one calculation suffice. In the graphics we use a dB scale, so there the both dB values L_{SE+} and L_{SE-} are used.

5.3.2 Field strength measurement results

The recorded measuring results are processed according the subsection above per group of locations and per frequency. First we consider the FS results, normalized to an effective isotropic radiated power of 1 Watt. In Figures 5.9 - 5.12 the normalized median values of the measured field strength levels are plotted for the three groups of locations and all locations totalized.

Also the calculated FS values for PEC and for seven types of ground according [57] are shown. We learn from the plots that the measured FS values are nearly all below or around the calculated values for Very Dry Ground, the least conducting type of ground in the ITU GW propagation model. Also we notice that the measured levels are lower with increasing density of habitation and decrease with frequency. Compare these figures with the results of the validation measurements, as reported in Subsection 5.2.1, Figure 5.3 - 5.8. In these plots the measured FS levels are all within the range of the ITU GW model. We may conclude from our measurement results that the propagation loss in urban areas is higher than what is expected from the ITU GW model.

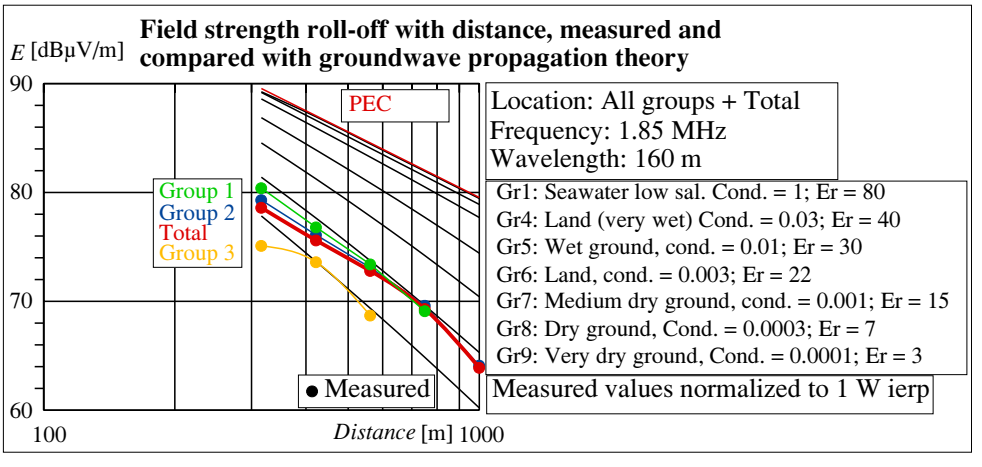

Figure 5.9. Normalized measured field strength levels compared with calculated values according existing models, 1.85 MHz. Notice: the curve Gr1 for sea-water is fully covered by the PEC curve, and so invisible.

5.3.3 Estimation of the propagation pdf

Next step is to estimate the propagation pdf from the measurement samples for each bin j. We use the t-statistics for an estimation as educated in [60]. By this estimation we look for an expectation value for the mean of the population of the loss l by taking the average or median value of the samples of l: $l_{Me,j}$. For the point estimate μ we calculate:

$$l_{\mu,j} = l_{Me,j} \pm t \cdot l_{SE,j} \text{ wherein } t = 0 \qquad (5.11)$$

$$= l_{Me,j} \tag{5.12}$$

$$L_{\mu,j} = 20 \log l_{\mu,j} \quad [\text{dB}] \tag{5.13}$$

From the estimated standard error in the propagation loss, we want to determine the Confidence Interval, *CI*, wherein $t \in CI$. Accepting the middle 90% of the distribution, 10% is left on both trails together, so $p = 0.10$. For degrees of freedom $df = n - 1$ we look up a value for t_j in the *t*-distribution table in [60]. The lower and upper end of the *CI* of $l_{\mu,j}$ is now given by:

$$l_{\mu\_lower,j} = l_{Me,j} - t_j \cdot l_{SE,j} \tag{5.14}$$

$$l_{\mu\_upper,j} = l_{Me,j} + t_j \cdot l_{SE,j} \tag{5.15}$$

$$L_{\mu\_lower,j} = 20 \log l_{\mu\_lower,j} \quad [\text{dB}] \tag{5.16}$$

$$L_{\mu\_upper,j} = 20 \log l_{\mu\_upper,j} \quad [\text{dB}] \tag{5.17}$$

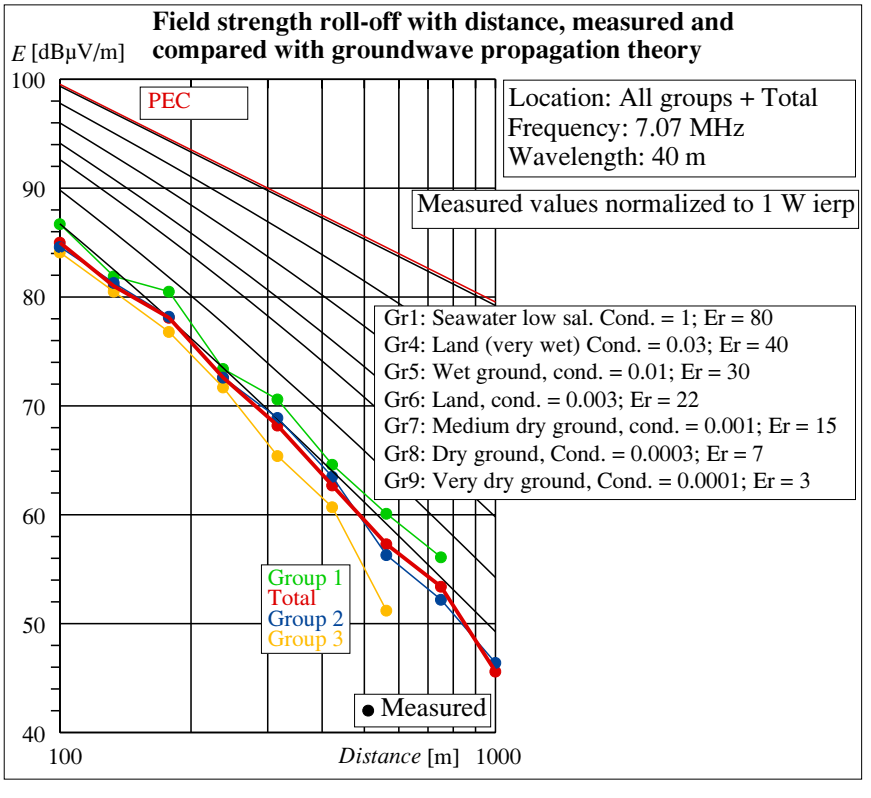

Figure 5.10. Normalized measured field strength levels compared with calculated values according existing models, 7.07 MHz.

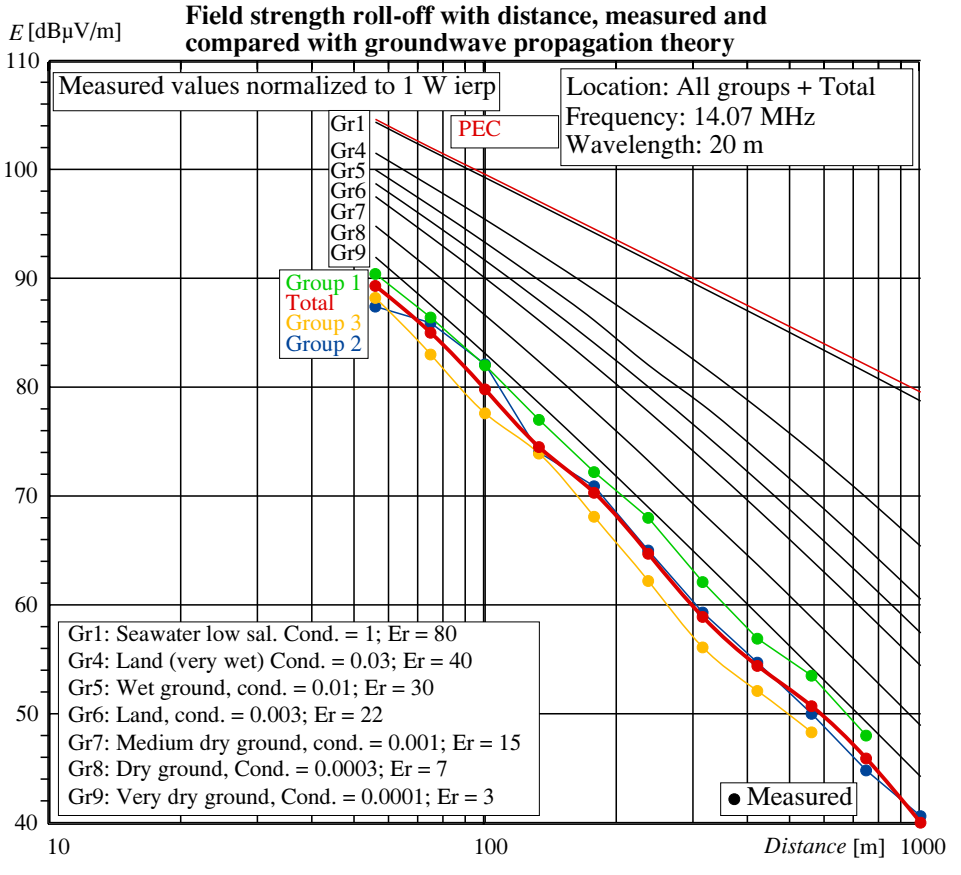

Figure 5.11. Normalized measured field strength levels compared with calculated values according existing models, 14.07 MHz.

These post-processing calculations were executed in a dedicated software program, written in C. Herein are the median FS values in each bin used as a basis for the propagation loss calculations, instead of the average values. This process is explained in Chapter 6.

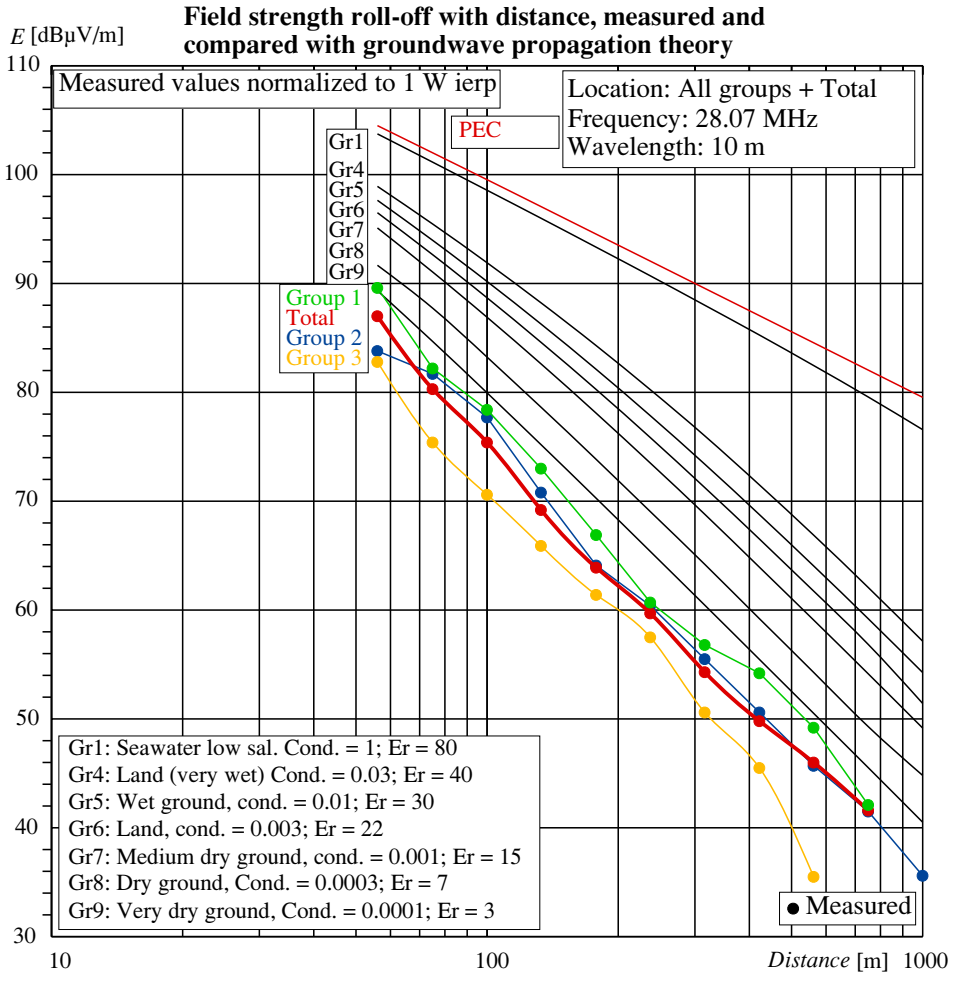

Figure 5.12. Normalized measured field strength levels compared with calculated values according existing models, 28.07 MHz.

5.3.4 Theory and the calculations of the propagation loss

In Appendix E the FS roll-off is calculated over a PEC ground. For distances d in the far field region and larger than the height of the transmitter and receiver antenna the FS values are approached by:

$$e_{PEC,d} \approx \frac{2}{d}\sqrt{(p_{tx}/2)\, g_{dip} \cdot 30} = \frac{1}{d}\sqrt{p_{tx} \cdot 90} \qquad (5.18)$$

Wherein d is the distance from transmitter to measurement location, p_{tx} is the effective isotropic radiated power, and g_{dip} the gain of a dipole antenna. Reference [84] defines several kinds of transmission loss. However, for calculating interference risks as in relevant CISPR EMC standards often the propagation characteristics of free space is used, resulting

in a 20 dB roll-off per decade of distance. So for reference it is relevant to know the increase of transmission loss with distance for the free space condition.

Under far field condition, assuming an electric dipole as transmitting antenna, we calculate the free space power density s_{fs} and the field strength e_{fs} as:

$$s_{fs} = \frac{p_{tx} g_{dip}}{4\pi d^2} \tag{5.19}$$

$$e_{fs} = \sqrt{s_{fs} Z_0} \approx \frac{1}{d}\sqrt{p_{tx} g_{dip} \cdot 120\pi / 4\pi} \tag{5.20}$$

$$\approx \frac{1}{d}\sqrt{p_{tx} \cdot 1.5 \times 30} \tag{5.21}$$

The free space propagation loss[1] L_{fs} we calculate from Equation (5.21):

$$L_{fs} = E_{d=1} - E_d \text{ [dB]} \tag{5.22}$$

$$= 20 \log\left(\frac{\sqrt{p_{tx} \cdot 1.5 \times 30}}{1}\right) - 20 \log\left(\frac{\sqrt{p_{tx} \cdot 1.5 \times 30}}{d}\right) \tag{5.23}$$

$$= 20 \log(d) \tag{5.24}$$

From our measured FS levels we want to calculate the "Excess Propagation Loss" by comparing with the FS calculated for PEC ground and with ITU ground type "Land" [57], [58] with a mediate conductivity of 3 mS/m and relative permittivity of 22. From Equation (5.5):

$$L_{excess\_PEC} = E_{PEC} - E_{N,Me} \text{ [dB]} \tag{5.25}$$

$$L_{excess\_Land} = E_{Land} - E_{N,Me} \text{ [dB]} \tag{5.26}$$

Limited to the far field ranges, we may calculate the full propagation loss L_{full} by:

$$L_{full} = L_{excess\_PEC} + L_{fs} \tag{5.27}$$

$$= L_{excess\_PEC} + 20 * \log(d) \tag{5.28}$$

5.4 Statistical Result Analysis

Applying the foregoing calculations on the measurement results are resulting in the Figures 5.13, 5.14 and 5.15 for resp. 1.85, 7, 14 and 28 MHz. In those plots the processing results are collected for the three groups of locations with increasing density of habitation, and for all locations totalized. Notice that the excess propagation loss curves related to "Land"

1 Here with "propagation loss" we only consider the effect of roll-off with distance of the field strength. Transmission loss as defined in [84] also takes into account the aperture of the receiving antenna, which is frequency dependent. It is defined as a ratio between the radiated power, ierp, and the received power from the lossless receiving antenna.

show a transition from increasing to constant at a distance related to the wavelength. We find this transition distance back in GW field strength curves in [57], where a transition in the roll-off from 20 dB/dec. to 40 dB/dec. takes place. This transition is characteristic for GW propagation model, see [71] and [57]. For example, at a wavelength of 20 m the transition is at a distance of approximately 300 meters, about 15 times the wavelength. In Figure 5.14 we find this transition back in the curves which compare the measured excess propagation loss with the propagation loss according ITU GW "Land" model. Here we find the bend, while comparing with the linear PEC line we find no bend. In Figure 5.13, concerning frequencies 1.85 and 7.07 MHz, wavelength resp. 160 and 40 m, these transition distances are over 1000 m, so out of range in these plots. We may conclude from the plots in Figures 5.13 - 5.15 that propagation in residential areas does not follow the ITU GW propagation model, but instead follow a constant slope with a constant number of dB per decade of distance.

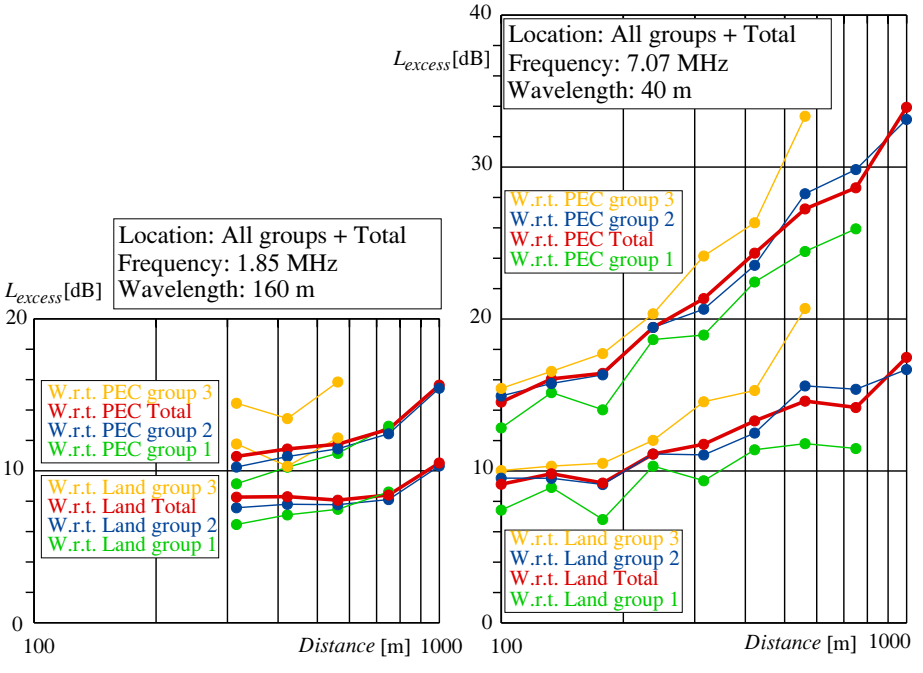

Figure 5.13. Excess Propagation loss curves for 1.85 and 7 MHz.

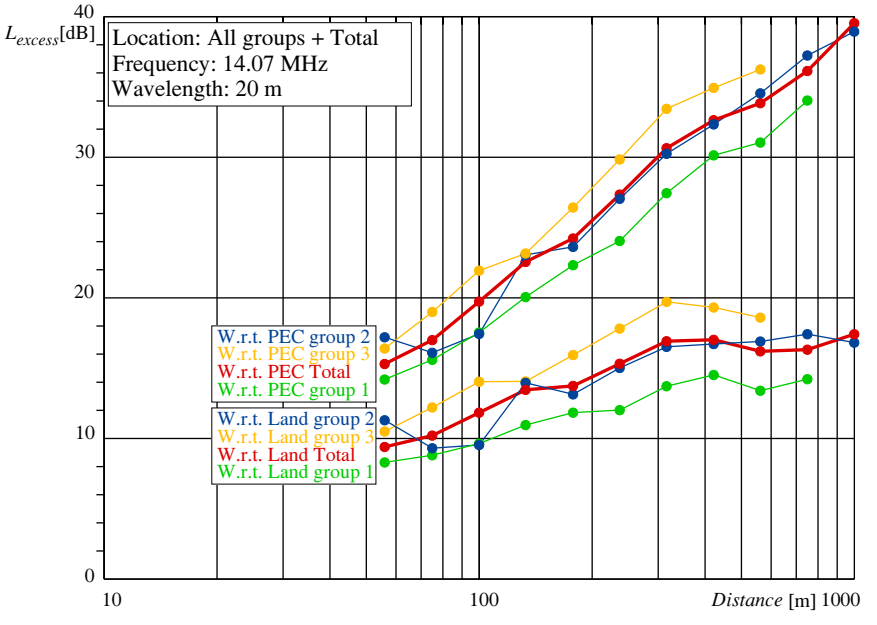

Figure 5.14. Excess Propagation loss curves for 14 MHz.

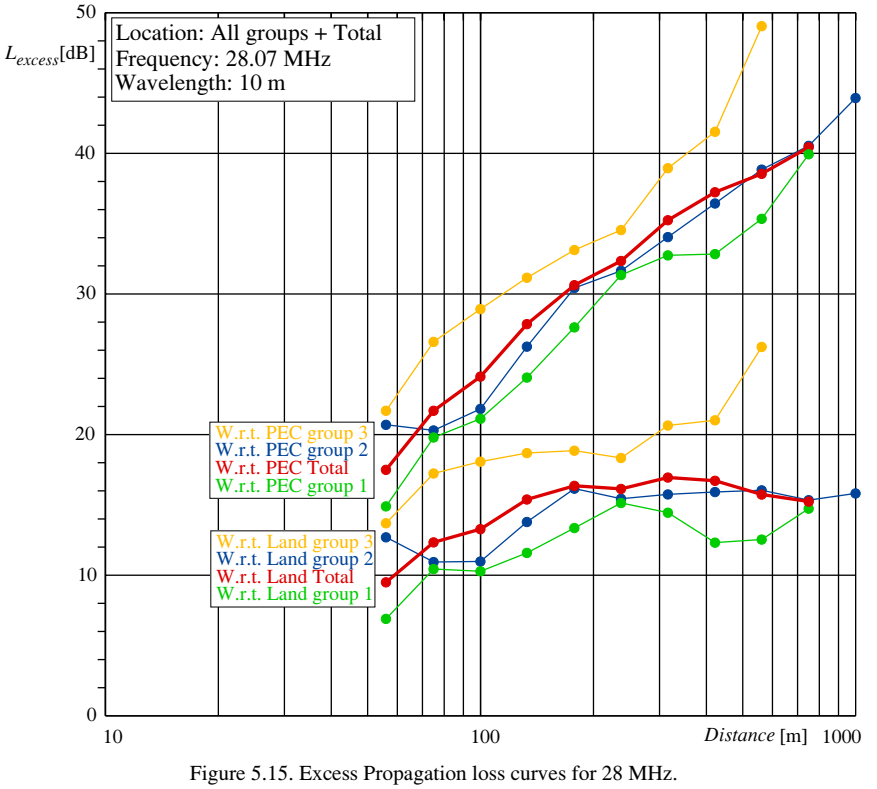

Figure 5.15. Excess Propagation loss curves for 28 MHz.

5.4.1 Regression analysis: Correlation to straight line and its slope

Inspecting the measurement results leads to the conclusion that the extra path loss above the loss according to GW propagation over PEC, in relation to the logarithmic value of the distance, is well approached by a straight line. For considering a correlation with a straight line we may write:

$$L_{full} = slope \cdot D + \alpha \tag{5.29}$$

Now we arrive at a linear relation between L_{full} in dB and $D = 20 \log(d)$. With this relation we assume a case of interval measures, implying we may apply the Pearson correlation test, using the Pearson product-moment coefficient, [60]. Here a measurement ensemble consists of the measurement results on a single frequency band on a number n of distances as samples $i = 1$ to $i = n$. In this study n varies from 3 to 11.

As mentioned before we want to compare our measurement results with the free space roll-off with distance of 20 dB/decade, starting at the reference distance of 10 meter. This means that we must force the regression line going through the point $L_{full} = 20$ dB and $D = 20 \log(d) = 20$. So $\alpha = 0$ for $slope = 1$ (= 20 dB/dec.). We can arrange that by, instead of the average values for L_{full} and D (27), (28), substitute $av\_L_{full} = 20$ and $av\_D = 20$ in the formula for the slope of the regression line (30):

$$slope = \frac{\sum_{i=1}^{n} (D_i - av\_D)(L_{full,i} - av\_L_{full})}{\sum_{i=1}^{n} (D_i - av\_D)^2} \tag{5.30}$$

$$= \frac{\sum_{i=1}^{n} (D_i - 20)(L_{full,i} - 20)}{\sum_{i=1}^{n} (D_i - 20)^2} \tag{5.31}$$

The degrees of freedom is now given by $df = n - 1$, one higher than in the standard Pearson correlation test, as one fixed sample point has been added. n is the number of bins involved.

The calculations has been performed for all three groups of locations and for all locations totalized. We show here the results for all locations totalised only and for four frequencies. Figures 5.16 - 5.19 are resulting. We find a high correlation coefficients r and roll-off slope of 26.6 to 43.1 dB/decade of the distance.

All resulting values for the Roll-Off slope are shown in Figure 5.20 as a function of the frequency. Also a regression line can be drawn here, which leads to a general approximation of the field strength roll-off with distance for frequencies between 1 and 30 MHz.

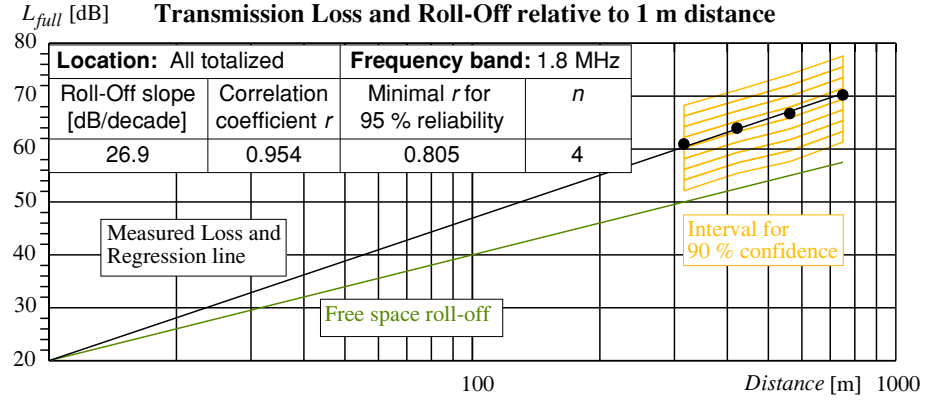

Figure 5.16. Transmission loss and Roll-Off relative to 1 m distance at 1.8 MHz.

The result is summarized in Table 5.2. We consider the numbers for Group I+II+III in Table 5.2 as the main outcome. It is composed of the results from the correlation of propagation loss with distance for six frequencies from all location groups, so giving eighteen samples for the correlation with frequency. See the schematic in Figure 5.21, wherein an overview of the processing of the measurement data and the statistical analysis is shown. For low and high density areas additional values for *a* and *b* are given. Also is, by way of checking, all samples from all locations put together and processed, resulting in the values at the last row of Table 5.2. These result were comparable with the values for Group I+II+III and for median density area.

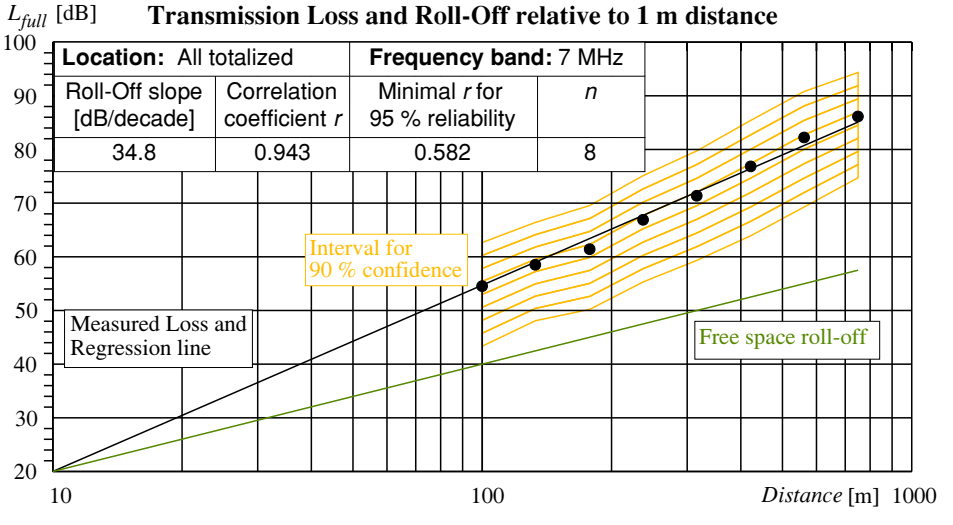

Figure 5.17. Transmission loss and Roll-Off relative to 1 m distance at 7 MHz.

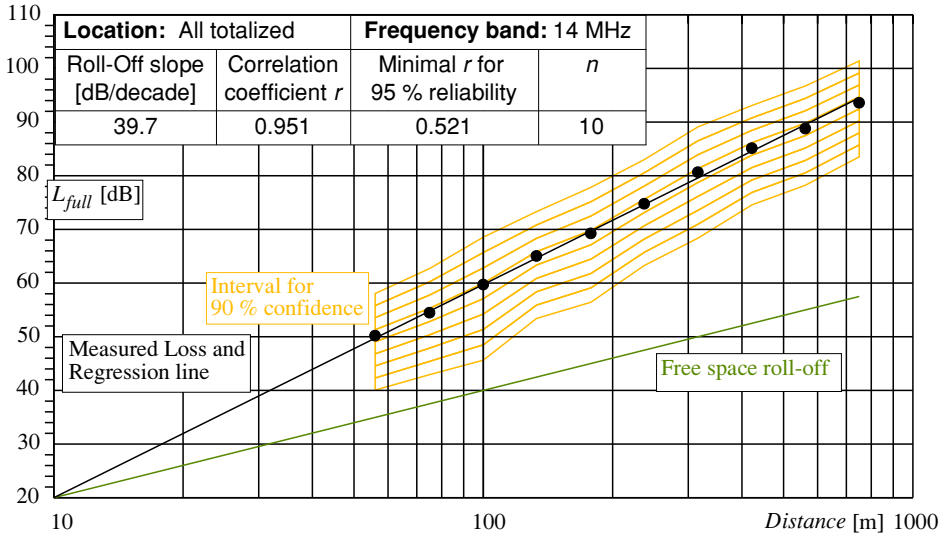

Figure 5.18. Transmission loss and Roll-Off relative to 1 m distance at 14 MHz.

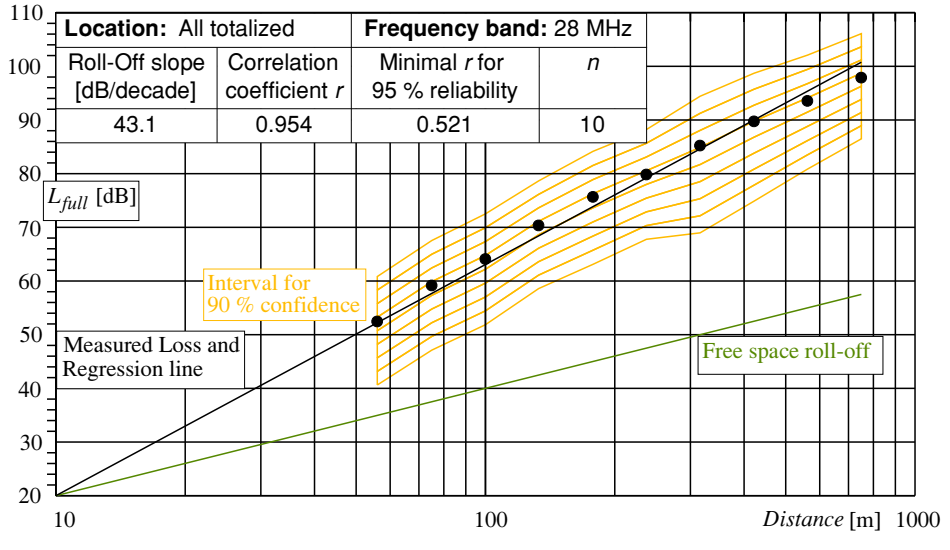

Figure 5.19. Transmission loss and Roll-Off relative to 1 m distance at 28 MHz.

Table 5.2. Roll-Off slope as found by measurement in The Netherlands.

Frequency range 1 - 30 MHz	*Roll-Off slope* = *a**log(*f* [MHz]) + *b* [dB/decade]				
Correlation over:	*n*	*r*	r_{min}	*a*	*b*
Group I + II + III	**18**	**0.963**	**0.378**	**14.3**	**23.0**
Low density area, group I	6	0.994	0.622	12.6	23.3
Median density area, group II	6	0.989	0.622	14.6	22.1
High density area, group III	6	0.992	0.622	15.6	23.7
All locations	6	0.993	0.622	14.5	22.4

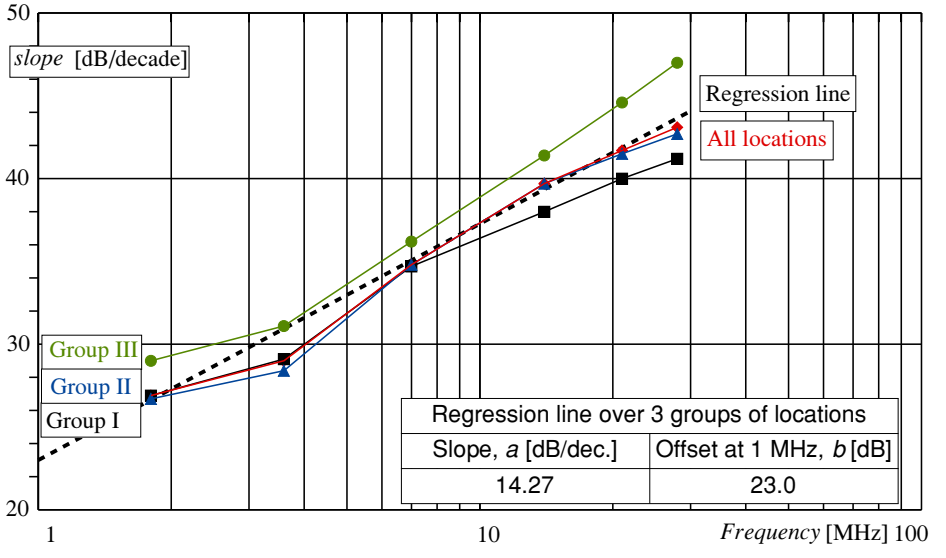

Figure 5.20. Roll-Off slope as a function of frequency. Results from the three groups and all locations together.

5.5 Conclusions

In the study of accumulation of man-made noise on MF and HF frequencies in urban areas the propagation within these areas may play a significant role. Information from foregoing propagation studies appear to be unsatisfying, so a new experiment had to be setup wherein a mobile field strength measurement system, in combination with a stationary beacon transmitter, performed propagation measurements at a small scale with hundreds of measurement points at propagation distances up to 1000 meter. This method produces a high number of data and allows to run a proper statistical analysis, giving very concise results.

From these measurements at sixteen locations in The Netherlands at six frequencies from 1.8 to 28 MHz the conclusion can be drawn that propagation in urban areas do not follow the ITU GW propagation model, but show higher propagation losses, increasing with frequency, and show a constant roll-off with distance. The slope of this roll-off is frequency dependant according a linear regression as depicted in Figure 5.20 and numerically displayed in Table 5.2. Stochastically there is a small dependency on the density of habitation, as shown in the table and visible in Figure 5.20, but at individual locations the local topography is strongly relevant.

The so found statistical information about propagation loss in residential areas may be used for building an accumulation model to lay a causality between source powers, source densities, and local MMN levels. We would recommend others to do propagation experiments in other urban places, using equivalent methods, to verify and broaden our results.

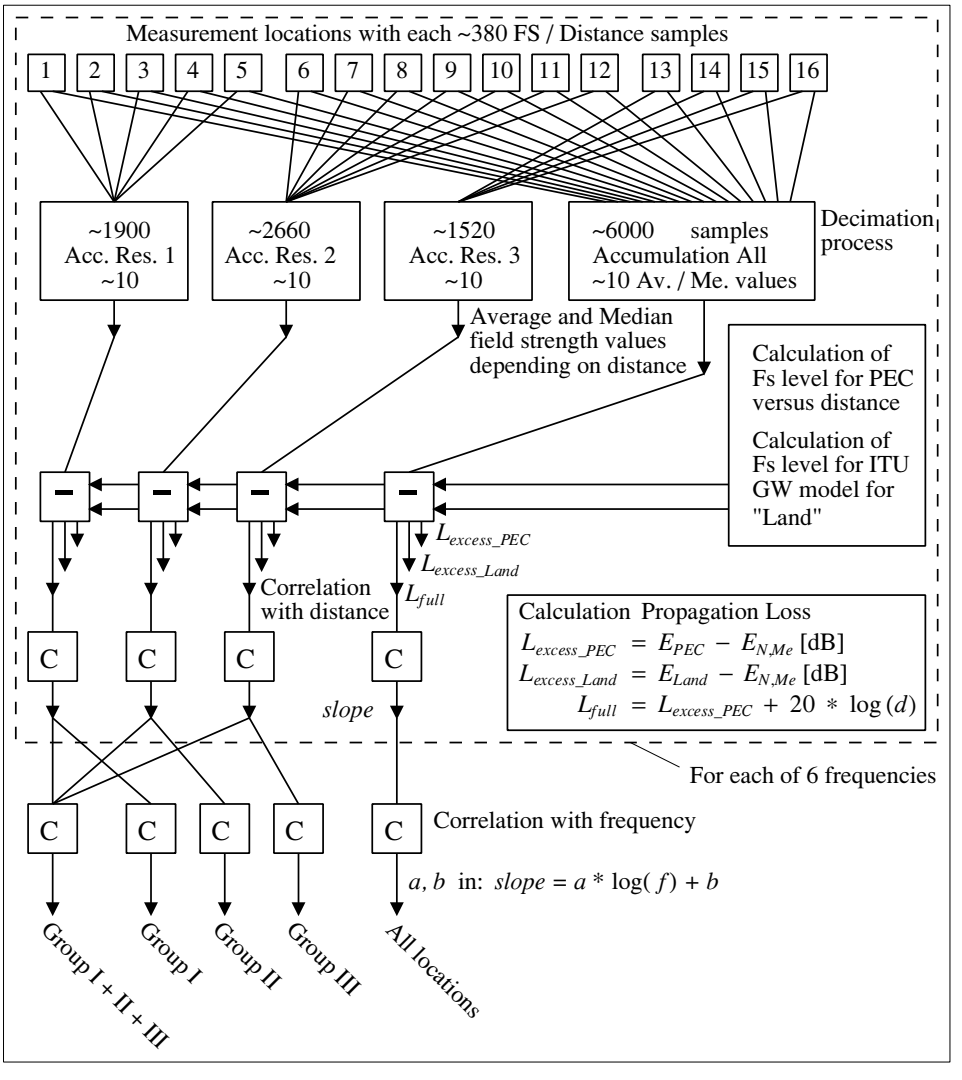

Figure 5.21. Schematic overview of the data processing and analysis.

Chapter 6

6 Propagation measurements to estimate the influence of seasons on the ground wave propagation loss

This chapter gives a report about longitudinal measurements of propagation over a fixed trajectory with the purpose to investigate the seasonal dependency of propagation loss. This study was already mentioned in Chapter 5, but not fully reported. The chapter enlightens more technical details about the used propagation measurement techniques.

6.1 Introduction

For building an accumulation model of Man-Made Noise an estimation of the propagation loss in residential areas is required. Therefor a measurement campaign to measure the loss of ground wave propagation at 16 locations has been performed. But these measurements are all carried out in the summer season, when the ground is relative dry. One might question if there is a significant difference in propagation loss when measured in the wintertime with a high level of precipitation and humidity.

To study this question a series of monthly measurements were performed throughout a period of a full year, using a single location and a fixed measurement trajectory. To simplify the implementation of the measurements a fixed location for the beacon transmitter was pinpointed in the backyard of author's house, located in rural area just outside of the village of Rietmolen. A measurement trajectory was set up, starting through the village, and next through rural area, resulting in a large arch returning to the starting point, see Figure 6.1. This trajectory leads through built-up area, open area, and around and

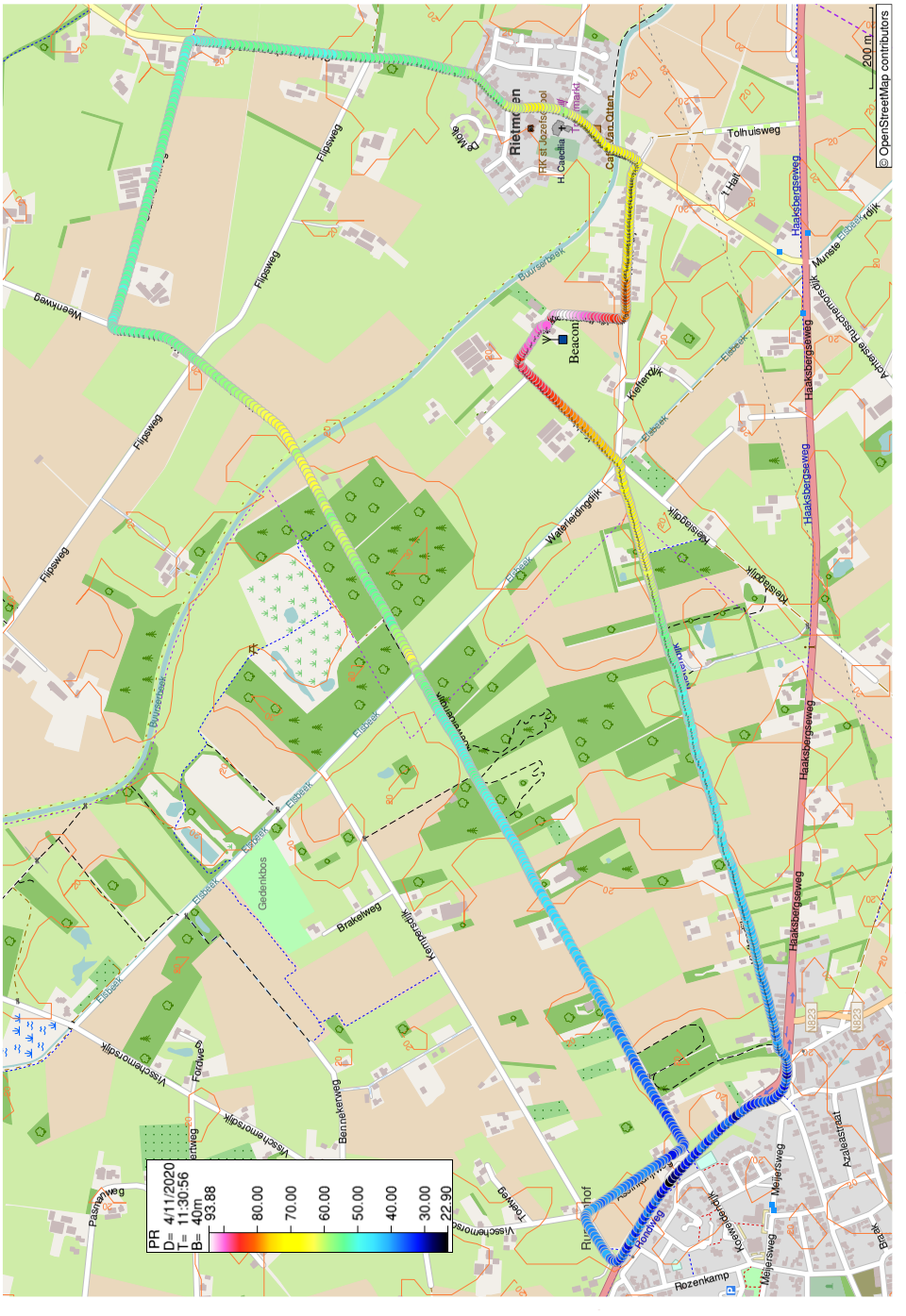

Figure 6.1. Map of the full trajectory for the propagation measurements.

through areas with vegetation and forest. In a second data processing phase the measurement samples from the part of the trajectory, passing the built-up area, are isolated to study the effects in residential area. In the measurements three frequencies are used: 1.85 MHz (low end of the band of interest), 28.07 MHz (high end), and 7.07 MHz (geometric middle).

6.2 Measurement method

A transmitter, "Beacon", is set up on a fixed location. A mobile field strength measurement setup is driven over the trajectory, while taken measurement samples of the field strength at regular distances travelled. In this section the method is described using the measurement results for the frequency of 7.07 MHz. In Figure 6.1 every coloured dot represents a measurement sample, wherein the colour codes for the values according to the colour bar, top left. In addition to that Figure 6.2 shows the the samples numbers in the X-ordinate and the measured values in the Y-direction. This figure is real-time plotted during the measurement drive.

Figure 6.2. Direct recording on the datalogger display. Horizontal: number of sample.

A first processing step is to plot the distance between the location of the beacon transmitter and the actual measurement position as the crow flies, and the field strength, see Figure 6.3. A second step is to reorder the samples for increasing distance and plot the field strength with a logarithmic distance X-axis, see Figure 6.4. Now we see in a scatter plot clearly the relationship between measured field strength and the log of the distance.

The next step is to combine samples into "bins", meaning ranges of distance, and calculate average and median values for every bin. For this purpose a software application has been written of which Figure 6.5 shows the window of the graphical users interface

(GUI). The CSV-file from the datalogger is dropped on this window and so loaded into the application.

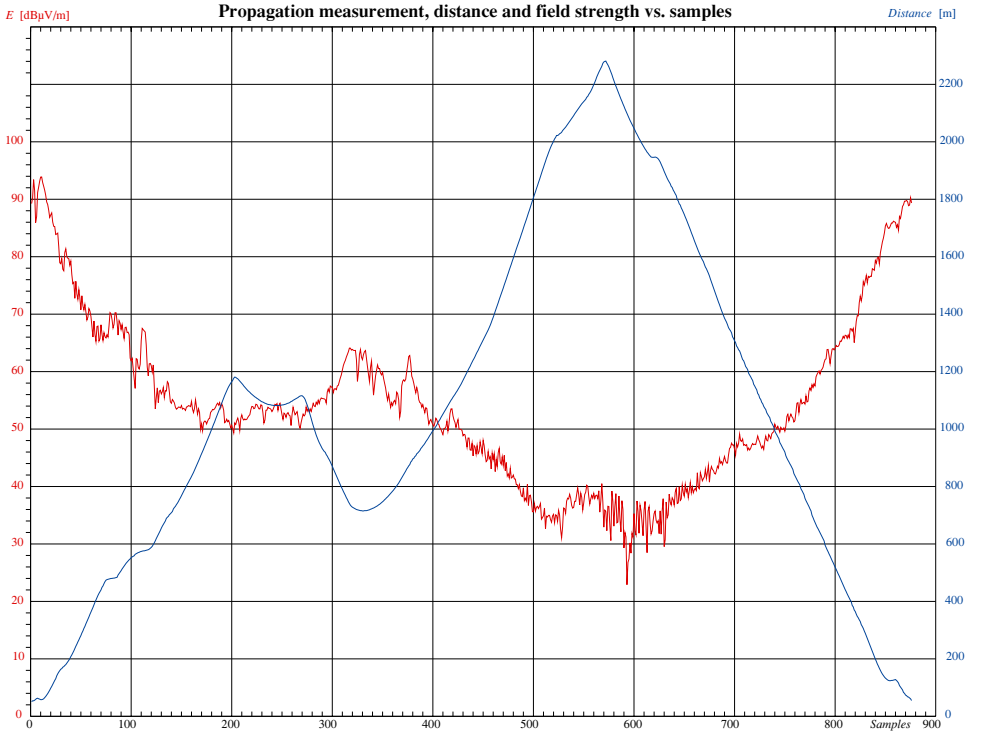

Figure 6.3. Distance and measured field strength by sample.

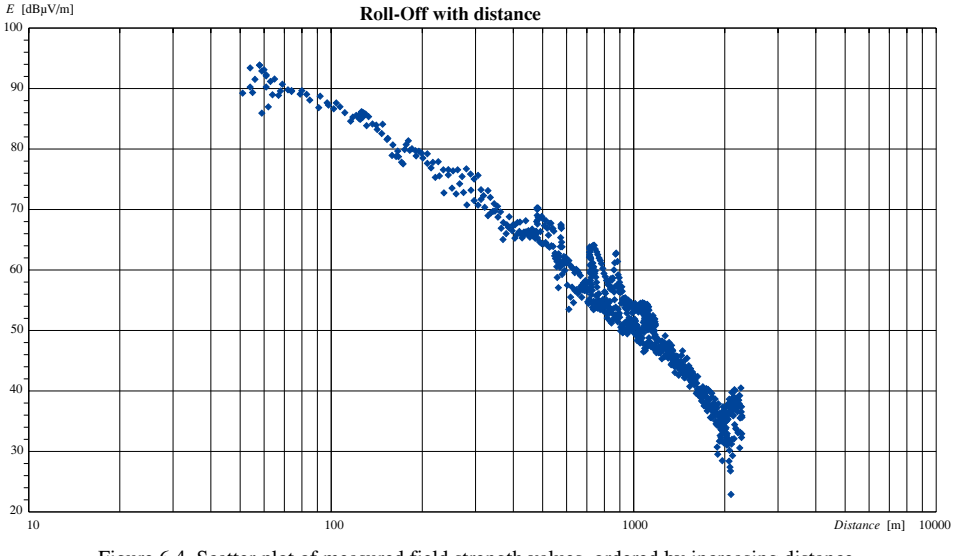

Figure 6.4. Scatter plot of measured field strength values, ordered by increasing distance.

The results are shown in the lower half of the window. The bin centres are shown together with the borders. Row "N" shows the number of samples loaded per bin. Button "Calculate first" starts a calculation of the average value of field strength in each bin. In this process samples, that are not on the centre distance of the bin, are translated to the centre while assuming a slope of -20 dB/decade.

After this the button "Calculate Def" is pressed several times until the resulting values in the rows "Av FS" and "Slope" are stable. This is an iterative process wherein the actual slope is calculated, and the average values are adapted. Finally the button "Finish Calc" is pressed to calculate the median field strength values. Button "Export" lets the results in a series of CSV files to be saved.

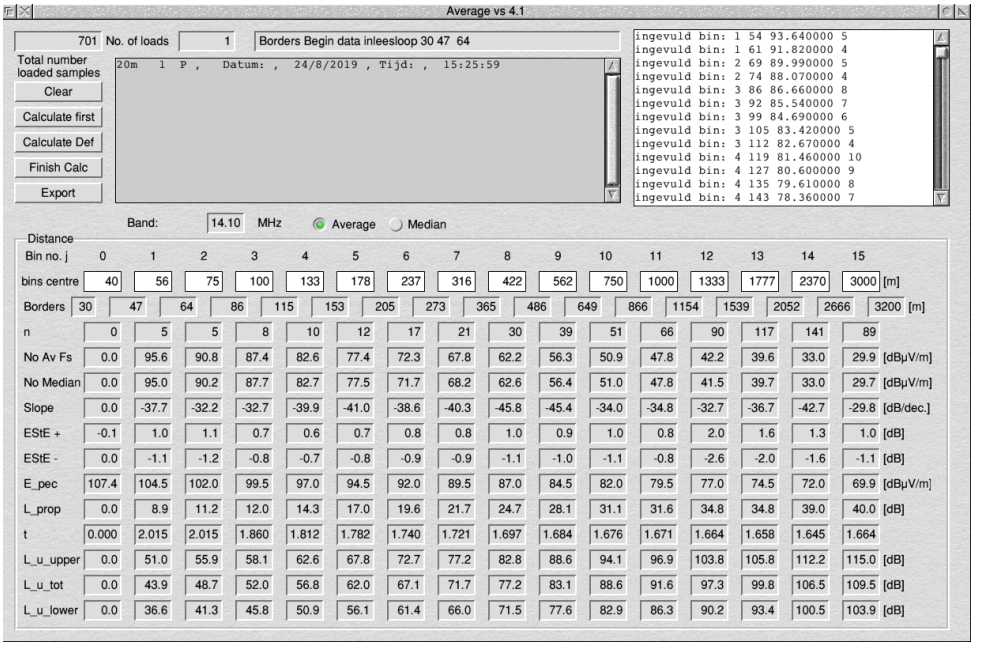

Figure 6.5. Window of data processing application "Average".

The next step in the processing is to plot the average and median values in a field strength vs. distance plot, alongside calculated values for Perfect Electric Conducting ground (PEC) and simulation results from the ITU ground wave propagation model [77]. Thereby the field strength values are normalized to a for the beacon transmitter radiated power of 1 Weirp, using the outcome of the calibration measurement of the beacon transmitter. Figure 6.6 is an example of such a plot. For the average values a curve is plotted. We see that this curve follows more of less the curves for the diverse types of ground with different conductivity, as defined in Rec. ITU-R P.368 [57]. In Figure 6.6 the measured curve is close to ground type 7, defined as "Medium dry ground" with a

conductivity σ = 0.001 S/m, and a relative permittivity, ε_r = 15. In Table 6.1 the relevant types are mentioned with their Rec. ITU-R P.368 names and conductivity. Remark that when *gr* is the type number, the conductivity is approached by

$$\sigma = \frac{1}{\sqrt{10^{(gr-1)}}} \quad \text{for } gr > 0 \tag{6.1}$$

$$\sigma = \infty \quad \text{for } gr = 0 \tag{6.2}$$

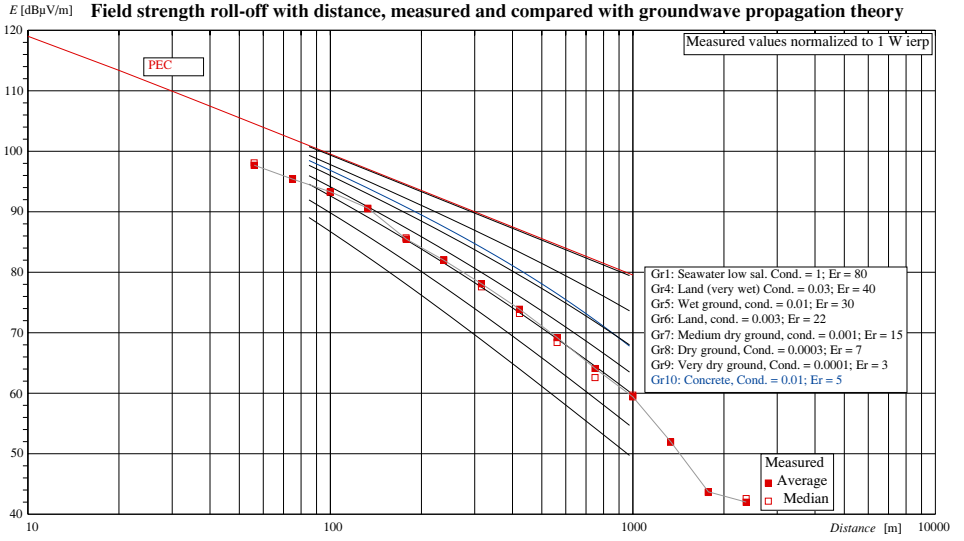

Figure 6.6. Normalized field strength values plotted against ITU model curves.

This continuous relationship (6.1) makes it feasible to quantify the measurement result into a single real number, *ATG*, that shows the proportionality with the inverse of the conductivity. In this way it is quantifying the ground from the field strength, and from there the propagation loss. A note must be made here. In the real environment the propagation loss is not only determined by the ground, but also by other environmental parameters as buildings, cables, vegetation, and forest. Trees must be considered as lossy conductors, depending on the season. Especial when the vertical dimensions of objects approach the quarter of a wavelength or longer, these objects may influence the propagation loss. That is the reason that the notation "Apparent type of ground" (*ATG*) is used.

The calculation of *ATG* is carried out in Table 6.1, where the field strength values at the distances of the centres of the bins, related to the series of ground types, are collected and the averaged value for all distances is given. In the most right handed column the measured field strength values are shown with a averaged value there below. This measured average is subtracted from the simulation averages and displayed in the row "Av. Diff." Here the results are a positive value in column Gr6 (2.59) and a negative value in Gr7 (-0.18). It

means that the measured curve lays for the greater part in between the ground type 6 and 7. By linear interpolation, using the both nearest ground type, a value for an Apparent type of ground, *ATG*, can be calculated, here 6.94.

Table 6.1. Calculating the Apparent type of ground, ATG.

Table for the purpose of calculating Apparent type of ground. *Frequency*: 7 MHz									
ITU Rec. 368 ground description	PEC	Gr1 Sea water low salinity	Gr4 Very wet land	Gr5 Wet ground	Gr6 Land	Gr7 Medium dry ground	Gr8 Dry ground	Gr9 Very dry ground	Averaged *E* [dBµV/m]
Conductivity σ/ε_ρ:		1/80	0.03/40	0.01/30	0.003/22	0.001/15	0.0003/7	0.0001/3	
Distance [m]	*gr* = 0	1	4	5	6	7	8	9	
237	92.05	91.83	89.34	86.50	83.72	81.54	77.59	73.49	82.00
316	89.55	89.33	86.38	83.09	79.96	77.53	73.11	68.81	78.10
422	87.04	86.80	83.32	79.50	76.00	73.33	68.60	64.01	73.90
562	84.55	84.29	80.15	75.77	71.90	68.99	63.94	59.16	69.20
750	82.04	81.76	76.81	71.80	67.58	64.46	59.13	54.23	64.10
1000	79.54	79.22	73.29	67.59	63.08	59.80	54.24	49.26	59.40
Av: [dBµV/m]	85.80	85.54	81.55	77.37	73.71	70.94	66.10	61.49	71.12
Av. Diff.: [dB]	14.68	14.42	10.43	6.25	2.59	-0.18	-5.02	-9.63	
Apparent type of Ground, *ATG*					6.94				

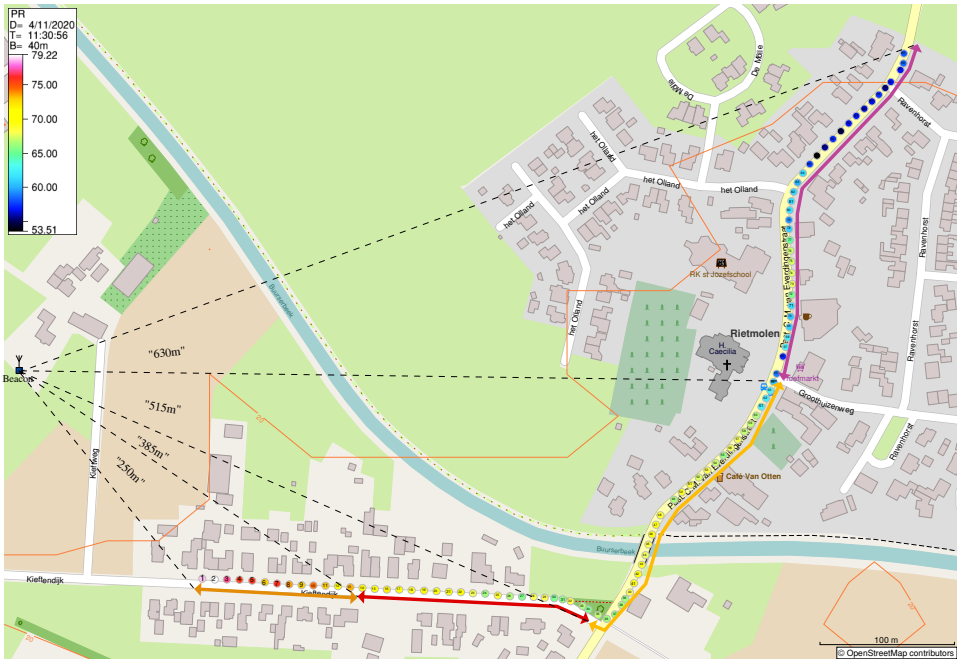

Figure 6.7. Limited trajectory through Rietmolen.

For the purpose of the study of propagation loss in residential areas it is more relevant to take a subset of the measurement samples, situated inside the build up area. Figure 6.7 shows a map in which the samples are plotted having a distance to the beacon in the range from 200 to 700 m. This trajectory is divided in four parts, 200 - 300, 300 - 470, 470 - 560,

and 560 - 700 m. The subranges form the bins in which the samples are combined, designated by resp. bin centre distances "250 m", "385 m", "560 m" and "630 m", and shown in Figure 6.7 by coloured curves. Segmentation lines show the respectively areas over which the propagation takes place.

So processing this subset of the measuring data results in four field strength values, which are plotted in Figure 6.8. In the same way as described above a value for *ATG* can be obtained via Table 6.2, now filled for this residential area.

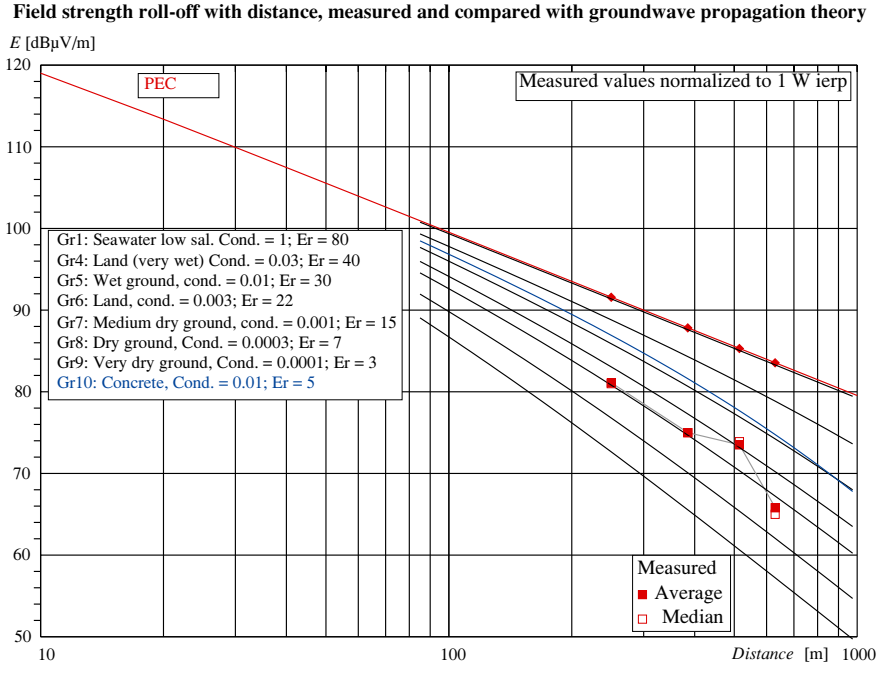

Figure 6.8. Results in residential area.

Table 6.2. Calculating the Apparent type of ground in residential area.

Table for the purpose of calculating Apparent type of ground. *Frequency*: 7 MHz									
ITU Rec. 368 ground description	PEC	Gr1 Sea water low salinity	Gr4 Very wet land	Gr5 Wet ground	Gr6 Land	Gr7 Medium dry ground	Gr8 Dry ground	Gr9 Very dry ground	Averaged *E* [dBµV/m]
Conductivity σ/ε_p:		1/80	0.03/40	0.01/30	0.003/22	0.001/15	0.0003/7	0.0001/3	
Distance [m]	*gr* = 0	1	4	5	6	7	8	9	
250	91.58	91.36	88.81	85.88	83.04	80.81	76.78	72.63	81.10
385	87.84	87.58	84.28	80.64	77.25	74.65	70.04	65.50	75.00
515	85.31	85.05	81.13	76.93	73.16	70.33	65.37	60.63	73.50
630	83.56	83.29	78.85	74.22	70.21	67.22	62.04	57.21	65.80
Av: [dBµV/m]	87.07	86.82	83.27	79.42	75.92	73.25	68.56	63.99	73.85
Av Diff.: [dB]	13.22	12.97	9.42	5.57	2.07	-0.60	-5.29	-9.86	
Apparent type of Ground, *ATG*					6.78				

6.3 Propagation loss

For the propagation study it is more relevant to consider the spread in the propagation loss for each frequency band and for each bin centre distance in the build-up area. The propagation loss may consists of several parameters as defined in [84]. There is the free-space propagation loss L_{bf}, defined as the loss between two isotropic antennas in free space condition, the basic propagation loss, L_b, defined for the real propagation path and between two isotropic antennas, excluding the effects of obstacles close to the antennas. Also there is the ray path transmission loss, L_t, which is multi-path effects taking into account.

In the setting of ground wave propagation the free-space propagation loss L_{bf} is linked to the field strength roll-off model of the cymomotive force, given by

$$e = \frac{C}{d}\sqrt{p_t}\,|F| \tag{6.3}$$

Herein is the constant C the cymomotive force [58], the value of which depends on the type and length of the radiator. When p_t is given in kW, d in km, and e in mV/m, then $C = 300$ for a short monopole, and $C = 314$ for a quarter wavelength monopole. We may use the same values for constant C when we modify expression (3) into

$$e = \frac{C}{d}\sqrt{\frac{p_t}{1000}}\,|F| \tag{6.4}$$

in combination with p_t given in W, d in m, and e in V/m.

Here, in the case of a small vertical antenna and PEC type of ground, applies $C = 300$, $F = 1$, so formula (4) changes in

$$e = \frac{300}{d}\sqrt{\frac{p_{tx}}{1000}} \tag{6.5}$$

$$E = 10\log(p_t) - 20\log(d) + 139.5 \text{ [dBµV/m]} \tag{6.6}$$

The ray path transmission loss, L_t, can be used when we want to take into account the two ray model with a free space path and a path with a reflection against ground. It is coupled with the PEC-curve as shown in Figure 6.6 and Figure 6.8 (red curve).

The absolute value of the propagation loss is defined by the difference between the isotropical transmitted power by a lossless transmitting antenna p_t and the available power from a lossless receiving antenna p_a, given by

$$p_a = A_{eff}s_t(d) \tag{6.7}$$

wherein A_{eff} is the effective aperture of the receiving antenna and $s_t(d)$ the power density at the location of the receiving antenna. For a lossless antenna equals:

$$A_{eff} = \frac{g\lambda^2}{4\pi} \tag{6.8}$$

$$s_t(d) = \frac{e^2(d)}{Z_0} \tag{6.9}$$

For the lower frequency bands the dimensions of the aperture is much larger than d, so e is not constant over this surface. So the concept of an absolute value of the propagation loss is not useful in this application. But the variations in propagation loss, the factor $|F|$, caused by ground wave propagation effects and other environmental parameters, can still be calculated from the electric field strength, and so the spread as caused by seasonal effects.

The absolute values of the propagation loss according the free space model and the values over PEC ground can be found in Table 6.3. Remark that at a minimal measurement distance of 56 m a small difference is visible between the free space model and the two ray PEC model, while at a shorter distance like 10 m the outcome is not realistic anymore, especially for the longer wavelengths.

Table 6.3. The absolute propagation loss.

Absolute propagation loss [dB]												
	Free space model L_{bf}						PEC ground wave model L_t					
Distance:	10	56	250	385	515	630	10	56	250	385	515	630
1.8 MHz	-7.747	7.217	20.21	23.96	26.49	28.24	-7.251	7.235	20.21	23.96	26.49	28.24
7 MHz	3.812	18.78	31.77	35.52	38.05	39.80	4.335	18.79	31.77	35.52	38.05	39.80
28 MHz	15.85	30.82	43.81	47.56	50.09	51.84	16.83	30,85	43.81	47.56	50.09	51.84

6.4 Measurement results

For studying the spread in the propagation loss due to seasonal variation of environmental conditions, the subject of this report, it is not necessarily to calculate the loss itself. It suffice to measure the field strength of the beacon signal. Then it is still possible to compare this with the values the field strength should show in case of a PEC ground, or in case of a general type of ground "Land" with intermediate conductivity properties: σ = 0.003 S/m, ε_r = 22. The reason for these choices is that in many standardisation activities interference ranges of RFI emitting devices are estimated using the free space model for simplicity very often. In CEPT an attempt is made to make a more real approach of interference ranges by using the ground wave propagation model [17].

The seasonal measurements result in measured field strength values for three frequency bands, which show a spread between consecutive measurement, which is partly due to stochastic phenomena and measurement inaccuracies, small local propagation effects, but also clearly due to a seasonal effect, as can be seen in Figure 6.9 and in Figure 6.10. Figure 6.9 shows the variation in the apparent type of ground, ATG, for the whole of the measuring

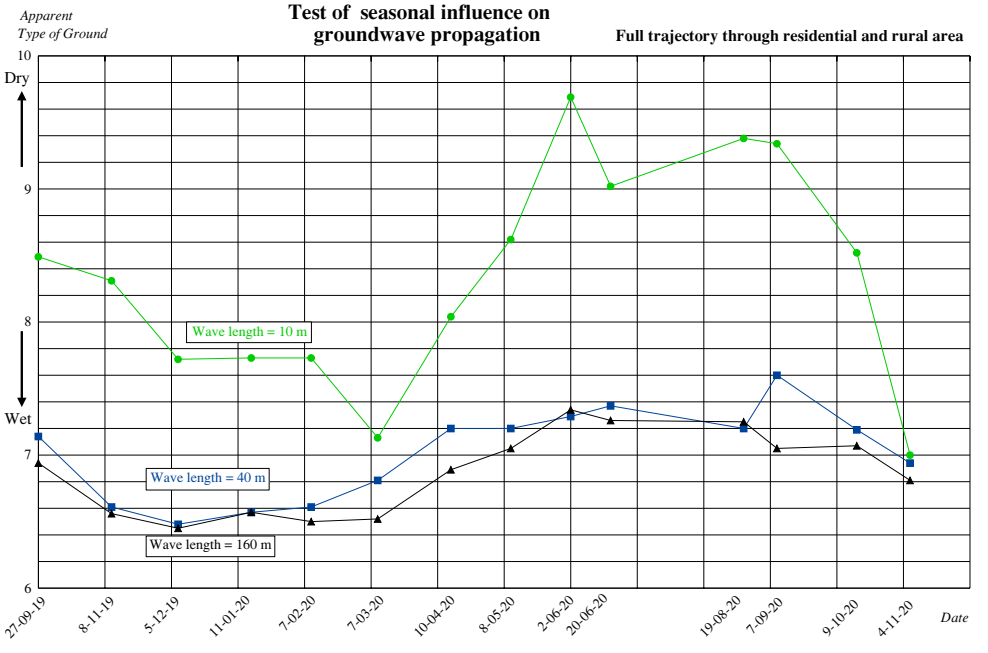

Figure 6.9. Result in ATG of a full year of measurements, full trajectory.

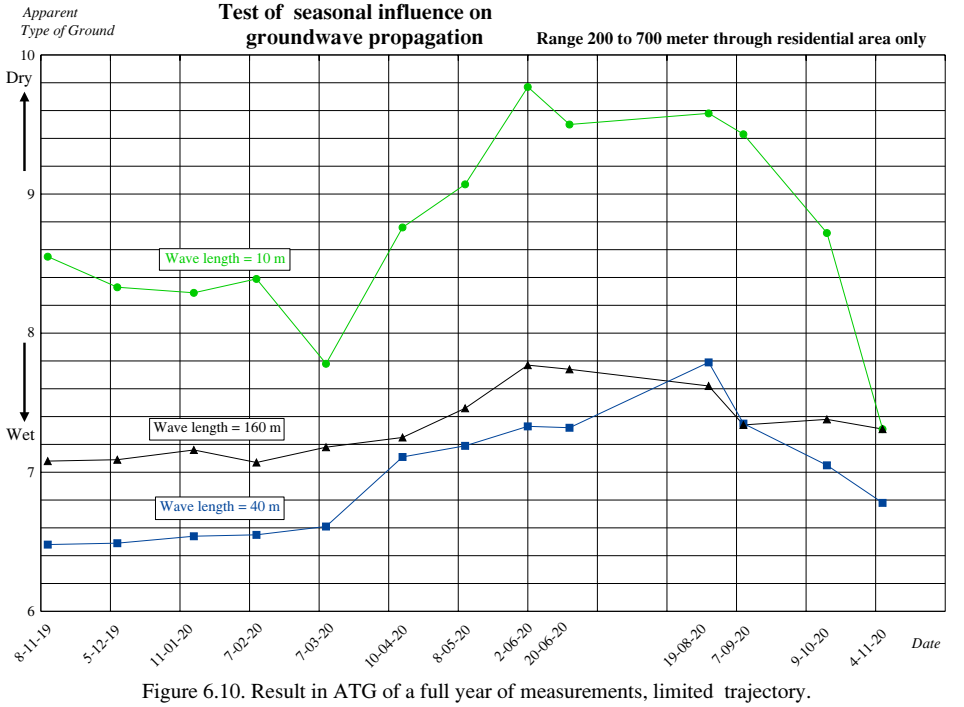

Figure 6.10. Result in ATG of a full year of measurements, limited trajectory.

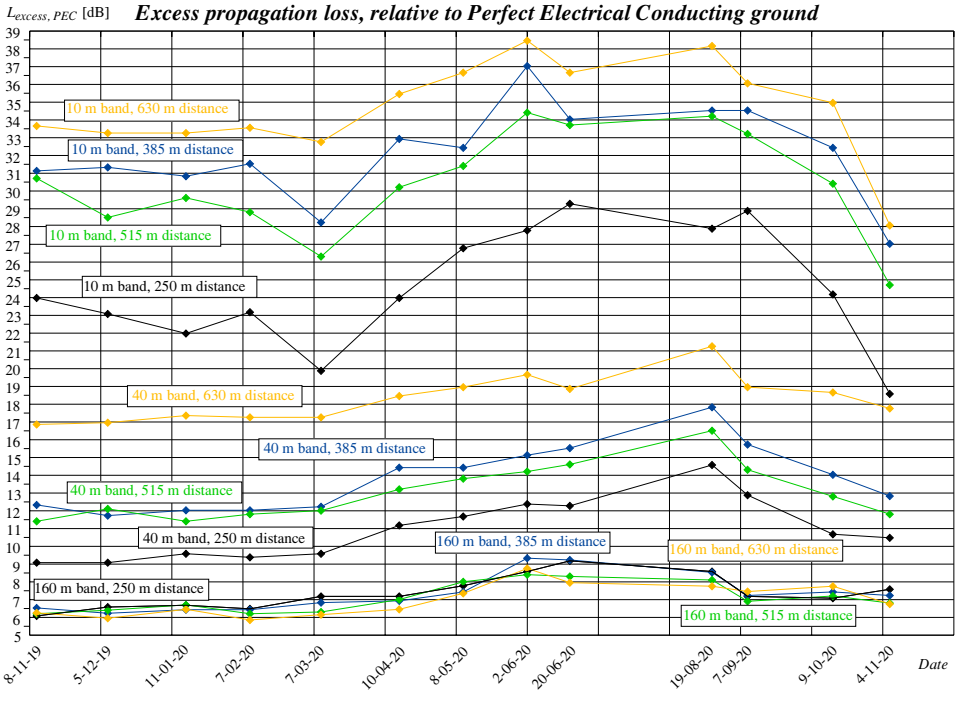

Figure 6.11. Result in excess propagation loss relative to PEC ground, for three distances.

trajectory. Figure 6.10 does the same but for the selected part of the measurement trajectory through the residential area only. Although the influence of vegetation is much less in the residential area than in the full rural trajectory, still the same tendency is apparent.

In the next step the extra propagation loss, $L_{excess,\,pec}$, relative to the absolute loss over PEC ground, L_t, is calculated for every bin distance in the residential area, and for each frequency, and plotted in Figure 6.11. This can also be done for the propagation loss, related to general type of ground "Land", resulting in $L_{excess,land}$. The result is plotted in Figure 6.12.

To present the spread, the same results are displayed in the bar plots in Figure 6.13. A further analysis, starting from the same numbers as used in Figure 6.12, reveal the the median values of the extra loss and the spread therein, see Table 6.4. It must be stressed here that these numbers result from a single measurement campaign at one location. It is not clear if these number are valid in general. But taking into consideration that the spread is relative small, 2.2 to 7.2 dB, more or less in the same order of other measurement uncertainties, the influence of this spread is expected to be not that much that it will have a serious influence on the results of the outcome of the measurement campaign on propagation loss in residential areas.

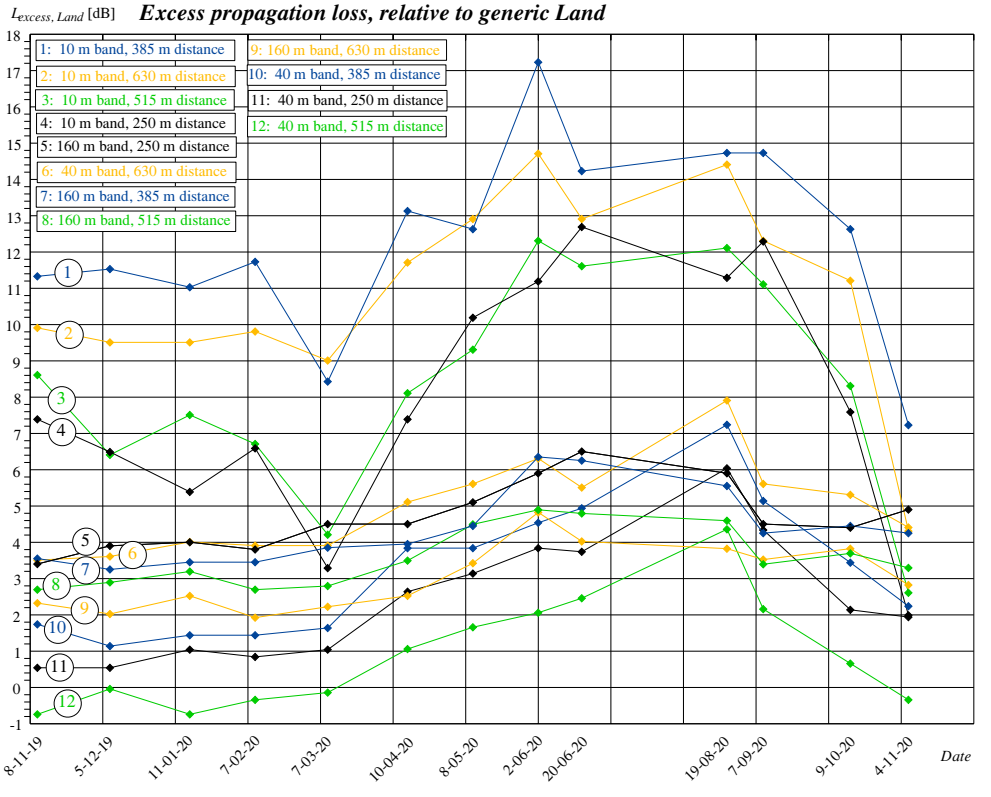

Figure 6.12. Result in excess propagation loss relative to ground type Land, for three distances.

Table 6.4. Propagation measurement results.

Results of propagation mesurements throughout residential area in Rietmolen in the period november 2019 to november 2020. Excess propagation loss relative to ground type "Land" with a *Conductivity* =0.003 S/m and relative permittivity, *Er*=22													
Band	160 m / 1.8 MHz				40 m / 7 MHz				10m / 28 MHz				
Distance	250	385	515	630	250	385	515	630	250	385	515	630	[m]
10% +	3.8	3.5	2.7	2.0	0.5	1.4	-0.7	3.6	3.3	8.4	4.2	9.0	$L_{rel,land}$ [dB]
median	4.5	4.3	3.4	2.8	2.1	3.4	0.7	5.1	7.4	12.6	8.3	11.2	
90% -	5.9	6.3	4.8	4.0	4.3	5.1	2.5	6.3	12.3	14.7	12.1	14.4	
Spread	2.1	2.8	2.1	2.0	3.8	3.7	3.2	2.7	9.0	6.3	7.9	5.4	[dB]
Av. Spread	2.2				3.3				7.2				[dB]
Av. Median	3.7				2.8				9.9				[dB]

6.5 Conclusions

From the seasonal measurements a spread in propagation loss in residential areas due to variation in the environmental conditions has been found. The size of this spread is not correlated to the distance, but increases with frequency. The size of the spread is in the order of other measurement uncertainties and does not necessarily reduce the accuracy of the propagation loss measurements in residential areas. As these measurements were carried out in the summer season, a small correction number, 1 to 3 dB, being the half of the spread, could be subtracted for compensation.

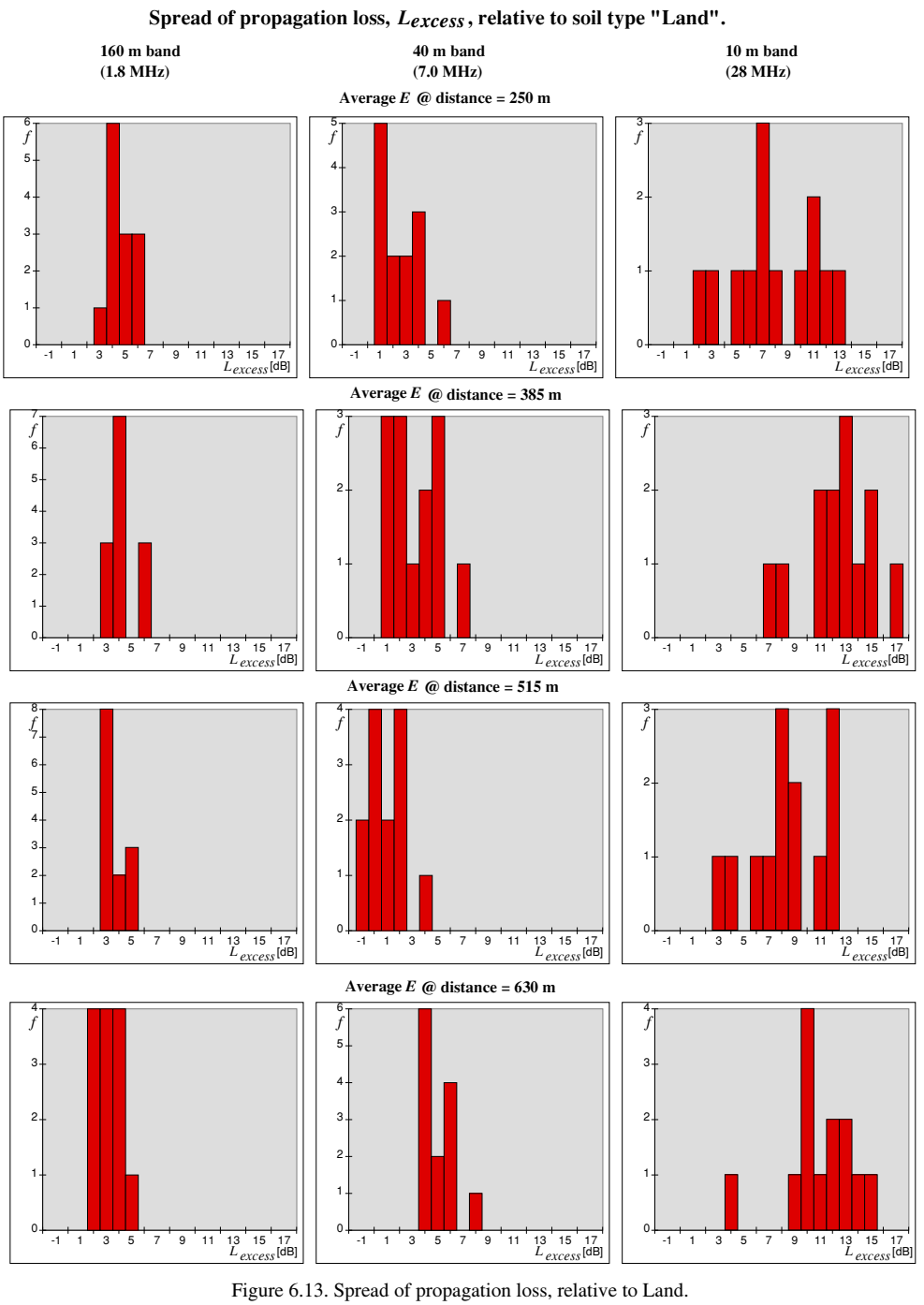

Figure 6.13. Spread of propagation loss, relative to Land.

Chapter 7

7 Model of cumulation of man-made radio noise, applied to sources of emissions limited by EMC standards, and compared to noise measurements

This chapter finalizes the study into cumulation effects of MMN. A model is presented of the cumulation effect of MMN in residential areas, using the propagation model from Chapter 5. Using the so obtained cumulation model MMN field strength levels are calculated under specified conditions, which results are compared to the measurements results of Chapters 3 and 4. The chapter is based on the publication "Model of cumulation of man-made radio noise, applied to sources of emissions limited by EMC standards, and compared with noise measurements", publication [V].

7.1 Introduction

In the last three decades radio spectrum users in residential areas are experiencing a gradual increase of man-made radio interference and noise. At first this was manifested by an increase of interference complaints concerning identifiable sources, being apparatus that demonstrable and verifiable not fulfilled the EMC requirements. Later, in the last two decades, an increase in AWG broadband background noise was observable in the residential and city areas. In 2015 and 2016 a measurement campaign was commissioned by the VERON, the Association for Experimental Radio Research in The Netherlands, member of the International Amateur Radio Union, IARU. The measurements in the

frequency range from 472 kHz to 50 MHz showed a clear increase in Man-Made Noise (MMN) compared with man-made noise data as given in the ITU Recommendation P.372-15 [13]. These measurements are reported in Chapter 3. The increase in MMN level in residential areas has been continued in the period from the measurements until now, according reports from VERON members to its EMC-EMF committee and according individual contact of the authors with colleague radio amateurs. Currently the reception at home in the MF and HF range is not feasible any more for many radio users, and they bail out to practice their hobby outdoors in rural areas. Or they flee in the use of external reception sites, situated in quiet areas, like the so-called web-sdrs [87] or even private remote controlled radio equipment, installed in quiet locations. Although some people may see these developments as a technical progress, we consider it as an harmful impediment towards the self-training, intercommunication and technical investigation possibilities as defined in the definition of the *Amateur Radio Service* in the ITU Radio Regulations. More important, we received knowledge of harmful interference to other radio services, including broadcasting and safety and security relevant services, because of the broadband nature of the MMN. Interference and reduction of transmitting range of the last services is a very serious problem.

In this chapter we will make an attempt for an elucidation of the phenomenon of the rise of the broadband noise floor by human activity in residential environments. We will assume a cumulation effect by large numbers of small noise sources, spread over residential areas. In fact we assume a large number of sources in every home or apartment like many switch mode power supplies in adapter for laptops, PCs, and many other apparatus. Other sources are LED lighting, multi-media equipment, internet of things, LAN equipment, ventilation systems, PV installations, etc., etc. In this way we will build a model for the cumulation effect of large numbers of man-made noise sources.

The need for a cumulation model became apparent during the discussions about EMC standards for broadband cable networks, starting in the nineties of the last centennial. In particular EMC of high speed data communication over mains networks (Powerline communication, PLC) and over telephone lines (xDSL), and also leaky coaxial TV networks was addressed. Jonathan Stott from BBC Research did an in depth analysis of cumulation effects of interference from broadband communication systems in 1999 [88]. He included accumulation via groundwave, via skywave (reflection against the ionosphere), and in free space, concerning interference to reception in airplanes. Although he mainly focused on PLC in that section, a generalized analysis is given in [89]. In [35] an extensive study is published about all aspects of interference from wire-line broadband telecommunication systems, including cumulation effects. For the same purpose the Swiss

Federal Office of Communications (OFCOM, in the German language BAKOM) did measurements in cooperation with the Swiss telecom firm ASCOM on the radiation of PLC signals, and presented the results as isotropic effective antenna gain factors. They used three injection points: a) the median voltage (MV) transformer in the street, b) the house access point (HAP), and c) indoor wall outlets. Antenna gains were measured separately for skywave radiation, as well as for groundwave, [90]-[93]. Also the Netherlands Radio Agency did antenna gain measurements of mains networks [94].

The study in this chapter is not directed on wire-line broadband telecommunication systems, but is focussed on MMN sources in ordinary house-hold environments, e.g. on situations wherein appliances inject electric disturbance into mains networks. In the preparation of this study we investigated the MMN floor in Chapter 3, the correlation between the MMN floor levels and the density of habitation in Chapter 4, and the propagation in residential areas in Chapter 5. For details about the measurements we refer to Chapter 3, 5 and 6.

The chapter is organized as follows: In Section 7.2 the theory of the cumulation process is clarified using the propagation model from Chapter 5, in Section 7.3 we consider the input parameters for the MMN field strength calculations, and in Section 7.4 we show the calculations and discuss their results in Section 7.5. The conclusions appear in Section 7.6.

7.2 Theory of cumulation of Noise from Multiple Sources

Cumulative man-made noise (MMN) is the addition of the signals of a large number of noise and EMI sources around the measurement location. Figure 7.1 depicts an area with a measurement location M, several source locations S_i with each a propagation traject distance r_i.

The sources are uncorrelated, so we must add the signal powers of these signals to arrive at a power density s and a field strength E in general written as:

$$s_M = \sum_{i=1}^{N} p_i g_i l(r_i) \tag{7.1}$$

Herein is: p_i, the source power of source i, g_i the antenna gain of source i, and $l(r_i)$, the transmission loss with distance, r_i. Then the field strength e_M at location M follows from:

$$e_M = \sqrt{s_M Z_0} \tag{7.2}$$

wherein $Z_0 \approx 120\pi \approx 377$ ohm. Independently from the signal shapes of the individual sources the cumulation of various uncorrelated signals will lead to Gaussian noise at the measurement location M for a high number of sources.

Later on we will consider the sources s_i in Figure 7.1 as the houses wherein a large

series of pieces of equipment act as sources and inject noise and EMI in mains and in other wires and conductors. As we suppose linear processes we may add all noise sources in a house together, and combine them with the corresponding antenna gain of each house. In this paper we write the number of homes in an area as *Nh*, and the number of sources as *Ns*. The number of sources per home *m* is given as $m = Ns/Nh$.

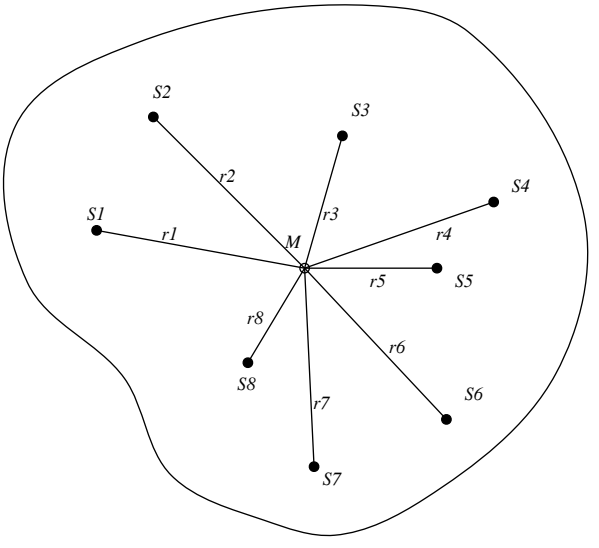

Figure 7.1. Sources S_i with distances r_i to measurement location M.

7.2.1 Propagation loss

In Chapter 5 a propagation loss *L* is defined as the ratio between a (fictitious far field) field strength (FS) *E* at a distance of 1 meter to the FS at a distance of *r* meters:

$$L = E_{r=1} - E_r \quad [\text{dB}] \tag{7.3}$$

$$l = \frac{e_{r=1}}{e_r} \tag{7.4}$$

The measurements in Chapter 5 showed that *L* for residential areas can be described by a linear relationship between the logarithm of the distance and the propagation loss in dB.

$$L = slope \log r \quad [\text{dB}] \tag{7.5}$$

Also was found that in the range from 1 to 30 MHz the slope of this linear relationship is linearly depending on the logarithm of the frequency *f* in MHz, and so on throughout this chapter:

$$slope = a \log f \ [\text{MHz}] + b \ [\text{dB/decade}] \tag{7.6}$$

The constants in this relationship were measured in Chapter 5 and are given in Table

7.1. Herein is n the number of measurement samples, r the correlation coefficient, and r_{min} the minimal correlation coefficient for a 95 % reliability.

Table 7.1. Constants in the frequency depending roll-off of propagation loss with distance.

Frequency range 1 - 30 MHz	*Roll-Off slope* = a*log(f[MHz]) + b [dB/decade]				
Correlation over:	n	r	r_{min}	a	b
Group I + II + III	**18**	**0.963**	**0.378**	**14.3**	**23.0**
Low density area, group I	6	0.994	0.622	12.6	23.3
Median density area, group II	6	0.989	0.622	14.6	22.1
High density area, group III	6	0.992	0.622	15.6	23.7
All locations	6	0.993	0.622	14.5	22.4

So the propagation loss can be written as:

$$L(r,f) = \left(a \log f + b\right) \log r \ \text{[dB]} \tag{7.7}$$

$$l(r,f) = 10^{\frac{\left(a \log f + b\right) \log r}{20}} \tag{7.8}$$

The calculation of accumulated noise is always performed for a fixed frequency. As we may handle f as a constant, we can simplify Equation (7.8). If

$$slope = a \log f + b \tag{7.9}$$

then:

$$l(r,f) = 10^{(slope(f)/20)\ \log r} = r^{(slope(f)/20)} \tag{7.10}$$

$$l^2(r,f) = r^{(slope(f)/10)} \tag{7.11}$$

7.2.2 Calculation for a single source

We have a source with an expectation value for the source power $\hat{p}_i$. We assume a perfect impedance match from the source into the mains network. The network partly radiates this power into a low elevation angle so that we may speak of ground-wave propagation. For such networks an apparent isotropic antenna gain g_i, which gain includes a radiation efficiency η, has been established by measurements [93]. That antenna gain can be used as a generalized expectation value $\hat{g}(f)$ for mains networks, frequency f dependent.

We can approximate the field strength at short distances. We assume a short electric monopole over a Perfect Electric Conducting (PEC) ground. The gain of a short monopole over PEC is: $g_{monopole} = 3$, or 4.77 dB, [84], [85]. For the free half space wave we find for the power density s_{pec} on zero elevation angle:

$$s_{pec} = \frac{p_{tx} g_{monopole}}{4\pi r^2} \tag{7.12}$$

$$e_{pec} = \sqrt{s_{pec} Z_0} \approx \frac{1}{r}\sqrt{p_{tx} g_{monopole} \cdot 120\pi / 4\pi} \tag{7.13}$$

$$\approx \frac{1}{r}\sqrt{p_{tx} \cdot 3 \times 30} \tag{7.14}$$

In the real environment we substitute $g_{monopole}$ in the expectation value of the antenna gain $\hat{g}(f)$, and divide by the expectation value of the extra propagation loss factor $\hat{l}_{excess}(f)$:

$$e_i \approx \frac{1}{r_i} \frac{1}{\hat{l}_{excess,i}(r_i, f)} \sqrt{\hat{p}_{tx}(f)\, \hat{g}(f) \cdot 30} \tag{7.15}$$

We combine $r_i \hat{l}_{excess,i}(r_i, f) \equiv \hat{l}_i(r_i, f)$. Values for $\hat{l}(r, f)$ are derived in Chapter 5. So for the field strength we can write:

$$e_i \approx \frac{1}{\hat{l}_i(r_i, f)} \sqrt{\hat{p}_{tx}(f)\, \hat{g}(f) \cdot 30} \tag{7.16}$$

The power density s_i, caused by source i at distance r_i, is:

$$s_i = \frac{e_i^2}{Z_0} = \frac{\hat{p}(f)\, \hat{g}(f) \cdot 30}{\hat{l}_i^2(r_i, f) \cdot 120\pi} = \frac{\hat{p}(f)\, \hat{g}(f)}{r^{(slope(f)/10)} \cdot 4\pi} \tag{7.17}$$

7.2.3 Accumulation of man-made noise sources. Case 1: A series of known sources

Now, as we can calculate the electric field strength at any distance from a single source i and so the power density s_i, we add the power densities from Ns sources around the measurement position M according formula (7.1).

$$s_M = \sum_{i=1}^{Ns} s_i = \sum_{i=1}^{Ns} \frac{\hat{p}(f)\, \hat{g}(f)}{\hat{l}_i^2(r_i, f) \cdot 4\pi} \tag{7.18}$$

$$e_M^2 = s_M Z_0 = \frac{\hat{p}(f)\, \hat{g}(f) \cdot 120\pi}{4\pi} \sum_{i=1}^{Ns} \frac{1}{\hat{l}_i^2(r_i, f)} \tag{7.19}$$

Now we write for the accumulation of Ns sources in technical units:

$$e_M^2[\mu V/m] = \hat{p}(f)[mW]\, \hat{g}(f) \cdot 30 \times 10^9 \cdot \sum_{i=1}^{Ns} \frac{1}{\hat{l}_{,i}^2(r_i, f)}$$

In dB:

$$E_M[dB\mu V/m] = \hat{\hat{P}}(f)[dBm] + \hat{\hat{G}}(f)[dB] + 104.8 +$$

$$-10 \log \sum_{i=1}^{Ns} \hat{l}_i^2(r_i, f) \tag{7.20}$$

$$= \hat{P}(f)\,[\mathrm{dBm}] + \hat{G}(f)\,[\mathrm{dB}] + 104.8 +$$

$$-10 \log \sum_{i=1}^{Ns} r_i^{(slope\,(f)\,/\,10)} \tag{7.21}$$

7.2.4 Case 2: A flat density of sources, density known

The function of E_M^2 as a cumulation of all man-made sources within the circle with radius r is of special interest, see Figure 7.2. Therefor we assume a density of MMN sources of n sources per m^2. The area A [m^2] within a circle with radius r is:

$$A = \pi r^2 \tag{7.22}$$

So the number of sources N_s within radius r is:

$$N_s = nA = n\pi r^2 \tag{7.23}$$

The number of sources dN_s in annular region dr is given by the first derivative:

$$dN_s = n\pi \cdot 2rdr \quad \text{for } r \gg dr \tag{7.24}$$

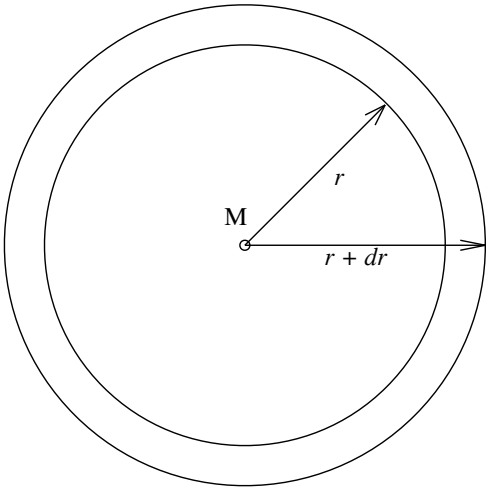

Figure 7.2. Depiction of the integration process with radius r.

For calculating the sum s_M of all contributions s_i from all sources between a minimum radius r_{min} and a maximum radius r_{max} we have to integrate over radius range r_{min} to r_{max}, taking into account the varying number of sources per increase of r and the increase of propagation loss $\hat{l}_i(r_i, f)$ with distance. Implicitly we use Wald's equation, (7.25), here, which says that the expectation value of the sum of N independent observations X_N with a random outcome, in which $\hat{N}$ itself is the expectation value of the total number of observations, is equal to the product of the expectation values:

$$E(X_1 + X_2 + .. + X_N) = \hat{N} \cdot \hat{X} \tag{7.25}$$

In our application $\hat{N}$ stands for the expected number of sources, dN_s, in area dA and $\hat{X}$ for the power density $\hat{s}_i$ at location M. Although we consider the source density n as an deterministic input parameter, the division of sources over the area dA is a stochastic variable.

$$dA = 2\pi r dr \tag{7.26}$$

$$dN_s = ndA = n{\cdot}2\pi r dr \tag{7.27}$$

$$s_m = \int_{r=r_{min}}^{r_{max}} n{\cdot}2\pi r s_i.dr \tag{7.28}$$

$$= \int_{r=r_{min}}^{r_{max}} n{\cdot}2\pi r \frac{\hat{p}(f)\,\hat{g}(f)}{\hat{l}^2(r,f)\cdot 4\pi}{\cdot}dr \tag{7.29}$$

$$= n\hat{p}(f)\,\hat{g}(f) \int_{r=r_{min}}^{r_{max}} \frac{2\pi r}{\hat{l}^2(r,f){\cdot}4\pi} dr \tag{7.30}$$

$$= \frac{n{\cdot}\hat{p}(f)\,\hat{g}(f)}{2} \int_{r=r_{min}}^{r_{max}} \frac{r}{\hat{l}^2(r,f)} dr \tag{7.31}$$

With

$$\hat{l}(r,f) = 10^{\frac{a\log f + b\log r}{20}} \equiv r^{(slope(f)/20)} \tag{7.32}$$

The electric field strength follows from:

$$e_M = \sqrt{s_M Z_0} \tag{7.33}$$

$$\approx \sqrt{\frac{n\hat{p}(f)\,\hat{g}(f)}{2} 120\pi \int_{r=r_{min}}^{r_{max}} \frac{r}{\hat{l}^2(r,f)} dr} \tag{7.34}$$

We consider the frequency f as a constant, we may do so because we apply the integration at a single frequency. When we define $sl \equiv slope(f)/10$, and use Equation (7.11), we may simplify the integration:

$$integral \equiv \int_{r=r_{min}}^{r_{max}} \frac{r}{\hat{l}^2(r,f)} dr = \int_{r=r_{min}}^{r_{max}} \frac{r}{r^{sl}} dr \tag{7.35}$$

$$= \int_{r=r_{min}}^{r_{max}} r^{1-sl} dr \tag{7.36}$$

$$= \frac{1}{sl-2}\left(\frac{1}{r_{min}^{sl-2}} - \frac{1}{r_{max}^{sl-2}}\right) \tag{7.37}$$

This solution of the integral exists when: $sl \neq 2$, $slope(f)/10 \neq 2$, $slope(f) \neq 20$ dB/dec. In practice this means that the propagation loss should be larger than the loss in free space, which is always the case here. So the complete solution is:

$$e_M = \sqrt{n\hat{p}(f)\,\hat{g}(f)\cdot 60\pi \frac{1}{sl-2}\left(\frac{1}{r_{min}^{sl-2}} - \frac{1}{r_{max}^{sl-2}}\right)} \tag{7.38}$$

7.2.5 Maximum range relevant for cumulation

A very relevant question is: "Up to what range do the sources contribute to the total noise power?" Therefor we go back to Equation (7.37). Herein we find the relationship between the maximum distance r_{max} and the integral term *integral* of the power density s_M with the slope factor *sl* and the minimum distance r_{min} as a chosen parameters: We find a maximum of *integral* for $r_{max} \rightarrow \infty$:

$$integral_{max} = \frac{1}{sl-2}\,\frac{1}{r_{min}^{sl-2}} \tag{7.39}$$

The maximum MMN FS at location *M* can now be calculated from Equation (7.38) under the condition $r_{max} \rightarrow \infty$:

$$e_{M,max} = \sqrt{n\hat{p}(f)\,\hat{g}(f)\cdot 60\pi \frac{1}{sl-2}\,\frac{1}{r_{min}^{sl-2}}} \tag{7.40}$$

Now we define a border value for $r_{max}(k)$ for a ratio k from where the extra contribution to the noise power is limited to:

$$k \equiv \frac{integral}{integral_{max}} \text{ for } k < 1 \tag{7.41}$$

$$k = \left(\frac{1}{r_{min}^{sl-2}} - \frac{1}{r_{max}^{sl-2}}\right) \Big/ \left(\frac{1}{r_{min}^{sl-2}}\right) \tag{7.42}$$

$$\frac{k}{r_{min}^{sl-2}} = \frac{1}{r_{min}^{sl-2}} - \frac{1}{r_{max}^{sl-2}} \tag{7.43}$$

$$\frac{1}{r_{max}^{sl-2}} = \frac{1-k}{r_{min}^{sl-2}} \tag{7.44}$$

$$r_{max}(k) = \frac{r_{min}}{(1-k)^{1/(sl-2)}} \tag{7.45}$$

7.3 Input Parameters

Man-made noise is generated by electric, electronic, IT equipment and installations. Every electric current or voltage, that is switched between two amplitude or phase conditions, generates electric noise over a broad spectrum, what may be radiated as an EM wave by the connected wiring. In particular switched mode power supplies generate high frequency components as a result of high dV/dt-voltages, caused by the switching currents, which switching is continuously and with a high frequency. They are for any kind of use, from very small, for example in LED lamps, up to high power units as in frequency and PV

convertors. The disturbance power of these sources, available at the mains port, varies over a large range. It's level depends heavily on the internal switched currents, and how far the manufacturer of these equipment succeeds in suppressing the noise at the port by filtering.

The radiation of man-made noise is legally limited by the EMC Directive in Europe [29] as explained in [95], and by the FCC rules in the USA. Although the EMC Directive legally only tells that radio services shall not be interfered by harmful interference, it places the responsibility on the manufacturers of electric and electronic apparatus. To fulfil the EMC requirements they may use EMC standards to show compliance. So is the IEC 61000-6 [96] series of generic standards, that applies when there is no product standard available, and sets the basis for many limits that also appear in product standards like the CISPR 11 [97] for industrial, scientific and medical equipment, CISPR 14 [98] for household appliances, electric tools and similar apparatus, CISPR 32 [99] for multimedia equipment. In essence they all share the same limit values for conducted disturbances on (AC) mains power ports for class B (domestic) equipment. Also the limits on DC power ports, telecom and other wired ports are equivalent between the standards, but differ from the AC port limits. They share field strength limits for radiated emissions.

The limits for conducted emissions on the AC power port are of our primary interest, because a) they are applicable for our frequency range of interest: 150 kHz to 30 MHz, and b) these limits apply to the largest amount of electric and electronic equipment used in residential environment, c) we have access to the emission properties of mains networks in homes, to be discussed later in this section, useful for cumulation calculations.

In these standards radiation limits are only available for frequencies above 30 MHz, so they are not of interest in this study. Below 30 MHz the wavelength is so much larger than the dimensions of the equipment that generally is accepted that the radiation direct from the cabinet, and from the circuits inside of the equipment, is negligible.

Wires, connected to DC power ports, telecom ports and other wired ports, may be playing a significant role in radiation of electromagnetic disturbances, but these emissions are difficult to use in a cumulation model because of lack of stochastic data about the emission properties. We will ignore this form of radiation initially, but come back on this subject in the Section 7.5.

In the EMC standards the voltage at the mains port is limited, and the resulting radiation depends on the attached wiring and especially the extensiveness of the wiring inside the house and the structure of the mains wiring. E.g. parts of the mains wiring may show loops and dipole-like structures.

The limit values in the mentioned EMC standards correspond to a measuring bandwidth of 9 kHz in the frequency range 150 kHz to 30 MHz. *A priory* there is no knowledge about

the character of the disturbance. In case of an unmodulated carrier the measuring bandwidth and type of detector is not relevant. Secondly, it may consist of a complex waveform, more or less pulsed. Here the Quasi-Peak detector, as defined in CISPR 16-1-1 [100], is used for EMC measurements and the bandwidth of the disturbances often exceeds 9 kHz. Thirdly, the disturbance may be stochastic and broadband of nature (AWGN). In this case the required detector is the RMS detector, but may be replaced by the Average detector in combination with a correction. Also the measurement bandwidth is relevant, so usually there is a conversion into a power density, giving the noise power in 1 Hz bandwidth, or into a common user bandwidth. To do the calculations to estimate cumulative MMN FS levels at a location we have to fill in a few input parameters:

a) The expectation value of the available power per source.
b) The expectation value of the antenna gain for a home mains network.
c) The expectation value of the number of sources per home.
d) The expectation value of the number of home per square meter.
e) The minimal distance r_{min}, the exclusion zone.
f) The expectation value of the propagation loss, $\hat{l}$.

7.3.1 Available source power

Selection of the expectation value of the available power per source is a very relevant factor which has a direct effect on the calculated cumulative MMN field strength. A very interesting choice is the available power value derived from the earlier mentioned limits for the residential environment (class B) conductive disturbance limit at the mains port. Because all electronic equipment in homes is expected to meet this requirement, and so forming an upper limit for the value of the available power of sources. From the result we would conclude if this standard is sufficient strict to protect radio users in residential areas from interference from cumulative MMN from large numbers of sources. The values, given by the standard, is given in Table 7.2. Herein a line impedance of 50 ohm is assumed.

Table 7.2. Limits for conducted disturbance at the mains ports for equipment to be used in residential areas (class B).

Frequency [MHz]	*Limits Quasi Peak* [dBµV]	*Limits Average* [dBµV]
0.15 to 0.50	66 to 56	56 to 46
0.50 - 5	56	46
5 - 30	60	50

For the frequency range from 150 kHz to 30 MHz the measurement bandwidth is 9 kHz. For the case of the cumulation study we choose for handling MMN as being AWGN noise, because after cumulation of the large number of uncorrelated sources the result will be AWGN as described by the Central Limit Theorem. Further, we choose to use 2.7 kHz as

the reference bandwidth, because the most used receiver and channel bandwidth on MF and HF is 2.7 kHz. This reference bandwidth was also used for the measurements in Chapter 3. The difference on the levels of Gaussian noise from this bandwidth to the 9 kHz bandwidth as defined in CISPR 16-1-1 is 5.2 dB. We may use the limit values for the Average detector for setting the source disturbance voltage that is being injected in mains wiring. These limit are converted into an available source power in a bandwidth of 9 kHz. Hereafter we refer to these power values as Equivalent CISPR Source (ECS). Taking into account the conversion from average value into r.m.s value (+1.05 dB) the available source power @9 kHz, P:

$$P_{9kHz} = V_{av}\ [\text{dB}\mu\text{V}] - 107 + 1.05\ [\text{dBm}] \tag{7.46}$$

$$P_{2.7kHz} = P_{9kHz} - 10\log(9/2.7)$$

$$P_{ECS} \equiv P_{2.7kHz} = P_{9kHz} - 5.2\ \ [\text{dBm}] \tag{7.47}$$

Also we can derive a power density:

$$PDF_{ECS} = P_{9kHz} - 10\log(9000)$$

$$= P_{9kHz} - 39.5\ \ [\text{dBm/Hz}] \tag{7.48}$$

See the Table 7.3, where also the frequency dependant available source powers are inserted, derived from the Average limits in Table 7.3.

Table 7.3. ECS power, derived from data in Table 7.2.

Frequency [MHz]	*Available source power* [dBm], *BW* = 9 kHz	*Power density* [dBm/Hz]	*Available source power* [dBm], *BW* = 2.7 kHz
1.85	-60	-99.5	-65.2
3.65	-60	-99.5	-65.2
5.35	-56	-95.5	-61.2
7.1	-56	-95.5	-61.2
10.1	-56	-95.5	-61.2
14.2	-56	-95.5	-61.2
18.1	-56	-95.5	-61.2
21.1	-56	-95.5	-61.2
25.0	-56	-95.5	-61.2
28.5	-56	-95.5	-61.2

7.3.2 Antenna gain

To calculate the isotropic radiated power the expected value of the antenna gain of the radiating elements in the mains network must be added to the ECS values. Reference [93] shows the equivalent antenna gain for groundwave radiation of the inhouse part of Low Voltage Distribution Networks.

Reference [92] discusses the measurement method. The results are shown in Figure 7.3

and Figure 7 from [93]. Three types of injection points are identified: a) the Indoor, using mains sockets; b) House Access Point (HAP), the connection from the street cable to the meter; c) the 230 V crossbar in the transformer substation. The exact measurement frequencies are 2.0, 3.5, 10, 20, and 30 MHz.

From Figure 7.3 it is clear that the measurements, using the Indoor injection points, show the highest antenna gain figure, and so are most relevant for our study. We use the trend line "Indoor" to calculate equivalent antenna gains for our frequencies of interest, see Table 7.4. Antenna gain measurements have also been performed in the Netherlands [95]. Although these measurements are less extensive than those in [93], the results are about the same, see Figure 7.4.

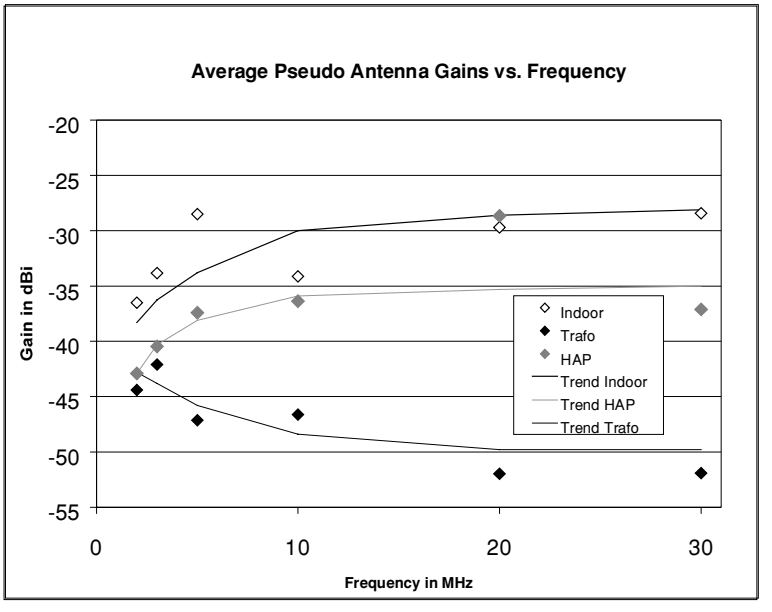

Figure 7.3. Resulting average pseudo antenna gains of LVDN vs. frequency with trend lines, Figure 7 in [94].

In both references the test signal has been injected in the Differential Mode (DM). In Appendix H we conclude that the Longitudinal Conversion Loss (LCL) value is, averaged over the frequency range, maximal 6 dB for real world domestical environments. That means that the CM currents, induced by the injected the DM current, has, averaged over a large frequency range, half the value of the DM current. The in Subsection 7.3.1 calculated available source power is valid for the Normal Mode, that means on one line, Live or Neutral. Disturbances from equipment are mostly present on both lines, often in phase so CM, but in counter phase, DM, is also possible. So in practice the injected power is 3 - 6 dB higher, which compensates for the 6 dB LCL, for which the estimated antenna gains are valid.

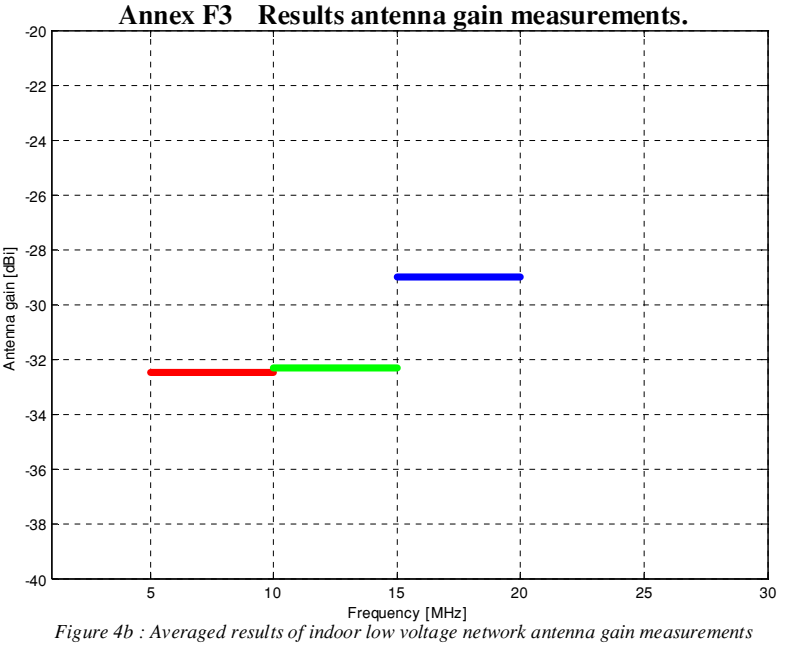

Figure 4b : Averaged results of indoor low voltage network antenna gain measurements in the frequency ranges 5 MHz-10 MHz, 10 MHz-15 MHz and 15 MHz-20 MHz . Total number of measurements: 113 measurements at 13 different houses in 3 frequency ranges.

Figure 7.4. Antenna gain measured in the Netherlands, from [95].

Table 7.4. Expectation values of antenna gain of inhouse mains networks.

Frequency [MHz]	1.85	3.65	5.35	7.1	10.1	14.2	18.1	21.1	25.0	28.5
Isotropic antenna gain [dB]	-38.3	-35.7	-33.7	-32.3	-30.0	-29.4	-28.8	-28.3	-27.8	-27.2

7.3.3 Number of sources per home

A number of 50 sources per home, m, is assumed for all types of environments.

7.3.4 Density of habitation, exclusion zone and propagation loss

The calculations are based on a flat density of sources. In practice the spread of the sources is never flat, but these calculations may give some insight in fundamental aspects. The expectation value of the number of homes per square meter is depending on the type of environment. We will apply the calculations for four types of environments with increasing density of habitation, and so the density of sources. This density also has an effect on the minimum value of r_{min}, the radius of the exclusion zone, and the fine tuning in the propagation loss, the values for a and b. A minimal value for r_{min} is not only necessary for the solution for the integral, but it defines the free space around a detached house wherein

no source is expected, or being under control of the victim habitant. In the EMC standards the exclusion range is considered as the range wherein possible interference sources are considered to be under control of the resident and so are excluded from the ruling. In the integration process we consider r_{min} being the averaged range to the most neighbouring homes, depending on the type of environment. In a first approach we use a rough estimation for the values of r_{min}. As these values have a considerable influence on the calculated FS levels according Equation (7.40) a further discussion of the values may be necessary. For comparison we will also show calculations using a fixed value of $r_{min} = 10$ m.

In Chapter 3 we defined sub-divisions of the residential area as already defined in [13]. In residential-1 area the number of residences within a range of 100 m from the measurement location, $Nh_{r=100}$, is 11 to 50 homes according the definition. This means detached houses with spacious gardens. From the dataset, collected for the MMN measurements in Chapter 3, we calculate the average number of houses in a circle of 500 m, $Nh_{r=500}$, as being 1070. So the density of sources becomes $n = 68 \cdot 10^{-3}$ sources / m^2. For the distance to neighbouring houses we estimate an in all directions averaged value for r_{min} of 50 m. For the propagation loss parameters we take according Chapter 5 $a = 12.6$, $b = 23.3$.

In the residential-2 areas $Nh_{r=100} = 51$ to 100 is 51 homes. In general this means linked houses with gardens. Here we arrived at $Nh_{r=500} = 2388$ and $n = 152 \cdot 10^{-3}$ sources / m^2. We estimate r_{min} =25 m, and select according Chapter 5 $a = 14.3$, $b = 23$.

In the residential-3 areas $Nh_{r=100} > 100$ homes, $n = 274 \cdot 10^{-3}$ sources / m^2. In general this means (multi-floor) linked houses with little or no gardens in dense habituated areas. Here we arrived at $Nh_{r=500} = 3878$, estimate r_{min} =15 m, and select according Chapter 5 $a = 15.6$, $b = 23.7$.

In the area, marked as Residential (1+2+3) we put all the data of all three sub-residential areas together to compare it directly with the residential environment as defined by ITU in [13] and in Chapter 3. Here $Nh_{500} = 2225$, $n = 142 \cdot 10^{-3}$ sources / m^2, we take r_{min} =25 m, and select according Chapter 5 $a = 14.3$, $b = 23$.

In the city areas, defined by $Nh_{100} > 150$ and $Nh_{500} > 2000$, is $Nh_{500} = 4802$ and $n = 287 \cdot 10^{-3}$ sources / m^2. This is an area of dense habitation with a commercial centre. Large apartment buildings are included here. We take r_{min} =10 m, and select according Chapter 5 $a = 15.6$, $b = 23.7$. All these input data is gathered in Table 7.5.

Table 7.5. Input data.

Average number of homes in a circle of 500 m radius: Number of sources/home: m=50	Residential 1 Nh_{100}= 11 - 50	Residential 2 Nh_{100}= 51 - 100	Residential 3 Nh_{100} > 100	Residential (1+2+3) Nh_{100}>10	City Nh_{100} > 150 Commercial center Nh_{500} > 2000
Nh as found in [11]	1070	2388	3878	2225	4502
Source density n [1/m²]	0.068	0.152	0.274	0.142	0.287
a	12.6	14.3	15.6	14.3	15.6
b	23.3	23	23.7	23	23.7
r_{min} [m]	50	25	15	25	10

7.4 Simulations

Now we have the cumulation theory and the input parameters available, we can execute some simulations. First we will look at the relationship between the calculated MMN level and the outer limit of the integration area, defined by r_{max}. In Figure 7.5 we show the results for three frequencies, low (1.8 MHz / 160 m), middle (14 MHz / 20 m), and high (28 MHz / 10 m). Also we use three values for the exclusion range r_{min}: 10, 25 and 50 m. A source power of -40 dBm is used, but for the shape of the curves this parameter is not relevant. We see in all curves that the field strength level stabilizes for high values of r_{max}. The minimal value of r_{max} from where the increase nearly stops is strongly depending on the exclusion zone r_{min}, and also on the frequency. In Equation (7.41) we defined a ratio k.

Using Equation (7.45) a maximum range $r_{max}(k)$ can be calculated wherein the attribution of noise sources is relevant, depending on the chosen ratio k and frequency. Factor k is in the graphs given as a dB number K according

$$K = 10 \log (k) \tag{7.49}$$

From Figure 7.6 for $K = -0.5$ dB we learn that the range $r_{max}(K)$, wherein the radiated power from each source participate in the total noise FS at location M, is very limited and depending on frequency and on the exclusion distance r_{min}. The value of this distance appears to be in the same order of magnitude as we concluded in Chapter 4, namely up to 300 m, frequency depending.

Secondly, we will study the cumulative levels under several conditions. We start with assuming that the expectation value for the available power of the sources is equivalent to the class B limit for the conducted disturbance (the in Table 7.3 defined ECS values), and the discerning values for r_{min} according Table 7.5. The resulting calculated field strength values are shown in Figure 7.7 alongside with the published MMN field strength levels according [13] and the measured levels according Chapter 3.

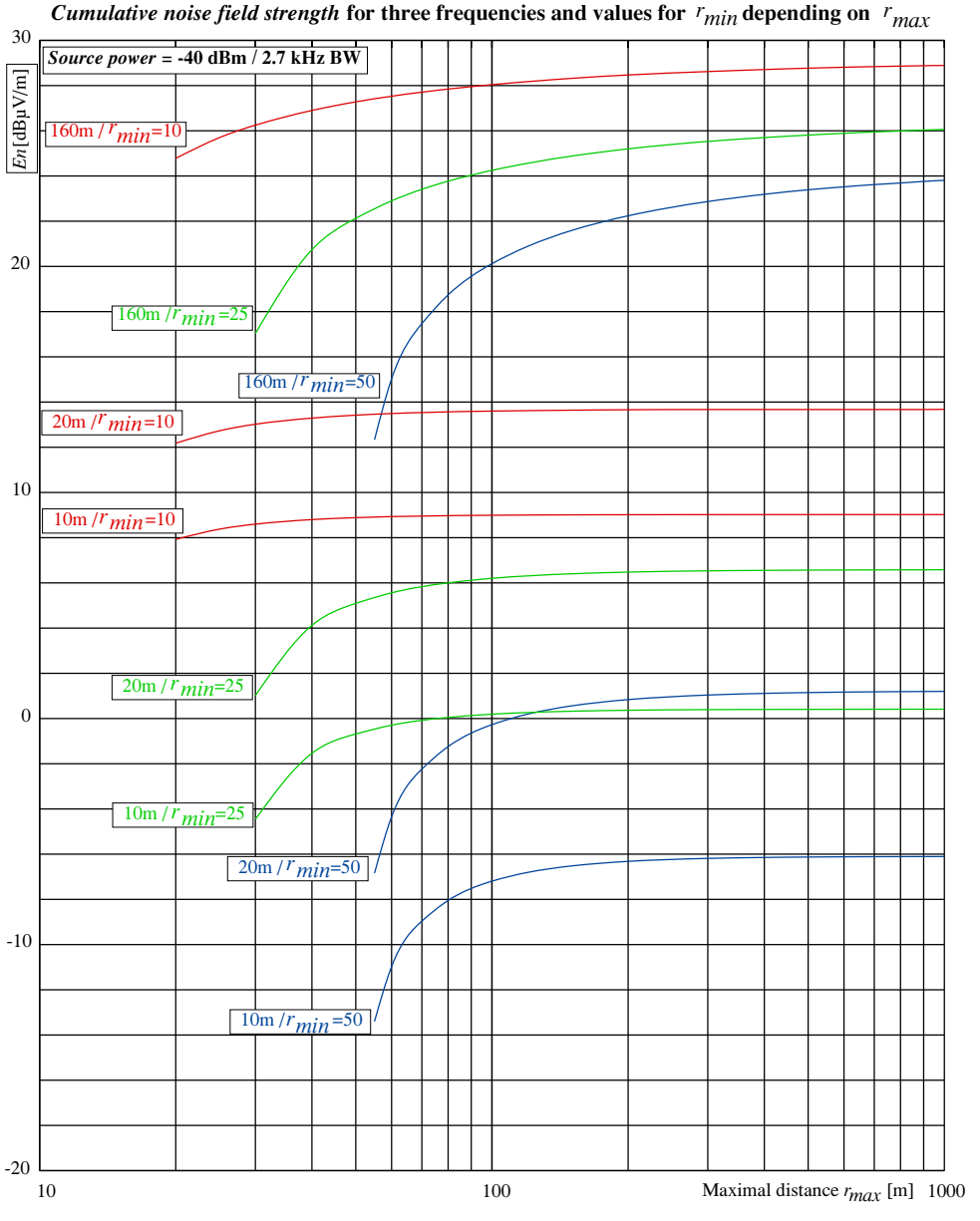

Figure 7.5. Cumulative noise field strength for the three frequencies and values for r_{min} depending on r_{max}.

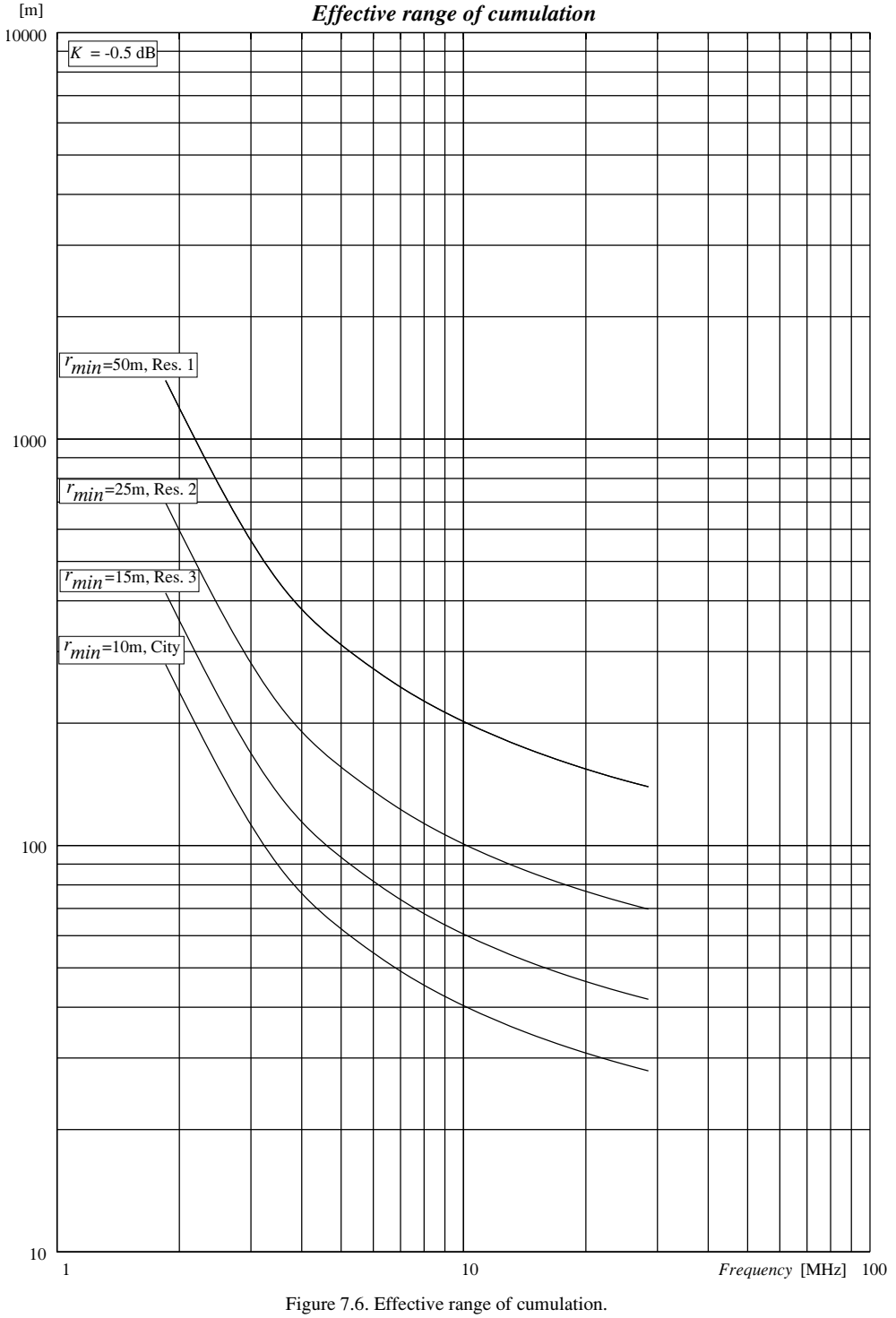

Figure 7.6. Effective range of cumulation.

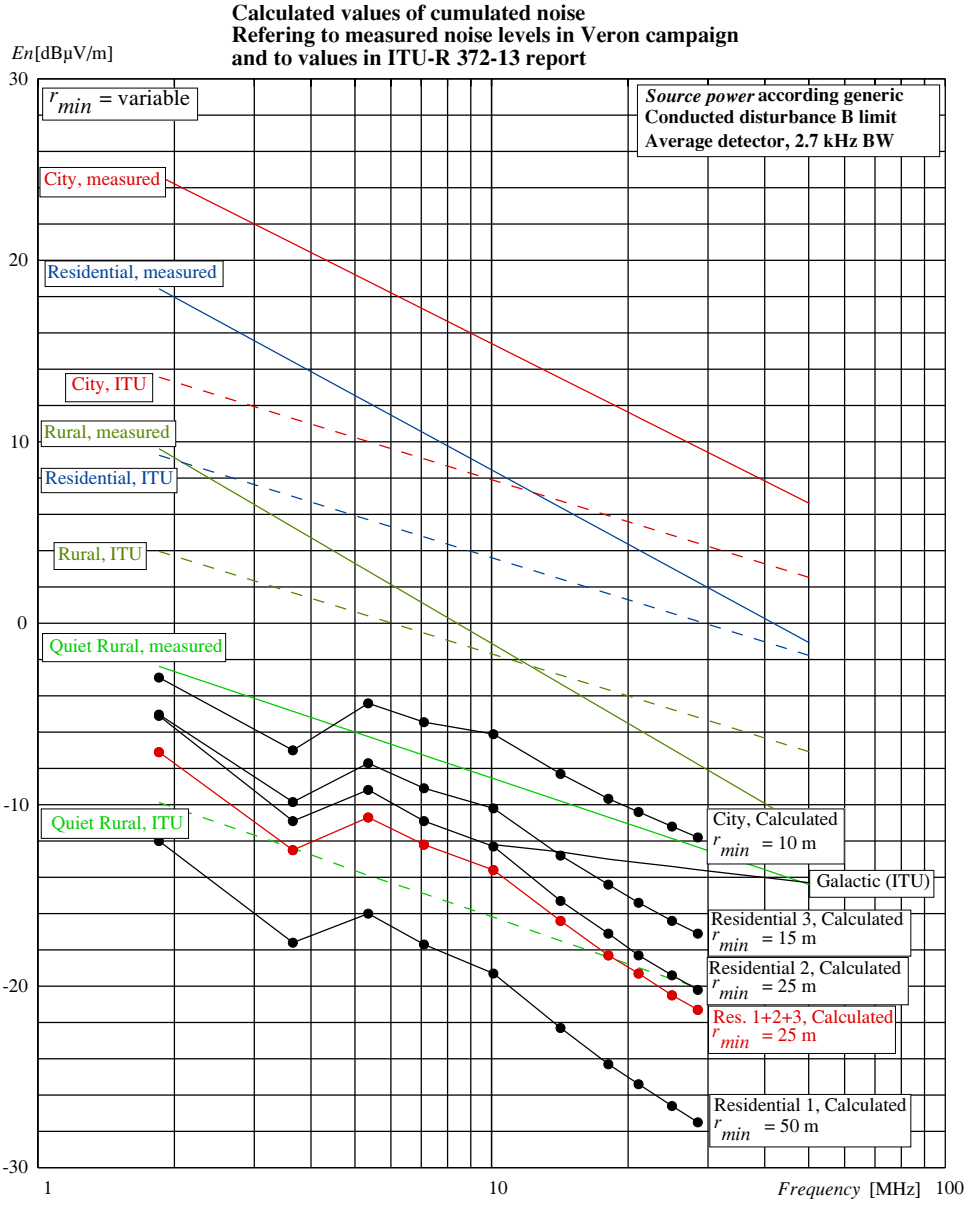

Figure 7.7. Outcome of noise floor simulations (black) using source powers according ECS values with real minimum distance values.

We conclude that the calculated FS levels are very low. Even for the curve of the environment, where MMN is at the highest level, namely the city area, the calculated values match more or less the measured values for the Quiet Rural area. At the lowest frequencies the levels are lower because of the lower limit levels for frequencies below 5

MHz, see Table 7.2. When we assume a fixed value for r_{min} = 10 m, then the curves approach each other, but the mean level is still around the measured Quiet Rural curve, see Figure 7.8. The conclusion we draw from these simulations is that the measured MMN levels in Chapter 3 cannot be explained with noise sources with power levels at the ECS values.

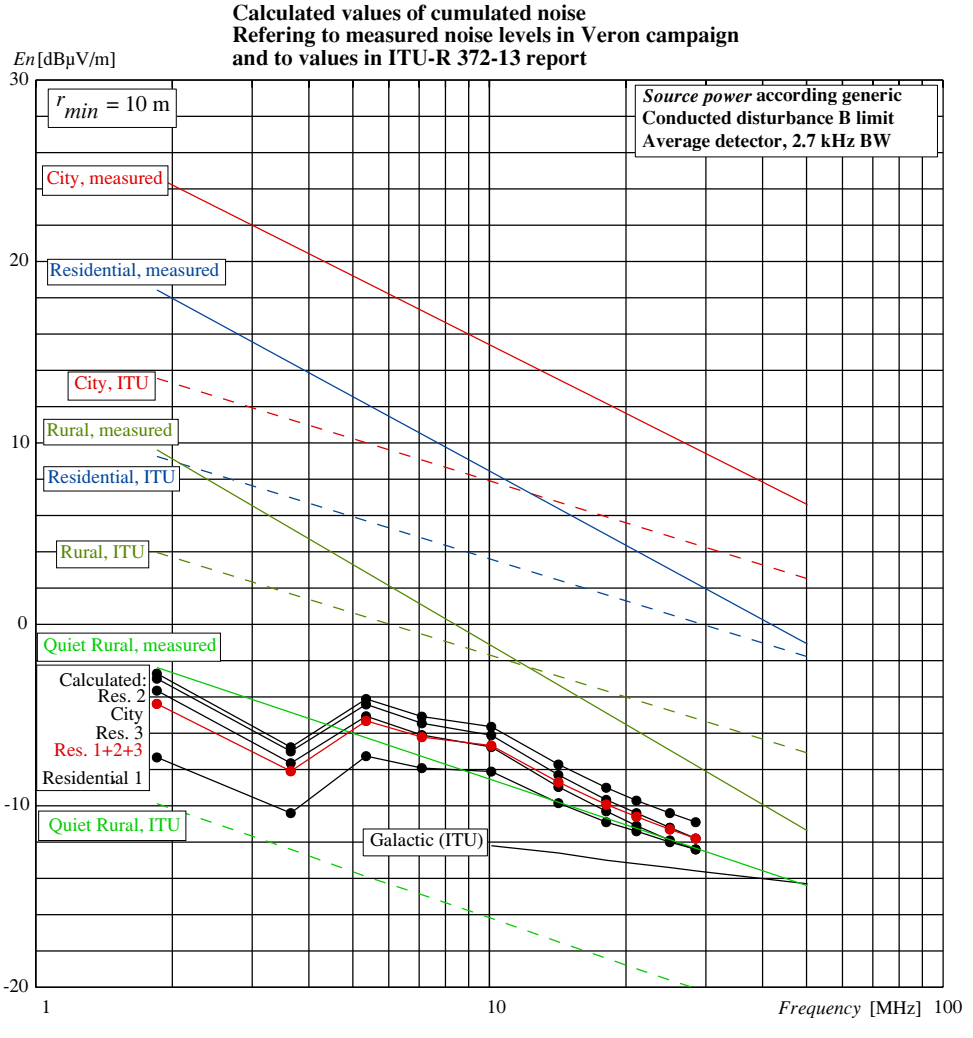

Figure 7.8. Outcome of noise floor simulations (black) using source powers according ECS values and a fixed minimum distance of 10 m.

In a second experiment we assume an expectation value for the available power from the mains ports of -40 dBm for all frequencies. The results of those simulations are shown in Figure 7.9 for discerning values for r_{min}. The results for each type of environment approach the measured values pretty well.

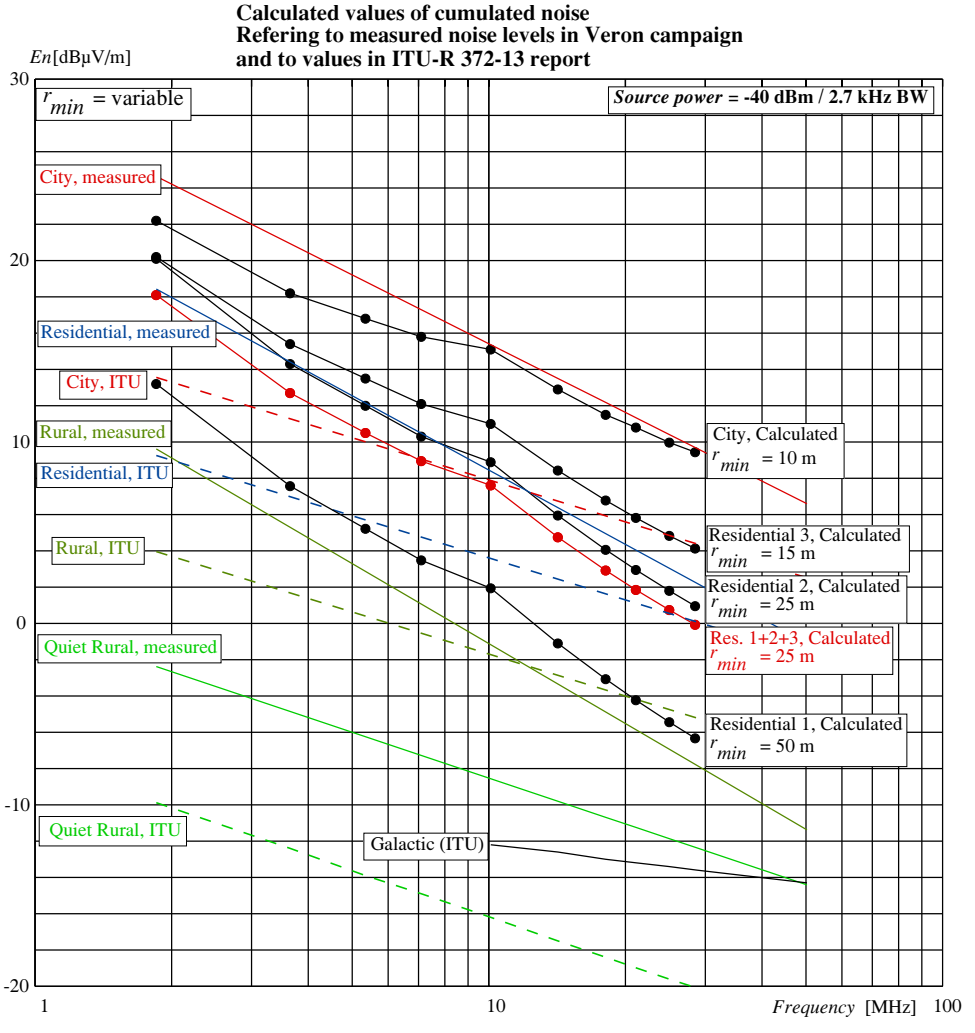

Figure 7.9. Outcome of noise floor simulations (black) using a source power of -40 dBm in 2.7 kHz bandwidth with real minimum distances.

Further, remember that for frequencies below 10 MHz the antenna gain of the radiating home mains networks reduces, see Figure 7.3 and Table 7.4. It is interesting to see that the slopes of the calculated curves are matching the slopes of the measured curves very well. From this latest observation can be concluded that the cumulation model, described in Section 7.2, gives a good description of the measured cumulation effect.

In relation to the absolute height of the calculated MMN levels four dependencies are identified:

1 the expectation value of the source power, $P_{2.7kHz}$,

2 the expectation value of the source density, n [1/m^2], including the number of sources per home, m, and the density of habitation in the area,

3 the expectation value of the antenna gain,

4 the expectation value of the propagation loss.

Dependency 1 is the main input parameter of our experiments. The number of sources per home in dependency 2 is an estimation, but the Nh is a result of counting residences in the considered areas. A doubling in m does a mere increase in the noise floor of only 3 dB. Dependency 4 is determined by the outcome of the propagation loss measurements in Chapter 5. As the propagation measurements are done in the same locations as used for the MMN measurements in Chapter 3 we do not doubt the values of the propagation loss. Left over is the dependency 3, the antenna gain. As we have seen that the antenna gain measurement campaign result in nearly the same results in Switzerland [92], [93] as in The Netherlands [94], we conclude that dependency 3 cannot explain large absolute MMN level deviations of 10 dB and more.

In a first instance this means that the assumption for the available power per source, being equal to the ECS values, is far to low (about 22 dB) to explain the measured values for the MMN floor. Following this conclusion it is worthwhile doing some optimizations in the input parameters for the simulations so that the outcome of the FS simulations match the measurement results in an optimum way. Doing the optimization we start with the simulation for the city area. We leave $r_{min} = 10$ m and adapt the source power so that we find a best match for the calculated FS with the measured FS, that means that for all frequency points, mentioned in Table 7.3 (in MHz), the difference is minimal:

$$\sum_{f=1.85}^{f=28.5} \left(E_{measured}(f) - E_{M,max}(f) \right) \approx 0 \tag{7.50}$$

Equation (7.50) appear to be true when we assume $P_{2.7kHz} = -39$ dBm. In the next steps we use this power level for the other areas. There we align r_{min} to such a value that for the case of residential 2 area, as well as for the case of all residential areas combined, the result matches to the measured FS for the residential area in Chapter 3. Finally, we match the simulation results for the residential-3 area to halfway residential and city measurement results, and for residential-1 to halfway rural and residential environment. The result of the optimizations is displayed in Figure 7.10, while the numerical results are summarized in Table 7.6. Comparing the values of r_{min} in this table with those in Table 7.5 reveals that the differences are small.

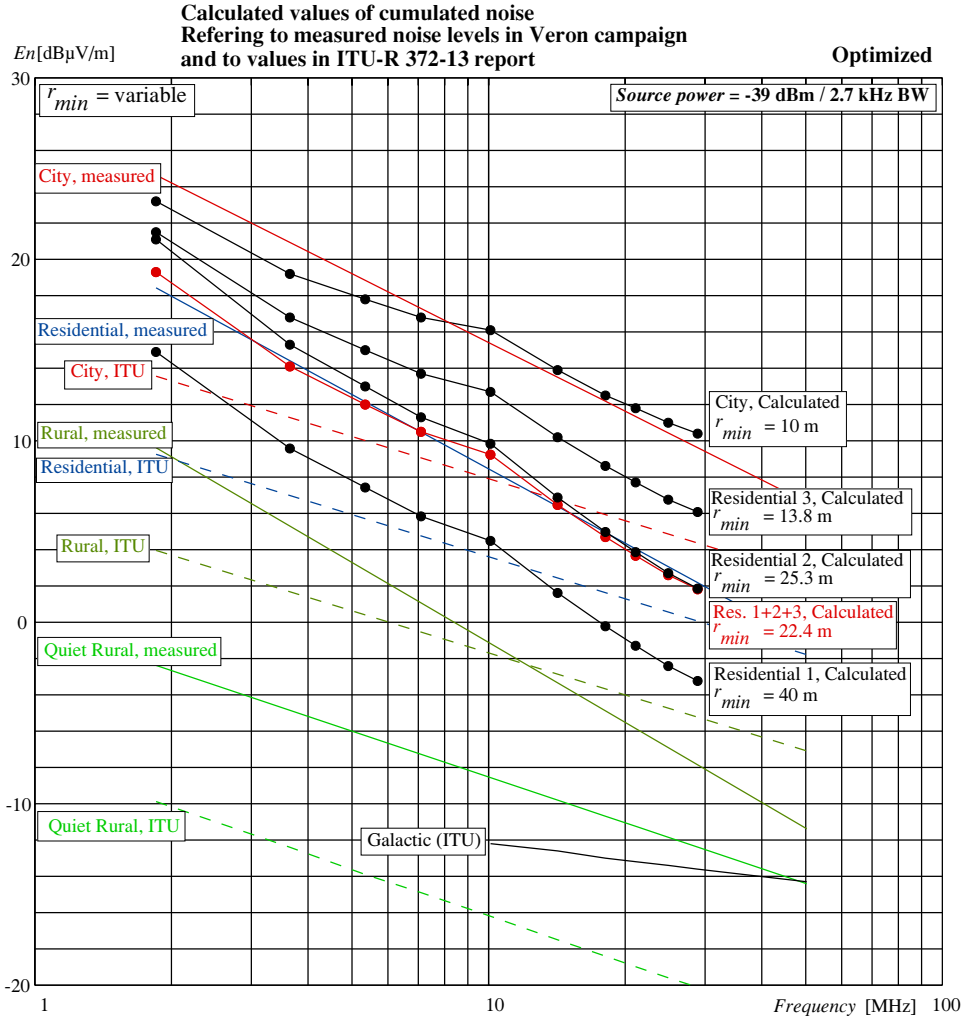

Figure 7.10. Outcome of noise floor simulations (black) using a source power of -39 dBm in 2.7 kHz bandwidth, see text.

Table 7.6. Summary of input parameters after optimization.

Environment:	Residential-1	Residential-2	Residential-3	Residential (1+2+3)	City
m [1/home]	50				
n [1/m^2]	0.068	0.152	0.247	0.142	0.287
$P_{2.7kHz}$ [dBm]	-39				
r_{min} [m]	40	25.2	13.8	23.0	10

7.5 Discussion

From Table 7.6 we must conclude that the mean available source power per source is apparently much higher (~22 dB) than we can explain by adding the MMN originating from the mains port. In Section 7.3 we already mentioned that radiation from wiring, connected to DC power, telecom and other wired ports, were not taken into account because we have no stochastic data about antenna gains related to the wiring, connected to these ports. However, we can make some observations. From the relevant EMC standards Table 7.7 can be extracted. In the same way as we calculated the available source power in Table 7.3 for the mains port, we can do this for the auxiliary ports in Table 7.8.

We arrive at a level of -52.2 dBm in a bandwidth of 2.7 kHz as available source power for all of our measurement frequencies. This is 9 dB higher compared to the mains port (ECS value), but still 13 dB lacking from what has been measured in Chapter 3. Once more we have to stress that these comparisons have a limited value because of the lack of information about the average antenna gain. It could mean that the antenna gain in question is higher because the currents are mostly asymmetrical, i.e. in common mode, whereby the radio frequency conducting wiring has been looped through by multi pieces of interconnected equipment. Also protected earth wiring can take part in the radiation of MMN in this way. This will illustrated by an example in Subsection 7.51.

Table 7.7. EMC limits for DC, Telecom and other wired ports.

EMC limits for DC, Telecom, and other wired ports, class B equipment.				
Frequency [MHz]	*Limits Quasi Peak* [dBµV]	*Limits Average* [dBµV]	*Limits Quasi Peak* [dBµA]	*Limits Average* [dBµA]
0.15 to 0.50	84 to 74	74 to 64	40 -> 30	30 -> 20
0.50 - 30	74	64	30	20

Table 7.8. Available source power.

Available source power from DC, Telecom, and other wired ports, class B equipment, frequency range 0.50 - 30 MHz.				
Voltage limit, *Z* = 150 ohm: [dBµV]	*Current limit*: [dBµA]	*Available source power* [dBm], BW = 9 kHz	*Power density* [dBm/Hz]	*Available source power* [dBm], BW = 2.7 kHz
64	20	-47	-86.5	-52.2

7.5.1 Example of mismatch in testmethod: charging electric bicycle

An in real world existing example of mismatch between a test setup and the real world is that of the electric bicycle being charged while the battery is still placed in the holder on the bike. In Figure 7.11 a very probable setup is shown. The bicycle is standing on the floor of the garage, having a relative large capacitance to the floor and the surroundings. The battery on the bike is connected to wiring in the bike and most probable also to the

framework. The charger, laying on the floor, or table or something similar, contains a common mode noise source, which induces a CM current in both cables, to the battery and via the mains cable into the mains network. This network is mostly lead through the ceiling of the garage inside the main building, and then into the HAP. This can be a long piece of wiring, 10 - 20 m at least, and may act as a perfect radiating antenna.

Figure 7.12 shows the measurement setup as defined in CISPR 14, [98]. Herein the charger is the EUT and the battery the AuxEq. As can be concluded the capacitance to the surroundings from the battery, here mostly the capacitance to the Reference Ground Plane, RGP, is relative small. That means that the CM current, induced in the cable between the charger and the battery, meets a much higher serial impedance and will be smaller than in the practical environment as shown in Figure 7.11. Above that a large part of the CM current on the mains cable is not measured by the AMN, because the PE wire is shorted in the AMN. Another problem is that the AMN measures in the Normal Mode, that means that the voltages on the Live an Neutral line are measured independently, so the ratio between DM and CM is not measured.

The result is that the potential of radiating harmful EMI in a practical situation, as depicted by Figure 7.11, is much higher than what is measured in the test setup, as defined in CISPR 14. Note that in this example, although the mismatch in testing is caused by the measurement method on the DC cable, the resulting radiating of EMI is actually done by the mains cabling.

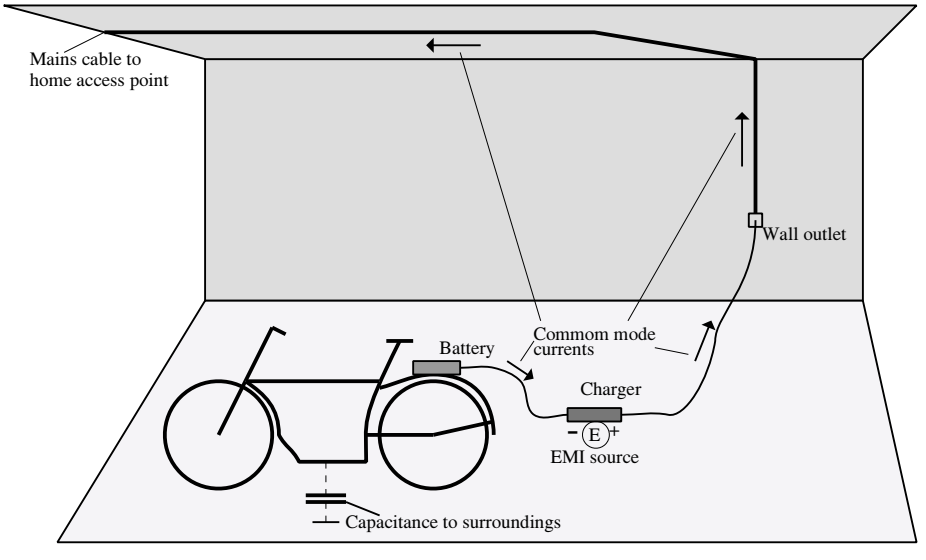

Figure 7.11. EMI radiating by common mode current.

As the serial impedance in the CM current on the DC cable to the battery, formed by the reactance of the capacitance to the surroundings, is still relative high, solving this interference problem is not easily done by putting some ferrite beads on the DC or mains cable, but a parallel tuned circuit is necessary. This tuned circuit can be made by winding the DC/AC cable multiple times through a high-Q ferrite bead and connect a tuning capacitor in parallel. In this way the interference problem can be solved for a selected frequency band only.

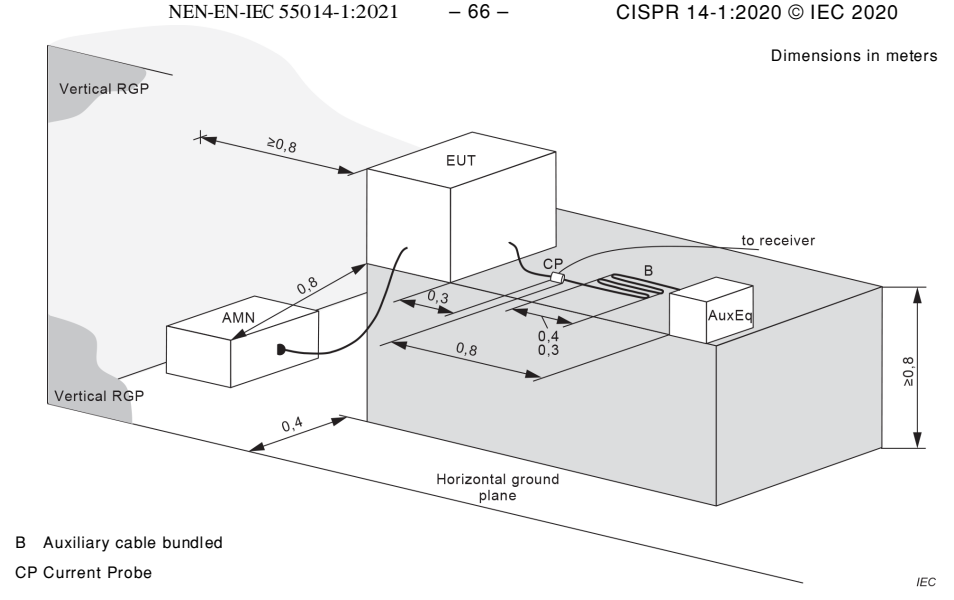

Figure 24 – Example of alternative test setup (vertical RGP) for measurements on table-top EUT (disturbance voltage on mains port and disturbance current on auxiliary port)

Figure 7.12. Conducted test setup. From [99].

This is only one of many examples wherein there is a strong discrepancy between the measurement method and the way wherein equipment is connected and used in practice. Other fields of application wherein this mismatch form an issue are for example in PV installations, installations with motor controllers, frequency convertors, etc.

7.6 Conclusion

The presented model concerning the cumulation of Man-Made Noise in residential areas is supported by earlier MMN field strength measurements in Chapter 3. The maximum range according the cumulation model, wherein the contribution of MMN source is relevant to the accumulated field strength level, is equal to what is found by correlation between measured field strength levels and the local density of habitation in Chapter 4, and reaches up to

about 300 m, depending on frequency.

It is unlikely that noise sources, emitted by the low voltage mains port, with the available powers limited by the CISPR standards, using the class B conductive disturbance voltage limit, are causing the high MMN floor levels as measured in residential areas. Comparing with our noise floor measurements a ratio of 22 dB in source power is missing.

Radiation from cabling, connected to ports for DC power, telecom, or other wiring, is a reasonable candidate for explaining the extra noise level because of a) the 9 dB higher level of source power, available at those ports compared with the mains port, and b) the extensive wiring that may be connected to these ports in the practical residential situation. One should remember that the amount of apparatus with extra ports to the existing main port has extensively grown in the electronic age, that means after the year 1975.

The meaning of the findings could be that the limits values for the mains port itself are acceptable from the point of EMC ruling, but that the limits for the DC power ports, telecom ports and ports for other wiring should be addressed, concerning the available power limit, as well as concerning the radiation properties of the connected wiring in the real practical world.

We can not exclude the possibility that there is a large number of apparatus in the field that does not comply with the EMC standards for several reasons, like showing much higher emission source power levels by design of the apparatus, or because of shortcomings in the installation and/or application.

Chapter 8

8 Conclusions and recommendations

8.1 Conclusions

In this dissertation the research question was defined as "Is there a scientifical stochastic model possible that explains and predicts broadband noise field strength levels in residential areas, starting from a distribution of individual MMN sources with a known expectation value of available power?". From Chapter 7 we may conclude that the answer is "Yes".

In Chapter 3 we conclude from our extensive measurements, which results has been compared with measurements in the sixties and seventies of the last century [13], that it is unmistakable that the MMN floor in residential areas has risen, and referring to the many complaints received from radio spectrum users, up to a level where radio reception in a wide context is seriously interfered.

In Chapter 7 a model of the cumulation effects of MMN has been derived. From this cumulation model we also conclude that the contribution of individual MMN sources to the cumulated noise floor is practically limited to sources within a maximal radius from the measurement position, depending on the frequency and on the ensity of habitation. This was already concluded in Chapter 4 from the measurement results.

The experiments with different sets of input data in applying the cumulation model revealed that it is unlikely that noise sources, emitted by the low voltage mains port, with the available powers limited by the CISPR standards using the class B conductive disturbance voltage limit, are causing the high MMN floor levels as measured in residential

areas. It was concluded that radiation from cabling, connected to ports for DC power, telecom, or other wiring, is a reasonable candidate for explaining the measured excess noise.

That does not exclude the possibility that noise sources with high emissions powers are in the field, and having a substantial contribution to the noise floor. Such equipment must be considered as being illegal on the market, resulting from shortcomings in the enforcement of the EMC regulations.

In Chapter 5 we learned that statistical values of propagation losses of MMN in residential areas for frequencies below 30 MHz can be estimated very well by applying linear equations (5.29), (7.5), (7.6). Those losses are larger than values calculated from the free space or even the ITU ground-wave propagation model [57], [58].

8.2 Further research

The subject of increased MMN levels is far from closed. Measurements and studies of radio noise levels under the real environmental conditions of the radio user should be carried out in far more countries. These measurements should be extended to higher frequency bands, like VHF, UHF and even SHF because of the shift of the use of ever higher frequencies and because of the use of components with increasing switching speed that increases the frequency range wherein MMN is produced.

More research into the propagation of MMN, also for higher frequencies, is needed. Chapter 5 has shown that the often used propagation models for free space and ground-wave are not applicable for MMN in residential areas below 30 MHz. Also the propagation mechanism on higher frequencies in residential environments differ from that below 30 MHz.

Knowledge about radiation properties from home AC mains wiring is very limited, as it is of the radiation from the feeding cables, both underground and overhead. This also counts for telecom cabling. More measurements, including extended methods, for example the use of drones or other mobile vehicles, should be performed.

A fundamental new approach is needed for testing EMC in relation to the emission of cabling and networks that are connected to other ports of apparatus than the AC mains port.

The assumptions made for the existing measurement methods, like the lenghts of connected external cables, the ways they are layed out, the termination of those cables, interconnecting of different pieces of equipment, in short the practical use of the equipment, are not valid anymore and the methods do not correspond with the existing use of the apparatus. Special attention should be given to the situations wherein the apparatus

form a current source, differential between the mains port and the DC or data port, so that common mode currents can be injected in long cables, both in the mains network as in the DC or data network. An example has been given in Chapter 7, Subsection 7.5.1.

8.3 Recommendations

Carefully selecting and documentation of the measurement locations for MMN research is very important for arriving at measurement results of scientific relevance, see Chapter 3. Noise measurements should be performed, preferable manually, by operators experienced in radio communication to be able to discriminate between the several sources of noise, as of natural origin, like Atmospheric and Galactic, MMN, EMI, and wanted radio signals. Although existing algorithms differentiating between noise and wanted radio signals, as mentioned in References [7] - [11], are working reasonably well, results from automatic measurements methods should be interpreted with care. The saying "To measure is to know" is only true when one knows what is measured.

For the enforcement of EMC Directive of the European Union [29] it is important to prosecute offenders who violate the essential requirements of the EMC Directive. Generic and product EMC standards, giving a presumption of compliance to the directive, are only tools to simplify the process of market surveillance, but are not sufficient for protecting the radio spectrum from interference. Meeting the requirements of the standards does not guarantee EMC. For example, the derivation of limit values by using statistical mitigation factors as defined in CISPR 16-4-4 [105], implies the existence of practical situations wherein the so calculated limit values are not suitable to protect the radio spectrum from interference. This is because of such mitigation factors are calculated using averaged parameters describing co-location, co-frequency, coincident in the time domain, etc., determining a statistical risk for causing interference. In practice these factors are mainly selected from the perspective of the equipment manufacturer. However, the statistical risk seen from the position of the victim may be very different[1]. Moreover, in real life the legal means to prosecute offenders, violating the essential requirements, are experienced to be not sufficient. So the estimation of risk of interference for a radio spectrum user, as well as the enforcement of the EU EMC Directive, needs a lot of attention.

For frequencies below 30 MHz field strength limits are necessary, for all products and for fixed installations. Former assumptions were, that enclosures are too small to radiate for

1 For example, in a situation wherein 1 of 10 houses in a street having a PV-installation installed the density of PV-installation is 10%. With a density of 1 radio amateur per 1000 family homes the chance that a PV-installation is adjacent to a radio amateur is 4/1000, see [IEC DTR CISPR 16-4-4/TR/A2/Ed2, CIS/H/402/CD]. Seen from the position of the radio amateur the chance he is adjacent to a PV-installation is 4/10, so the risk he is interfered by a PV-installation is relative high when that installation is emitting noise.

those frequencies, are irrelevant today; it is the, today often extensive, connected cabling to the apparatus that radiate. So field strength measurements, especially when apparatus is installed in a practical application or in an installation, are required to provide a proof of compliance, in particular in case of interference.

In the current time and circumstances under which accumulation of Man-Made Noise does occur or the risk of interference from a single source is significant, that noise need to be considered as a kind of environmental pollution. Many rules about environmental pollution consist of limits for the emission of the pollution sources on one side, and of limits for the level of pollution in the environments on the other side, for example limits about dust particles and for pollution by chemicals. The current standards, used to show compliance with the EU EMC Directive, only focus on limitation of emissions from apparatus and installations. What is missing in the EMC standards are environmental limits, so MMN and EMI field strength limits in defined areas. Future versions of ITU-R Recommendation P.372 could set those limits. Such limits or reference values could be relevant in the assessing whether the essential requirements are met, and could be used as a legal base for enforcement of the EU EMC Directive. Enforcement can be simplified in a significant way by establishing that the EMI, generated by a detected source, does exceed such an environmental limit or does increase the existing noise floor, which is higher, with more than x dB, for example 3 dB, at the location of the victim at any distance from the source larger than the exclusion distance of 10 meter. This approach of the enforcement would be new, but very well in line with the meaning of the EU EMC Directive. Moreover, the definition of "Harmful Interference" as defined by the ITU Radio Regulations: "Interference which endangers the functioning of a radionavigation service or of other safety services or seriously degrades, obstructs, or repeatedly interrupts a radiocommuniction service operating in accordance with these Regulations", could be filled in with a measureable parameter. This approach will have a very important side effect on the developement of the emission standards in that the limits and measurement methods therein need to be sufficient strict to match the environmental requirements.

References

[1] Eugene J. Cummins, Stephen Jaurggui, and Wilbur Ray Vincent, "Time and frequency domain characteristics of man-made radio noise affecting HF-communications sites," *IEEE Transactions on Electromagnetic Compatibility,* vol. EMC-21, no. 3. pp. 182-189, August 1979, 10.1109/ TEMC.1979.303730.

[2] F. Leferink, F. Silva, J. Catrysse, S. Batteman, V.Beauvois, and A. Roc'h, "Man-made noise in our living environments," *URSI Radio Science Bulletin.* vol. 83, no. 3. pp. 49-57, September 2010.

[3] W.R. Lauber, J.M. Bertrand, and P.R. Bouliane, "An Update of CCIR Business and Residential Noise Levels," *Proceedings of IEEE Symposium on Electromagnetic Compatibility*, Chicago, IL, USA, August 1994, pp. 348-353, 10.1109/SEMC.1994.385632.

[4] A. Wagstaff and N. Merricks, "Man-made noise measurement programme," *IEE Proceedings - Communications,* vol. 152, no. 3, pp. 371-377 July 2005, 10.1049/ip-com:20045025.

[5] M. Iwama, "Estimation of Background Noise in HF Band", *2008 Asia-Pacific Symposium on Electromagnetic Compatibility & 19th International Zurich symposium on Electromagnetic Compatibility*, Singapore, May 2008, pp. 478-481.

[6] R. Dalke, R. Achatz, Y. Lo, P.Papazian, and G. Hufford, "Measurement and Analysis of Man-made Noise in VHF and UHF Bands," *Proc.1997 Wireless Communications Conference,* Boulder, CO, USA, August 1997, pp. 229-233, 10.1109/WCC.1997.622284.

[7] "Radio noise measurements, European harmonisation of measurement methods", Radiocommunications Agency Netherlands, 2005. Available from the author.

[8] Erik van Maanen, "Practical Radio Noise Measurements," *18th International Wroclaw Symposium and Exhibition on Electromagnetic Compatibility,* Wroclaw, Poland, June 2006. [Online]. Available: https:// www.researchgate.net/publication/264829264.

[9] Report ITU-R SM.2055, "Radio Noise measurements," Geneva, 2006. [Online]. Available: https://www.itu.int/pub/R-REP-SM.2055.

[10] Report ITU-R SM.2155, "MMN measurements in the HF range," Geneva, 2009. [Online]. Available: https://www.itu.int/pub/R-REP-SM.2155.

[11] Recommendation ITU-R SM.1753-2, "Methods for measurements of radio noise," Sept. 2012. [Online]. Available: https://www.itu.int/rec/R-REC-SM.1753/en.

[12] B.A. Witvliet, Erik van Maanen, Mark J. Bentum, C. H. Slump, and R. Schiphorst, "A Novel Method for the Evaluation of Polarization and Hemisphere Coverage of HF Radio Noise Measurement Antennas," *2015 IEEE international symposium on Electromagnetic Compatibility (EMC),* Dresden, Germany, Aug. 2015, pp. 289-294, 10.1109/ISEMC.2015.7256174.

[13] *Recommendation ITU-R P.372-15* "Radio noise," International Telecommunication Union. Geneva. Sept. 2021. [Online]. Available: https://www.itu.int/rec/R-REC-P.372/en.

[14] *Handbook of Atmospheric Electrodynamics*, vol. 1, Radioastronimical Institute, University of Bonn, Germany, CRC Press, 1995, ISBN 0-8493-8647-0.

[15] Wilfred R. Lauber, Jean M. Bertrand, "HF Atmospheric Noise Levels in the Canadian Arctic", *IEEE Transactions on EMC,* vol. 36, no. 2, May 1994.

[16] Propagation of Radiowaves, *Les Barclay, The Institution of Engineering and Technology, 2013. ISBN 978-1-84919-578-2.*

[17] ERC Report 069, "*Propagation model and interference range calculation for inductive systems 10 kHz - 30 MHz*." Marbella, February 1999. https://docdb.cept.org/document/637.

[18] E.N. Skomal, "Distribution and Frequency Dependence of Unintentionally Generated Man-Made VHF/UHF Noise in Metropolitan Areas," *IEEE Transactions on Electromagnetic Compatibility,* vol. 7, no. 3, pp. 263-278, Sept. 1965, 10.1109/TEMC.1965.4307416.

[19] E.N. Skomal, "Distribution and Frequency Dependence of Unintentionally Generated Man-Made VHF/UHF Noise in Metropolitan Areas, Part II-

Theory," *IEEE Transactions on Electromagnetic Compatibility, v*ol. 7, no. 4. pp. 420-427, Dec. 1965, 10.1109/TEMC.1965.4307437.

[20] W.E. Buelherand and C.D. Lunden, "Signature of man-made high-frequency radio noise," *IEEE Transactions on Electromagnetic Compatibility,* vol. EMC-8, no. 3, pp. 143-152, Sept. 1966, 10.1109/TEMC.1966.304417.

[21] Jules Deitz, "Man-Made Noise," *8th Symposium Digest: 8th National Symposium on Electromagnetic Compatibility,* San Francisco, CA, USA, July 1966, pp. 1-4, 10.1109/ISEMC.1966.7567028.

[22] E.N. Skomal, "Comparative Radio Noise Levels of Transmission Lines, Automotive Traffic, and RF Stabilized Arc Welders," *IEEE Transactions on EMC*, vol. EMC-9, no. 2. Year 1967. Pages 73 - 77.

[23] E.N. Skomal, "Distribution and Frequency Dependence of Incidental Man-Made HF/VHF Noise in Metropolitan Areas," *IEEE Transactions on EMC*, vol. EMC-11, no. 2, pp. 66-75, May 1969, 10.1109/TEMC.1969.303014.

[24] E.N. Skomal, "The Dimensions of Radio Noise," *IEEE Electromagnetic Compatibility Symposium Record,* Asbury Park, NJ, USA, June 1969. Pages 18 - 28, 10.1109/TEMC.1969.4307173.

[25] E.N. Skomal, "An Analysis of Metropolitan Incidental Radio Noise Data," *IEEE Transactions on EMC*, vol. EMC-15, no. 2, pp. 45-57, May 1973, 10.1109/TEMC.1973.303236.

[26] D. Middleton, "Statistical-Physical Models of Electromagnetic Interference," *IEEE Transactions on EMC*, vol. EMC-19, no. 3. Year 1977. Pages 106 - 127.

[27] E.N. Skomal, "Definition, Distribution, and Sources of Radio Noise," *Man-made Radio Noise*, New York, N.Y. Van Nostrand Reinhold Co, 1978. pp. 1–11.

[28] CISPR/F/683/INF ITU SG1/WP1A, "LED lighting interference to broadcasting services," *Liason statement to CISPR/F and CISPR/H,* July 2016, unpublished, available on request by the author.

[29] Directive 2014/30/EU of the European Parliament and of the Counsel of 29 February 2014, on the harmonisation of the laws of the Member States

relating to electromagnetic compatibility. *Official Journal of the European Union*, No. L 96 March 29, 2014, pp. 79-106. [Online]. Available: https://eur-lex-europa-eu.ezproxy2.utwente.nl/legal-content/EN/PDF/?uri= CELEX:32014L0030&rid=4.

[30] "(Radio Equipment) Directive 2014/53/EU", *Official Journal of the European Union*, No. L 153 May 22, 2014, pp. 62-106.

[31] E.N. Skomal, "The Conversion of Area distributed, Incidental Radio Noise Envelope Distribution Functions by Radio Propagation Processes," *IEEE Transactions on Electromagnetic Compatibility, v*ol. EMC-12, no. 3, pp. 83-88, Aug. 1970, 10.1109/TEMC.1970.303075.

[32] E.N. Skomal, "Recent Extensions of composite, incidental man-made radio noise data and their relevance to the hypothesis of the noise envelope statistic transformation," *IEEE International Electromagnetic Compatibility Symposium Record,* Philadelphia, Pa, USA, July 1971, pp. 1-13, 10.1109/ ISEMC.1971.7567946.

[33] E.N. Skomal, "Evidence for the Conversion of Noise Envelope Statistics by Radio Propagation Process," *IEEE Transactions on Electromagnetic Compatibility*, vol. EMC-24, no. 3. pp. 330-334, Aug. 1982, 10.1109/ TEMC.1982.304044.

[34] ECC Report 24, annex 7, "Cumulative effect of Broadband PLT Below 30 MHz", Cavtat, May 2003, http://www.erodocdb.dk/doks/relation.aspx?docid= 1941.

[35] NATO Research and Technology Organisation "HF Interference, Procedures and Tools," *RTO Technical Report TR-IST-050*, June 2007.

[36] E.N. Skomal, "A Long Term Trend in Urban Zone Man Made Radio Noise and the UHF Automotive Ignition Resonance," *IEEE International Symposium on Electromagnetic Compatibility,* Wakefield, Massachusetts, USA, Aug. 1985, pp. 312-317.

[37] E.N. Skomal, "The range and frequency dependence of VHF & UHF man-made noise in and above metropolitan areas," *IEEE Transactions on Vehicular Technology, v*ol. 19, no. 2, pp. 213 - 221, May 1970, 10.1109/T-

VT.1970.23452.

[38] P. Ångskog, C. Karlsson, J.F. Coll, J. Chilo, and P.F. Stenumgaard, "Sources of Disturbances on Wireless Communication in Industrial and Factory Environments," *Asia-Pacific International Symposium on Electromagnetic Compatibility,* Beijng, China, April 2010, pp. 281-284, 10.1109/ APEMC.2010.5475862.

[39] Frank Weinmann and Klaus Dostert, "Verification of background noise in the shortwave frequency range according to recommendation ITU-R P.372," *AEU-International Journal of Electronics and Communications, v*ol. 60, no. 3. pp. 208-216, March 2006. [Online]. Available: https://doi.org/10.1016/ j.aeue.2005.03.005.

[40] Tatsushiko Kagoshima, Satoshi Ito, and Keiichi Ohizumi, "How should electromagnetic waves below 30 MHz be handled?" *Proceedings of 6th International Conference on Modelling, Identification and Control*, Melbourne, Australia, Dec. 2014, pp. 38 - 41, 10.1109/ICMIC.2014.7020724.

[41] Iratxe Landa, Amaia Arrinda, Iñaki Eizmenda, Manuel M Velez, and Igor Fernandez, "Man-made Noise Measurements in Indoor Locations in Medium Wave Band," *Proceedings of the 4th European Conference on Antennas and Propagation (EuCAP2010),* Barcelona, Spain, April 2010, pp. 1-5.

[42] Iratxe Landa, Manuel Velez, Amaia Arrinda, Pablo Angueria, and Iñaki Eizmenda, "Revision of the Methodology for Processing Radio Noise Measurements in the Medium Wave Band," *IEEE Antennas and Propagation Magazine,* vol. 54, no. 6, Dec. 2012, pp. 214-226, 10.1109/ MAP.2012.6387824.

[43] Iratxe Landa, Manual Maria Velez, and Amaia Arrinda, "Procedure for radio noise measurements in Medium Wave band," *IEEE International Instrumentation and Measurement Technology Conference (I2MTC),* Minneapolis, MN, USA, May 2013, pp. 166-171, 10.1109/ I2MTC.2013.6555403.

[44] "Man-Made Radio Noise," *CCIR Report 258-4*, International Radio Consultive Committee, International Telecommunicatons Union, 1982.

[45] A.D. Spaulding and R.T. Disney, "Man-made Radio Noise, Part 1: Estimates for business, residential, and rural areas," *US Department of commerce / Office of Telecommunications Report, OT Report 74-38*, June 1974.

[46] "Characteristics and Applications of Atmospheric Radio Noise Data", *CCIR Report 322-4*, International Radio Consultive Committee, International Telecommunicatons Union, 1988.

[47] "Man-Made Radio Noise" *CCIR Report 258-4* (1982), *Recommendation CCIR 372-4, International Radio Consultive Committee, International Telecommunicatons Union, 1986.*

[48] *Electromagnetic Fields and Waves,* Paul Lorrain, Dale P. Corson, and François Lorrain, 3rd edition, W.H. Freeman and Company, 1988. ISBN: 0-716-71823-5.

[49] Erik van Maanen, "Practical Radio Noise Measurements," *18th International Wroclaw Symposium and Exhibition on Electromagnetic Compatibility,* Wroclaw, Poland, June 2006. [Online]. Available: https:// www.researchgate.net/publication/264829264.

[50] W.Q. Crichlow, R.T. Disney, and M.A. Jenkins, "Essa Technical Report IER 18-ITSA18-31", *Quarterly Radio Noise Data, June, July, August 1966*, Institute for Telecommunication Sciences and Aeronomy, Boulder, Colorado, USA, August 1967, pp. 1-40.

[51] Carlo Carobbi, "Issues in E-field measurements between 10 kHz and 30 MHz", *2017 IEEE International Symposium on Electromagnetic Compatibility & Signal/Power Integrity (EMCSI)*, Oct. 2017. 10.1109/ ISEMC.2017.8078024.

[52] J. DeMarinis, "The Antenna Cable as a Source of Error in EMI Measurements", *1988 IEEE International Symposium on EMC*, Seattle, WA, USA, Aug. 1988, pp. 9-14. 10.1109/ISEMC.1988.14078.

[53] M. Zingarelli, "9 kHz - 30 MHz E-field Measurement by an Innovative ROD Antenna embedding a Fully CISPR 16-1-1 Receiver", *7th Asia Pacific International Symposium on Electromagnetic Compatibility*, May 2016, pp. 788-790. 10.1109/APEMC.2016.7522867.

[54] Frank S. Colligan, "An E-Field Rod Antenna and Preamplifier for A.M. Field Strength Measurements", *IEEE Transactions on Broadcasting*, vol. BC-26, no. 4, Dec. 1980. pp. 93-98. 10.1109/TBC.1980.266379.

[55] Harry W. Gaul, "Electromagnetic Modeling and Measurements of the 104 cm Rod and Biconical Antenna for Radiated Emissions Testing Below 30 MHz", 2013, pp. 434-438.

[56] L. Turnbull, "The Groundplane Resonance - Problems with Radiated Emissions Measurements below 30 MHz", Automotive EMC Conference 2007. Oct. 20007. pp. 1-13.

[57] *Recommendation ITU-R P.368-9* "Ground-wave propagation curves for frequencies between 10 kHz and 30 MHz," International Telecommunication Union. Geneva. Feb.. 2007. [Online]. Available: https://www.itu.int/rec/R-REC-P.368-9-200702-I/en.

[58] *Handbook on Ground Wave Propagation*, Ed. 2014, Radio Communication Bureau ITU, Geneva, Switzerland, pp.10.

[59] A. V. Nikitin and R. L. Davidchack, "Nonlinear Rank-Based Analog Loop Filters in Delta-Sigma Analog-to-Digital Convertors for Mitigation of Technogenic Interference," *October 2017. Military Communications Conference (MILCOM),* MILCOM 2017 *MILCOM,* Baltimore, MD, USA, Oct. 2017 *10.1109*/MILCOM 2017.8170770.

[60] Fr.J. Gravettes and L.B. Wallnau, "Statistics for the Behavioural sciences," 7th ed., Thomson - Wadsworth ISBN-13: 978-0-495-09521-7 London, UK, 2007.

[61] A. Wagstaff and N. Merricks, "Man-made noise measurement programme, Final Report, Issue2", https://webarchive.nationalarchives.gov.uk /20090904194002/ http://www.ofcom.org.uk/static/archive/ra/topics/research/ topics/man-made-noise_finalreport.pdf

[62] Björn Johansson and Tore Lindgren, "Man-made Noise measurement in Sweden." *2016 IEEE International Symposium on Electromagnetic Compatibility (EMC),* Ottawa, ON, Canada. DOI: 10.1109/ ISEMC.2016.7571598.

[63] Paul Bechet, Andrei Christian Bechet, Simona Miclaus, "HF urban noise level in variable channels of 3-24 kHz: a preliminary experimentel approach." *Loughborough Antennas & Propagation Conference (LAPC 2017)* Loughborough, UK. DOI: 10.1049/cp.2017.0270.

[64] A. Palaios, V.M. Miteva, P. Mähönen, "Contemporary Study of Radio Noise Characteristics in Diverse Environments." *IEEE Access,* vol. 6, May 2018, pg. 25621-25631. DOI: 10.1109/ACCESS.2017.2654064.

[65] J.H. Stott, BBC R&D, Technical Note, 1999 - pdfs.semanticscholar.org.

[66] OpenStreetMap organisation: <https://www.openstreetmap.org>.

[67] *Statistical Tables for Biological, Agriculturaland Medical Research,* R.A. Fisher and F. Yates, 6th ed. Longman Group Ltd. 1974, London.

[68] *Statistical Methods,* 7th ed. George W. Snedecor and William g. Cochran. 1980 Iowa State University Press.

[69] J. Zenneck, "Propagation of Plane EM Waves Along a Plane Conducting Surface," *Ann. Phys.* (Leipzig), 28, 1907, pp. 846-866.

[70] A.N. Sommerfeld, "Propagation of Waves in Wireless Telegraphy," *Ann. Phys.* (Leipzig), 28, 1909, pp. 665-737.

[71] K.A. Norton, "The Propagation of Radio Waves over the Surface of the Earth and in the Upper Atmosphere, Part I", *Proceeding of the IRE*, vol. 24, no. 10, 1936, pp. 1367-1387.

[72] K.A. Norton, "The Propagation of Radio Waves over the Surface of the Earth and in the Upper Atmosphere, Part II", *Proceeding of the IRE*, vol. 25, no. 9,September1937, pp. 1203-1236.

[73] K.A. Norton, "The Physical Reality of Space and Surface Waves in the Radiation field of Radio Antennas", *Proceeding of the IRE*, vol. 25, no. 9, September 1937, pp. 1192-1202.

[74] J.R. Wait, "The Ancient and Modern History of EM Ground-Wave Propagation", *IEEE Antennas and Propagation Magazine*, vol. 40, no. 5, October 1998, pp. 7-24.

[75] R.E. Collin, "Hertzian Dipole Radiating Over a Lossy Earth or Sea: Some

Early and Late 20th-Century Controversies", *IEEE Antennas and Propagation Magazine*, vol. 46, no. 2, April 2004, pp. 64-79.

[76] K.A. Norton, "The Calculation of Ground-Wave Field Intensity Over a Finitely Conducting Spherical Earth", *Proceeding of the IRE*, vol. 29, December 1941, pp. 623-639.

[77] *GRWAVE*. Ground-wave simulating tool from ITU-R. https://github.com/space-physics/grwave.

[78] Yoanne Corre, Yves Lostanlen, "Three-Dimensional Urban EM Wave Propagation Model for Radio Network Planning and Optimization Over Large Areas", *IEEE Transactions on Vehicular Technology,* vol. 58, no. 7, pp. 3112 - 3123, September 2009, DOI: 10.1109/TVT.2009.2016973.

[79] Vittorio Degli-Esposti, "A Diffuse Scattering Model for Urban Propagation Prediction", *IEEE Transaction on Antennas and Propagation*, vol. 49, no. 7, July 2001, pp. 111- 1113.

[80] J.H. Causebrook, "Medium-Wave propagation in built-up areas"*, Proceedings IEE,* vol. 125, no. 9, September 1978, pp. 804-808.

[81] M.P.C. Almeida, e.a. "Medium wave DRM field trials in Brazil - Some daytime and nighttime results in urban environment", *Measurement,* Elsevier, vol. 45, year 2012, pp. 2237-2245.

[82] M. J. Packer, R.I. Desourdis, "Rural and Urban Groundwave propagation in a desert environment", *Proceedings of MILCOM '93 - IEEE Military Communications Conference,* 1993, vol. 2, pp. 634-638.

[83] L. Lichun, "A New MF and HF Ground-Wave Model for Urban Areas", *IEEE Antennas and Propagation Magazine,* vol. 42, no. 1, February 2000, pp. 21-33.

[84] *The concept of transmission loss for radio links*. Rec. ITU-R P.341-7 (2019). https://www.itu.int/rec/R-REC-P.341-7-201908-l/en.

[85] *Antennas for All Applications.* John D. Kraus and Ronald J. Marhefka, MacGraw-Hill Higher Education, Edition 3, 2002. ISBN 0-07-112240-0.

[86] *Electromagnetic Fields and Waves,* Paul Lorrain, Dale P. Corson, and François Lorrain, 3rd edition, W.H. Freeman and Company, 1988. ISBN: 0-

716-71823-5.

[87] http://www.websdr.org/

[88] Jonathan Stott, "Protection of sensitive receiving sites", BBC R&D 1282C(99), 21 September 1999.

[89] Jonathan Stott, "Cumulative effects of distributed interferers", BBC R&D 1670(01) WHP 004, 24 August 2001.

[90] OFCOM, Switzerland and ASCOM, Switzerland, "A Novel Method for Measuring the Far Field Radiation Characteristics of Low Voltage Distribution Networks" (FAFIRA Report No. 1), CEPT/ERC PT SE35, London, 22-23 January 2001.

[91] OFCOM, Switzerland and ASCOM, Switzerland, "Measured Skywave Radiation Characteristics of Low Voltage Distribution Networks Excited by PLC Systems Transmitting in the HF-Band" (FAFIRA Report No. 2), CEPT/ ERC PT SE35, London, 22-23 Jan 2001.

[92] OFCOM, Switzerland and ASCOM, Switzerland, "Method for Measuring The Far Field Radiation Characteristics of Low Voltage Distribution Networks"Groundwave Radiation Characteristics of Low Voltage Electricity Distribution Networks" (FAFIRA Report No. 4), CEPT/ERC PT SE35, London, 22-23 Jan 2001.

[93] OFCOM, Switzerland and ASCOM, Switzerland, "Measured Ground-wave Radiation Characteristics of Low Voltage Electricity Distribution Networks Excited by PLC Systems Transmitting in the HF-Band" (FAFIRA Report No. 5), CEPT/ERC PT SE35, London, 22-23 Jan 2001.

[94] Jean Paul van Assche, Jan Coenraads, Radio Agency Netherlands, "Information on radiation properties of mains networks", JWG ETSI/ CENELEC, EMC of conducted transmission networks, 04/04/2003.

[95] Frank Leferink, "Gaps in the Application of the EMC Directive Due to Inadequate Harmonized Product Standards", IEEE 2010. [Online]. Available: https://ewh-ieee-org.ezproxy2.utwente.nl/soc/emcs/acstrial/newsletters/ summer10/PP_Gaps.pdf

[96] *International Standard, Electromagnetic compatibility (EMC)-Part 6:*

Generic standards, IEC 61000-6, [Online]. Available: https://webstore.iec.ch/publication/4253.

[97] CISPR 11:2015+A1:2016 en, "Industrial, scientific and medical equipment - Radio-frequency disturbance characteristics - Limits and methods of measurement". [Online]. Available: https://webstore.iec.ch/publication/64542.

[98] CISPR 14-1:2020 en, "Electromagnetic compatibility for household applicances, electric tools and similar apparatus - Part 1: Emissions". [Online]. Available: https://webstore.iec.ch/publication/60734.

[99] CISPR 32:2015+AMD1:2019, Electromagnetic compatibility of multimedia equipment - Emission requirements". [Online]. Available: https://webstore.iec.ch/searchform&q=CISPR%2032

[100] CISPR 16-1-1:2019, "Specification for radio disturbance and immunity measuring apparatus and methods - Part 1-1: Radio disturbance and immunity measuring apparatus - Measuring apparatus". [Online]. Available: https://webstore.iec.ch/publication/60774

[101] *Recommendation ITU-T O.9 (03/99)* "Measuring arrangements to assess the degree of unbalance about earth" International Telecommunication Union. Geneva. March 1999. [Online]. Available: https://www.itu.int/rec/T-REC-O.9-199903-I/en.

[102] *Recommendation ITU-T K.86 (11/11)* "Method for measuring longitudinal conversion loss (9 - 30 MHz)" International Telecommunication Union. Geneva. November 2011. [Online]. Available: https://www.itu.int/rec/K-REC-K.86-201111-I/en.

[103] A.K.M. Mahbub Ar Rashid, Faculty of Engineering, Kyushu Institute of Tech.,1-1 Sensui-Cho, Tobata-Ku, Kitakyushu-Shi, Fukuoka 804-8550, Japan, e.a. "Evaluation of Longitudinal Conversion Loss (LCL) for Indoor AC Mains Line", *2003 IEEE Symposium on EMC, vol. 2, pg. 771-776*. DOI: 10.1109/ISEMC.2003.

[104] K.Y. See, A. Kamarul, and P.L. So, "Longitudinal Conversion Loss of Power Line Network for Typical Singapore Household", *2005 International Power Engineering Conference,* November 29th, 2005, Singapore. DOI: 10.1109/

IPEC.2005.206918.

[105] CISPR 16-4-4:2017-06, "Specification for radio disturbance and immunity measuring apparatus and methods - Part 4-4: Uncertainties, statistics and limit modelling - Statistics of complaints and a model for the calculation of limits for the protection of radio services." [Online]. Available: https://webstore.iec.ch/publication/66963.

[106] J.L. Eaton, BBC Research Department, "The wave-tilt method of measuring electrical ground constants in hte l.f. and m.f. bands", *BBC Research Report RD 1976/15,* June 1076. www.bbc.uk/rd/pubs/reports/1976-15.pdf.

Appendices

Appendix A: Derivation of the relation between F_a and E_n

For the case of a half-wave dipole in free space we can make the following derivation. For the power density pd_n we write with noise field strength e_n:

$$pd_n = \frac{e_n^2}{120\pi} \tag{A.1}$$

Noise power received by the receiver p_n:

$$p_n = A_{eff} \cdot pd_n \tag{A.2}$$

where A_{eff} is the effective area of the antenna. In the general case A_{eff} is according reference [48]:

$$\begin{aligned} A_{eff} &= \frac{g\lambda^2}{4\pi} \\ &= \frac{g \cdot 300^2}{4\pi f^2} \qquad (f \text{ in MHz}) \end{aligned} \tag{A.3}$$

So

$$\begin{aligned} p_n &= \frac{g \cdot 300^2}{4\pi f^2} \frac{e_n^2}{120\pi} \\ &= \frac{19.0}{f^2} g e_n^2 \end{aligned} \tag{A.4}$$

Converting into logarithmic terms

$$\begin{aligned} 10 \log p_n &= 10 \log 19.0 + 10 \log g + 10 \log {e_n}^2 - 10 \log f^2 \\ &= 12.79 + 10 \log g + 20 \log e_n - 20 \log f \end{aligned} \tag{A.5}$$

$$20 \log e_n = 10 \log p_n + 20 \log f - 10 \log g - 12.79$$

$$E_n \text{ [dBµV/m]} - 120 = P_n + 20 \log f - G - 12.79 \tag{A.6}$$

$$E_n \text{ [dBµV/m]} = P_n \text{ [dBW]} + 20 \log f \text{ [MHz]} - G + 107.21 \tag{A.7}$$

But for a lossless antenna also Equation (1.7), Chapter 1, is valid:

$$P_n = F_a + 10 \log b - 204, \text{ so}$$

$$E_n = F_a + 10\log b - 204 + 20\log f[\text{MHz}] - G + 107.2$$

$$= F_a + 20\log f\ [\text{MHz}] + 10\log b - G - 96.8\ \ [\text{dB}\mu\text{V/m}] \qquad (A.8)$$

For an isotropic antenna in free space with $G = 0$ we arrive at:

$$E_n = F_a + 20\log f\ [\text{MHz}] + 10\log b - 96.8\ \ [\text{dB}\mu\text{V/m}] \qquad (A.9)$$

For a half-wave dipole in free space is known $G = 2.15$ so:

$$E_n = F_a + 20\log f\ [\text{MHz}] + 10\log b - 98.9\ \ [\text{dB}\mu\text{V/m}] \qquad (A.10)$$

For a Hertzian dipole, $G = 1.75$ dB, in free space we arrive at:

$$E_n = F_a + 20\log f\ [\text{MHz}] + 10\log b - 98.5\ \ [\text{dB}\mu\text{V/m}] \qquad (A.11)$$

A.1 Short Monople

For a short monopole over a perfect electric conducting (PEC) ground we know that the gain $g_{monopole} = 3$ and equal to the gain of a vertical Hertzian dipole just above PEC ground, see [16] and [84] and appendix E.

For antenna with gain g the effective area $A_{eff}(\theta)$ and elevation θ is according (*A*.3):

$$A_{eff}(\theta) = \frac{g \cdot 300^2}{4\pi f^2}\cos(\theta) \qquad (f \text{ in MHz}) \qquad (A.12)$$

$$= \frac{3 \times 300^2}{4\pi f^2}\cos(\theta) \quad \text{for a short monopole} \qquad (A.13)$$

For a noise field strength $e_{n,free\ space}$, defined in the far field region and propagating in free space:

$$pd_{n,free\ space} = \frac{e^2_{n,free\ space}}{120\pi} \qquad (A.14)$$

$$p_{n,free\ space} = A_{eff} pd_{n,free\ space}$$

$$= \frac{3}{4\pi}\left(\frac{300}{f}\right)^2 \cos(\theta)\frac{e^2_{n,free\ space}}{120\pi}$$

$$= \frac{1}{160\pi^2}\left(\frac{300}{f}\right)^2 \cos(\theta)\, e^2_{n,free\ space}$$

$$= \frac{57.0}{f^2}\cos(\theta)\, e^2_{n,free\ space} \qquad (A.15)$$

For the elevation angle with the highest gain ($\theta \rightarrow 0$) we get for the total received power:

$$p_{n,free\ space} = \frac{57.0}{f^2}\, e^2_{n,free\ space} \qquad (A.16)$$

A.2 Field strength values double just above ground

At the point of reflection over PEC ground the field strength values, E and H, doubles because of boundary conditions. This can be seen when we study what happens at the boundary between the half space above ground and that space below. In the case of the E-field of the incident wave is parallel to the plane of incidence (vertical polarisation), the components of the incident wave and of the reflected wave, that are parallel to the ground, will compensate each other at the point of reflection, according Fresnel's Equations [16]. The E-fields component normal to the ground will add, and so double when the ground is perfectly conducting. In this case the H-field is normal to the plane of incidence and parallel to the ground. The H-field of the incident wave will be added to the H-field of the reflected wave, and also double in strength at the point of reflection when the ground is perfectly conducting. In the case of the E-field of the incident wave is normal to the plane of incidence, and thus parallel to the ground, the E-field at the point of reflection is zero, so the reflected E-field has a 180 degrees phase shift. The H-field in this case is parallel to the plan of incidence. The H-field component, normal to the ground, will be cancelled, while the component parallel to the ground will be doubled at the point of reflection.

As the field strength values usually are measured with the well known field sensor antennas, like the magnetic loop or active E-field monopole probe, these doubled values are indicated, because the sensors are calibrated for field strengths in free space. So in noise measurements using Equation (1.8), like as referred to in ITU-R Rec. 372, the calculated field strength is that over PEC ground. So now we may write for the electrical field strength of noise e_n as measured by a field sensor just above ground:

$$e_n = 2e_{n,free\ space} \tag{A.17}$$

So from Equation (A.15):

$$p_n = \frac{14.25}{f^2} e_n^2 \tag{A.18}$$

Switching to dB:

$$P_n = E_n[\text{dBµV/m}] - 120 - 20\log f\,[\text{MHz}] + 11.5 \tag{A.19}$$

$$F_a + 10\log b - 204 = E_n[\text{dBµV/m}] - 20\log f\,[\text{MHz}] - 108.5 \tag{A.20}$$

$$E_n[\text{dBµV/m}] = F_a + 10\log b - 204 + 20\log f\,[\text{MHz}] + 108.5 \tag{A.21}$$

$$= F_a + 20\log f\,[\text{MHz}] + 10\log b - 95.5 \tag{A.22}$$

This result is in accordance with Reference [13], and shown in Equation (1.8) of Chapter 1.

Appendix B: Calculation of the antenna factor of a receiving antenna

When the field strength, E, or the power density, p, of a radio signal is known we are able to calculate the voltage, that is induced in a conductor with a length small in relation to the wavelength directly from the field strength pro meter. For a receiving antenna with dimensions that are not small compared with the wavelength, like a half wave dipole, we have to integrate the field strength over the length of the antenna and consider the dynamic behaviour of the antenna. We can avoid this calculation when we know the effective surface, the aperture, of the antenna. In general, for a receiving antenna is valid according reference [16] (any size, but zero loss):

$$A_{eff} = \frac{g\lambda^2}{4\pi} \tag{B.1}$$

with g as the antenna gain. For an electric dipole is that:

$$A_{eff} = \frac{3\lambda^2}{8\pi} \tag{B.2}$$

The power density is:

$$p = \frac{E^2}{120\pi} \quad [W/m^2] \tag{B.3}$$

Then the received power is:

$$P_{rx} = A_{eff}p = \frac{g\lambda^2}{4\pi}\frac{E^2}{120\pi} = \frac{g\lambda^2}{480\pi^2}E^2 \tag{B.4)}$$

But at the receiver input with input resistance, R_{rx}, is valid:

$$P_{rx} = \frac{V_{rx}^2}{R_{rx}} \tag{B.5}$$

with V_{rx} the voltage over the receiver input terminal, thus:

$$\frac{V_{rx}^2}{R_{rx}} = \frac{g\lambda^2}{480\pi^2}E^2 \tag{B.6}$$

$$V_{rx} = \frac{\lambda}{4\pi}\sqrt{\frac{gR_{rx}}{30}}E \tag{B.7}$$

This means for the antenna factor, k:

$$k \equiv \frac{E}{V_{rx}} = \frac{4\pi}{\lambda}\sqrt{\frac{30}{gR_{rx}}} \tag{B.8}$$

The antenna gain is g, mostly given in dB's as G, so:

$$G = 10\,log\,(g) \tag{B.9}$$

$$g = 10^{G/10} \qquad (B.10)$$

For a half wave dipole with a gain of 1.64 (2.14 dB) [84] relative to an isotropic radiator and a receiver input impedance of 50 ohm (real) we get:

$$k = \frac{4\pi}{\lambda} 0.605 \qquad (B.11)$$

or in dB:

$$K = 20\, log\,(k) \qquad (B.12)$$

For half wave dipoles that results in Table B.1 on several amateur bands:

Table B.1. Antenna factors and numbers for a half wave dipole in free space as a function of frequency

Antenna factor and number										
Band	1.8	3.6	7,0	10.1	14	18	21	24	28	[MHz]
k	0.046	0.091	0.177	0.256	0.360	0.459	0.537	0.631	0.732	[1/m]
K	-26.8	-20.8	-15.0	-11.8	-8.9	-6.8	-5.4	-4.0	-2.7	[dB/m]

Appendix C: Cumulation of noise powers when using two crossed loop antennas

Suppose we have a set of noise sources $S_1,\ S_2,\ \cdots S_n$ at n different positions all generating uncorrelated noise, which arrive at the position of the receiver antenna with an (equivalent) electric field strength of $E_1,\ E_2,\ \cdots E_n$, and a magnetic field strength $H_1,\ H_2,\ \cdots H_n$. We assume far field conditions at the measurement position. Also we assume vertical polarisation, and no noise arriving via skywave. We may make this assumption because of the considerations in Chapter 2, Subsections 2.2.2 and 2.3.6.

First, suppose the receiving antenna is a short monopole above a perfect conducting ground. All noise components from the n sources are added as noise powers, so the equivalent field strength of the summed noise is:

$$E_{total} = \sqrt{E_1^2 + E_2^2 + \cdots + E_n^2} \qquad (C.1)$$

Secondly, suppose the receiving antenna is a pair of crossed vertical small magnetic loop antennas. Each of the loop antennas is connected to a measuring receiver using a RMS detector, which converts the measure noise field strength into detector output voltages V_x and V_y. We see according Figure C.1:

$$S_1 : H_{1,x} = H_1 \cos\phi_1 \qquad H_{1,y} = H_1 \sin\phi_1$$

$$S_2 : H_{2,x} = H_2 \cos\phi_2 \qquad H_{2,y} = H_2 \sin\phi_2$$

$$* \qquad\qquad *$$

$$* \qquad\qquad *$$

$$S_n : H_{n,x}^* = H_n \cos \phi_n \qquad H_{n,y}^* = H_n \sin \phi_n \tag{C.2}$$

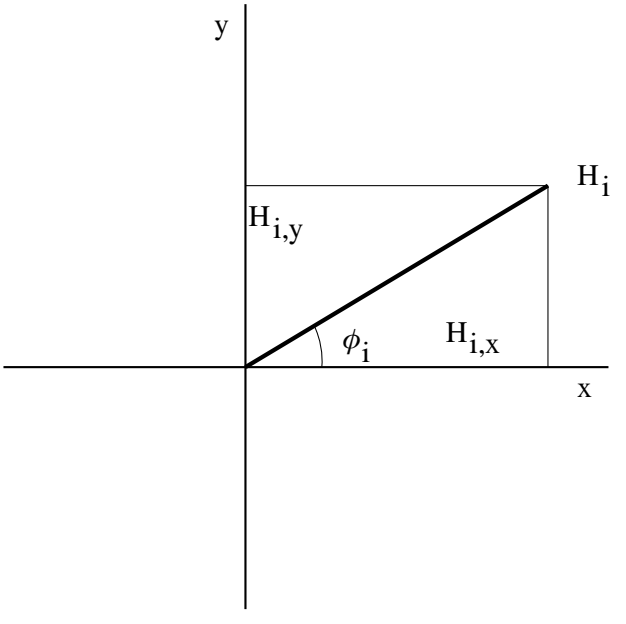

Figure C.1. Adding of noise in two orthogonal antenna loops.

Adding the powers in each receiver results in:

$$H_x = \sqrt{H_{1,x}^2 + H_{2,x}^2 + \cdots + H_{n,x}^2} \tag{C.3}$$

$$H_y = \sqrt{H_{1,y}^2 + H_{2,y}^2 + \cdots + H_{n,y}^2} \tag{C.4}$$

Defining a proportionality constant k the resulting detector outputs are:

$$V_x = kH_x \tag{C.5}$$

$$V_y = kH_y \tag{C.6}$$

To calculate the total amount of noise power and noise field strength we have to add the powers in the x and y direction, so the equivalent total noise field strength is:

$$\begin{aligned} H_{total} &= \frac{\sqrt{V_x^2 + V_y^2}}{k} \\ &= \frac{\sqrt{(kH_x)^2 + (kH_y)^2}}{k} \\ &= \sqrt{(H_{1,x}^2 + H_{2,x}^2 + \cdots + H_{n,x}^2) + (H_{1,y}^2 + H_{2,y}^2 + \cdots + H_{n,y}^2)} \\ &= \sqrt{H_{1,x}^2 + H_{1,y}^2 + H_{2,x}^2 + H_{2,y}^2 + \cdots + H_{n,x}^2 + H_{n,y}^2} \end{aligned} \tag{C.7}$$

As $H^2_i = H^2_{i,x} + H^2_{i,y}$ it follows:

$$H_{total} = \sqrt{H_1^2 + H_2^2 + \cdots + H_n^2} \qquad (C.8)$$

Equation (C.8) is conform to Equation (C.1), so the azimuthal directivity for man-made noise measurements in the case of a short monopole above a perfect conducting ground and that in the case of pair of crossed vertical small magnetic loop antennas, are identical. A necessary condition is that the detector outputs for both loop antennas are Root Sum Squares added.

Appendix D: Data of noise measurements

Table D.1. Measurement data from Chapter 3 as refered to in Chapter 4, Section 4.2: Density of habitation.

VERON noise floor measurement campaign			Number of livings within distance from measurement location:											
	Location:	Type of environment:	0-50 m	50-100m	100-200m	200-300m	300-400m	400-500m	0-50 m	0-100 m	0-200 m	0-300 m	0-400 m	0-500 m
1	Dwingelosche veld	Quiet Rural	0	0	0	0	0	0	0	0	0	0	0	0
2	Kootwijkerzand		0	0	0	0	0	0	0	0	0	0	0	0
3	Lake IJsselmeer		0	0	0	0	0	0	0	0	0	0	0	0
4	PA5CW	Rural	1	0.5	1	1	0.5	1	1	1	2	3	3	4
5	PA3FAU		1	0.5	6	8	9	24	1	1	7	15	24	48
6	PI4CC		1	0.5	1	8	15	54	1	1	2	10	25	79
7	PE1PUP		1	1	1	3	2	3	1	2	3	6	8	11
8	PA3FTZ		1	1	1	3	5	4	1	2	3	6	11	15
9	PA3ARM		1	1	4	8	11	13	1	2	6	14	25	38
10	PH4RTM		2	2	5	5	4	10	2	4	9	14	18	28
11	PE5T		3	2	7	2	5	3	3	5	12	14	19	22
12	PA0MER		1	4	3	5	3	9	1	5	8	13	16	25
13	PA0KDF		4	1	7	28	32	51	4	5	12	40	72	123
14	PA0RLM	Residential 1	6	2	48	108	258	249	6	8	56	164	422	671
15	PA2JAJ		5	6	45	52	40	47	5	11	56	108	148	195
16	PA3AWN		3	10	11	35	26	23	3	13	24	59	85	108
17	PA0JMG		7	7	66	110	107	130	7	14	80	190	297	427
18	PA0JBB		15	0.5	18	5	24	30	15	15	33	38	62	92
19	PA3ERO		4	11	69	63	92	65	4	15	84	147	239	304
20	PA2DTA		5	11	17	28	42	13	5	16	33	61	103	116
21	PE1KRY		3	14	69	120	191	248	3	17	86	206	397	645
22	PA0RYL		5	15	98	147	54	49	5	20	118	265	319	368
23	PA0WTA		6	14	62	225	261	225	6	20	82	307	568	793
24	PAoAST		9	29	128	196	337	552	9	38	166	362	699	1251
25	PD0RKC		16	27	63	84	83	81	16	43	106	190	273	354
26	PA8A		7	40	249	305	476	590	7	47	296	601	1077	1667
27	PC0WP		11	39	108	358	313	423	11	50	158	516	829	1252
28	PA3ECT	Residential 2	16	38	54	17	14	9	16	54	108	125	139	148
29	PA3ADC		17	40	83	49	36	5	17	57	140	189	225	230
30	PA2PIM		16	44	166	316	421	619	16	60	226	542	963	1582
31	PA0KLS		11	52	147	291	335	262	11	63	210	501	836	1098
32	PD0SBS		18	47	135	95	160	215	18	65	200	295	455	670
33	PA0HTT		12	54	153	176	144	112	12	66	219	395	539	651
34	PC7M		23	43	158	133	158	193	23	66	224	357	515	708
35	PA2MD		37	38	203	207	417	555	37	75	278	485	902	1457
36	PA0JNH		24	52	114	45	16	13	24	76	190	235	251	264
37	PA0WJG		22	55	348	540	446	518	22	77	425	965	1411	1929
38	PA1AT		24	63	152	382	406	308	24	87	239	621	1027	1335
39	PA3FTT		32	63	318	385	494	448	32	95	413	798	1292	1740
40	PB0AIR		31	64	366	363	447	626	31	95	461	824	1271	1897
41	PA0VBR		27	71	160	184	338	379	27	98	258	442	780	1159
42	PA0GJH	Residential 3	38	66	152	331	478	555	38	104	256	587	1065	1620
43	PA9RZ		19	90	268	390	531	478	19	109	377	767	1298	1776
44	PA0AOB		29	84	508	954	899	1063	29	113	621	1575	2474	3537
45	PA3BME		21	94	274	446	407	441	21	115	389	835	1242	1683
46	PA0WGV		12	104	359	268	364	337	12	116	475	743	1107	1444
47	PA0RSM		30	86	210	407	323	452	30	116	326	733	1056	1508
48	PE1RKS		41	91	138	288	337	322	41	132	270	558	895	1217
49	PD2HW		51	81	296	600	424	413	51	132	428	1028	1452	1865
50	PH1E	City	34	57	274	448	656	715	34	91	365	813	1469	2184
51	PE4WJ		20	72	234	252	263	458	20	92	326	578	841	1299
52	PA3GON		44	96	388	426	707	703	44	140	528	954	1661	2364
53	PA3GXD		52	106	369	511	533	575	52	158	527	1038	1571	2146
54	PA5ROB		45	114	320	652	934	634	45	159	479	1131	2065	2699
55	PA3EIO		100	63	299	353	554	551	100	163	462	815	1369	1920
56	PE1NRA		96	177	597	823	858	1246	96	273	870	1693	2551	3797
57	PA7WLL		48	225	842	1146	1787	2646	48	273	1115	2261	4048	6694
58	Lake Markermeer	Atypical	0	0	0	0	0	0	0	0	0	0	0	0
59	Goffertpark Nijmegen		0	0	1	2	88	210	0	0	1	3	91	301

Table D.2. Measurement data from Chapter 3 as refered to in Chapter 4, Section 4.2: Field strength levels.

VERON noise floor measurement campaign			Noise floor as field strength [dBµV/m], Averaged Total value, in Frequency bands:											
	Location:	Type of environment:	635 m	160 m	80 m	60 m	40 m	30 m	20 m	17 m	15 m	12 m	10 m	6 m
1	Dwingelosche veld	Quiet Rural	6.8	-5.2	-13.1	-11.7	-9.4	-8.0	-12.3	-10.0	-10.8	-12.2	-10.4	-10.7
2	Kootwijkerzand		12.2	-9.1	-16.3	-12.2	-12.0	-13.0	-8.2	-8.1	-9.9	-11.9	-11.9	-10.3
3	Lake IJsselmeer		6.6	0.6	-5.2	-4.9	-1.1	-4.6	-7.0	-6.8	-5.9	-13.0	-15.2	-17.2
4	PA5CW	Rural	23.4	4.9	-1.6	-0.9	0.1	-5.3	-4.7	-1.9	-1.8	-8.8	-17	-11.4
5	PA3FAU		18.0	11.3	3.9	6.7	7.6	1.5	8.5	-7.3	-5.9	-12.2	-9.8	-9.9
6	PI4CC		21.0	11.4	0.5	-5.4	-11.1	-8.2	-12.4	-12.9	-10.3	-14.7	-15.0	-11.5
7	PE1PUP		15.7	10.2	12.6	13.7	14.6	2.3	4.3	-6.5	-9.3	-14.7	-14.2	-11.1
8	PA3FTZ		12.8	10.7	2.5	2.6	-0.2	6.0	0.1	-4.5	0.3	-2.2	-7.6	-9.7
9	PA3ARM		16.8	12.4	4.3	-0.3	2.9	1.0	-9.7	-13.8	-11.0	-13.9	-12.7	-12.5
10	PH4RTM		17.6	10.6	1.3	4.7	11.2	4.9	-2.3	-5.5	-3.7	-5.8	-11.5	-14.8
11	PE5T		18.3	12.6	10.0	7.5	6.7	2.1	-0.5	9.0	6.4	13.0	-3.5	-2.1
12	PA0MER		14.0	15.0	2.1	0.6	0.2	-2.6	-4.3	-4.4	-4.7	-9.9	-16.2	-9.1
13	PA0KDF		15.3	6.8	3.1	-1.4	-1.1	-1.6	-1.1	-3.6	-5.8	-9.8	-10.9	-10.7
14	PA0RLM	Residential 1	20.7	12.7	12.3	8.1	9.5	1.6	15.0	13.1	4.0	1.9	1.0	0.7
15	PA2JAJ		13.1	11.7	17.7	7.3	2.5	2.2	2.6	-1.2	-2.1	-5.7	-9.5	-8.9
16	PA3AWN		16.2	9.6	9.5	3.8	-0.1	-0.3	2.9	-2.4	-7.8	-11.5	-11.1	-17
17	PA0JMG		12.7	15.1	18.7	19.3	14.9	7.0	6.1	3.5	4.7	1.9	-5.7	-8.1
18	PA0JBB		14.8	14.9	12.2	8.9	3.8	-2.5	2.6	-2.9	-4.9	-9.0	-7.6	-8.2
19	PA3ERO		14.4	12.6	10.0	10.2	6.4	1.4	0.4	***4***	2.2	-2.2	-4.8	-16.4
20	PA2DTA		7.5	6.4	4.5	2.8	0.2	1.9	-2.9	-1.6	-6.7	-10.6	-8.2	-15.1
21	PE1KRY		31.1	15.9	13.1	14.4	6.3	3.7	-0.7	-3.9	-2.3	-6.9	-8.3	-4.7
22	PA0RYL		14.8	5.7	3.5	-1.8	-1.5	-1.5	-3.7	2.6	0.9	-5.6	-7.2	-6.6
23	PA0WTA		31.4	13.0	18.0	10.7	4.3	12.7	6.9	1.4	1.3	-3.7	-6.9	-1.6
24	PAoAST		26.1	21.3	17.8	16.1	18.3	9.4	8.3	5.7	9.6	4.3	0.0	-4.1
25	PD0RKC		28.6	20.5	24.6	22.2	17.9	16.7	20.8	15.4	12.3	4.7	-0.3	2.6
26	PA8A		17.8	17.0	18.9	13.3	8.5	8.6	0.1	-2.3	-0.2	-8.7	-9.5	-6.6
27	PC0WP		24.3	16.1	14.0	8.9	7.8	14.4	9.5	5.9	9.7	-0.6	-1.2	-3.8
28	PA3ECT	Residential 2	17.6	14.3	13.1	12.1	11.4	10.6	7.7	5.5	1.2	-3.3	-2.3	-2.3
29	PA3ADC		36.6	19.4	19.5	14.3	12.1	5.7	14.0	13.0	7.0	7.8	4.4	-5.4
30	PA2PIM		20.4	19.2	18.8	11.3	7.5	15.2	6.3	9.8	8.9	-0.2	-1.0	-2.7
31	PA0KLS		16.8	19.5	16.9	14.5	19.5	14.8	8.3	7.7	7.5	7.0	3.7	8.9
32	PD0SBS		27.5	30.6	23.1	24.5	20.9	11.4	9.0	13.7	15.5	19.4	4.5	6.7
33	PA0HTT		21.6	20.8	16.5	14.2	12.1	9.2	11.4	6.9	18.8	9.7	5.5	10.0
34	PC7M		17.1	20.1	16.3	11.3	15.5	16.1	13.5	6.4	8.6	3.1	-5.2	-2.8
35	PA2MD		23.7	23.0	14.8	10.6	10.2	6.0	6.6	6.0	7.2	1.0	5.0	2.1
36	PA0JNH		18.8	16.4	17.4	15.0	14.0	13.2	15.3	10.3	11.1	10.1	6.9	2.0
37	PA0WJG		43.9	21.9	18.3	10.3	10.2	3.1	10.7	8.6	5.4	10.9	5.1	***2***
38	PA1AT		37.0	19.4	20.1	16.7	8.4	2.6	10.0	7.9	8.1	4.6	-1.4	-0.3
39	PA3FTT		45.7	30.7	31.5	21.3	18.3	15.4	13.6	10.1	9.2	4.8	1.0	4.2
40	PB0AIR		38.3	25.3	18.4	13.6	10.1	14.0	10.9	9.3	5.1	3.4	2.1	9.5
41	PA0VBR		22.9	13.1	14.4	15.0	15.6	14.6	6.5	6.1	6.2	12.1	1.3	-0.2
42	PA0GJH	Residential 3	31.1	20.3	19.4	11.8	7.8	6.7	8.3	6.2	6.2	-1.2	-4.9	-3.7
43	PA9RZ		20.7	18.5	17.3	11.42	9.8	7.9	6.1	-0.2	0.6	-1.3	-4.7	0.3
44	PA0AOB		28.7	20.0	17.7	16.7	14.0	13.7	15.2	9.2	7.8	13.0	9.2	7.4
45	PA3BME		34.1	16.8	17.5	15.2	12.6	9.0	12.8	17.5	16.8	4.4	-3.9	-7.7
46	PA0WGV		39.7	22.4	17.0	13.4	7.8	3.2	7.8	3.9	8.6	-0.7	-0.6	-4.2
47	PA0RSM		21.6	19.1	20.2	14.0	9.3	5.7	6.2	6.2	8.1	1.4	-3.1	4.0
48	PE1RKS		33.9	19.4	18.8	16.3	13.3	10.9	10.6	12.9	10.5	4.2	0.8	5.6
49	PD2HW		17.8	23.5	19.4	19.3	19.4	9.9	13.9	11.0	17.0	4.0	0.3	1.8
50	PH1E	City	23.2	19.8	19.3	18.3	17.2	8.5	10.7	11.6	10.8	8.9	2.2	3.6
51	PE4WJ		33.2	27.1	28.9	23.8	30.9	22.4	21.8	19.6	15.2	14.9	22.0	13.1
52	PA3GON		24.0	29.4	30.1	21.2	20.5	13.4	15.2	15.8	15.0	12.1	7.3	1.6
53	PA3GXD		28.5	35.1	24.8	25.7	18.6	14.6	12.5	10.3	8.6	9.3	2.8	5.6
54	PA5ROB		25.9	20.4	20.2	16.9	12.4	7.2	14.6	9.4	8.2	5.7	2.6	6.1
55	PA3EIO		16.9	20.5	21.4	17.3	13.2	16.2	4.2	3.5	3.6	1.1	-1.2	1.7
56	PE1NRA		33.4	28.5	28.9	22.4	16.0	13.9	16.2	14.4	11.2	4.2	3.7	-5.9
57	PA7WLL		30.4	35.4	26.9	22.9	19.4	16.7	18.6	18.5	16.5	20.6	21.5	10.8
58	Lake Markermeer	Atypical	16.6	7.7	1.7	-2.4	-4.18	-3.8	-5.9	-4.5	-6.7	-6.3	-0.5	-9.4
59	Goffertpark Nijmegen		14.3	6.6	-0.2	-1.9	-5.6	-6.7	-6.1	-6.4	-10.5	-12.9	-11.3	-9.2

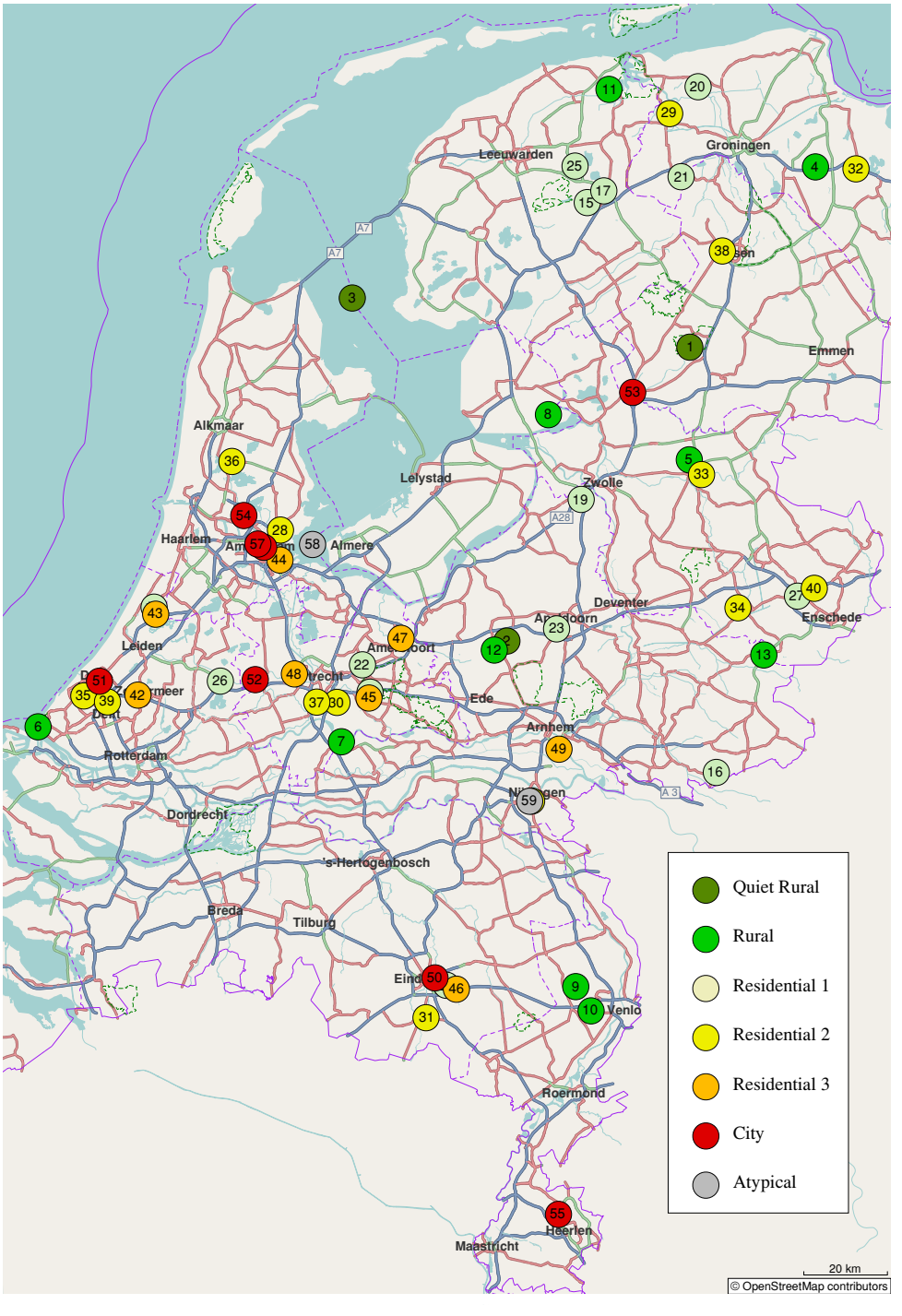

Figure D.1. Map of measurement locations.

Appendix E: Calculation of field strength above Perfect Electrical Conducting ground

As treated in Chapter 5 we use the propagation over PEC ground as a reference, so we need to calculate that. A simplified way, using PEC, is as follows. When we calculate the field strength, we start with the assumption that we have small and symmetrical dipole with a symmetrical feed. Then we place an infinite, electrical perfect conducting (PEC), sheet between both halves of the dipole and the transmission line, see Figure E.1. This conducting sheet is in the symmetry centre, and so does not interact with the dipole, feed line, or the generated EM fields. This means that the space is divided into two half-spaces, above the PEC sheet, forming a ground plane, and below, while there is no interaction between the fields in the two spaces. Just above the borderline, and in case the PEC sheet is absent, the power density s_{dipole} and the field strength e_{dipole} is:

$$s_{dipole} = \frac{g_{dipole}}{4\pi d^2} p_{tx} \qquad (E.1)$$

$$e_{dipole} = \sqrt{s_{dipole} Z_0} \approx \frac{1}{d}\sqrt{p_{tx} g_{dipole} \cdot 30} \qquad (E.2)$$

Herein is the gain $g_{dipole} = 1.5$ according [84].

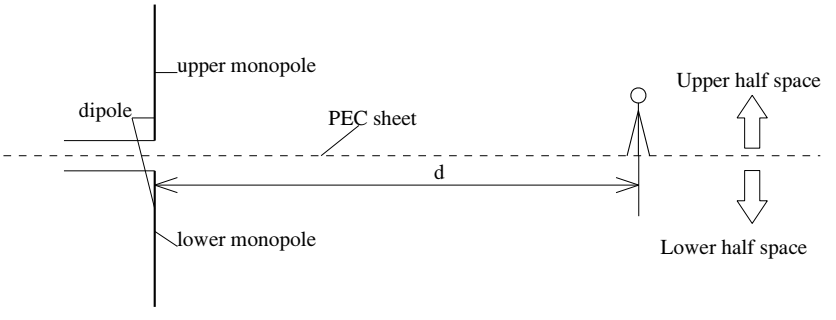

Figure E.1. Derivation of the gain of a monopole.

When we place the PEC sheet, the power density and the field strength at any position in both the half spaces do not change, but the power $p_{tx,\,dipole}$, fed to the dipole, is now divided over the two dipole halves and the half spaces. If we consider the one dipole half above the PEC ground as the monopole, with power $p_{tx,\,monopole}$, we may write:

$$p_{tx,\,monopole} = \frac{p_{tx,\,dipole}}{2} \qquad (E.3)$$

$$e_{monopole} \equiv e_{dipole} \qquad (E.4)$$

$$\frac{1}{d}\sqrt{p_{tx,\,monopole} g_{monopole} \cdot 30} = \frac{1}{d}\sqrt{p_{tx,\,dipole} g_{dipole} \cdot 30} \qquad (E.5)$$

(E.5) is true when $g_{monopole} = 2g_{dipole} = 3$. Now we can rewrite (E.2):

$$e_{monopole} = \frac{1}{d}\sqrt{p_{tx} \cdot 90} \tag{E.6}$$

When the antenna height of the monopole is much smaller than a quarter of the wavelength we may extent (E.6) for all elevation angles θ:

$$e_{monopole}(\theta) = \frac{1}{d}\sqrt{p_{tx} \cdot 90}\cos(\theta) \tag{E.7}$$

Appendix F: Compensation for measuring in the near field

Reference [86], Chapter 38, gives a good description of the near, intermediate and far fields, electric and magnetic, of a small oscillating dipole. From there it is not difficult to derive equations that describe the distance function in the main radiation direction for the E- and H-field:

$$|E| = \frac{[p]}{4\pi\varepsilon_0 \lambda\!\!\!^{-2} d}\sqrt{\left(\frac{\lambda\!\!\!^{-2}}{d^2} - 1\right)^2 + \left(\frac{\lambda\!\!\!^{-}}{d}\right)^2} \tag{F.1}$$

$$= \frac{[p]}{4\pi\varepsilon_0 \lambda\!\!\!^{-2} d}\, k_E \tag{F.2}$$

$$k_E = \sqrt{\left(\frac{\lambda\!\!\!^{-2}}{d^2} - 1\right)^2 + \left(\frac{\lambda\!\!\!^{-}}{d}\right)^2} \tag{F.3}$$

$$|H| = \frac{c\,[p]}{4\pi \lambda\!\!\!^{-2} d}\sqrt{(-1)^2 + \left(\frac{\lambda\!\!\!^{-}}{d}\right)^2} \tag{F.4}$$

$$= \frac{c\,[p]}{4\pi \lambda\!\!\!^{-2}}\, k_H \tag{F.5}$$

$$k_H = \sqrt{1 + \left(\frac{\lambda\!\!\!^{-}}{d}\right)^2} \tag{F.6}$$

Wherein k_E and k_H represents the correction factors in the near field for the electric, resp. the magnetic field component. In the far field with $d \gg \lambda\!\!\!^{-}$: $k_E = 1$ and $k_H = 1$. Herein the radian wavelength $\lambda\!\!\!^{-}$ is defined by:

$$\lambda\!\!\!^{-} = \frac{\lambda}{2\pi} \tag{F.7}$$

We can show the roll-off of the field strengths in the near and intermediate regions by plotting the relative field strengths, electric E_{rel} and magnetic H_{rel}:

$$E_{rel} = \frac{1}{d}\sqrt{\left(\frac{\lambda\!\!\!^{-2}}{d^2} - 1\right)^2 + \left(\frac{\lambda\!\!\!^{-}}{d}\right)^2} \tag{F.8}$$

$$H_{rel} = \frac{1}{d}\sqrt{1 + \left(\frac{\lambda}{d}\right)^2} \tag{F.9}$$

The results are shown in Figure F.1

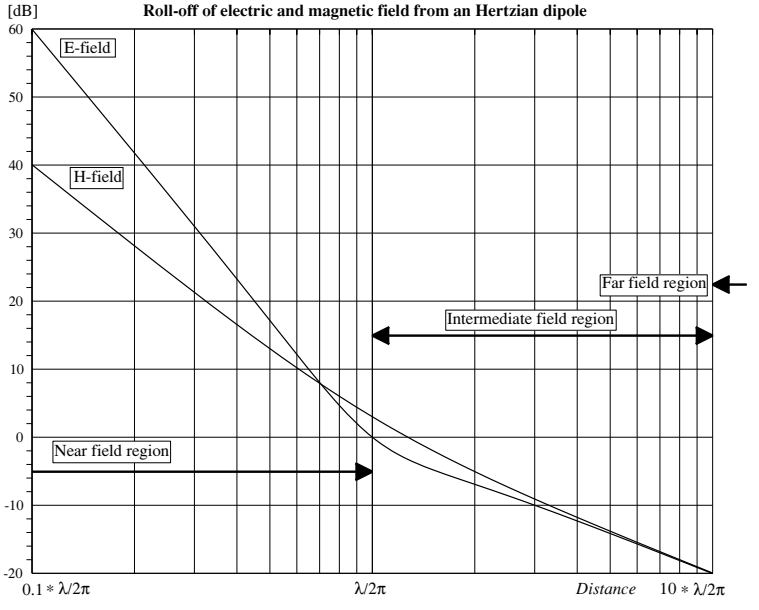

Figure F.1. Roll-off of electric and magnetic field from an Herzian dipole.

For the impedance of the field, radiated by a small electric dipole we find:

$$|Z_{electric\ dipole}| \equiv \frac{|E|}{|H|} = \frac{\dfrac{[p]}{4\pi\varepsilon_0\lambda^2 d}\sqrt{\left(\dfrac{\lambda^2}{d^2} - 1\right)^2 + \left(\dfrac{\lambda}{d}\right)^2}}{\dfrac{c\,[p]}{4\pi\lambda^2 d}\sqrt{(-1)^2 + \left(\dfrac{\lambda}{d}\right)^2}} \tag{F.10}$$

$$= \frac{\sqrt{\left(\frac{\lambda^2}{d^2} - 1\right)^2 + \left(\frac{\lambda}{d}\right)^2}}{4\pi\varepsilon_0 c\sqrt{(-1)^2 + \left(\frac{\lambda}{d}\right)^2}} \tag{F.11}$$

As

$$c = 1/\sqrt{\varepsilon_0\mu_0} \tag{F.12}$$

$$Z_0 = \sqrt{\frac{\mu_0}{\varepsilon_0}} \tag{F.13}$$

we end up with:

$$|Z_{electric\ dipole}| = Z_0\,\frac{\sqrt{\lambda^4 - \lambda^2 r^2 + r^4}}{r\sqrt{r^2 + \lambda^2}} \tag{F.14}$$

Even so we can find the field impedance from a magnetic dipole. The absolute value of the

magnetic field strength from a magnetic dipole is given by:

$$|H| = \frac{m}{4\pi}\frac{\sqrt{\lambda^4 - \lambda^2 r^2 + r^4}}{\lambda^2 r^3} \qquad (F.15)$$

and

$$|E| = \frac{\mu_0 cm}{4\pi\lambda^2 r}\sqrt{1 + \frac{\lambda^2}{r^2}} \qquad (F.16)$$

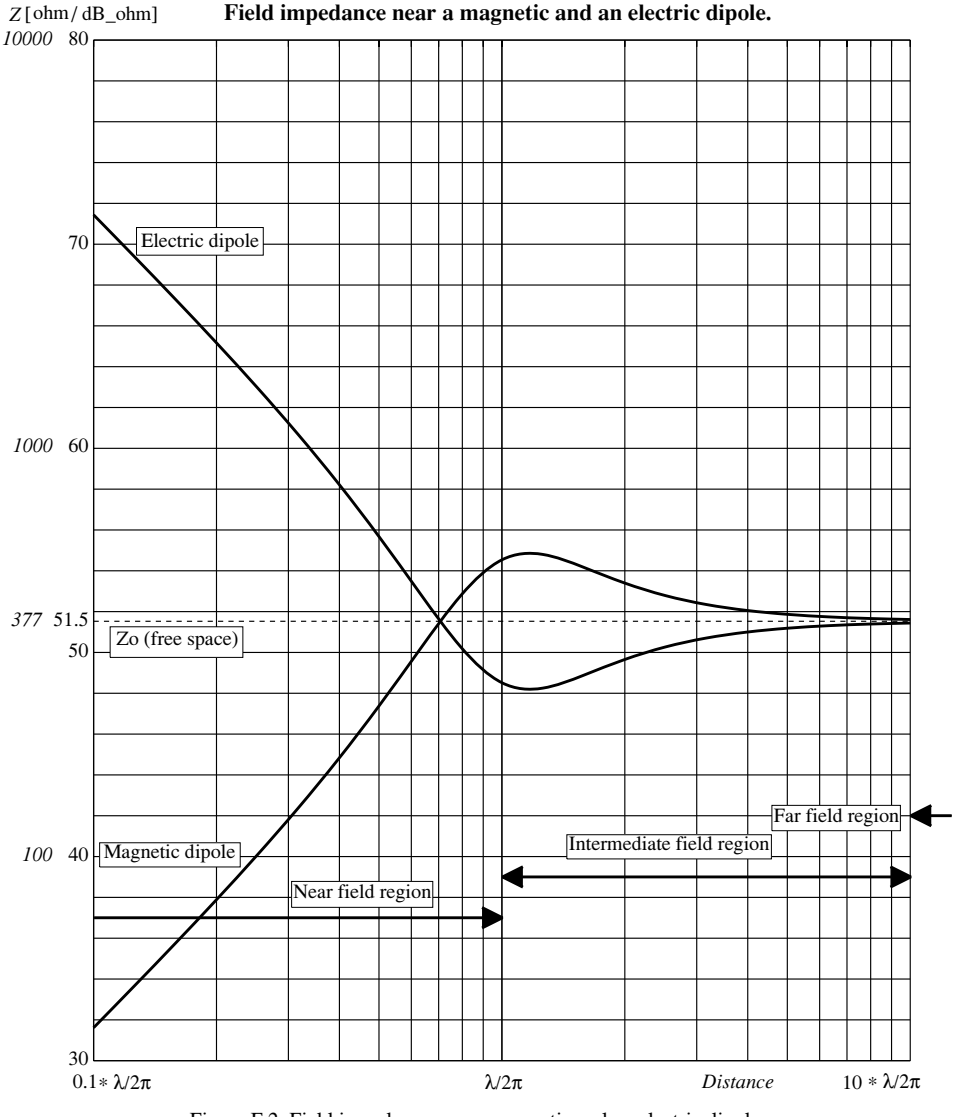

Figure F.2. Field impedance near a magnetic and an electric dipole.

So for the impedance of a field from a radiating magnetic dipole we find:

$$|Z_{magnetic\ dipole}| \equiv \frac{|E|}{|H|} = \frac{\frac{\mu_0 cm}{4\pi\lambda^2 r}\sqrt{1 + \frac{\lambda^2}{r^r}}}{\frac{m}{4\pi}\frac{\sqrt{\lambda^4 - \lambda^2 r^2 + r^4}}{\lambda^2 r^3}} \qquad (F.17)$$

$$= \mu_0 c r^2 \frac{\sqrt{1 + \lambda^2/r^2}}{\sqrt{\lambda^4 - \lambda^2 r^2 + r^4}} \qquad (F.18)$$

$$= Z_0 \frac{r\sqrt{r^2 + \lambda^2}}{\sqrt{\lambda^4 - \lambda^2 r^2 + r^4}} \qquad (F.19)$$

Figure F.2 shows the field impedance near a magnetic and an electric dipole.

Appendix G: Errors due to polarisation

In the field strenght measurements, in the noise as well as the propagation experiment, ground-wave propagation is assumed, and therefore the polarisation of the received waves vertical. But it is known that ground-wave propagated waves show a forward tilted E-field when there are ground losses. In reference [106], J.L. Eaton, BBC, the relationship is shown between this tilt and the ground constants. Especially the in [106] given equation:

$$\left|\frac{E_s}{E_n}\right| = \frac{1}{120\pi}\sqrt{\frac{\omega\mu}{\sqrt{\sigma^2 + \omega^2\varepsilon^2}}} \qquad (G.1)$$

gives us the opportunity to estimate the error that occurs when we try to estimate the total electrical field E_{total} strength by measuring the vertical component E_n. E_s is the field strength parallel to the surface. Table G.1 shows $|E_s/E_n|$ as function of ground constants and frequency.

Table G.1. Ratio of horizontal / vertical E-field as a function of ground constants.

Type of ground	σ [S/m]	ε_r	Horizontal / vertical E-field ratio [dB] @ frequency [MHz]										
			0.47	1.85	3.65	5.36	7.1	10.1	14.2	18.1	21.2	25	28.5
Sea water, av. salinity	5	70	-52.8	-46.9	-43.9	-42.2	-41.0	-39.5	-38.0	-37.0	-36.3	-35.6	-35.0
Sea water, low salinity	1	80	-45.8	-39.9	-36.9	-35.3	-34.0	-32.5	-31.0	-30.0	-29.3	-28.6	-28.0
Fresh water	0.003	80	-21.4	-19.3	-19.1	-19.1	-19.1	-19.0	-19.0	-19.0	-19.0	-19.0	-19.0
Wet land	0.030	40	-30.6	-24.7	-21.9	-20.3	-19.3	-18.2	-17.4	-17.0	-16.8	-16.6	-16.5
Wet ground	0.010	30	-25.8	-20.1	-17.6	-16.5	-15.9	-15.4	-15.1	-15.0	-14.9	-14.9	-14.9
Land	0.003	22	-20.7	-15.7	-14.2	-13.8	-13.7	-13.6	-13.5	-13.5	-13.5	-13.4	-13.4
Medium dry ground	0.001	15	-16.1	-12.5	-12.0	-11.9	-11.8	-11.8	-11.8	-11.8	-11.8	-11.8	-11.8
Dry ground	0.0003	7	-11.3	-8.81	-8.55	-8.50	-8.48	-8.47	-8.46	-8.46	-8.46	-8.46	-8.46
Very dry ground	0.0001	3	-6.86	-5.00	-4.83	-4.80	-4.79	-4.78	-4.78	-4.78	-4.78	-4.78	-4.78

The phase difference between E_s and E_n is given by:

$$\tan(2\phi) = \frac{\sigma}{\omega\varepsilon} \qquad (G.2)$$

The phase difference makes that the polarisation is elliptical with tilted axis. Table G.2 shows the calculated phase differences, depending on ground constants and frequency. As the instantaneous values of E_s and E_n are maximal together when the phase difference $\phi = 0$, the sum vector E_{total} maximizes for $\phi = 0$. So we may assume that the worse case situation occurs when there is no phase difference between E_n and E_s. Then

$$E_{total} = \sqrt{E_n^2 + E_s^2} \qquad (G.3)$$

Now we can express the error in dB by

$$Error = 20 \log\left(\frac{E_n}{E_{total}}\right) \qquad (G.4)$$

When

$$r \equiv \left|\frac{E_s}{E_n}\right| \qquad (G.5)$$

$$Error = 20 \log\left(\frac{1}{\sqrt{r^2 + 1}}\right) \text{ [dB]} \qquad (G.6)$$

Table G.3 shows the calculated results of *Error*. The maximal error is for very dry ground, 1.25 dB, all other cases the error is smaller than 1 dB,

Table G.2. Phase difference between E_s and E_n, depending on ground constants.

Type of ground	σ [S/m]	ε_r	**Phase difference between E_s and E_n @ frequency [MHz] in degrees [°]**										
			0.47	1.85	3.65	5.36	7.1	10.1	14.2	18.1	21.2	25	28.5
Sea water, av. salinity	5	70	45.0	45.0	44.9	44.9	44.8	44.8	44.7	44.6	44.5	44.4	44.4
Sea water, low salinity	1	80	44.9	44.8	44.5	44.3	44.1	43.7	43.2	42.7	42.3	41.8	41.4
Fresh water	0.003	80	27.5	10.1	5.23	3.58	2.71	1.90	1.36	1.07	0.911	0.772	0.677
Wet land	0.030	40	44.0	41.1	37.4	34.2	31.1	26.5	21.8	18.3	16.2	14.2	12.7
Wet ground	0.010	30	42.7	36.5	29.3	24.1	20.1	15.3	11.4	9.16	7.89	6.74	5.94
Land	0.003	22	39.6	26.6	16.9	12.3	9.52	6.80	4.90	3.86	3.30	2.80	2.46
Medium dry ground	0.001	15	34.3	16.6	9.09	6.30	4.79	3.37	2.41	1.89	1.62	1.37	1.20
Dry ground	0.0003	7	29.3	11.4	5.96	4.09	3.10	2.18	1.55	1.22	1.04	0.882	0.774
Very dry ground	0.0001	3	25.9	9.06	4.66	3.19	2.41	1.69	1.21	0.948	0.809	0.686	0.602

Table G.3. Error in estimation of total field strength by measuring vertical component.

Type of ground	σ [S/m]	ε_r	***Error* in estimation E_{total} by measuring E_{normal} @ frequency [MHz] in [dB]**										
			0.47	1.85	3.65	5.36	7.1	10.1	14.2	18.1	21.2	25	28.5
Sea water, av. salinity	5	70	0> *Error* >-0.01										
Sea water, low salinity	1	80	0> *Error* >-0.01										
Fresh water	0.003	80	-0.031	-0.051	-0.053	-0.053	-0.054	-0.054	-0.054	-0.054	-0.054	-0.054	-0.054
Wet land	0.030	40	-0.004	-0.015	-0.028	-0.040	-0.050	-0.065	-0.078	-0.086	-0.091	-0.094	-0.097
Wet ground	0.010	30	-0.011	-0.042	-0.075	-0.095	-0.11	-0.12	-0.13	-0.14	-0.14	-0.14	-0.14
Land	0.003	22	-0.03	-0.116	-0.16	-0.17	-0.18	-0.18	-0.190	-0.191	-0.192	-0.192	-0.192
Medium dry ground	0.001	15	-0.10	-0.24	-0.27	-0.27	-0.28	-0.28	-0.28	-0.28	-0.28	-0.28	-0.28
Dry ground	0.0003	7	-0.31	-0.54	-0.57	-0.57	-0.58	-0.58	-0.58	-0.58	-0.58	-0.58	-0.58
Very dry ground	0.0001	3	-1.24	-1.25	-1.25	-1.25	-1.25	-1.25	-1.25	-1.25	-1.25	-1.25	-1.25

Appendix H: Longitudinal Conversion Loss in mains networks

H.1 Introduction

In Chapter 7 the Longitudinal Conversion Loss (LCL) is mentioned. LCL is a well-known parameter for telecom and data transmision lines and associated equipment. It is related to the symmetry of the line or the connected port. Basically it concerns lines existing of two wires without branching.

According to ITU-T Recommendation O.9 [101] and [102] *the Longitudinal Conversion Loss (LCL) of a one- or two-port network is a measure (a ration expressed in dB) of the degree of unwanted transverse signal produced at the terminals of the network due to the presence of a longitudinal signal on the connecting leads*, defined in Equation (H.1) and in Figure H.1:

$$LCL = 20 \log \left| \frac{V_{L1}}{V_{T1}} \right| \text{[dB]} \qquad (H.1)$$

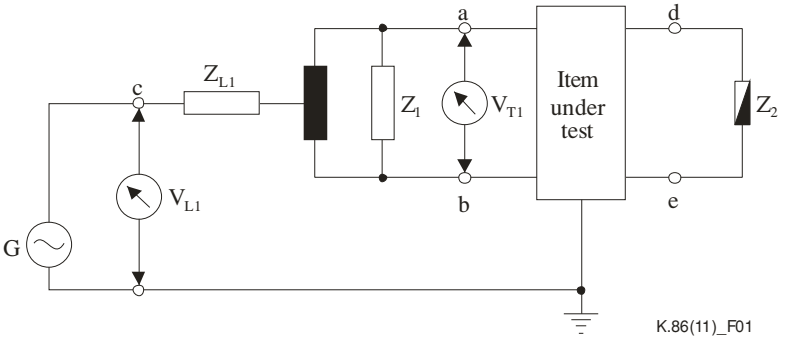

G: Signal generator.

Figure H.1. Definition of Longitudinal Conversion Loss. From [103].

H.2 LCL values of mains networks

The mains wiring inside a residence may be considered as a network for which LCL values can be defined. This subject has been studied over the last three decades because of the use of the mains network for Power Line Communication. In that application a Differential Mode (DM) radio frequency signal is supplied to one entry point of the network (wall outlet) with the intention that at another entry point that signal is received as a DM voltage. If the currents on the network were strictly differential at all places in the entire network, no radio disturbance would be radiated from the wiring. However, the symmetry of the wiring in a mains network is poor, because it has not been designed for. Even worse, the network is extensively meshed, including splitted wiring causing current loops and dipole-like

structures, see below. In such an application the ratio between DM current and Common Mode (CM) current is relevant for the degree of radiation. So we define the LCL value in a slight different way as the ratio between the CM current at position B and the injected DM current at the feedpoint (A) of the network. Figure H.2 shows a basic schematic view of a mains network. The sum of the disturbance currents on both lines, I_{Live} and $I_{Neutral}$, form the CM current, $I_{CM}(B)$ at position B, and the difference the DM current $I_{DM}(B)$. As reference we use the DM current at the injection point, $I_{DM}(A)$, because that value is determined by the injection source. The protective earth wire PE may be present or not, and has an additional influence on the currents, at least because of the capacitive and inductive coupling between the individual wires.

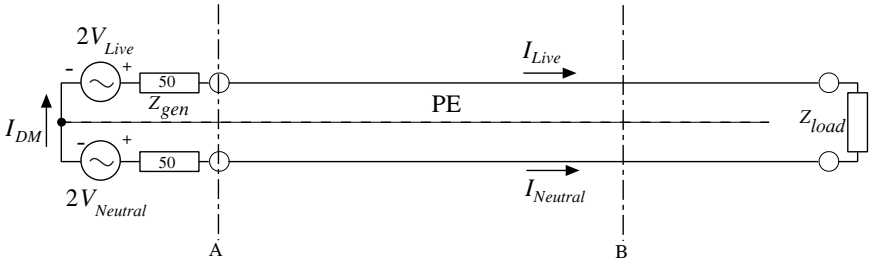

Figure H.2. Basic schematic view of mains network.

Equation (H.2) defines the LCL value $LCL(B)$ at location B:

$$LCL(B) = -20 \log \left| \frac{I_{CM}(B)}{I_{DM}(A)} \right| \text{ [dB]} \qquad (H.2)$$

$$I_{CM}(B) = \left| I_{Live}(B) + I_{Neutral}(B) \right| \qquad (H.3)$$

$$I_{DM}(B) = \left| I_{Live}(B) - I_{Neutral}(B) \right| \qquad (H.4)$$

$$I_{DM}(A) = I_{Live}(A) = -I_{Neutral}(A) \qquad (H.5)$$

$$= \frac{2V_{Live} - 2V_{Neutral}}{2Z_{source} + Z_{Live} + Z_{Neutral}} \qquad (H.6)$$

For symmetrical injection $V_{Live} = -V_{Neutral}$ so

$$I_{DM}(A) = \frac{4V_{Live}}{4 \times 50} = \frac{V_{Live}}{50} \qquad (H.7)$$

wherein we assume an input impedance of the mains network lines, $Z_{Live} = Z_{Neutral} = 50$ ohms. These input impedances are depending on the practical lay-out of the network and may vary around 50 ohms strongly. We may compare V_{Live} and $V_{Neutral}$ directly with the limits given in Table 7.2, Chapter 7, Subsection 7.3.1, and so with the ECS available powers given in Table 7.3.

For finding suitable values for LCL, we look back into the history of the discussions

about EMC for Power Line Communication. In the beginning, around the year 2000, the PLC lobby claimed a LCL value of 60 dB (CEPT working party SE35). During the discussions in the CENELEC/ETSI Joint Working Group on EMC of conducted transmission networks (2002 - 2007) the claims were reduced to 40 dB, which was still far too optimistic in the eyes of the radio spectrum users. Reference [103] uses a more extended mains network for making LCL measurements, depicted in Figure H.3. The resulted in measurements and calculations are shown in Figure H.4. We see an averaged values of *LCL*, varying around 40 dB, with low values below 20 dB.

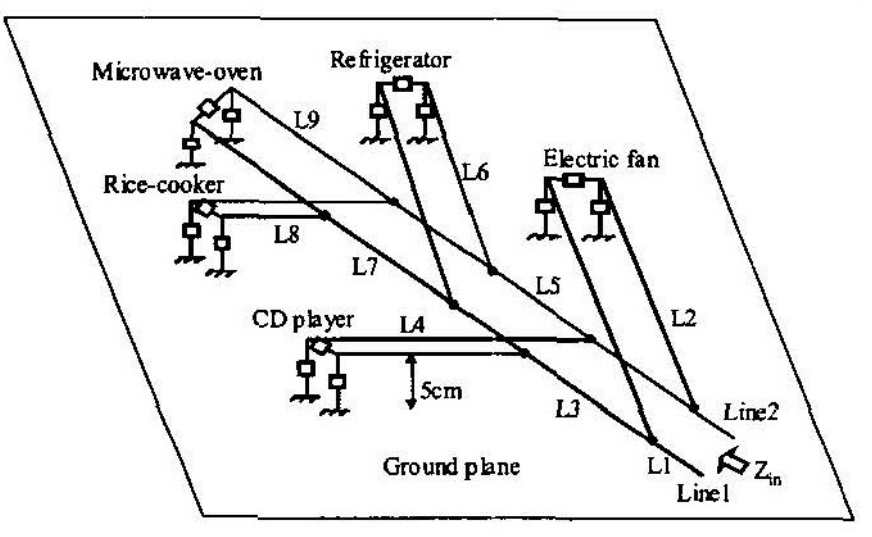

Figure 6. Experimental set-up for measuring LCL and input impedance

Figure H.3. More extended mains network for LCL measurements, from [103].

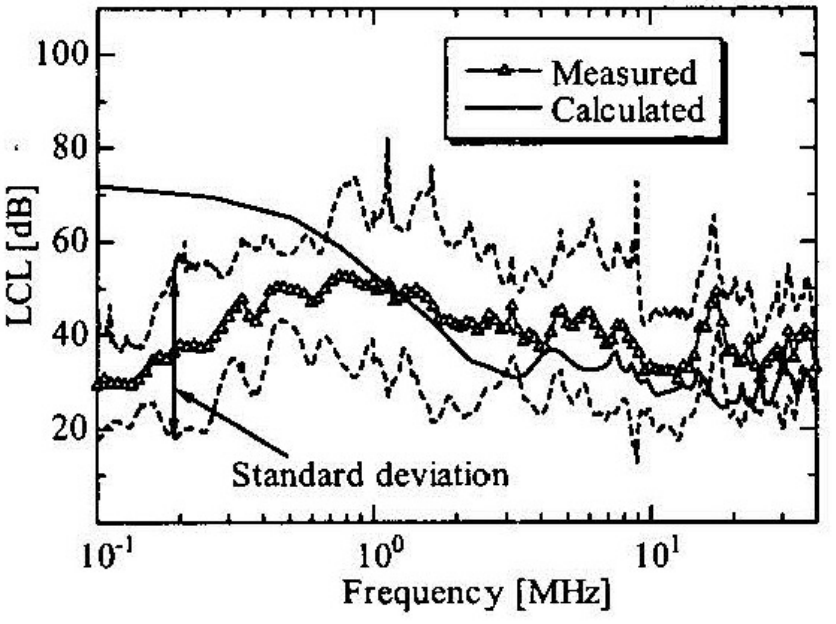

Figure 12. LCL characteristics of AC mains line

Figure H.4. Measurement and calculation results, from [103].

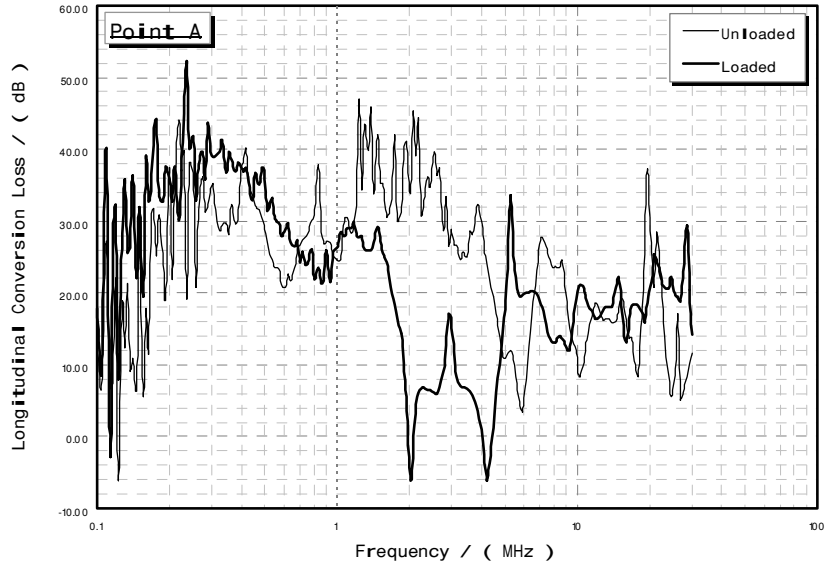

Fig. 10. Measured electrical unbalance at point A in a four-room housing unit.

Figure H.5. LCL values measured in a typical Singapore house. From [104].

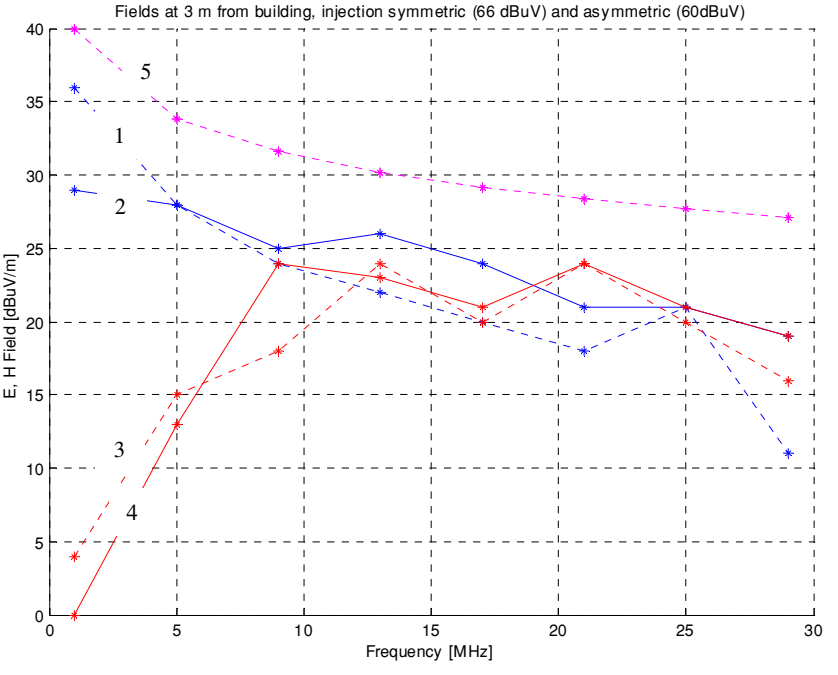

Figure 8.6. Field strength measurements. 1: Asymmetric H-field; 2: Asymmetric E-field; 3: Symmetric H-field; 4: Symmetric E-field; 5: NB30 limit, provisonal, Germany. From [94].

Work in CENELEC TC 210 WG11 for a draft standard CENELEC prEN50561-1 for in-home PLC networks started in 2008. The discussion around the LCL value arose again. Proposals were made for a compromise value of 24 dB. More studies and measurement became available. In [104] very low values of *LCL* were found, even negative values. See Figure H.5.

Reference [94] also shows field strength measurements, E-field and H-field, both from symmetrical and asymmetrical injection. The results are displayed in Figure H.6. We see that the symmetric (DM) curves, and the asymmetric (CM) curves coincide quite well. Only at frequencies below 7 MHz the apparent antenna gain differs.

H.3 LCL measurements

At Nedap N.V., involved in the PLC studies because of risks of interference to their EAS and RFID systems, measurements were performed on AC mains networks with layouts that are common in Dutch houses. It concerns the layout with an overhead distribution box which is placed near the centre of the ceiling of each room. This box is fed from the House Access Point, forms the feeding point of the main lighting in that room, and is further

connected to all switches and wall outlets in that room. In Figure H.7 a simplified two dimensional drawing is shown, together with the measurement set-up. From this figure it is clear that the layout of the wires in the room form a kind of folded dipole antenna. In reality there are more branches, 3 or 4, in each room, and this is repeated for most of the other rooms. This means that in nearly all houses in the Netherland, and probably also in other countries, there is a plurality of electric dipole antennas, each with different resonance frequencies.

The test set-up in Figure H.7 is based on a spectrum analyzer with a tracking generator, Rohde & Schwarz, type FSP 3. The Mains Connector Device, containing a 1:4 balun transformer, injects a symmetrical test signal into the mains network, which is fed with 230 V AC by the AMN. A EZ-17 type current probe measures currents at the indicated measurement positions, MPx. There are four measurement conditions:

a. No apparatus connected and switch open.
b. No apparatus connected and switch closed.
c. An apparatus is connected and switch open.
d. An apparatus is connected and switch closed.

"An apparatus is connected" means here that a capacitor is connected over the outlet, so forming a short circuit for the test signal. The individual measurements are enumerated in Table H.1. As only ratios of current amplitudes are needed, only the voltage input value in dBµVs on the display of the spectrum analyzer is noted. The LCL values are a substraction in dB of the differential mode (DM) current minus the common mode (CM) current. The DM current, where is referred to, is read from the frequency plot of the DM current for that frequency where the CM current peaks. For example in Figure H.8 the frequency plot of DM current is displayed. In Figure H.9 the CM current at MP 2, which shows a peak at 18.4 MHz. At this frequency the DM current is read in Figure H.7. The LCL value at the position of MP 2, at that frequency, is now given by

$$LCL = 74 - 80.66 = -6.66\ [dB]\,. \qquad (H.8)$$

The most right column of Table H.1 displays the measured LCL values in this experiment. This delivers an average LCL value of -1.25 dB, using the resonance frequencies of the dipole structure. That means that because of the resonance the actual CM currents values are higher than the driving DM current!

Table H.1.

Measurement results of Longitudinal Conversion Loss in test network. Nedap R&D.							
Measurement number	*Measurement point in Fig.*	Details of measurements	*Indication on FSP3* of maximal DM current [dBµV]	*Indication on FSP3* of maximal CM current [dBµV]	*Maximum @ Frequency* [MHz]	*DM current* @ Maximum Frequency of CM current	*LCL* value compared @ maximal freq.
1	MP0	Calibration measurement, without testciruit	77.34				
2	MP0	DM current to NMA, testciruit connected.	76.97		18.2		
3	MP1	CM to testcircuit, condition. a		57	7.3	73	16
4	MP1	CM to testcircuit, condition. b		63.90	7.4	60	-3.90
5	MP1	CM to testcircuit, condition. c		58.51	7.4	52	-6.51
6	MP1	CM to testcircuit, condition. d		60.25	19.1	76	15.75
7	MP1	DM to testcircuit, condition. a	81.33		6.8		
8	MP1	DM to testcircuit, condition. b	81.88		9.3		
9	MP1	DM to testcircuit, condition. c	81		19.4		
10	MP1	DM to testcircuit, condition. d	81.31		15.7		
11	MP2	CM in right hand branch, cond. a		76.92	17.6	70	-6.92
12	MP2	CM in right hand branch, cond. b		80.66	18.4	74	-6.66
13	MP2	CM in right hand branch, cond. c		81.54	17.7	77	-4.54
14	MP2	CM in right hand branch, cond. d		77.62	18.7	77	-0.62
15	MP3	CM in left hand branch, cond. a		77.25	17.6	70	-7.25
16	MP3	CM in left hand branch, cond. b		80.24	18.4	74	-6.24
17	MP3	CM in left hand branch, cond. c		81.21	17.7	77	-4.21
18	MP3	CM in left hand branch, cond. d		76.87	18.6	77	0.13

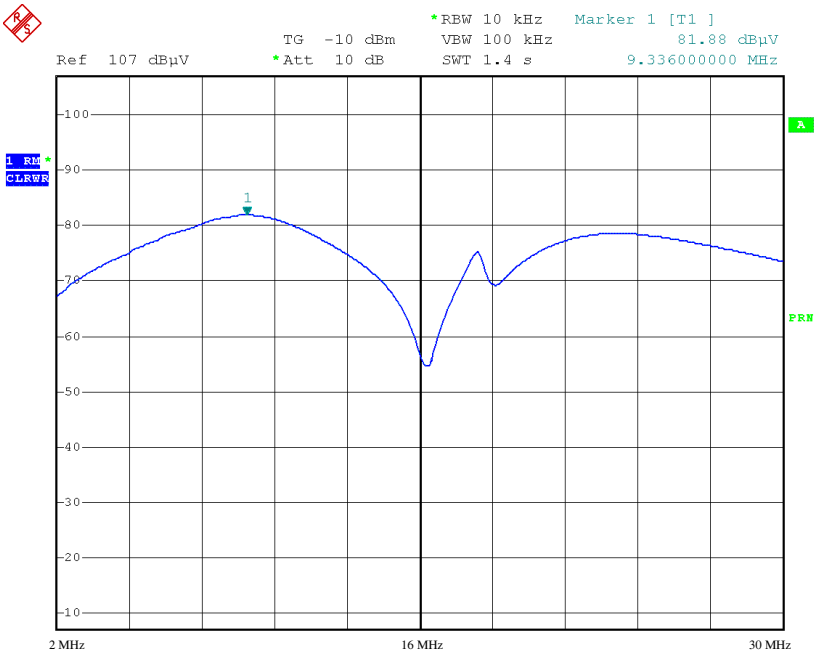

Comment: Trace1: Sink, Trace2 r=24mm, Trace3 r=25mm
Date: 23.APR.2008 13:36:35

Figure H.8. DM current at MP 1.

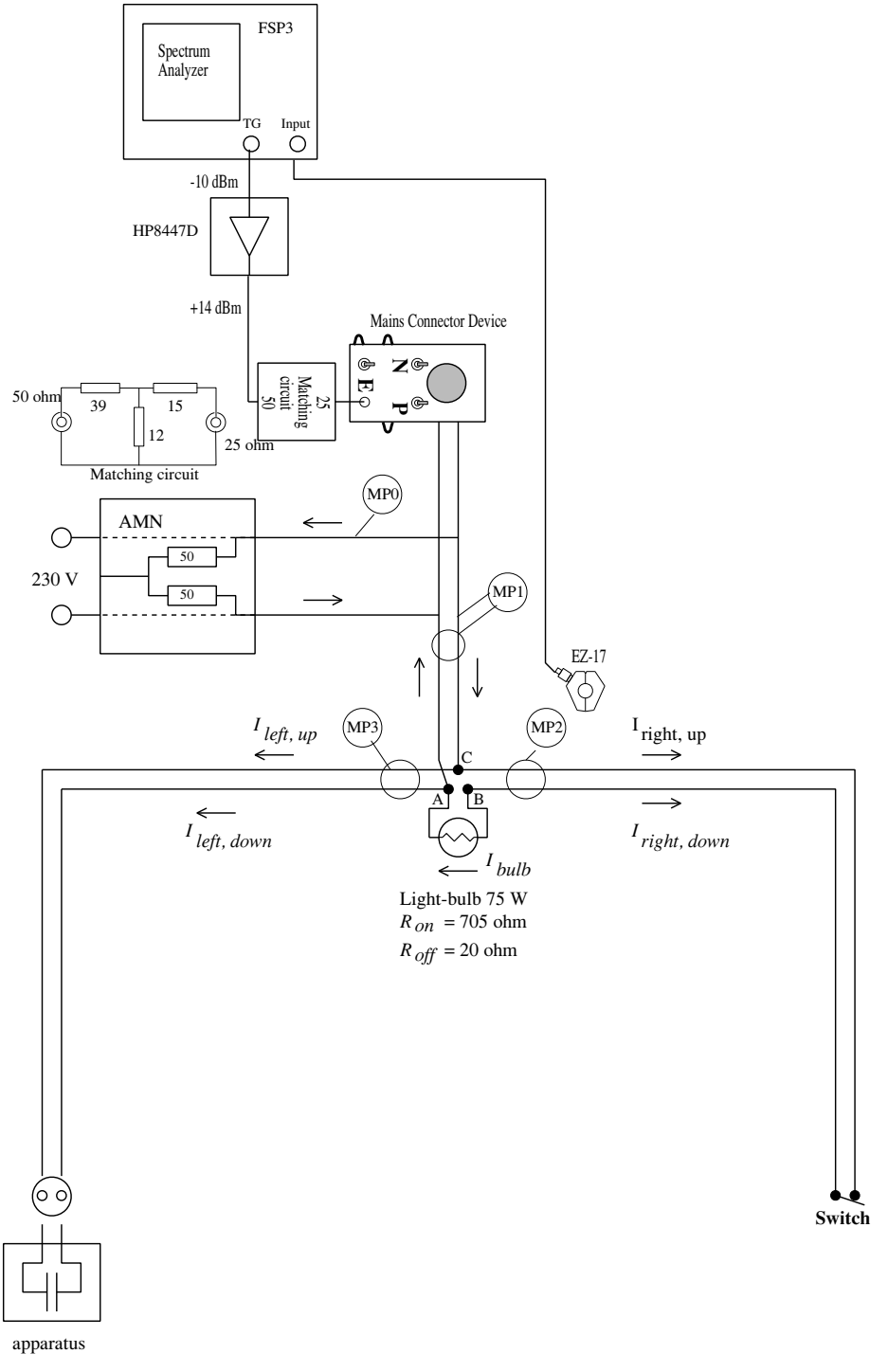
FSP3
Spectrum Analyzer
TG
Input
-10 dBm
HP8447D
+14 dBm
Mains Connector Device
50 ohm
39
15
12
25 ohm
Matching circuit
Matching circuit 50 25
MP0
AMN
50
50
230 V
MP1
EZ-17
I left, up
MP3
MP2
I right, up
C
A
B
I left, down
I right, down
I bulb
Light-bulb 75 W
R on = 705 ohm
R off = 20 ohm
Switch
apparatus

Figure H.7.

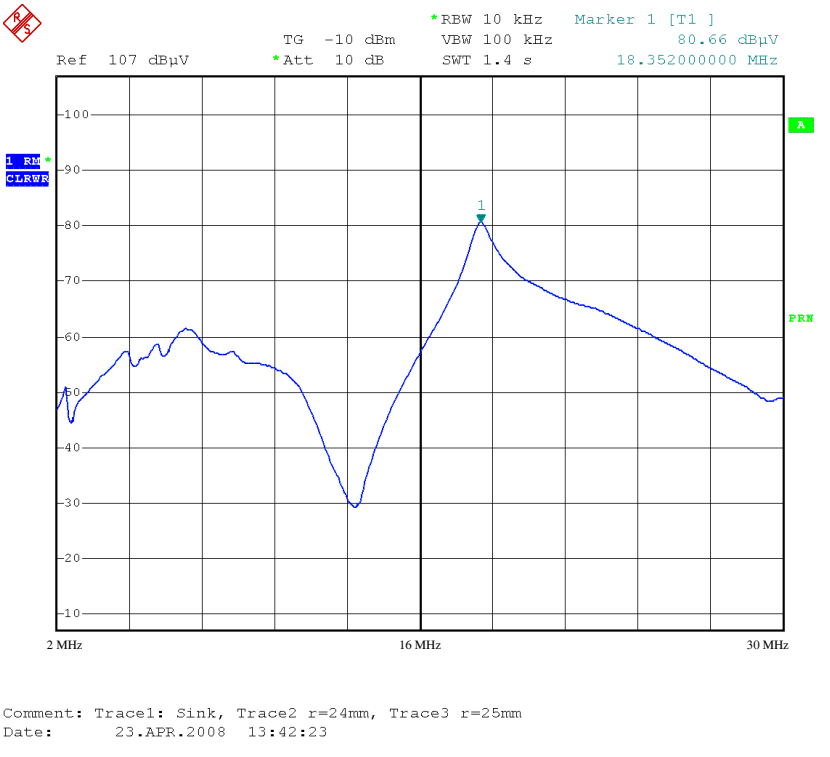

Figure H.9. CM current at MP 2.

H.4 Conclusion

Realizing, that this test network is still a rather strong simplification of the real world, that every dipole and other resonating structures have a different resonance frequency, that also the Protective Earth wires have a strong RF coupling with the power lines, they may show resonances of their own, and radiate by themselves, indicate that those low level of LCL values, measured at spot frequencies, result in a far more broadband low level of LCL values. Also taking into account the earlier mentioned results of studies of [94], [103], and [104], it is in the author's view reasonable to conclude that 6 dB is a conservative value for the LCL value for a real world mains network, averaged over a large frequency range.

Used computer hardware and software

In this project minimal use is made of traditionally used computers, operating systems, and software. Instead systems based on the ARM processor architecture (Advanced RISC Machine) were used in combination with RiscOS, a desktop operating system. Originally developed for the educational and home market by Acorn Computers Ltd., Cambridge, it is an open source project now, and further supported and developed by RiscOS Open Ltd. Info: https://www.riscosopen.org/. This dissertation is fully written on the ARMX6.

Computers and software used for this dissertation

Hardware			
1	ARMX6	RComp Interactive	My workstation, based on the i.MX6 Cortex-A9 industrial ARM board system. Running RiscOS 5.
2	Raspberry Pi 2	Raspberry Pi Foundation	Used in the data loggers. Running RiscOS 5.
3	USB-D/A/IO-pcb	KITT-Engineering	Used in the data loggers for AD-conversion.
Software from external sources			
1	!Draw	Part of the OS	Vector oriented drawing application.
2	!StrongEd	Torrens.org.uk	Very effective text / ASCI editor. Also useful for manipulating of CSV files and writing source files.
3	!TechWriter Pro	Martin Würthner *et al*	Technical Document Processor, developed in association with Acorn Computers Ltd.
4	!TableMate	G. Buchanan	Tablemaker with simple spreadsheet functions including direct cell input. Used for table making and many simple calculations, very useful for manipulating of CSV files.
5	!Praktikum	Feldner&Braun	Data series processor. Used for median complex calculations and in particulary for plotting.
6	!CsvExtrct	Feldner&Braun	Extracting single data columns from multiple column CSV file.
7	DDE Acorn C/C++	Risc OS Open Limited	Desktop Development Environment including C compiler. C programs are used for complex calculations.
8	!CadMust	Usarc Software Development	Schematic & Pcb Design.
9	!RiscOSM	H.M. Phillips	Open Street Map application for RiscOS.
10	!PhotoDesk	Photodesk Ltd/ © XAT 2022	Image processor
Special software, written by the author			
1	!RFIlogger	Datalogger application for the noise field strength measurements.	
2	!PROPlogger	Datalogger application for the mobile propagation measurements.	
3	!Average	Post processing application for the propagation measurements.	
4	!Transfer	Post processing application to transfer mobile propagation or noise measurement data into the !RiscOSM mapping application.	

List of Publications

1 Publications, peer reviewed, related to this dissertation

[I] T.W.H. Fockens and F. Leferink, "Issues Concerning Radio Noise Floor Measurements using a Portable Measurement Set-up", *Proc. of the 2018 International Symposium on Electromagnetic Compatibility (EMC Europe 2018)*, Amsterdam, The Netherlands, August 27-30, 2018 DOI: 10.1109/ EMCEurope.2018.8485041.

[II] T.W.H. Fockens, A.P.M. Zwamborn, and F. Leferink, "Measurements of the Man-made Noise Floor on HF in The Netherlands", *IEEE Transactions on EMC,* vol. 61, no. 2, April 2019 DOI: 10.1109/TEMC.2018.2830512.

[III] T.W.H. Fockens and F. Leferink, "Correlation Between Measured Man-Made Noise Levels and the Density of Habitation", *IEEE Transactions on EMC,* vol. 62, no. 6, December 2020, DOI: 10.1109/TEMC.2020.3001979.

[IV] T.W.H. Fockens, Robert Vogt-Ardatjew, F. Leferink, "Propagation measurements and analysis on MF and HF bands in urban areas in The Netherlands", *IEEE Transactions on EMC,* vol. 64, issue 3, June 2022, DOI: 10.1109/TEMC.2021.3137237.

[V] T.W.H. Fockens and F. Leferink, "Model of Cumulation of Man-Made Radio Noise, Applied to Sources of Emission Limitedby EMC Standards, and Compared With Noise Measurements", *IEEE Transactions on EMC,* vol. 64, no. 6, December 2022, pg. 1994-2004, DOI: 10.1109/TEMC.2022.3188539.

2 Publication, peer reviewed, not related

[VI] A.W. Breukelaar, Abraham bij de Vaate, Koos Fockens, Inland migration study of sea trout (Salmon trutta) into the rivers Rhine and Meuse (The Netherlands), based on inductive coupling radio telemetry, *Hydrobiologia 372*, May 1998, DOI: 10.1023/A:1017058718334.

3 Publications, not peer reviewed

[VII] Koos Fockens, "The radio amateur and the effects of the use of the 230 Volt power line for broadband data communication (PLC)", Technical Report,

VERON, 2002-06-27, DOI:10.13140/RG.2.2.32525.00487.

[VIII] Koos Fockens, System model for Inductive ID systems, Technical Report, Nedap N.V., 2003-10-16. DOI: 10.13140/RG.2.2.24975.25769.

Dankwoord

Het begon allemaal in 2013, in een periode waarin bij de VERON EMC-EMF commissie steeds meer klachten binnen kwamen over radiostoringen en verhoogde ruisniveau's, toen de voorzitter van de commissie, Jan Janssen, mij de ruimte gaf om ideëen over een ruismeetcampagne uit te werken en aan het VERON Hoofdbestuur voor te leggen. De opdracht volgde in november van dat jaar onder voorwaarde dat het onderzoek zou moeten resulteren in een wetenschappelijke publicatie. Daarvoor ben ik in het speciaal hoofdbestuurlid Peter Zwamborn dank verschuldigd. Na een jaar van voorbereidingen kon de campagne in 2015 beginnen. De commissieleden Jan Janssen, Fred Marks en Anton Steenbakker hebben mij, elk in hun eigen regio, geholpen bij het uitvoeren van de metingen bij de vrijwilligers[1] waar we op hun thuislokaties mochten meten. In het bijzonder ben ik dank verschuldigd aan het gemengde team van de opleidingen maritiem officier en elektrotechniek van de Hogeschool van Amsterdam o.l.v. Ton Vaes en op initiatief van Frits Brouwer, die met hun opleidingsschip, de *Gyrinus*, het mogelijk maakte ruismetingen uit te voeren op het IJsselmeer. Met windkracht 7 was dat een unieke ervaring. Dit experiment leerde ook dat het noodzakelijk was alle elektrische systemen op het schip uit te zetten om goed metingen te kunnen doen. Ook de ruismetingen op het Markermeer met de boot van Klaas van der Ham**,** samen met Peer Touber (†) en Gijs Lamsvelt (†), waren interessant doordat we ook op 28 MHz nog sterke grondgolf propagatie over water van ruis, afkomstig uit het centrum van Amsterdam, konden vaststellen. Ik wil graag Norbert IJzereef, Defensie, en zijn collega's bedanken voor hun inzet om propagatiemetingen mogelijk te maken op de landingsbaan van vliegbasis Deelen.

Het waren Peter Zwamborn en Robert Langenhuysen, die mij de suggestie aan de hand deden het onderzoek uit te breiden met een promotie pad. Peter zorgde voor kontakt met zijn collega Prof. Frank Leferink. In juni 2017 heb ik met Prof. Leferink gesproken en gevraagd voor een PhD plek en om als promotor op te willen treden. Heel veel dank Frank dat je mij de gelegenheid gaf om dit nieuwe avontuur te beginnen.

1 A. v. Asperen, A. Baltes*, A. Bauer, D. v. d. Berg, H. v.d. Berg, A. Den Boer, P.T. De Boer, J. Bosch*, A. v. Bronkhorst*, R. v. Dongen, W. Drenten*, H. v. Enckevort, J. Evers, W. v. Gaalen*, W. Geven, W. Groen, K. v. d. Ham, H. v.d. Heuvel*, H. Hilbink*, J. Hoek, P. v. d. Hulst, J. Janssen*, G.J. Huysman, P. Jelgersma, K. de Jonge, P. Kats*, E. Kattenberg, B. v. d. Kleij, W.Kurvers, E. Krijger*, R. Langenhuysen*, D. Lucas (†), F. Marks, S. Nestra, G. Nieboer*, P. Niessen, K. Nijdam, W. Peezenkamp*, A. Reuvekamp*, K. Robers, H. Roenhorst*, A. Steenbakker**,** J. S. v.d. Stoel, F. Tak*, K. Timmer, F. Timmerman, W. J.Ubbels, H. Verkaik, J. Vos, A. Westers, K. Wiegers, C. Wielenga, H. Wilmink, R. v. d. Zaal, Q. v. Zon. *Hebben ook geparticipeerd in de propagatiemetingen.

Voor de calibratie van mijn meetantennes was ik afhankelijk externe referentiebronnen. De eerste poging daartoe werd uitgevoerd in de grote anechoïsche kamer van Tüv Niekerk met hulp van Ties Koning**.** Bevreesd voor het effect van resonanties in de kamer zijn de calibratiemetingen overgedaan op de OATS van Agentschap Telecom**,** nu genoemd Rijksinspectie Digitale Infrastructuur**,** door Jos Kamer**.** De ruisvloer niveau's van het gehele meetsysteem zijn gemeten in de kleine anechoïsche kamer van Nedap N.V. Daar heb ik ook de ENR-waarde van mijn ruisbron mogen calibreren, nodig om de effectieve ruisbandbreedtes van de meetontvangers te bepalen. Dit is gebeurd d.m.v. een gecalibreerde spectrum analyzer van Rohde & Schwarz, type FSV30.

Zoals genoemd in Chapter 1 speelden computers draaiende onder RiscOS een centrale rol in dit project, en maakten mij onafhankelijk van andere, duurdere, software die gewoonlijk gebruikt wordt in deze situaties. Ik wil Andries Lohmeijer en Peter van der Vos, beiden van KITT Engineering, bedanken voor de langdurige samenwerking die in mijn Nedap tijdperk begon: Andries voor de hardware ontwikkelingen voor RFID labelmeetsystemen, daarna ook toegepast in de dataloggers, en Peter, die mij geduldig hielp met leren van programmeren in C in combinatie met RiscOS.

Tevens wil ik dank zeggen aan Matthew en Hilary Phillips (UK) voor hun "RiscOSM", Open Street Map applicatie, die ik uitgebreid gebruikt heb in het hele project en in het bijzonder voor hun bereidheid hun software uit te breiden met de optie om CSV bestanden te importeren, die GPS data en veldsterkte informatie bevatten, wat de mogelijkheid geeft om kleurgecodeerde stippen te plotten op de kaart.

Ik ben ook veel dank verschuldigd aan mijn dochter Marijke, die op het juiste moment aan kwam zetten met haar studieboek over statistiek, Referentie [60]. Een voor mij nieuw terrein dat wel van essentieel belang was voor de verwerking en interpretatie van de meetresultaten.

Naast Prof. Leferink moet ik anderen in de vakgroep Power Engineering & EMC bedanken, zoals Cees Keijer, die helaas niet meer onder ons is, en Frits Buessink, met welke twee ik de in de eerste jaren de werkkamer deelde en mij een prettige werkomgeving bezorgden, Lillian Hannink voor de vele en snelle hulp in allerlei praktische en administratieve zaken, Robert Vogt-Ardatjew als dagelijkse begeleider, en vele anderen in de vakgroep. Robert Fennis wil ik bedanken voor zijn studie inzake grondgolf propagatie.

Tenslotte ben ik ook zeer veel dank verschuldigd aan mijn lieve echtgenote Stella, voor haar geduld terwijl zij in de loop van het promotie-traject om medische redenen de zwaarste jaren van haar leven doormaakte.

Acknowledgement

It all begun in 2013, in a period when increasing numbers of complaints were received by the VERON EMC-EMF committee about radio interference and risen noise levels, when the chairman, Jan Janssen, give me room to develop ideas about a noise measuring campaign and presented it to the VERON Board. The mandate followed in November of that year with the condition that the investigation should result in a scientific publication. Therefor I am indebted to Board member Peter Zwamborn especially. After one year of preparations the campaign could start in 2015. Each in their own region, committee members Jan Janssen, Fred Marks and Anton Steenbakker assisted me in excecuting the measurements at the home locations of the volunteers[2], where we were allowed to measure. In particular I am grateful for help of the mixed team from the Amsterdam University of Applied Sciences, the maritime officer training and electrical engineering, led by Ton Vaes an on initiative from Frits Brouwer, who gave me the oppertunity to do noise measurements on Lake IJsselmeer with their training ship *Gyrinus*. With wind force 7 that was an unique experience. Also this experiment learned us the necessity to switch off all electrical systems on the ship for being able to perform the noise measurements correctly. Noise measurements on Lake Markermeer too by using the sailing boat of Klaas van der Ham, together with Peer Touber (†) and Gijs Lamsvelt (†), were interesting by the fact that we could determine on 28 MHz strong ground-wave propagation over water of noise, arriving from the city centre of Amsterdam. I would like to thank to Norbert IJzereef and his collegues of the Ministery of Defense, for his commitment to enable propagation measurements on the runway of airbase Deelen.

It were Peter Zwamborn en Robert Langenhuysen suggesting me to extend the investigation project with an PhD trajectory. Peter made me in contact with his colleague Prof. Frank Leferink. June 2017 I spoke Prof. Leferink and ask him for a position and to act as a promotor. Many thank Frank that you gave me the opportunity to start this new adventure.

2 A. v. Asperen, A. Baltes*, A. Bauer, D. v. d. Berg, H. v.d. Berg, A. Den Boer, P.T. De Boer, J. Bosch*, A. v. Bronkhorst*, R. v. Dongen, W. Drenten*, H. v. Enckevort, J. Evers, W. v. Gaalen*, W. Geven, W. Groen, K. v. d. Ham, H. v.d. Heuvel*, H. Hilbink*, J. Hoek, P. v. d. Hulst, J. Janssen*, G.J. Huysman, P. Jelgersma, K. de Jonge, P. Kats*, E. Kattenberg, B. v. d. Kleij, W.Kurvers, E. Krijger*, R. Langenhuysen*, D. Lucas (†), F. Marks, S. Nestra, G. Nieboer*, P. Niessen, K. Nijdam, W. Peezenkamp*, A. Reuvekamp*, K. Robers, H. Roenhorst*, A. Steenbakker**,** J. S. v.d. Stoel, F. Tak*, K. Timmer, F. Timmerman, W. J.Ubbels, H. Verkaik, J. Vos, A. Westers, K. Wiegers, C. Wielenga, H. Wilmink, R. v. d. Zaal, Q. v. Zon. *Did also participate in the propagation measurements.

For calibration of my measurement antennas I was depending on external references. The first attemp was carried out in the large anechoic room of Tüv Niekerk with help from Ties Koning**.** Afraid of effects of resonances in the room, calibration measurements were repeated on the OATS of Netherlands Radio Agency by Jos Kamer. The noise floor of the complete measurement system were measurement in the small anechoic room of Nedap N.V. Also I could calibrate the ENR value of my noise source, needed to measure the effective noise bandwidths of the measurement receivers. For this purpose a calibrated Spectrum Analyzer from Rohde & Schwarz, type FSV30, is used.

As mentioned in Chapter 1 Computers running under RiscOS played a key role in this project, and made me independent from other, more expensive, software that is usual used in these situations. I wil thank Andries Lohmeijer and Peter van der Vos, both from KITT Engineering, for the long standing cooperation that started in my Nedap era: Andries for the hardware developments, among other applied in the dataloggers, and Peter, who helped me patiently with learning programming in C in combination with RiscOS.

Also I would like to thank Matthew and Hilary Phillips for their RiscOSM, Open Street Map, application, which I extensively used throughout the entire project and especially for their kindness to extent their software with the option to import CVS files, containing GPS data and field strength levels, giving the option to plot colour coded dots on the map.

I am indebted to my daughter Marijke, who at the right moment arrived with her textbook about statistics, Reference [60]. A new field for me that proofed to be of essential importance for the processing and interpretation of the measurement results.

Next to Prof. Leferink I must say thanks to others in the department of Power Engineering & EMC as the late Cees Keijer, who left us too early, and Frits Buessink, with both I shared the office and provided me with a pleasant working environment, Lillian Hannink for the many and quick help in all kinds of practical and administrative matters, Robert Vogt-Ardatjew as my daily supervisor, and many others in the department.

At last I am very grateful to my dear wife Stella for her patience while she went through the toughest years of her life during my PhD work because of medical reasons.

Biography

Tallienco Wieand Harm (Koos) Fockens was born in the City of Groningen on September 8th 1946. Raised as the youngest son of a farmer's family on the farm between Luddeweer and Woltersum, on the Lowland of Groningen. In 1959 he went to the Rijks HBS in the City, started studying Electrical Engineering at the Technische Hogeschool Twente in 1965, now University of Twente, and received his masters degree, Ir, in Januari 1974 on the subjects of instrumental electronics and telecommunication in the Chair of Professor Rodenburg.

He has been with NEDAP NV, Groenlo, The Netherlands, since 1974 until his retirement in 2011. His work concerned the development of, and research into, EAS (Electronic Article Surveillance) and RFID systems, including a new technical solution for fish migration telemetry. Special interest was for the research into the behaviour of RFID tags, the qualifying and testing thereof. Later on, he became involved in international standardisation working parties, ETSI, CENELEC, CEPT and ISO, on RFID, Short Range Devices, and EMC. He has published three papers before, about fish migration telemetry, about Inductive RFID systems and about the effects of PLC inhouse, and wrote many patents. In August 2017 he joined the Telecommunication Engineering group of the University of Twente as a Ph.D. student.

Ir. Fockens has an amateur radio license since 1966 (radio callsign: pa0kdf), is a member of the VERON (Association for Experimental Radio Research in The Netherlands) since 1963, member of its EMC-EMF comittee (2001), was a member of NERG (Netherlands Society of Electronics and Radio engineering) until its closure, and is now a member of Royal Institute of Engineers (KIVI).

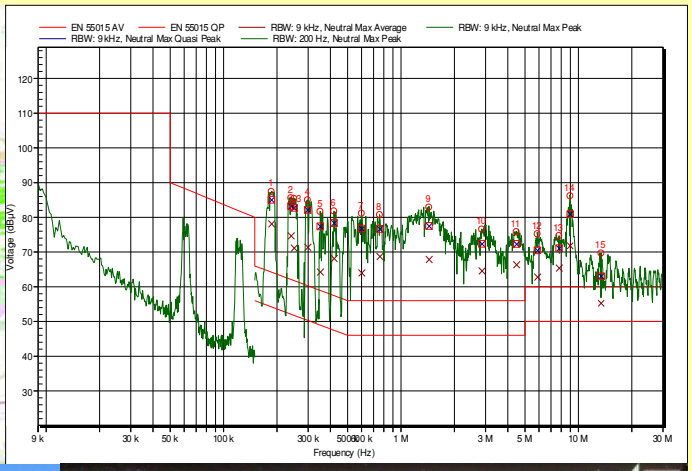
EN 55015 AV
EN 55015 QP
RBW: 9 kHz, Neutral Max Average
RBW: 9 kHz, Neutral Max Peak
RBW: 9 kHz, Neutral Max Quasi Peak
RBW: 200 Hz, Neutral Max Peak
Voltage (dBµV)
Frequency (Hz)
9 k
30 k
50 k
100 k
300 k
500 k
1 M
3 M
5 M
10 M
30 M

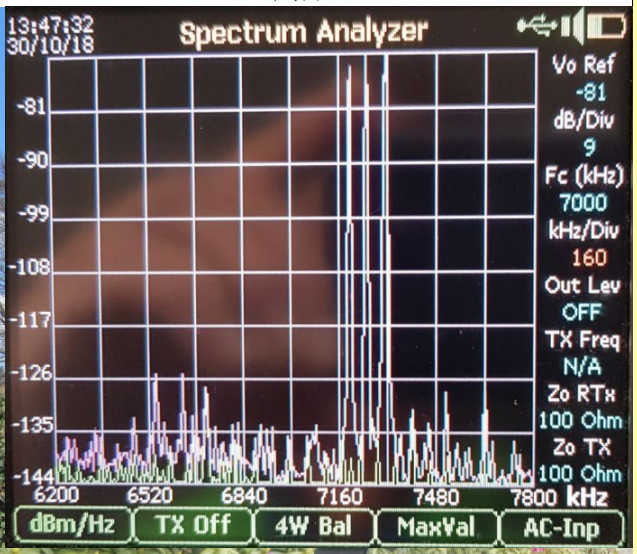
13:47:32
30/10/18
Spectrum Analyzer
Vo Ref
-81
dB/Div
9
Fc (kHz)
7000
kHz/Div
160
Out Lev
OFF
TX Freq
N/A
Zo RTx
100 Ohm
Zo TX
100 Ohm
-81
-90
-99
-108
-117
-126
-135
-144
6200
6520
6840
7160
7480
7800 kHz
dBm/Hz
TX Off
4W Bal
MaxVal
AC-Inp